QUANTIFYING SPATIAL GEOTECHNICAL UNCERTAINTY TO ADVANCE THE PRACTICE OF RISK ASSESSMENT AND DECISION-MAKING IN TUNNEL PROJECTS

FINAL PROJECT REPORT

by
Gangrade R[1]
Mooney M[1]
Trainor-Guitton W[1]
[1] Colorado School of Mines

Sponsorship
UTC-UTI

For

University Transportation Center for
Underground Transportation Infrastructure
(UTC-UTI)

August 17th, 2021

Disclaimer

1. Report No.	2. Government Accession No.	3. Recipient's Catalog No.	
4. Title and Subtitle Quantifying spatial geotechnical uncertainty to advance the practice of risk assessment and decision-making in tunnel projects		5. Report Date August 17th, 2021	
		6. Performing Organization Code	
7. Author(s) Rajat Gangrade, Mike Mooney, and Whitney Trainor-Guitton		8. Performing Organization Report No.	
9. Performing Organization Name and Address University Transportation Center for Underground Transportation Infrastructure (UTC-UTI) Tier 1 University Transportation Center Colorado School of Mines Coolbaugh 308, 1012 14th St., Golden, CO 80401		10. Work Unit No. (TRAIS)	
		11. Contract or Grant No.	
12. Sponsoring Agency Name and Address United States of America Department of Transportation Research and Innovative Technology Administration		13. Type of Report and Period Covered	
		14. Sponsoring Agency Code	
15. Supplementary Notes Report also available at: https://zenodo.org/communities/utc-uti			
16. Abstract The largest element of technical and financial risk on any tunnel project lies in the ground conditions. The conventional practice of developing deterministic interpretations of ground conditions does not account for ground spatial variability nor quantify uncertainty. With the increased number of claims and litigations, it is evident that the conventional practice is ineffective in assessing ground spatial variability and uncertainty. Geostatistics-based methodologies are developed in this report to provide advantages over the qualitative and subjective deterministic interpretation of ground conditions with the probabilistic assessment of ground conditions as outputs. The geostatistics-based methodologies presented in this report are developed with a vision to assist the tunneling community in (a) analyzing ground spatial variability and uncertainty and (b) tying the results from geostatistical modeling to tunnel risk assessment. The latter is expected to help the tunneling community realize the advantages of geostatistical modeling-based methodologies in improving tunnel construction performance.			
17. Key Words Geostatistics; Spatial variability; Geotechnical uncertainty; Tunneling; Risk assessment; Probabilistic assessment		18. Distribution Statement No restrictions.	
19. Security Classification (of this report) Unclassified	20. Security Classification (of this page) Unclassified	21. No of Pages 190	22. Price NA

Table of Contents

List of Figures

List of Tables

EXECUTIVE SUMMARY

The largest element of technical and financial risk on any tunnel project lies in the ground conditions. The conventional practice of developing deterministic interpretations of ground conditions does not account for ground spatial variability nor quantify uncertainty. With the increased number of claims and litigations in the tunneling industry, it is evident that the conventional practice is ineffective in assessing ground spatial variability and uncertainty. Geostatistics-based methodologies are developed in this report to provide advantages over the qualitative and subjective deterministic interpretation of ground conditions with the probabilistic assessment of ground conditions as outputs. Geotechnical site investigation data from varied geological settings are utilized to offer effective solutions for unique challenges in tunnel projects and improve ground awareness.

As the first contribution of the report, a probabilistic geostatistical methodology is developed to quantify the soil transition location uncertainty in the longitudinal and transverse directions of tunneling. Results from application to a soil tunnel project reveal that soil transition locations identified from the methodology agree reasonably well with the ground truth transitions, estimated via the difference in the rates of chamber pressure dissipation at the tunnel springline.

Next, a geostatistics-based methodology is developed to generate quantitative estimates of karstic features' size, number, occurrence probability, and occurrence location within the tunnel envelope. Applying the methodology to a mixed-ground tunnel project in Malaysia reveals a presence of 2% to 6% average volumetric karstic void fraction for every 50 m of tunnel excavation. The results are utilized to estimate an average cumulative grout volume of 4000 m^3 for the complete tunnel section.

Next, a risk-based methodology is developed to optimize geotechnical SI from quantifying geotechnical parameter uncertainty. For the risk created by uncertainty in tool wear rate, geospatial assessments of geotechnical parameter uncertainty, tunnel risk consequences, and investigation accessibility are developed to identify additional investigation locations. The results revealed that additional investigations reduced geotechnical parameter uncertainty by about 40 % that led to a reduction in the location uncertainty of the first two cutterhead interventions by about 90 rings.

Lastly, a methodology is developed to quantify the geostatistical model accuracy in predicting soil conditions, emphasizing predicting soil transitions. The methodology was applied to two soil tunnel projects to investigate the effect of geotechnical SI density and geological environment on geostatistical model accuracy. The results revealed that for a 100 m borehole spacing, geostatistical model accuracy in capturing soil transitions in a sedimentary and sequenced stratigraphy is about 60 %; whereas, for the heterogeneous glacial environment is less than 50 %.

The geostatistics-based methodologies presented in this report are developed with a vision to assist the tunneling community in (a) analyzing ground spatial variability and uncertainty and (b) tying the results from geostatistical modeling to tunnel risk assessment. The latter is expected to help the tunneling community realize the advantages of geostatistical modeling-based methodologies in improving tunnel construction performance.

CHAPTER 1- INTRODUCTION

1.1 Motivation

Subsurface conditions are among the greatest source of unknown prior to the actual construction of tunnel projects. Interpretation of the expected ground conditions on a tunnel project site is a key aspect in tunnel procurement, planning, design, and construction decisions. As a result, the most prominent technical and financial risk element on any tunnel project lies in the ground conditions.

Essex (2007) discusses that *"The design and construction process must account for the variability of subsurface conditions, and the potential project costs associated with the variability."* In the current tunneling practice, geological and geotechnical profiles of the anticipated ground conditions are presented in the geotechnical baseline report (GBR) and geotechnical data report (GDR). The profiles are intended to advise the tunnel designers and contractors of the anticipated ground conditions, construction means and methods, and potential tunnel risks. The profiles and the baseline conditions in the GBRs are used to demarcate risk allocation between the tunnel project owner and the contractor, resolve differing site condition (DSC) claims and financial litigations (Essex 2007; Davis 2021). To get the magnitude of DSC claims, in early 2014, Seattle Tunnel Partners, the design-build team constructing the Alaska Way Viaduct Tunnel, submitted a DSC claim worth the US $20 million to Washington State Department of Transportation, after completing about 10 % of the TBM drive (van der Pouw Kraan 2014).

With the increase in the number of DSC and litigations arising out of ground spatial variability and uncertainty, tunnel project owners typically use the GBR as a risk transfer mechanism by presenting a limited interpretation of the ground conditions. Tunnel designers and contractors may not recognize the potential ground risk, resulting in overbidding/underbidding on tunnel projects and poor decisions on design and construction. During excavation, unanticipated ground conditions may mobilize a large part of the ground volume, excessive settlements, endanger work crew and community, and lead to significant delays in project delivery. Spyridis and Proske (2021) discuss that from a total 321 tunnel collapse case studies, 92% of the tunnel collapses occurred during construction, predominantly due to unanticipated ground conditions or poor decision-making arising from inadequate knowledge of the ground conditions. Database and catalogs of tunnel collapse and accidents can be found in (Seidenfuss 2006; Zhao 2009; Sousa 2010a; Reiner 2011; Zhang et al. 2015). Thus, inadequate knowledge of the ground spatial variability and uncertainty remains a practical problem in tunneling and geotechnical engineering projects.

Tunnel projects are unique as it involves fitting an operating engineering system into the unknown subsurface with a life span of just over 100 years. The report aims to develop methodologies that can minimize the *unknowns* in the subsurface through quantitative outputs of ground spatial variability and uncertainty. The methodologies are aimed to provide advantages over the qualitative and subjective deterministic interpretation of ground conditions with probabilistic assessment of ground conditions as outputs. An application of these methodologies is expected to provide a realistic interpretation of the ground conditions. The report aims to use the geotechnical SI data from tunnel projects to develop these methodologies and thereby provide quantitative improvement in (a) ground awareness, (b) risk characterization, (c) risk mitigation planning, and (d) decision-making on tunnel projects.

The report utilizes the theory of geostatistics as a tool to develop these methodologies. Geostatistics uses a specific modeling approach on available data to interpolate between known data points, thus creating a spatial representation of the ground conditions. Modeling ground spatial variability and uncertainty has gained increased attention over the past couple of decades. A number of researchers have focused on the description of ground spatial variability using geostatistics in mining, geological, and geotechnical engineering applications (Matheron 1971; Deutsch and Journel 1992; Phoon and Kulhawy 1999a; Baecher and Christian 2005; Uzielli et al. 2006; Caers et al. 2007; Chiles and Delfiner 2009; Phoon and Ching 2014; Pyrcz and Deutsch 2014). Over the past few years, geostatistical techniques have been applied to characterize the uncertainty ground conditions and geotechnical parameters for tunnel projects (El Gonnouni et al. 2006; Marache et al. 2009; Stavropoulou et al. 2010; Ozturk and Simdi 2014; Pinheiro et al. 2017; Chen et al. 2017; Huang et al. 2017; Boyd et al. 2019, 2020; Grasmick et al. 2020a, b; Grasmick and Mooney 2021).

The geostatistics-based methodologies presented in this report are developed with a vision to assist the tunneling community in (a) analyzing ground spatial variability and uncertainty and (b) tying the results from geostatistical modeling to tunnel risk assessment. The latter is expected to help the tunneling community realize the advantages of geostatistical modeling-based methodologies in improving tunnel construction performance. Within these methodologies, geotechnical SI data from tunnel projects in varied geological settings are utilized to offer effective solutions for unique challenges in tunnel projects to improve ground awareness. The following paragraphs introduce the engineering challenges focused upon in this report and highlight the features of respective geostatistics-based methodologies developed herein.

1.1.1 Quantifying soil transition location uncertainty

In geotechnical and tunneling applications, engineers are often concerned about stratigraphic transitions. Their occurrence may lead to reduced tunnel boring machine (TBM) advance rates, loss of face stability, and the creation of sinkholes causing heavy water inrush (Sousa 2010; Wang et al. 2016). Stratigraphic transitions can include the movement of a TBM from one soil/rock type into another, or it can include mixed face conditions, i.e., a horizontal transition between disparate soil/rock types. A lack of quantifiable knowledge of mixed-face conditions has led to major tunnel incidents involving excessive ground deformations in about 55% of tunnel projects worldwide (British Tunneling Society 2005). The uncertainty in stratigraphic transitions is addressed qualitatively with a "?" along a unique boundary between stratigraphic units in the geological profiles (see Figure 1.1).

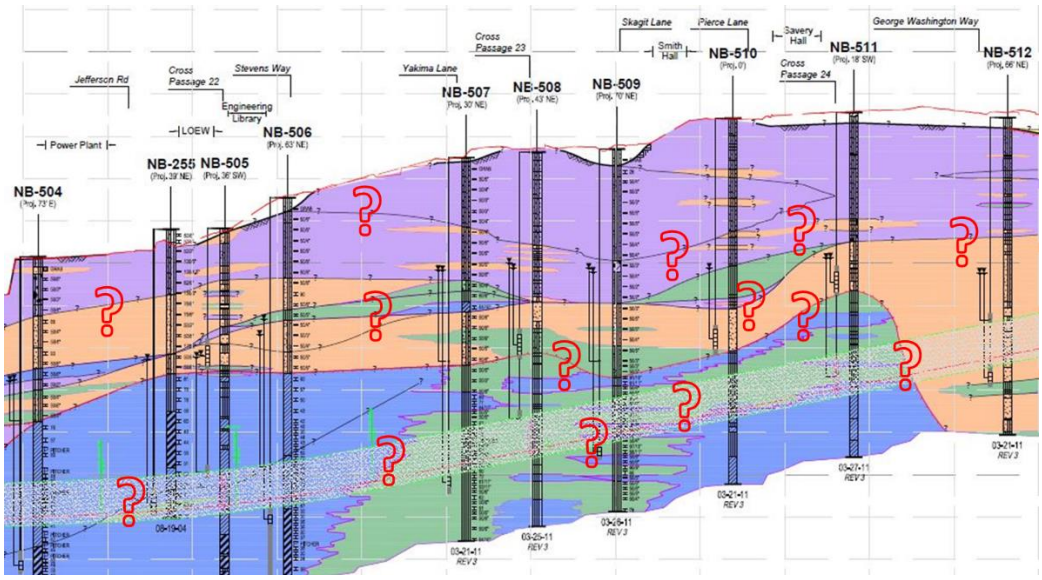

Figure 1.1 Deterministic soil profile from GBR for the Northgate Link extension project in Seattle (Jacobs 2013).

A lag in the regulation of TBM operational parameters to adapt to the occurrence of mixed-face conditions has led to tunneling-induced ground deformations or face stability issues on tunnel projects worldwide (Ma et al. 2015; Zhang et al. 2020). Significant ground movements were observed due to the occurrence of mixed-face conditions (sand overlying clay within tunnel envelope) in the TBM excavated projects undertaken by Washington Metro Area Transit Authority (WMATA) (Clough and Leca 1993). On Changsha Metro Line 4 in China, an unexpected surface settlement of 50 mm (2 inches) was observed due to the lag in chamber pressure regulation as the TBM advanced from low permeability ground to high permeability ground (Zhang et al. 2020). Tunneling-induced settlement of up to 20 mm (0.8 inches) was observed on the Edmonton South Light Rail Transit Extension project, Canada, due to tunneling in mixed-face conditions of glacial till, Edmonton clay, sands, and silts (Bossé 2005). Similar significant tunneling issues related to ground movement, cutter tool consumption, and water inflows were observed on Kranji tunnel of the Deep Tunnel Sewage System in Singapore (Zhao et al. 2007), Metro line 1 tunnel in Chengdu, China (Gao et al. 2013; He et al. 2013), and Metro line 3 tunnel in Guangzhou, China (Ren et al. 2016). From tunneling case histories worldwide, it is evident that quantification of stratigraphic transition location uncertainty requires more attention for efficient tunneling performance.

Due to a deterministic interpretation of the tunnel excavation environment, a quantification of stratigraphic transition location uncertainty remains to be a practical problem in the design and construction of tunnel projects. From the perspectives of efficient tunnel construction and tunnel risk mitigation, it is of great interest to quantify the uncertainty in locations of stratigraphic transitions.

This report presents a geostatistics-based probabilistic approach to quantify soil transition location uncertainty (in the longitudinal and transverse direction) within the tunnel envelope. The methodology aims to quantify the soil transition location uncertainty using the occurrence

probability of soil types along the tunnel length and mixed-ground transition plane (vis-à-vis TBM cutterhead). The methodology is applied to a soil tunnel project in North America where soil transition location uncertainty at two different locations along tunnel alignment is quantified. The results obtained from the probabilistic approach are validated with the TBM operational data from the project to justify the efficacy of the methodology in identifying soil transition locations. The proposed approach is applied to another soil tunnel project in North America to verify the methodology's performance in a different geological setting. The results from the two tunnel projects are validated with a data-driven model developed by Yu and Mooney (2021) that characterized the as-encountered ground conditions using relevant TBM operational data.

1.1.2 Quantifying void risk occurrence for tunnel projects

Like stratigraphic transitions, solution cavities and voids formed in karstic geological environments are another critical subsurface feature affecting tunnel planning, design, and construction. For tunnel projects planned in geological formations exhibiting karstic features, detecting voids in the driving path of the TBM has always been a critical issue. Tunnel excavation in a karstic geological setting can induce severe geotechnical hazards leading to high construction costs and schedule delays (Yau et al. 2020).

Several researchers have discussed the design and construction issues due to the presence of karstic void features on tunnel projects in Malaysia (Zabidi and De Freitas, 2013; Boon et al. 2020), China (Cui et al. 2015; Ren et al. 2016; Wang et al. 2020), Iran (Zarei et al. 2010; Shahriar et al. 2008), and North America (Day 2004). These case studies show that unpreparedness in estimating karstic features in tunnel projects has influenced tunnel geotechnical hazards. Typically, with limited and sparse geotechnical SI on tunnel projects, there is significant uncertainty regarding karstic voids' location and occurrence frequency estimates. Irregular distribution of the karstic voids and their various shapes and sizes compounds the problem of evaluating the void fraction within the tunnel envelope.

Like any other tunnel risk, karstic risk assessments are included in the geotechnical baseline report (GBR). Interestingly, although GBRs are used increasingly to demarcate risk allocation and resolve financial disputes, the karstic risk evaluation incorporated in GBRs is qualitative or semi-quantitative (Yau et al. 2020). The risk assessments from GBR, lacking consideration of spatial variability and distribution of voids, may influence project pricing and construction means and methods and can potentially result in an increased number of DSC claims. Therefore, it is worthwhile to develop quantitative assessments of karstic features considering spatial variability from SI data for efficient planning and construction of tunnel projects.

To address this issue, a geostatistics-based methodology is developed to advance the qualitative/semi-quantitative assessments (from conventional practice) of karstic feature occurrence within the tunnel envelope. The methodology involves modeling karstic features of different radii as a geological unit to quantify the volume of karstic features within the tunnel envelope. The quantitative estimates – the size, number, occurrence probability, and occurrence location of karstic features within the tunnel envelope are utilized to develop probabilistic estimates of grout volume required to treat karstic features. The developed methodology is applied to a mixed-ground tunnel project in Malaysia, and probabilistic estimates of karstic feature occurrence and grout volume required are developed for every 50 m of tunnel excavation.

1.1.3 Optimizing site investigations for tunneling applications

Tunnel geotechnical SI campaigns recover less than 1 % of the ground compared to tunnel excavated volume. The scope of this limited and sparse tunnel geotechnical SI is driven by the budget constraints and subjective engineering experience rather than characterizing the expected ground variability. Walters et al. (2011) discussed that the typical allocated budget for tunnel geotechnical SI (detailed fieldwork, data collection, interpretation, and baseline preparation) is about 0.75 % of the project budget. Designing geotechnical SI campaigns in geotechnical and tunnel projects is a process of decision-making under uncertainty.

Published studies present methodologies to locate boreholes at locations of highest uncertainty and design an optimal configuration of boreholes that maximizes knowledge gain of ground spatial variability (Gong et al. 2014; Sousa et al. 2016; Pinheiro et al. 2017). However, none of these methodologies is based on UCT risks, which are unique. While FHWA (2009) recommends an average spacing of 100-150 m to determine the number and locations of boreholes for tunnel geotechnical SI, the effect of limited and sparse geotechnical SI on tunnel risks is not known. The disputes and claims reported in the tunnel and geotechnical engineering projects (National Research Council 1984; Tonks et al. 2017), due to flawed interpretation of ground conditions from low-quality SI, imply that the prevailing practice of locating boreholes does not necessarily capture the ground variability. For efficient tunnel construction and risk mitigation, the tunnel engineering community has realized that ground spatial variability and uncertainty are significant challenges that need to be addressed (Dong et al. 2016; Sotiropoulos et al. 2016; Xia et al. 2017). Shirlaw (2016) presented a case history on the misinterpretation of rock head level on the C855 Circle Line project in Singapore, resulting in sinkhole formation within a short distance of tunneling (Figure 1.2). Although several boreholes were later drilled to interpret the rock head level, the study highlighted the need for an optimized effort of tunnel geotechnical SI considering geotechnical risks.

This led to the motivation of improving the quality of SI on tunnel projects to reduce the uncertainty in tunnel risk occurrence by specifically accounting for the spatial variability in the ground conditions related to one or more tunnel risks. It is of great interest to incorporate the tunnel project site conditions and resources constraints for the owner, engineer, and contractor to make informed decisions for planning, design, and construction.

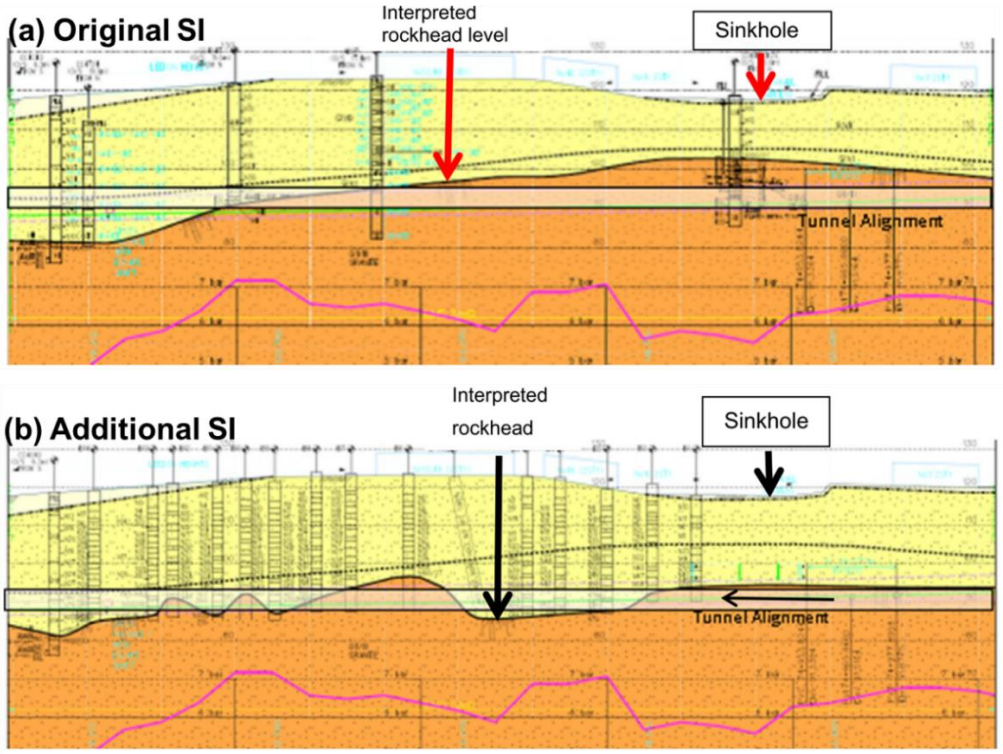

Figure 1.2 (a) Original investigation on 250 m section of C855 Circle Line, Singapore. The interpretation of rock head is based on five boreholes, (b) Same 250 m tunnel section with the reassessment of rock head level from additional 15 boreholes (Shirlaw 2016).

A risk-based methodology to optimize geotechnical SI from geotechnical parameter uncertainty modeling is developed to address this motivation. The methodology generates a geospatial quantification of the geotechnical parameter uncertainty, tunnel risk consequences, and investigation accessibility. An index that integrates the geotechnical parameter uncertainty and tunnel site conditions is defined to identify priority locations of additional investigations based on a tunnel risk. The methodology is applied to a soil tunnel project in North America where additional boreholes are located, considering the risk created by uncertainty in tool wear rates. The results are used to derive quantitative estimates of the uncertainty in the location of cutterhead interventions.

1.1.4 Evaluating the accuracy of geostatistical models

Geostatistical models of ground conditions are increasingly applied for risk assessment and decision-making on underground construction and tunneling projects (Grasmick et al. 2018; Boyd et al. 2020; Mahmoudi et al. 2021; Nebbia et al. 2021). However, the accuracy of the developed geostatistical models is universally not reported nor quantified. Unfortunately, no specific guidelines, techniques, or procedures exist that can be applied to quantify geostatistical model accuracy in predicting the ground conditions. The expected growth in the number of tunnel projects and the increased awareness about applying geostatistical techniques to estimate ground conditions needs a discussion on the accuracy of the developed geostatistical models. Applying geostatistical

models for tunnel risk assessment and decision-making raises an important question of the influence of tunnel project geotechnical SI density and geological environment type on the geostatistical model accuracy.

Existing techniques on geostatistical model validation include cross-validation, jack-knife, histogram reproduction, variogram reproduction to evaluate the geostatistical models (Goovaerts 2001; Leuangthong et al. 2004). The applicability of these cross-validation techniques in evaluating geostatistical models of ground conditions for tunnel projects is questionable. These techniques use only a portion of the data that leads to biased and less-reliable estimates. Leaving out a set of boreholes may not necessarily offer insights on model performance in predicting ground conditions, especially the geologic transitions, one of the significant risks in geotechnical and tunnel applications. In addition to the limitations on the techniques, one of the key knowledge gaps in the existing research is the lack of a diagnostic tool to quantify the accuracy of ground-type geostatistical models. Existing methods of using accuracy plots show high inadequacies in assessing the prediction accuracy of ground types with low proportions (Deutsch and Deutsch, 2012). For a quantitative assessment of ground type geostatistical models, there exists a need for a diagnostic tool that captures the presence/absence of all soil types and not skew the accuracy results in favor of high proportion ground types.

This motivated the identification of a suitable diagnostic tool that quantified the geostatistical model accuracy for each ground type, irrespective of the ground type proportions. The influence of investigations and geological environment on geostatistical model accuracy is of great interest to understand the efficacy of geostatistical models in predicting ground conditions.

To address this motivation, a methodology that quantifies geostatistical model accuracy in predicting soil conditions (in the complete tunnel envelope) and soil transitions at a relatively finer resolution is developed. The proposed methodology uses a multi-class confusion matrix to evaluate the model accuracy in predicting each soil type, irrespective of the proportions. The methodology is applied to two soil tunnel projects in North America in different geological settings. The accuracy of the modeled ground conditions is compared from the two tunnel projects for different densities of investigations.

Collectively, the contributions in this report aid the tunneling community in advancing the practice of tunnel risk assessment and informed decision-making on tunnel projects. The developed methodologies aim to show the success and advantages of geostatistical techniques in developing a realistic representation of the ground conditions. Additionally, the results from the methodologies are exclusively tied to tunnel risk assessment for the tunneling community to relate to the challenges encountered in typical tunnel projects.

1.2 Research Objectives

The following research objectives are pursued to address the abovementioned practical problem statements

1. Develop a probabilistic geostatistical modeling-based approach to characterize, quantify, and visualize the uncertainty in stratigraphic transitions in the longitudinal and transverse directions within the tunneling envelope; Validate the results from the probabilistic geostatistical

modeling-based approach using tunnel boring machine (TBM) operation data from a soil tunnel project.
2. Develop a geostatistical modeling approach to quantify the occurrence of karstic features within the tunneling envelope; apply the probabilistic results from geostatistical modeling to quantify the remediation measures for the treatment of karstic features.
3. Develop a tunnel risk-based framework to optimize geotechnical SI that integrates knowledge of spatial variability and uncertainty in ground conditions related to the tunnel risk, the consequences severity from tunnel risks, and actual project site conditions; Employ the proposed methodology on an actual soil tunnel project to evaluate the reduction in uncertainty in tunnel risk occurrence from additional SI.
4. Evaluate the accuracy of geostatistical models in characterizing stratigraphic transitions within tunnel envelope and investigate the effect of sampling density, geological depositional environment, and efficiency of the geostatistical technique on the accuracy of developed models.

1.3 Report organization

This is a manuscript-based report and is divided into eight chapters. Chapter 4 to Chapter 7 include the manuscripts. All but one (Chapter 7) of the main Chapters have been published or are under review with peer-reviewed international journals as of the date of report publication. The main Chapters, as included in this report, are nearly identical to the published or submitted manuscripts. The references cited in each manuscript are presented in a comprehensive list at the end of the report. Besides the current chapter for introduction, the remaining six are organized as follows.

Chapter 2 provides the necessary background for the development of this report. A review of the relevant geostatistical modeling algorithms for continuous (geotechnical parameters) and categorical (geological units) is provided. In addition, the general geostatistical modeling workflow adopted in this report is presented.

Chapter 3 provides a review of the prior work relevant to the research objectives pursued in the report. Relevant research efforts on the quantification of soil transition uncertainty are first presented. Research work on void risk assessment for tunneling applications is reviewed. Previous research on optimization of geotechnical site investigations (SI) is reviewed. Previous research efforts on evaluating the accuracy of geostatistical models are presented.

Chapter 4 presents the probabilistic geostatistical approach to quantify the soil transition location uncertainty. The proposed modeling approach is demonstrated using geotechnical data from Anacostia River Tunnel (ART) project, and the location uncertainty for two soil transitions within the ART tunnel envelope is quantified. The details of the modeling approach and the validation of the results from the probabilistic assessment with field data are presented.

Chapter 5 presents the geostatistics-based methodology to quantify the occurrence frequency, number, and size of karstic voids for a tunneling project in Malaysia. An application of the probabilistic approach in developing quantitative estimates of void occurrence within the tunnel envelope is presented. The study is applied to generate probabilistic estimates of grout volume required for the treatment of karstic voids.

Chapter 6 introduces an effort to optimize geotechnical SI programs for tunneling projects considering tunnel risk, project site conditions, and budget constraints. The proposed approach quantifies the tunnel risk created by tool wear on the North East Boundary Tunnel (NEBT) project. The reduction in the location uncertainty of cutterhead interventions with additional boreholes at priority locations on the NEBT project is presented.

Chapter 7 introduces a quantitative evaluation of geostatistical model accuracy in predicting soil conditions within the tunnel envelope, emphasizing accuracy in predicting the soil transitions. The influence of geotechnical SI density and geological environment on geostatistical model accuracy is quantified for the ART project and N125 project sections.

Concluding remarks are provided in Chapter 8. The chapter starts with a summary of the contributions and results. The potential and limitations of geostatistics in tunnel applications and recommendations for future research are outlined in Chapter 8.

Additional results are presented in appendices (A-E) to elaborate on additional analyses, different validation approaches, and efficacy of different geostatistical techniques that help explain the methodological details fully described in the individual Chapters. Table 1.1 lists the appendices alongside the Chapters in which they are referenced.

Table 1.1 List of appendices associated with the main Chapters.

Chapter #	Chapter Title	Appendices
4	Quantification of soil transition uncertainty for tunnel projects	A, B, C
5	Probabilistic assessment of void risk and grouting volume for tunneling applications	-
6	Risk-based methodology to optimize geotechnical site investigations for tunnel projects	D, E
7	Evaluation of geostatistical model accuracy in predicting soil type transitions for tunnel projects	-

CHAPTER 2- BACKGROUND AND FUNDAMENTALS

Uncertainty and risk have been the central features of the core fields of geotechnical and geological engineering and the associated field of underground construction and tunneling (Baecher and Christian 2005). This is largely due to the inherent spatial variability of soil and rock properties that is not completely captured from rigorous site investigation programs (Phoon and Kulhawy 1999a). The nature of geotechnical, geological and underground construction engineering fields demands for tools capable of predicting variations and uncertainties in material properties (Hammah and Curran 2006).

Geostatistics and random field theory enable the spatial interpolation of geological-geotechnical data and quantify the associated uncertainty. Cromer (1996) discussed geostatistics as a powerful analytical tool capable of integrating engineering methods with scientific reasoning and professional knowledge to develop conceptual interpretations comparable to direct measurements. Estimating the spatial correlation/variability of geotechnical parameters using geotechnical SI data has increasingly gained interest, particularly for specific tests/parameters including standard penetration test (SPT), CPT, pressuremeter, soil type, and rock mass characterization (Stavropoulou et al. 2010; Zhu and Zhang 2013; Ozturk and Simdi 2014; Huber et al. 2015; Kaewkongkaew et al. 2015; Chen et al. 2017; Huang et al. 2017; Wang et al. 2017; Gangrade et al. 2020; Grasmick and Mooney 2021;). Grasmick (2019), Grasmick et al. (2020b), Grasmick and Mooney (2021) assessed the spatial variability and uncertainty of key geotechnical parameters, such as SPTs, plasticity index (PI), and moisture content, and applied the results from geostatistical assessment towards tunneling risk assessment, decision-making, and optimizing risk mitigation plans for tunnel projects.. Boyd (2019) focused on quantifying the aleatoric geologic variability, a component of the spatial uncertainty, at multiple spatial scales and demonstrated the integration of geotechnical data in geostatistical algorithms to quantify and understand the spatial uncertainty in tunnel projects. In most recent works, Vanarelli (2021) applied geostatistical methods to estimate the grounwater inflows in deep rock tunnels. Sánchez Rodríguez et al. (2020) applied geostatistical techniques to predict rock mass conditions ahead of the tunnel face for three tunnel projects.

2.1 Modeling spatial continuity of geotechnical parameters

There are generally two common approaches for estimating the spatial correlation of geotechnical parameters; one uses an autocorrelation function from random field theory and time series analysis, and the other uses the semivariance function from geostatistics. These functions are related and are based on comprehensive population sampling. Other methods include average local theory and the maximum likelihood method (Caers et al. 2007).

The semivariogram, also called variogram, $\gamma(h)$, measures the average dissimilarity between two variables (Oliver and Webster 2014) —for example, between the values of a parameter (Z) at location u and at a location ($u+h$). The concept of second-order stationarity underpins variogram-based geostatistical analyses. In second-order stationarity, the expectation and variance of $Z(u)$, $E[Z(u)]$ and $Var[Z(u)]$, are constant over the entire study domain, and do not depend on location u. Also, that the covariance between two observations separated by a distance h, only relies on the distance h between the observations and not on the spatial location u in the domain. The assumption of weak second-order stationarity allows calculation of the covariance. Assuming

second-order stationarity, the semi-variance between two data points, γ (*Z(u), Z(u+h)*) depends on a lag vector *h*: γ (*h*). Thus, the experimental variogram (2.1) is computed as

$$\gamma(h) = \frac{1}{2N(h)} \sum_{\alpha=1}^{N(h)} [Z(u) - Z(u+h)]^2 \tag{2.1}$$

In this description, *Z(u)* is the value of the parameter at location *u*, and *N (h)* is the number of data pairs separated by vector *h*.

An advantage of the variogram approach is that it does not require the mean of the random function *Z(u)* to be known, since it is eliminated in the squared difference between two data points in Eq. (2.1). Variograms established from the spatially distributed data are called experimental variograms. The components of the variograms consist of the nugget, sill, and correlation length, also known as range. The nugget represents microscale variability and measurement error. The sill represents the global variability in the direction of vector *h*. The correlation length (range) represents the distance at which the data are no longer spatially correlated. Experimental variograms are modeled with analytical functions, which serve three primary purposes of (a) computation of semi-variance values at any lag vector, (b) filter the noise from imperfect measurements or lack of data, and (c) ensure unique solutions (Lark and Webster 2006; Lark et al. 2006; Karacan et al. 2012; Lark 2012). Modeling variograms along different directions enables capturing the directional and zonal anisotropies. Directional anisotropy accounts for the difference in the variogram range in multiple directions. Due to geological processes, typically the range in the horizontal direction is larger than in the vertical direction. The zonal anisotropy accounts for the difference in the overall variance in multiple directions.

In random field theory, the autocorrelation function is the primary method to model the spatial variability of a geotechnical parameter and estimate the scale of fluctuation (θ) (DeGroot and Baecher 1994; Rackwitz 2000; Phoon et al. 2003; Baecher and Christian 2005; Griffiths and Fenton 2008; Vanmarcke 2010). The autocorrelation function has been widely used for investigating the spatial variability in the context of geotechnical engineering applications (Jaksa 1995, 2007, 2014; Phoon and Kulhawy 1999b; Jaksa and Fenton 2002; Phoon et al. 2004; Nadim et al. 2005; Uzielli et al. 2005).

The autocorrelation function characterizes the variation of the strength of spatial correlation with respect to the separation distance between two spatial locations. Uzielli et al. (2006) discussed that it is not possible to evaluate the real autocorrelation function for a parameter due to limited sample size. A sample autocorrelation function, an approximation of the real auto-correlation function, calculated from the limited available data is given by:

$$\rho_k = \frac{\sum_{i=1}^{N-k}(x_i - \mu_x)(x_{i+h} - \mu_x)}{\sum_{i=1}^{N}(x_i - \mu_x)^2} \tag{2.2}$$

where, ρ_k is the autocorrelation at lag h, μ_x is the mean of the data set, x_i and x_{i+k} are data values at location i and $i+h$, respectively. N is the number of data points, k is the maximum number of lags. Generally, $k = N/4$.

A plot of the autocorrelation coefficient versus the distance classes or lag bins is called the correlogram. The autocorrelation at zero separation distance is equal to 1 and decays to zero with increasing separation distance and can assume negative values. The scale of fluctuation (θ) from a sample autocorrelation function can be evaluated by fitting a number of theoretical models used in the literature (DeGroot and Baecher 1994; Phoon et al. 2003; Uzielli et al. 2006). Some of the theoretical models used in the literature are single exponential, cosine exponential, second-order Markov, and squared exponential (Onyejekwe et al. 2016). Table 2.1 presents an analytical relationship as proposed by Elkateb et al. (2003) between the scale of fluctuation and range from the variogram model. In this description, c_0 is the nugget, c is the sill, h is the lag distance and a is the effective (or practical) range, defined as the distance at which the semivariance value reaches 95% of the sill.

Table 2.1 Relationship between the scale of fluctuation and range of influence from respective semivariogram models (Elkateb et al. 2003).

Model	**Analytical variogram**	**Scale of fluctuation**
Exponential	$\gamma(h) = c_0 + (c - c_0)[1 - e^{(\frac{-3h}{a})}]$	$\theta = 2a_{EXP}/3$
Spherical	$\gamma(h) = c_0 + (c - c_0)[\frac{3h}{2a} - \frac{h^3}{2a^3}]$	$\theta = 0.55a_{SPH}$
Gaussian	$\gamma(h) = c_0 + (c - c_0)[1 - e^{(\frac{-3h^2}{a^2})}]$	$\theta = a_{GAU}$

2.2 Modeling spatial continuity of geological units

In addition to the continuous geotechnical parameters, it is typically desired to model the spatial correlation of categorical data (geologic units, soil/rock type). Two common approaches to model the spatial continuity of categorical data include the indicator variograms and transition probabilities.

In indicator modeling, the domain space characterized with multiple categorical units, presence of category k can be shown by a binary variable called indicator as in Eq. (2.3) for any point u in the domain space.

$$I_k(u) = \begin{cases} 1, & if\ u\ belongs\ to\ k \\ 0, & otherwise \end{cases} \quad (2.3)$$

The expected value (E) of $I_k(u)$ presents the probability (p) of finding category k at point u is presented in Eq. (2.4).

$$p_k(x) = E\{I_k(x)\} \tag{2.4}$$

For indicator variogram modeling, the indicators $I_k(u)$ replace *Z(u)* and *Z(u+h)* in semivariogram Eq. (2.1). The indicator variograms convey geometrical information about the categorical unit layout in the domain space and can be used to validate the consistency of the interpreted geological model (Maleki et al. 2017). For a categorical unit, the height of the indicator variogram (where the variograms plateau to sill) reflects the proportion of the unit.

A brief description of the transition probability approach to model the spatial continuity is presented in Section 2.3.1.

2.3 Modeling spatial variability and uncertainty

Most of the estimation methods, including kriging, involve a smoothing effect in simulating spatial ground conditions, in which the small values are usually overestimated and large values are underestimated, thus reducing the heterogeneity in conditions within the estimations. The models developed using kriging techniques represent the expected mean of geotechnical property with extreme values underestimated or overestimated (Deutsch and Journel 1992; Yamamoto 2005; Pyrcz and Deutsch 2014). Because of the smoothing effect, the kriging estimates do not reproduce the histogram and the spatial variability from the variogram model. Consequently, the results from kriging are insufficient for assessing the uncertainty and the effects of extreme values. However, for geotechnical engineering, and in particular for tunneling applications, high-quality knowledge of the ground conditions governs the project procurement, progress, and success. Therefore, as engineers, we are interested in ground models that are geologically realistic, incorporate small-scale variability, and can reproduce the high and low values from the available data. To overcome these challenges, stochastic sequential simulation techniques discussed in detail by Goovaerts (1998) and Deutsch and Journel (1992) are adopted herein. It is to be noted that inference of local statistical parameters (mean and variance) of cumulative distribution functions (CDFs) from estimation methods is the basis for stochastic simulation techniques and for the assessment of spatial uncertainty.

Stochastic simulation techniques attempt to reproduce the heterogeneity, mitigate the smoothing effect, and quantify the uncertainty of the property. A stochastic process is a collection of random variables and can have many outcomes, and each outcome is termed as a realization. The set of realizations differ from one another in terms of properties of modeling techniques but are considered equiprobable under the assumption of reproduction of prior probability distributions and spatial continuity model (from variograms). For second-order stationarity, a stochastic process generates realizations with an identical mean, variance, and covariance function (Ma 2019). It is important to note that all realizations from a stochastic modeling algorithm, for a given set of inputs, are only mathematically equiprobable but not necessarily equiprobable physically (Ma 2019).

Several methods and algorithms have been discussed to simulate the stochastic process – tessellation, turning bands, spectral, and sequential (Emery and Lantuéjoul 2014). Since honoring the geotechnical site investigation and laboratory test data is paramount for geotechnical and tunneling applications, stochastic processes capable of honoring the data are utilized in this report.

2.3.1 Transition probability-based Markov Chain approach (TPROGS)

A transition probability-based Markov Chain approach were adopted in the 1990s to describe heterogeneity in ground conditions in terms of geologic units (or so-called categorical data). From Carle and Fogg (1997), Carle (1999), Sartore (2013), and Carle and Fogg (2020), the transition probability from a unit *k* to a unit *j* is defined in Eq. (2.5)

$$t_{ij}\,(h) = Probability\ that\ k\ occurs\ at\ (u+h)\ given\ that\ j\ occurs\ at\ (u) \quad (2.5)$$

where *u* is the point in the simulation domain, and *h* is a lag vector.

The transition probability between units is conveyed from indicator cross-variograms. The transition probability between units *j* and *k* is conveyed in Eq. (2.6)

$$2\gamma_{jk}(h) = p_j[2t_{jk}(0) - t_{jk}(h) - t_{jk}(-h)] \quad (2.6)$$

where $p_j = E[I_j(u)]$ is the volumetric proportion of unit *j*, assuming stationarity, $I_j(u)$ is the indicator variable of unit *j*, i.e. I_j = 1 if point *u* is inside unit *j*, and zero otherwise.

The abovementioned definition of transition probability is a Markovian approach: the probability of unit *k* occurring at a location *u+h* is only dependent on location *u*. The continuous-lag Markov chain model defines the function that relates to the transition probability $t_{jk}(h)$ to lag *h*. the function is assumed exponential with distance, with the coefficients of the exponential denote the conditional rates of change from unit *j* to *k* per unit of lag distance *h*. The transition probabilities are calculated along the borehole, as the shortest separation lag is well informed. The resulting transition matrices are helpful for the definition of geological unit contacts. The transition matrices are asymmetrical and are calculated downward and upwards along the drilling path, as illustrated in Figure 2.1.

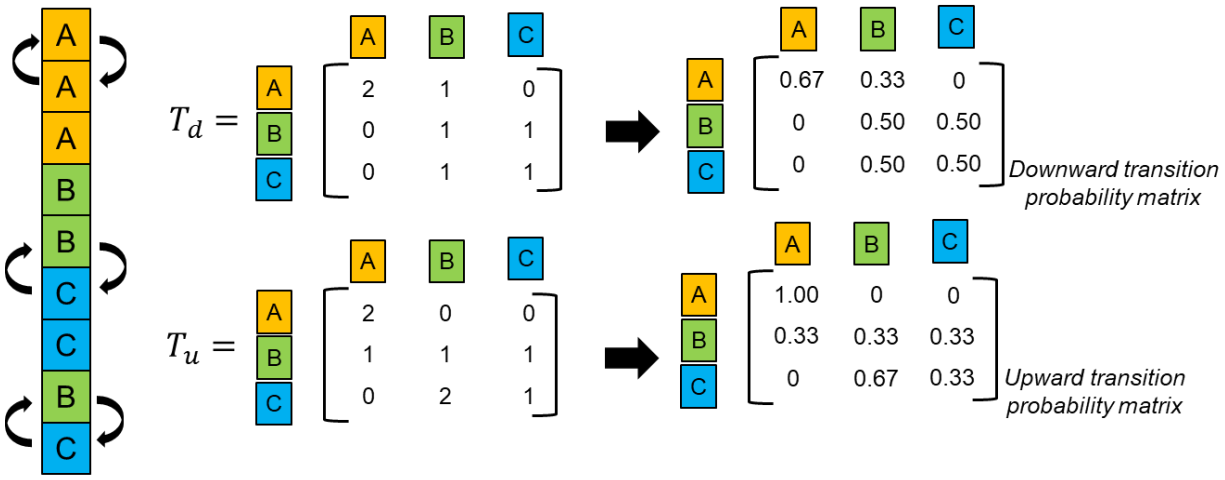

Figure 2.1 Illustration of the upward and downward transition probability calculation for a single string of categorical data along a borehole.

Carle (1999) discussed that the coefficients of the exponential model could be directly related to the interpretable properties of the geologic domain, such as proportions of units, mean length, and juxtaposition tendencies. The first step in the Markov-based approach is the calibration of these parameters on the data, similar to the calibration of variograms in traditional geostatistics-based modeling. Conditional simulations of ground conditions are generated similar to any stochastic modeling approach. de Marsily et al. (2005) argued that it is easier to calibrate the matrix of transition probabilities (and easier to fit models to the data) than in an indicator variogram-based approach. Additional discussions on the Markov-based approach and its comparison with an indicator variable-based approach can be found in Chilès et al. (2004), Chiles and Delfiner (2009), and Lee et al. (2007).

2.3.2 Pluri-Gaussian simulation technique

The pluri-Gaussian simulation (PGSIM) technique is a complete approach as geological constraints can be applied to the simulated domains. The technique overcomes most categorical simulation method limitations of not capturing the spatial changes in geological unit proportions, contact relationships, and geological realism within realizations (Madani and Emery 2015; Madani et al. 2019). Due to the advantages of better characterizing spatial transitions and contact relationships between geological units, PGSIM is used to model geological conditions for projects in this report.

With a stochastic modeling framework, the simulations from PGSIM attempt to preserve and reproduce the heterogeneity of parameters of interest (Pyrcz and Deutsch 2014; Ma 2019). Like any other stochastic modeling technique, multiple realizations of geological conditions are generated with PGSIM, with each realization capturing the degree of heterogeneity and spatial variability of the modeled units. Among a number of stochastic simulation techniques for modeling geological data, PGSIM offers a flexible framework, as it aims to reproduce (1) the contact relationships between units, (2) the unit proportions, (3) spatial correlation structure, and (4) available conditioning data. PGSIM has found applications in modeling petroleum reservoirs and

environmental science problems (Emery 2007; Armstrong et al. 2011). Madani et al. (2019) presented tools to validate the reproduction of stratigraphy in individual realizations generated from PGSIM. Madani and Emery (2015) presented a split-sample validation of the individual realizations using calibration plots, thus showing the deviation of simulated proportion of geologic units from actual proportions.

The PGSIM technique requires the definition of (a) geological units for simulations, (b) the simulation grid, (c) the relative proportions of units and the transition probability matrix, (d) the spatial variability characterization, and (e) the number of simulations. Figure 2.2 schematically illustrates the following key steps in generating realizations from PGSIM.

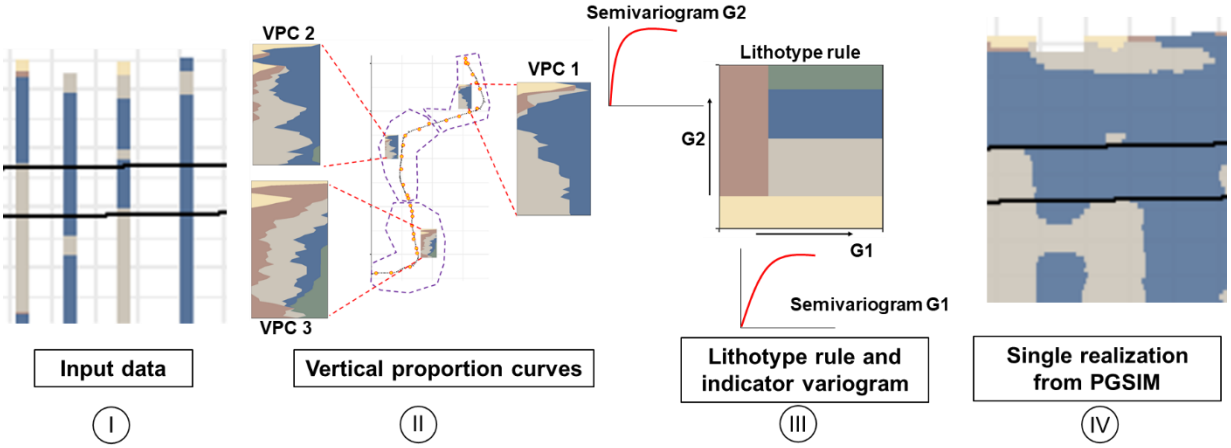

Figure 2.2 Schematic flow chart showing key steps involved in the PGSIM technique.

Step I- Data input: Geological units, as interpreted from the site investigation boreholes, is encoded as an indicator variable that takes a value of 1 if a specific category is present and 0 otherwise.

Step II- Production of vertical proportion curves (VPC): VPCs is a simple tool for quantifying the proportions of geological units present as a function of elevation or depth (Huber et al. 2015). The VPCs are computed along the lines vertical to a chosen reference level. The tunnel alignment is subdivided into multiple sections, and within each section, multiple VPCs are generated to capture the lateral variation in the unit's proportions for geostatistical modeling.

Step III- Definition of lithotype rule and variogram fitting: The *lithotype* rule derived from the available boreholes controls the permissible and forbidden contacts between pairs of units and reproduces the units' ordering. In this technique, the correlation of the geological units is quantified using indicator variograms generated for the vertical and horizontal directions. Variograms generated in multiple directions capture the anisotropy within the available data. The variogram range, the distance beyond which no correlation exists between the data in each direction and sill, is the maximum value of the variogram and defines it. The range of a stratigraphic unit indicator variogram is a function of heterogeneity and stratigraphic unit occurrence frequency. Dubrule (2017) provided an overview of indicator variograms for geostatistical modeling in three dimensions. Maleki et al. (2017) discussed that indicator variograms convey valuable information on the proportions of geological units, spatial correlation structure, and contact relationships

between the units. Indicator variograms can also be used to validate the consistency of the interpreted geostatistical model (Madani et al. 2019).

Step IV- Conditioning to geotechnical investigation data: Following the indicator variogram model, the geological units are transformed into Gaussian values in appropriate intervals using the Gibbs sampler algorithm. A search neighborhood is defined, and the available Gaussian values within the neighborhood, called conditioning data, are used to simulate Gaussian values within the neighborhood. Gaussian fields are iteratively co-simulated at points within the modeling domain that contain sampled borehole data. Within each iteration, a random point among the borehole samples is selected, and the Gaussian fields are updated based on the values taken by the Gaussian fields at other sampled locations. Gibbs sampler, an optimization algorithm, is used to perform the Gaussian fields' iteration and modeling. Next, the Gaussian fields are simulated at the unsampled locations using the turning bands algorithm. Since the Gaussian fields are independent, each field is conditioned to its previously simulated values. The regionalized VPCs and the *lithotype* rule are applied to the simulated Gaussian fields to convert Gaussian variables to the actual unit. The process is repeated multiple types leading to the generation of multiple realizations of the geological conditions. The realizations generated from PGSIM are constrained to the available data, therefore exhibiting realistic representations of geologic configurations.

Figure 2.3 shows the application of PGSIM from a rock deposit modeling study by Madani and Emery (2017). The study demonstrates that, even with 125 conditioning data points over an area of 1.87 km^2, it is possible to simulate rock-type domains in agreement with the geologist's lithological interpretation using PGSIM. The stochastic modeling technique allows for a realistic assessment of geological uncertainty and quantifies the gains in mineral resource evaluations.

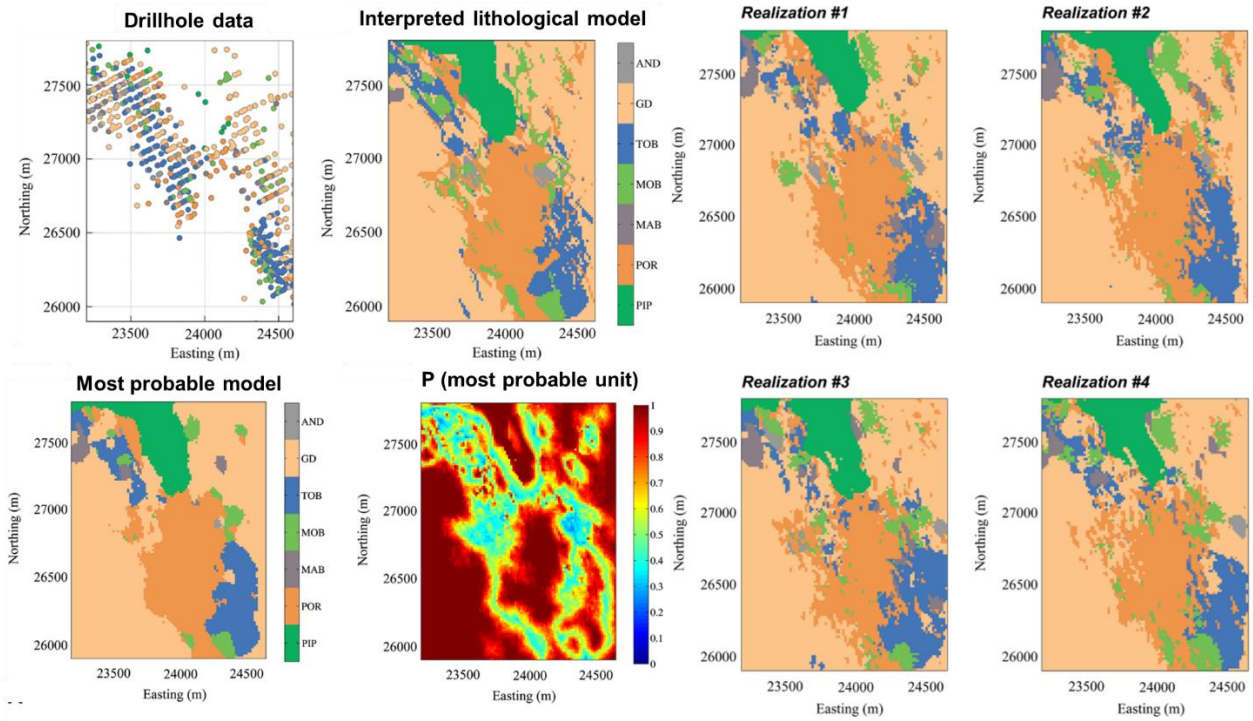

Figure 2.3 Plan view showing the drill hole data, interpreted lithological model, multiple PGSIM realizations, most probable model from PGSIM, and occurrence probability of the most probable unit (Madani and Emery 2017).

2.3.3 Sequential Gaussian simulation technique

Sequential Gaussian simulation (SGSIM) technique is a stochastic simulation algorithm that takes advantage of properties of Gaussian random functions (Szatmári and Pásztor 2019). Within this approach, the property being modeled needs to have a Gaussian distribution; otherwise, a normal score transforms that changes the data into a standardized normal distribution. Within this transformation, the highly frequent values are stretched into more bins, and the less frequent data are squeezed into fewer bins such that the original distribution is transformed into a normal distribution. The conditional mean and variance of the Gaussian distributed variable is fully characterized at any location within the simulation domain using estimation methods, such as kriging. The simulated results, or so-called realizations, render spatial patterns consistent with the input data and spatial structure. Figure 2.4 schematically illustrates a few steps in generating realizations from SGSIM.

SGSIM can be summarized in the following sequence of steps:

1. Transform the original Z data to a standard normal distribution. Go to a random location (random walk) and perform kriging to obtain the kriged estimate and the corresponding kriging variance.

2. Draw a random residual $R(u)$, which follows a normal distribution with a mean of 0.0 and a variance equal to the kriging variance $\sigma_E^2(u)$. Sum the kriged estimate and the residual to get the simulated value is presented in Eq. (2.7).

$$Z_s(u) = Z^*(u) + R(u) \tag{2.7}$$

3. Add the simulated value to the set of conditioning data. Previously simulated values are considered as conditioning data so that the covariance between all simulated values is reproduced. This is a key idea of sequential simulation.
4. All simulated locations are visiting in random order. Back transform the data once the model is populated.
5. Repeat with different random number seeds (different random paths and residuals for each simulated node) to create a desired number of realizations.

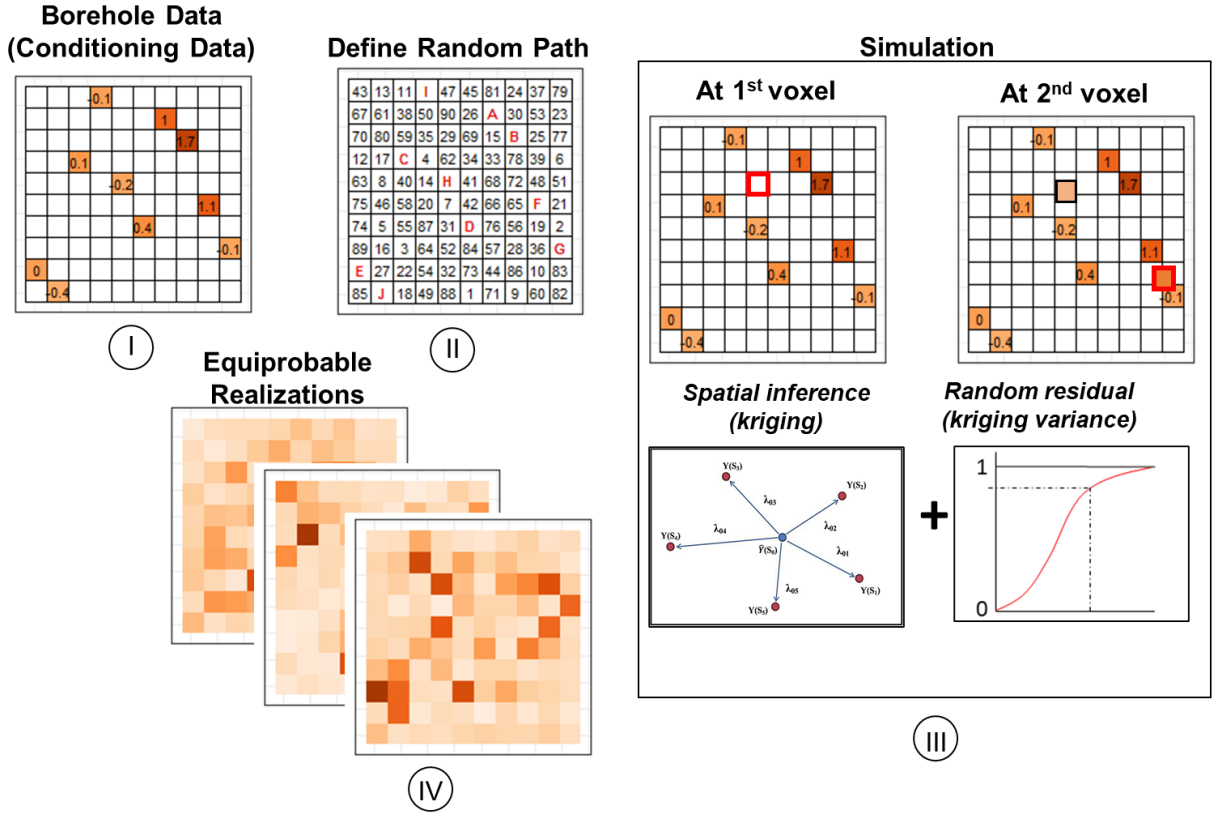

Figure 2.4 Schematic flow chart showing key steps involved in SGSIM technique.

Figure 2.5 illustrates seven realizations from SGSIM of the depth of the bedrock surface (Grasmick 2019). The borehole records from geotechnical SI were used for the variogram modeling and conditioning data in the simulation. The spatial correlation of each realization matches the input

variogram; high and low values are grouped together. The set of realizations can be used to assess the spatial uncertainty by examining the variance of all realizations at each simulation node.

Several researchers have applied SGSIM in geotechnical engineering applications such as fault detection (Esfahani and Asghari 2013); underground construction and tunneling (Wang 2018; Gao et al. 2019; Hu and Wang 2019; Grasmick and Mooney 2020; Grasmick et al. 2020); modeling rock mass heterogeneity (Mayer et al. 2014); deep excavations (Gholampour and Johari 2019; Sainea-Vargas and Torres-Suárez 2020); seismic risk assessment (Johari et al. 2020; Salsabili et al. 2020); and slope stability analysis (Kring and Chatterjee 2020).

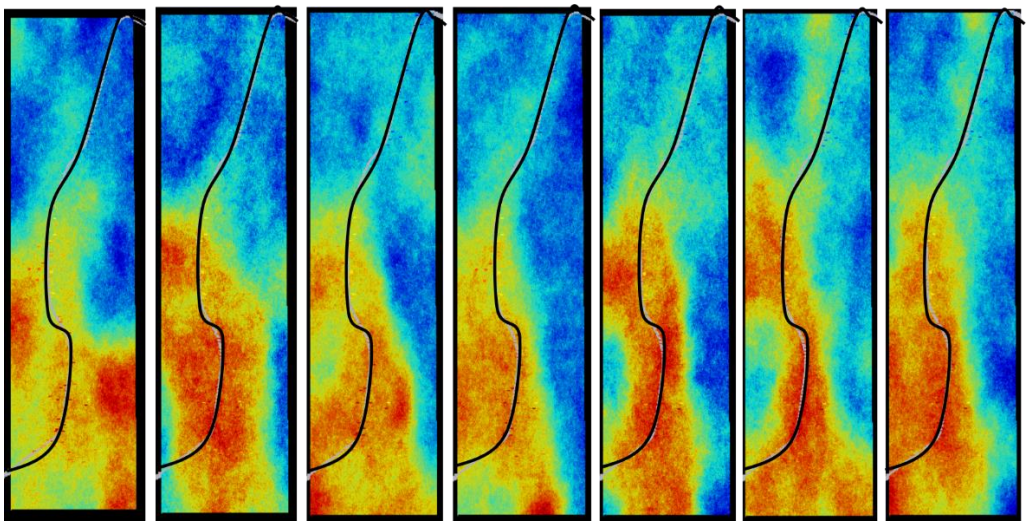

Figure 2.5 SGSIM realizations of the depth of bedrock surface with hotter colors indicating a relatively shallow depth of the bedrock (Grasmick 2019).

2.4 Quantification of uncertainty in geological and geotechnical data

For geological models (typically, soil or rock types), the concept of information entropy, introduced by (Shannon 1948), has been applied previously as a measure of uncertainty (dell'Arciprete et al. 2012; Bianchi et al. 2015). For a system with a discrete number of probable outcomes, normalized information entropy is a relative measure of 'missing information'. The information entropy is equal to 0 when only one outcome is possible, a maximum of 1.0 when all outcomes are equally likely, and any value in between. Wellmann and Regenauer-Lieb (2012) proposed to use information entropy as an objective measure to analyze and communicate uncertainty in geological models. The information entropy (H) for probability of outcome k (p_k) out of N possible outcomes is presented in Eq. (2.8).

$$H = -\sum_{k=1}^{N} p_k \cdot log p_k \tag{2.8}$$

Figure 2.6 illustrates the calculation of information entropy using the occurrence probabilities of individual units from geostatistical modeling. In this report, the individual realizations of geologic units (or so-called categorical data) are post-processed to identify the category with the maximum number of occurrences at each location from all realizations. Alternatively, the occurrence probabilities of the units are utilized to calculate the uncertainty associated with the occurrence of geologic units.

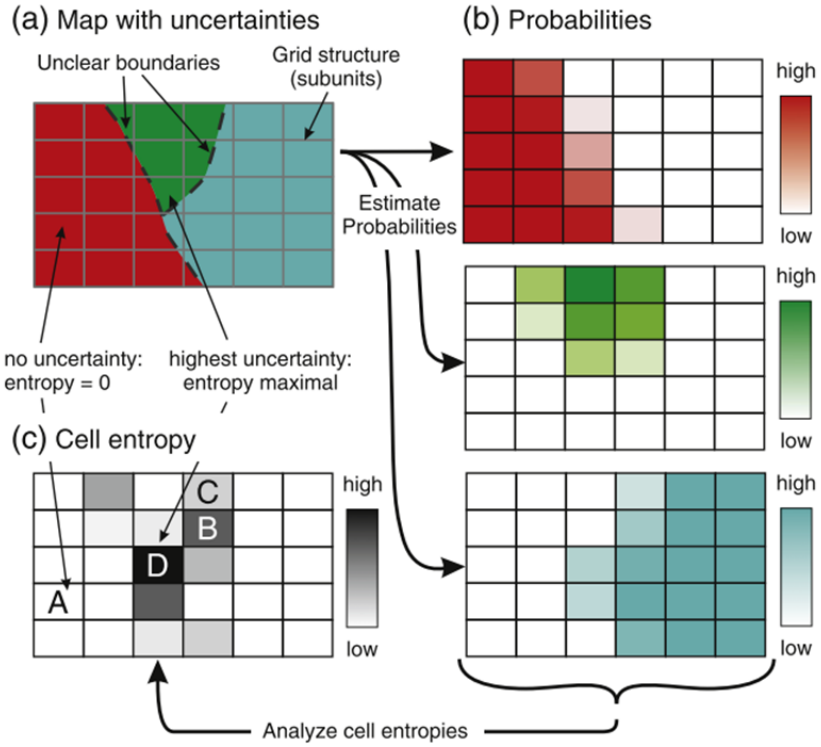

Figure 2.6 Application of information entropy to quantify uncertainties. Occurrence probabilities of units (as quantified from geostatistical modeling) are utilized to calculate the entropy. Higher entropy exists where more outcomes are equally likely (Wellmann and Regenauer-Lieb 2012).

For continuous variables (geotechnical parameters such as PI, SPT, soil abrasivity index (SAI)) uncertainty in simulated values can be expressed as absolute and relative uncertainty (Pyrcz and Deutsch 2014). Standard deviation (σ) of the parameter from multiple geostatistical realizations is an example of the absolute uncertainty. Relative uncertainty is the absolute uncertainty normalized by the mean (e.g., coefficient of variation, COV), which accounts for heteroscedasticity when the uncertainty scales with the predicted value (Pyrcz and Deutsch 2014). Empirical cumulative distribution function (ECDFs) and confidence intervals (CI) can be used as tools to quantify uncertainty in the probabilistic assessment framework. In the current tunnel practice, the magnitude of the CI bounds is seldom calculated, and the implication of this uncertainty is generally under-appreciated. CI is a measure of the level of confidence that the parameter of interest lies within a specific interval range. A higher probability associated with the CI means

there is a higher degree of certainty of parameter value falling within the interval range. Thus, CI is a robust measurement of uncertainty. In this report, individual realizations of geotechnical parameters are utilized to develop the CI bands of geotechnical parameter uncertainty. Figure 2.7 presents an illustration of geotechnical parameter uncertainty expressed in terms of CI.

ECDFs is a plot of the data specifically designed to display the percentiles by plotting percentages versus data values. The vertical axis represents the percentages from 0 to 100%, while the horizontal axis presents the data values—ECDFs aid in capturing the true probabilistic distribution of a parameter, as illustrated in Figure 2.8. The ECDFs provide insights into (a) percentile value for a given percentage and (b) the percentage corresponding to a particular data value.

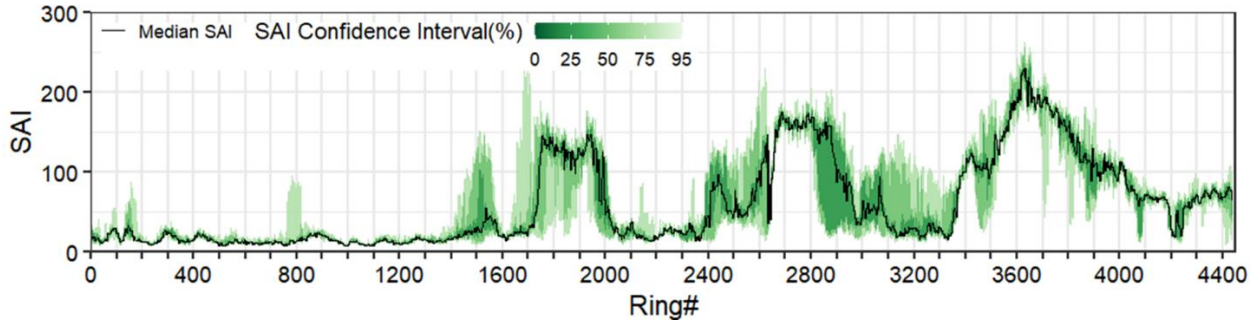

Figure 2.7 Example of geotechnical parameter uncertainty conveyed in a spatial context in terms of confidence intervals (CI).

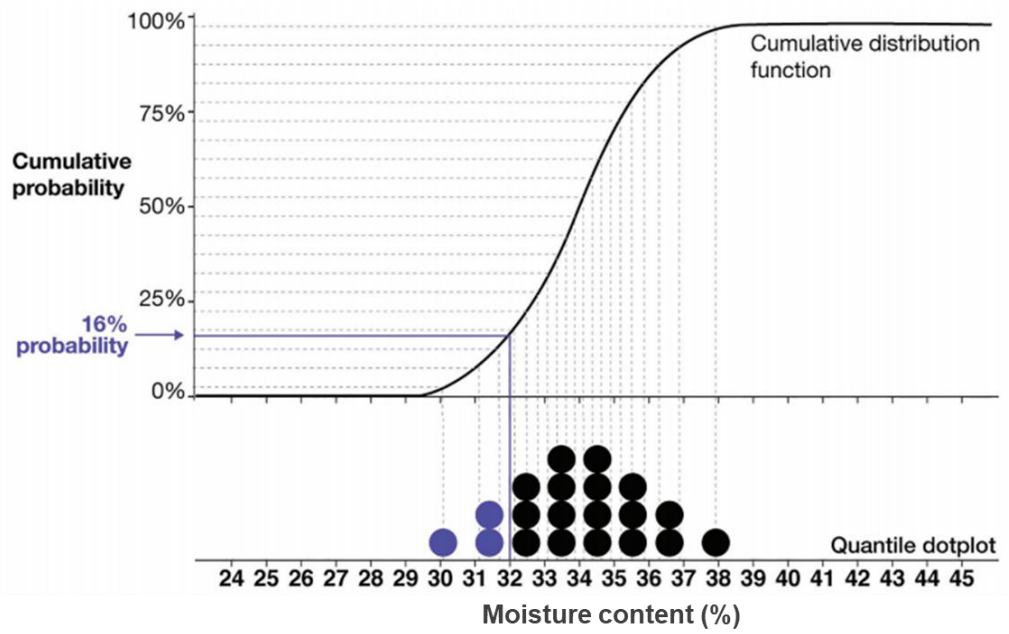

Figure 2.8 An illustration of empirical cumulative distribution function (ECDF) curve for moisture content (%) of soils. Each dot represents a 5 % probability (after Padilla et al. 2020).

2.5 Geostatistical modeling workflow for tunnel projects

For the geostatistical modeling of geotechnical/geological parameters, a 3D simulation grid is first developed along with the longitudinal and transverse directions of the tunnel alignment. In tunneling applications, geotechnical SI boreholes are drilled at an offset from the tunnel alignment, owing to accessibility constraints on the tunnel project site. Developing a 3D simulation grid allows honoring the geotechnical SI data at an offset from tunnel alignment. The practice is undertaken to overcome the limitations presented by a 2D ground model. Although the time required to generate a 2D geostatistical modeling will be significantly low than in the 3D model, developing a 2D model does not allow capturing the heterogeneities in the transverse directions. Phoon et al. (2021) argued that a 2D section could not be spatially variable as the out-of-plane dimension (transverse direction) adheres to the plain strain assumption. The results presented in the report are 2D only for presentation purposes, although the modeling and the post-processing of the geostatistical realizations are applied on the 3D grid. Figure 2.9 presents the typical steps of the 3D geostatistical modeling approach adopted in the report.

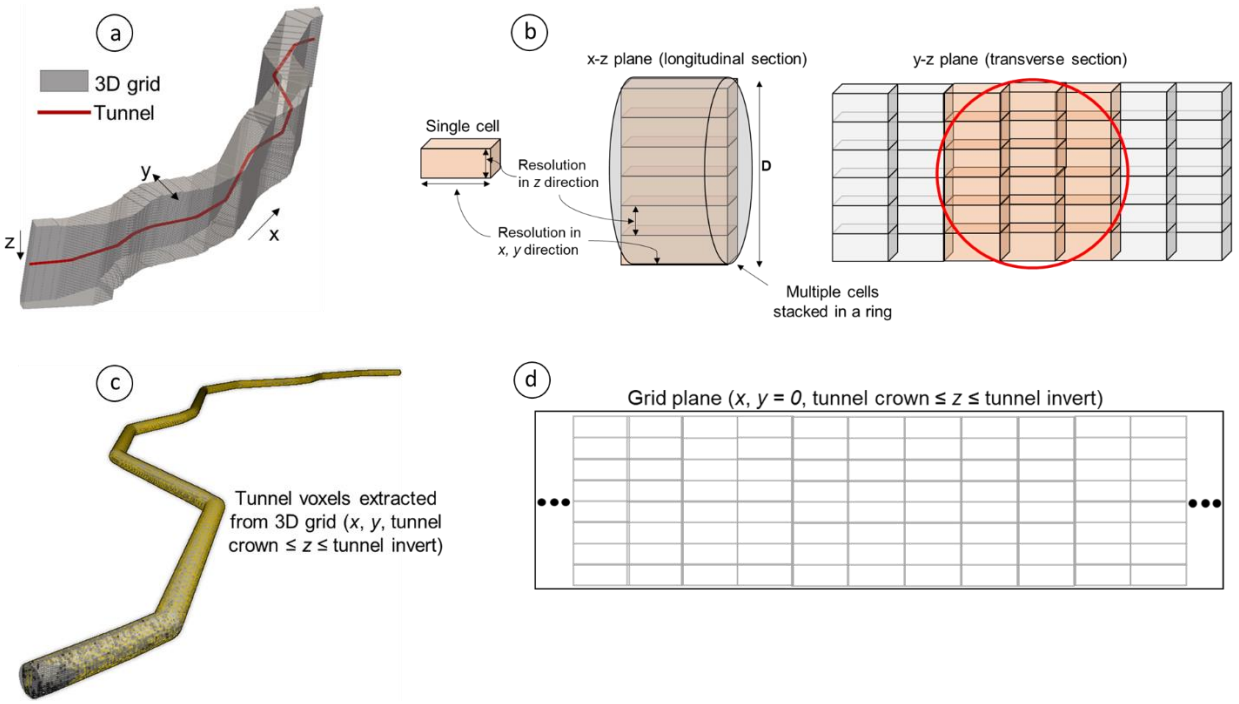

Figure 2.9 (a), (b) Grid structure for geostatistical modeling. (c) Extracted grid cells within the 3D tunnel envelope and (d) 2D plane presenting grid cells along tunnel alignment centerline.

Critical steps in the modeling are listed below

Step (a): A 3D simulation grid for geostatistical modeling is developed along the *x* (longitudinal), *y* (transverse), and *z* (vertical) directions along the tunnel alignment. The extents of the grid in each direction are decided based on the extent of the tunnel alignment and the spatial coordinates of the geotechnical SI. In cases where the geotechnical SI extent is beyond the longitudinal length of the tunnel alignment, the longitudinal extent of the 3D simulation grid is trimmed up to tunnel length. The transverse extent of the grid is decided based on the spatial extent of geotechnical SI (typically 50-80 m in tunnel projects). The vertical extent of the 3D simulation grid is based on the maximum depth of geotechnical SI that is at least two tunnel diameters below the tunnel invert.

Step (b): This step includes a decision on the resolution of the 3D simulation grid in the *x*, *y*, and *z* directions. The resolution of the 3D grid is decided based on the tunnel length, spacing between the geotechnical SI, and computational capacity. For the tunnel applications presented in the report, a resolution of 5 m in the *x* and *y* directions and 1 m in the *z*-direction is adopted. However, for two tunnel projects, it was computationally possible to develop a 3D grid of resolution 1.8 m x 1.8 m x 1 m (note that 1.8 m is based on the ring length from the projects).

Step (c): For the objectives pursued in the report, it was of interest to extract the geostatistical simulations within the tunnel envelope. This decision was based on the type of tunnel risk considered in the report. For example, for the risk related to tool wear and critical subsurface features such as soil transitions and karstic voids, the knowledge of the tunnel excavation environment is relatively more critical than the knowledge of subsurface conditions above the tunnel up to the ground surface. This step is not applicable when the consideration of overburden

stratigraphic profile is critical such as in the risk related to tunneling-induced ground deformation and groundwater inflow.

Step (d): For visualization of geotechnical conditions within the tunnel envelope, the 3D simulation grid is cut to develop a 2D profile capturing the geotechnical conditions within the tunnel envelope (tunnel crown $\leq z \leq$ tunnel invert) for complete tunnel length in the longitudinal direction (x) and tunnel centerline ($y = 0$).

Figure 2.10 presents the typical modeling workflow adopted in the report. Geotechnical SI data is utilized to develop a soil type model. This is a critical step as the soil type model is the basis for geostatistical modeling of geotechnical parameters using the *local* simulation approach as described by Grasmick et al. (2020). Geotechnical parameters such as SPTs, PI, water content are modeled for each soil type, and relevant geostatistical models are generated. The geostatistical models of soil type (geological conditions) and the geotechnical parameters are utilized to develop maps/profiles of tunnel risk related to geotechnical parameters. For example, the risk created by tool wear involves forced cutterhead interventions, significant impact on project schedule, cost, and impact to the community – is related to the SAI. The uncertainty in tool wear rate is quantified from the uncertainty in soil types and SAI conditions within the tunnel envelope. These risk maps serve as a valuable communication tool for the owners, engineers, contractors, and involved stakeholders.

The literature review undertaken and the other relevant information presented in this chapter provides the background required for the further reading of this report. Additional literature exists that is not covered here; however, the provided review synthesizes the most relevant research available that is important to this research subject.

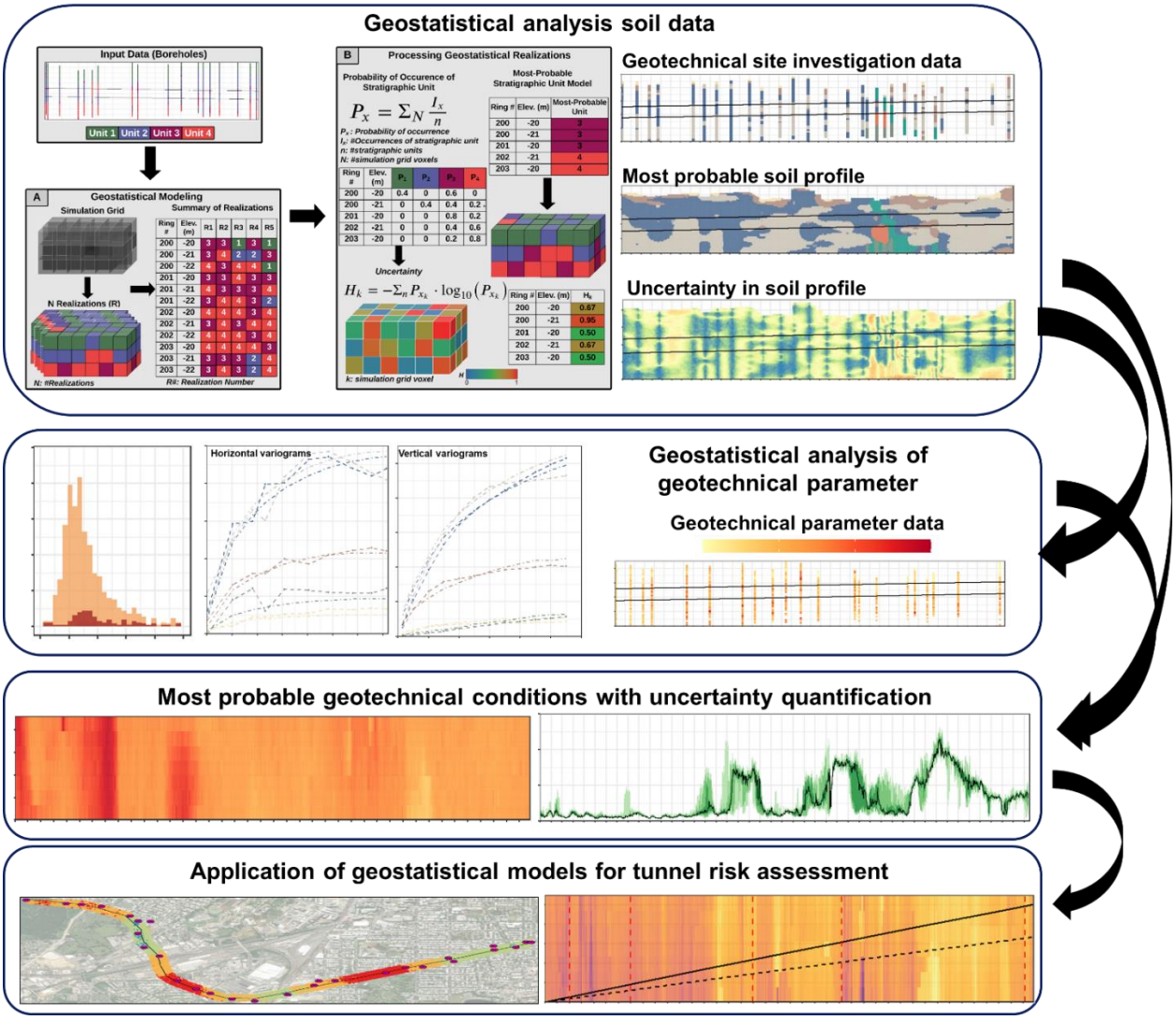

Figure 2.10. Workflow to generate geostatistical models for ground conditions (soil types + geotechnical parameter) utilizing geotechnical SI and laboratory test data.

CHAPTER 3- REVIEW OF PRIOR WORK

This chapter provides a review of the prior work relevant to the research objectives pursued in the report. Relevant research efforts on the quantification of soil transition uncertainty are first presented. Research work on void risk assessment for tunneling applications is reviewed. Previous research on optimization of geotechnical site investigations (SI) is reviewed. Previous research efforts on evaluating the accuracy of geostatistical models are presented.

3.1 Quantifying uncertainty in soil transitions

Over the years, several researchers have attempted to identify the boundaries between homogenous soil layers. Since cone penetration tests (CPT) produce nearly continuous records of the vertical soil profile, CPTs have attracted significant attention for stratigraphic profiling. Phoon et al. (2003) developed a statistical-based soil boundary identification procedure using Bartlett test statistic on a piezocone sounding record. Within the procedure, the coefficient of variation in cone tip resistance between sand and clay is characterized using the auto-correlation function to identify the soil layer boundary. In another attempt using CPTs, Uzielli et al. (2008) applied a moving-window statistical procedure to identify layer boundary on a site in the Venice lagoon. Ching et al. (2015) proposed a stratigraphic profiling approach based on the soil behavior type index interpreted from the CPTs. The approach involved using the wavelet transform modulus maxima (WTMM) method to identify the change points of soil behavior type index. Wang et al. (2013) developed a rigorous approach from applying Bayesian methods on CPTs to determine the number of soil layers and locations of boundaries based on the largest probability. However, these studies on single CPT identify only the vertical contact points between the stratigraphic units and do not quantify the uncertainty in layer boundary. In another attempt, Wang et al. (2014) developed a Bayesian approach to facilitate the identification of soil strata in the London Clay Formation (LCF) using water content data. The results revealed that a measurement interval of 0.1 to 0.3 m is required to identify the soil strata in LCF with sufficient accuracy. However, both sophisticated methods require advanced knowledge of Bayesian decision analysis, are computationally intensive, and focus only on identifying the layer boundary in the vertical direction.

Several approaches based on interpolation methods such as geostatistics and the Markov-Chain have been developed to interpret the stratigraphic configuration at unsampled locations (Blanchin and Chilès 1993; Chilès et al. 2004; Wellmann et al. 2010). The stratigraphic configuration is defined as the spatial interpolation of the subsurface strata using the available borehole data. These approaches quantify the uncertainty in stratigraphic configurations in terms information entropy (see Chapter 2, section 2.4); however, do not quantify the stratigraphic transition location uncertainty, which is the uncertainty in the boundary location between two stratigraphic units heterogeneous from a compositional or mechanical point of view.

Wang et al. (2016) presented a stochastic geological modeling approach based on Markov random field (MRF) with specific energy functions to quantify the uncertainties related to the inference of stratigraphic configurations, also known as stratigraphic uncertainty. The results of the study involved quantifying stratigraphic uncertainty by quantifying the information entropy from the generated realizations. The research utilized the stratigraphic configurations into finite element analysis (FEA) program to study the effect of stratigraphic uncertainty on the structural behavior of the tunnel. However, the study only highlights the uncertainty in stratigraphic configurations

without highlighting the uncertainty in stratigraphic transition locations. Further, the approach lacks a validation of the developed stochastic modeling approach in quantifying the stratigraphic configuration uncertainty. It is evident that the uncertainty in stratigraphic configurations does not provide insights into the uncertainty in locations stratigraphic transitions. Figure 3.1 presents a generated realization and quantification of uncertainty in stratigraphic configuration. As illustrated in Figure 3.1, the uncertainty in the most-likely stratigraphic configuration only quantifies the uncertainty in the occurrence of geologic units. The approach does not quantify the uncertainty in the locations of longitudinal and vertical transitions between different geologic units.

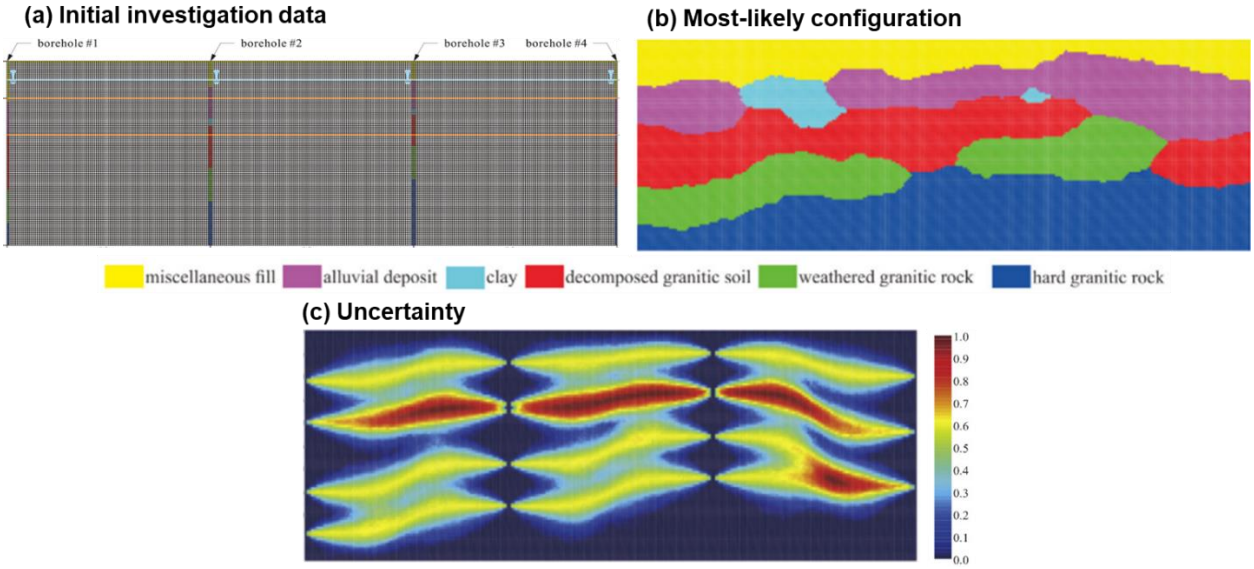

Figure 3.1 Quantification of uncertainty in stratigraphic configuration from four boreholes using MRF approach (Wang et al. 2016).

Xiao et al. (2017) developed a three-level probabilistic framework that considered stratigraphic uncertainty, a combination of boundary-based and couple Markov chain models to characterize soil layer stratification for a construction site in Hong Kong. The study revealed the advantage of accounting for the spatial trends and engineering judgment; however, the study is limited to modeling stratigraphy using only the transition probabilities between stratigraphic units.

For a probabilistic identification of soil stratification at the unsampled locations, Li et al. (2016a) proposed a kriging-based technique to characterize the soil stratification using 26 CPT profiles. The study estimated the soil types at the unsampled locations using the CPT parameter (i.e., cone tip resistance, sleeve friction, and pore pressure) estimates and soil classification method proposed by Robertson (2010). Soil types for respective CPT parameter values within the 95 % confidence interval of the estimated CPT parameters were estimated. The results were validated with the profiles interpreted from the existing CPTs. The results from the study showed satisfactory agreement between the predicted stratification and the CPT tests in the horizontal plane and vertical unsampled locations. The use of the kriging technique to interpolate the CPT parameters, assumption of the isotropic spatial structure (no anisotropy), and correlation length to model the CPT parameters are the study's major limitations.

CPT tests were also utilized by Wang et al. (2019) to develop a method for providing a 2D continuous soil classification and stratification profile. However, the methodology only provided a deterministic 2D cross-section discounting the uncertainties from 2D interpolation with a limited number of CPT tests and the uncertainty associated with the soil behavior type from CPT data. To overcome this limitation, Hu and Wang (2020) proposed a 2D probabilistic soil classification and stratification method using random field theory and Monte Carlo simulation (MCS). The study results indicated that the uncertainty associated with stratification is reasonably quantified, accounting for the underlying soil classification and stratification (see Figure 3.2). However, the study is limited to using CPT data with spatial trends, and the use of the methodology to CPT data without spatial trends is questionable.

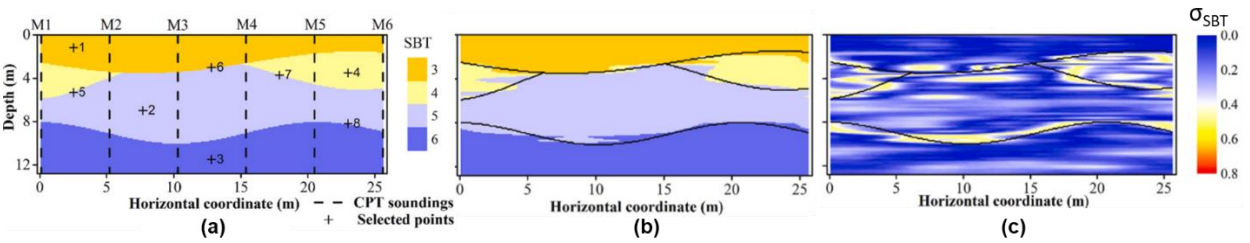

Figure 3.2 (a) Simulated geological model of soil stratification and zonation with CPT soundings; (b) the most likely SBT cross-section; (c) standard deviation of 500 SBT cross-sections (Hu and Wang 2020).

Gong et al. (2020) proposed a modified random field-based approach for characterizing stratigraphic configurations and the associated uncertainty in 2D. The study used the autocorrelation function to model the most likely (most probable) stratigraphic configurations. In another attempt to improve the uncertainty quantification, Zhao et al. (2021) presented a random field-based modeling method with the advantages of accounting for spatial correlation structure of the strata over the approach presented by Gong et al. (2020). The study focused on improving the stratigraphic realizations by removing the local anomalies from conditional random field modeling using the Markov Chain Monte Carlo (MCMC)-based updating. The study results showed a quantification of uncertainty associated with the most likely stratigraphic configuration (see Figure 3.3); however, the effectiveness of the study in characterizing stratigraphic layer uncertainty is not validated.

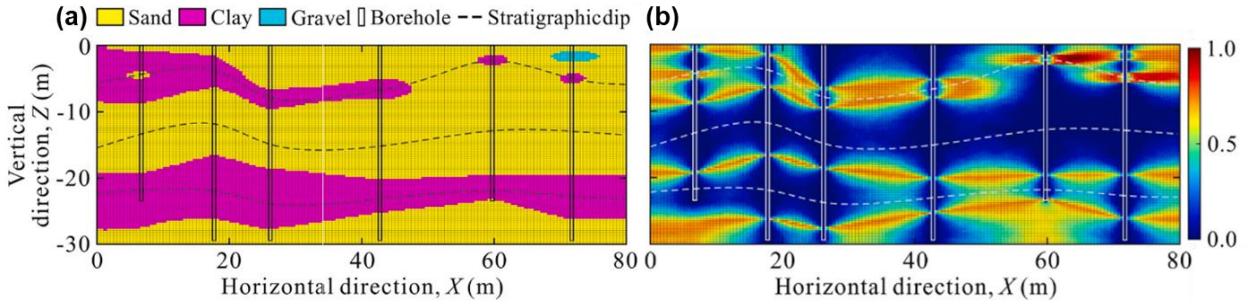

Figure 3.3 Stratigraphic uncertainty modeling results from random field-based modeling approach (a) Most likely stratigraphic configuration; (b) Spatial distribution of the modeled information entropy (Zhao et al. 2021).

Shi and Wang (2021) presented a data-driven method based on multiple-point statistics (MPS) to interpolate subsurface stratigraphy for a construction site in Hong Kong from six CPT soundings. Using MPS methodology, a training image is used to reflect the existing engineering knowledge of stratigraphic conditions. The connectivity and spatial measurements from the training image were extracted to generate multiple realizations of the stratigraphic configurations. The uncertainty in stratigraphic configuration is quantified from the generated realizations. A significant limitation of the study is the use of a training image, a deterministic 2D stratigraphic profile, to evaluate the uncertainty in the interpolation. Emery and Lantuéjoul (2014) showed that MPS only produces random fields when the size of the training image tends to infinity. MPS algorithms do not approximate random functions for the stratigraphic units with a finite training image, thus comprising the random function theory and model consistency.

Although the aforementioned probabilistic approaches allow generating possible stratigraphic realizations based on CPT data or borehole data, they have certain limitations on the consideration of transition probability matrices, statistical coefficients for random-field modeling, and spatial correlation structure. In addition, the estimated uncertainty in stratigraphic configurations does not capture the uncertainty in the stratigraphic layers in the sense of direct application to tunnel projects. These studies discussed are limited to quantifying the uncertainty in stratigraphic configurations without highlighting the uncertainty in stratigraphic transition locations in the vertical and horizontal directions within the subsurface.

3.2 Quantifying void risk occurrence for tunnel projects

A number of studies have attempted to examine the spatial variability of karstic features. Paraskevopoulou and Benardos (2013) indicated that the spatial variability and the associated risk of uncertainty need to be carefully considered and assessed prior to tunnel design and construction as encountering unforeseen conditions could lead to catastrophic delays and cost overruns. Ford and Williams (2013) highlighted the uncertainty arising from the spatial variability of karstic voids and discussed a number of factors–rock variability, topographical features, geomorphological features, rock discontinuities, and permeability affecting karstic void spatial variability. The study discussed the need to characterize karstic void variability for subsurface projects.

Zabidi and De Freitas (2013) developed a geospatial analysis-based methodology to generate deterministic estimates of karst void fraction in the ground from volumetric analysis of the boreholes drilled for Stormwater Management and Road Tunnel (SMART) in Kuala Lumpur. For the analysis, triangles formed by joining the three nearest boreholes were used to represent the karst percentage within the volume of ground along the tunnel alignment. The study employed a geometric method to calculate the volume of rock cores and karst within the boreholes and considered the length variations of rock core and the karst between the three boreholes. Triangular and trapezoidal geometric shapes were used to calculate the volume of rock core and karst between the three boreholes. The results from the study were limited only to identifying the karstic volume of the ground, without investigating into a quantitative assessment of occurrence of karstic features.

Cheng et al. (2017) proposed a fractal analysis model describing the relationship between drilled boreholes and karst caverns' diameters to predict the grouting volume for treating karst caverns along a tunnel alignment. The study utilized the fractal number-size model to estimate the total volume of karst caverns in the project region. Longitudinal distribution profiles and surface plane profiles of the karst caverns were developed from the drilled borehole data. From these profiles, the fractal parameters (height, spacing) of the karst caverns were calculated to estimate the volume of karsts within the ground. The grout volume required for karst treatment was estimated from the karst volume. A major limitation of the study is projecting the fractal characteristics of karstic features on the longitudinal profiles and surface profiles from limited borehole data.

Yau et al. (2020) used a random distribution of karstic voids and developed a numerical model to quantify the impact of karstic voids of water pressure expected and the structural capacity of the tunnel liners. The study utilized a MATLAB script to simulate a random distribution of karstic voids with a higher bound volume of 2 m^3. Within the 2D numerical model examining the structural capacity, the karst cavities were generated until 10 % of the total ground volume within the numerical model were occupied by the karst cavities. The study is limited in developing a random distribution of karstic cavities up to 10 % of ground volume without investigating into the spatial variability aspect. The spatial locations of karstic cavity occurrence, number of karstic features, the size and frequency of occurrence around and within the tunnel envelope is not considered within the study.

Kovačević et al. (2020) presented a customized neural network (NN) model, trained to learn the complex non-linear relationship between rock mass parameters in a karstic environment and tunnel design parameters. However, the study is limited to using empirical correlations to determine reduced rock stiffness in the presence of karstic features.

It is evident from the abovementioned geotechnical hazards that a quantified knowledge of karstic void size, occurrence frequency, and locations of occurrence within tunnel envelope would be beneficial for active risk management and decision-making on tunnel projects. Probabilistic approaches capable of characterizing the spatial variability and the associated uncertainty of subsurface features could be implemented for a comprehensive quantitative assessment.

3.3 Optimizing geotechnical SI for tunnel projects

For tunneling and mining applications, several researchers have developed methodologies to optimize geotechnical SI. Pinheiro et al. (2017) combined geostatistical simulation of rock mass rating (RMR) and applied a simulated annealing approach to identify optimal locations for additional investigation boreholes. The study used the variance and the width of 95 % probability interval of the simulated RMR values as the objective functions to identify optimal locations of SI. The study outcome showed that the objective function approach could contribute to a rational approach in formulating SI plans. The study is limited in discussing the rationale in selecting the optimal sampling locations and configuration of additional SI boreholes.

To determine an optimal level of SI effort for compelling predictions of tunneling-induced settlement in clays, Gong et al. (2014) developed a random field of geotechnical parameters affecting tunneling-induced settlement and applied a multi-objective optimization. An artificial dataset of undrained shear strength was developed, and the tunnel face support pressure was

assumed to be constant in predicting the ground deformation using the analytical model proposed by Loganathan and Poulos (1998). The study identified the best candidate SI program by comparing the settlement prediction from each candidate SI program and the field observations (see Figure 3.4). A significant limitation of the study is the lack of characterization of the scale of fluctuation and the coefficient of variation of the geotechnical property. In addition, the study lacks an analysis on the choice of geotechnical parameter and sensitivity of face support pressure towards tunneling-induced ground deformation.

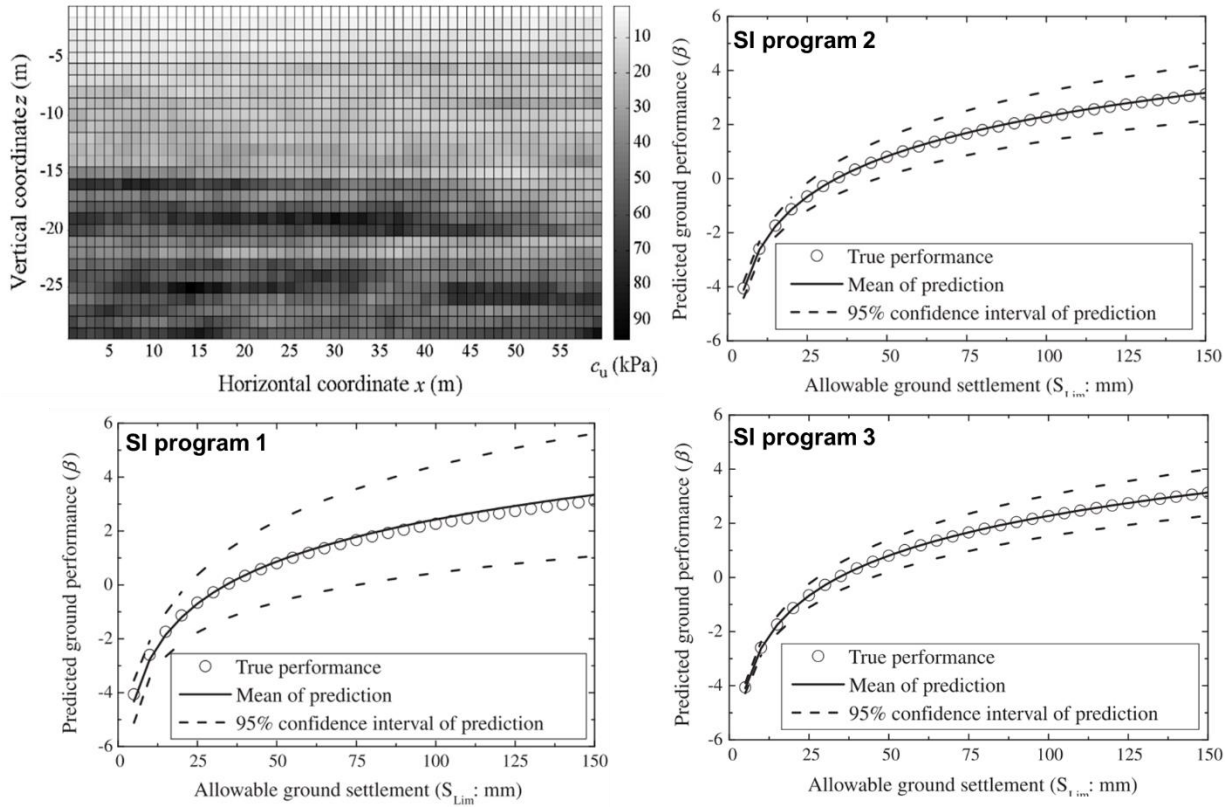

Figure 3.4 Example of the artificial dataset of undrained shear strength (c_u) and comparison among three different levels of SI effort (Gong et al. 2014).

A few researchers focused on the economic benefit uncertainty in SI planning for tunneling applications. Karam et al. (2007a) and Karam et al. (2007b) considered ground and cost uncertainties in exploration decision-making and planning based on the application of decision theory to exploration planning presented by Einstein et al. (1978). The study incorporated ground uncertainties by specifying (if known) or assuming (if unknown) probability distributions of parameters using MCS. The study helped in identifying the probability of beneficial exploration with regards to the cost of exploration along the tunnel length. Sousa et al. (2016) advanced the study by Karam et al. (2007b) and presented an SI planning approach for decision-making in geotechnical engineering based on the virtual exploration and Bayesian updating on the information gained from the boreholes. The study considered two functions–linear and inverse-squared decay propagation to model the information decay away from the boreholes. The expected value of the additional investigation helped in identifying the trade-off between the knowledge

gain and the cost of geotechnical investigations on Masdar City Metro subway tunnels. A limitation of the study is the application of the proposed approach to homogenous tunnel sections and the modeling of spatial distribution of geological conditions using information decay functions. The study did not discuss the benefit of investigations with regards to tunnel risk assessment.

Zetterlund et al. (2015) advanced the work use of decision theory to identify the value of additional investigations (see Figure 3.5). The study presented a methodology that checked two investigation alternatives and presented an economic justification of adding boreholes for planning grouting operations in a hard rock tunnel project. The results from the study aided in decision-making regarding investigation strategies on the tunnel project through the value of information analyses (VOIA). However, the models for VOIA tend to become complicated for tunneling applications, and the complexity of the models increases with the use of quantitative simulation models (e.g., ground condition model) used as input data (Zetterlund et al. 2015). In addition, the study only investigates the cost aspect of SI without looking into the knowledge gain from additional SI.

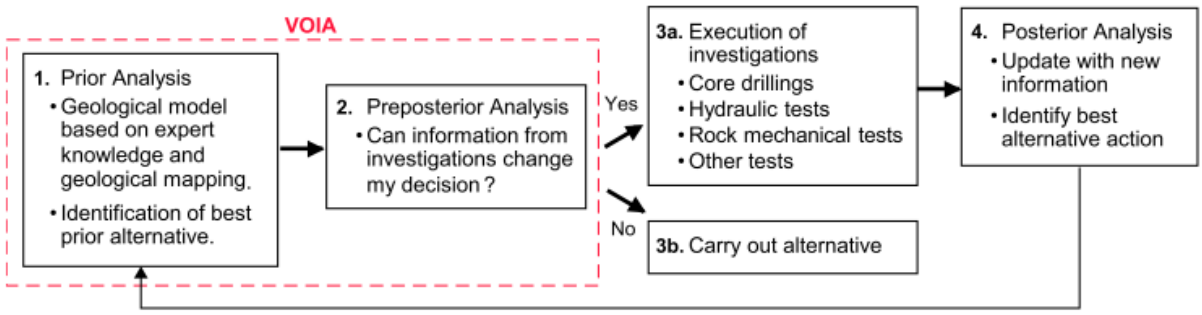

Figure 3.5 Framework for the value of information analysis (VOIA) in rock engineering investigations (Zetterlund et al. 2015).

In broader geotechnical engineering applications, Zhao and Wang (2019) presented a quantitative approach for determining efficient sampling locations in geotechnical site characterization using information entropy and Bayesian compressive sampling for one-dimensional case (depth of measurement within one soil layer) using CPT data. The study quantified the variance in the vertical direction for one CPT sounding using the autocorrelation function and identified the sampling location from maximum variance. A limitation of the study is dealing with high-resolution CPT data to make sampling decisions, and an assumed spatial structure of the CPT parameters.

For slope stability applications, Jiang et al. (2020) investigated the optimal test design of site exploration considering the impact of probability of slope failure while accounting for the spatial variability of soil properties. The study generated a non-stationary random field to model the undrained shear strength of the soils and identified the optimal borehole location at the slope crest. Hu et al. (2021) attempted to optimize the SI programs and developed a computationally efficient value of information (VoI) approach to analyze the effectiveness of SI programs for slope reliability assessment. The study assumed a lognormal distribution of undrained shear strength to model it as a random variable. Schweckendiek and Vrouwenvelder (2013) assessed the

effectiveness of the pore pressure monitoring strategy on the stability assessment of levees. Crisp et al. (2020) adopted a VoI approach to assessing the effectiveness of different geotechnical SI programs through the total expected project cost.

Although several researchers convey methodologies to optimize SI, they have certain limitations on the consideration of spatial variability in ground conditions. Most of the aforementioned studies are based on synthetic examples and use the spatial variability of ground properties based on general experience and the literature. Specifically, none of the studies focus on quantifying the spatial correlation structure and transition probabilities based on SI data. Further, none of the existing studies are based on considering the project site conditions and constraints (budget, time) in the optimization framework. More importantly, none of the studies in tunneling applications optimize SI programs with respect to one or more geotechnical risks. However, in broader geotechnical engineering applications, a handful of studies consider slope failure as a risk and design SI programs accordingly.

3.4 Evaluating the accuracy of geostatistical models

Numerous researchers discuss the application of geostatistical techniques to develop subsurface models of geological-geotechnical conditions and use these models for tunnel risk assessment and forecasting tunnel performance (Felletti and Beretta 2009; Stavropoulou et al. 2010; Kaewkongkaew et al. 2015; Chen et al. 2017; Grasmick 2019). However, limited studies have focused on evaluating the accuracy of developed geostatistical models. In previous works discussing the accuracy of geostatistical models, in the field of soil sciences, Kravchenko (2003) evaluated the effect of sampling density on mapping the accuracy of soil properties with different spatial structures and variability. The study used cross-validation techniques to evaluate the accuracy of the interpreted geostatistical model. In traditional geostatistics, Goovaerts (2001) and Leuangthong et al. (2004) presented techniques such as cross-validation, jack-knife, histogram reproduction, and variograms reproduction to evaluate the geostatistical models. The cross-validation techniques give a measure of variability expected by withholding data but do not provide an accuracy measure of the suite of categorical geostatistical models. Leaving out a set of boreholes may not necessarily offer insights on model performance in capturing the soil transitions, one of the significant risks in geotechnical and tunnel applications.

Grasmick et al. (2020) developed geostatistical models from continuous geotechnical parameters such as moisture content, standard penetration tests (SPT), plasticity index (PI) for tunnel risk assessment and evaluated the accuracy of models for *global* and *local simulation approaches*. The study used accuracy plots (also known as reliability diagrams) as a diagnostic tool to evaluate the geostatistical models and revealed the significance of evaluating models of uncertainty in selecting the appropriate modeling approach. The points on the accuracy plot summarized the fairness of the predicted uncertainty of the geotechnical parameters. Points close to the 45-degree line indicated fair or accurate probabilities. From accuracy plots, the average variance is a measure of the prediction precision; the lower the average variance the more precise are the distributions of uncertainty.

Boyd et al. (2019) used a synthetic dataset and evaluated the performance of 2D categorical geostatistical models from seven boreholes, for varying variogram parameters, by comparing them to a geologist's interpretation of subsurface conditions. The study used accuracy plots and R^2

values to evaluate the prediction performance of geostatistical models. However, global accuracy evaluation of a geostatistical model through R^2 values and accuracy plots is insufficient, as it does not guarantee that model is valid everywhere in its domain.

With the increased research and awareness in applying geostatistics to UCT projects, it is imperative to evaluate the accuracy of the geostatistical models prior to utilizing the models in risk assessment and decision-making framework.

CHAPTER 4- QUANTIFICATION OF SOIL TRANSITION LOCATION UNCERTAINTY FOR TUNNEL PROJECTS

4.1 Abstract

Stratigraphic transitions within the tunnel envelope cause a rapid change in tunnel boring machine (TBM) operating parameters and impose a significant challenge to TBM tunnel projects. This paper presents a geostatistical modeling-based probabilistic approach to quantify the stratigraphic transition location uncertainty in the longitudinal direction of tunneling and at the tunnel face. Geotechnical data from a soil tunneling project is used to elucidate the capability of the approach. A deterministic soil profile and TBM operation data from the project are examined to evaluate the results from the approach. The results reveal that the stratigraphic transition location uncertainty (for 90 % confidence interval) in the longitudinal direction, for the two stratigraphic transitions within the tunnel envelope, extends over a longitudinal distance of 28 rings and 130 rings. The occurrence of the stratigraphic transitions in the longitudinal direction at ring# 275 and ring# 550, for a 95 % probability of occurrence (P_{95}), match the locations of the change in maximum dissipation of chamber pressure from recorded TBM data. The assessment reveals that the stratigraphic transitions (P_{95}) occur 15 rings before and 30 rings after the locations suggested in the ground profiles suggested in the geotechnical baseline report (GBR). At the tunnel face, the probability of encountering stratigraphic transitions is the highest between ring# 200 and ring# 300 and varies between 60 % and 90 %.

4.2 Introduction

In a tunnel project, geotechnical site investigations (SI) through borehole sampling and lab testing are used to characterize the ground conditions. However, the information obtained from these investigations is location-specific, and sampling locations are sparse, which often leads to uncertainties in estimating ground conditions at unsampled locations. The resulting uncertainty can be attributed to two main sources (a) the inherent spatial variability of soil properties (within the same soil unit) from one point in space to another and (b) stratigraphic transitions, which are transitions between stratigraphic units that are heterogeneous in composition and in geological and mechanical properties (Uzielli et al. 2006). Over the years, the geotechnical community has focused on quantifying the inherent spatial variability and uncertainty of soil and rock properties (Pinheiro et al. 2016; Chen et al. 2017; Huang et al. 2017; Gong et al. 2018; Boyd 2019; Grasmick 2019); however, limited research exists on characterizing the stratigraphic transition location uncertainty.

In geotechnical and tunneling applications, engineers are often concerned about stratigraphic transitions since a lack of quantifiable knowledge about its occurrence may lead to reduced tunnel boring machine (TBM) advance rates, loss of face stability leading to the creation of sinkholes, and heavy water inrush (Sousa 2010; Wang et al. 2016). A lack of quantifiable knowledge of the stratigraphic transitions occurrence at the TBM face, also referred to as mixed-face conditions, has led to major tunnel incidents involving excessive ground deformations in about 55% of tunnel projects worldwide (British Tunneling Society 2005). For example, significant ground movements were observed due to the occurrence of mixed-face conditions in the projects undertaken by the Washington Metro Area Transit Authority (WMATA) (Clough and Leca 1993). From tunneling

case histories worldwide, it is evident that quantification of stratigraphic transition location uncertainty requires more attention for efficient tunneling performance.

In current geotechnical and tunneling practice, the uncertainty in stratigraphic transition locations is often addressed qualitatively with a "?" in ground profiles incorporated into the geotechnical baseline report (GBR), an integral risk allocation document for tunnel projects. Since the tunnel excavation environment is interpreted deterministically, the ground profiles within the GBR provide one unique boundary between stratigraphic units. The ground profiles fail to include a level of confidence for the stratigraphic transition location, and consequently do not quantify the associated uncertainty in the longitudinal direction and at the TBM face. Figure 4.1 presents a schematic representation of the qualitative stratigraphic transition location uncertainty as typically depicted in tunnel projects.

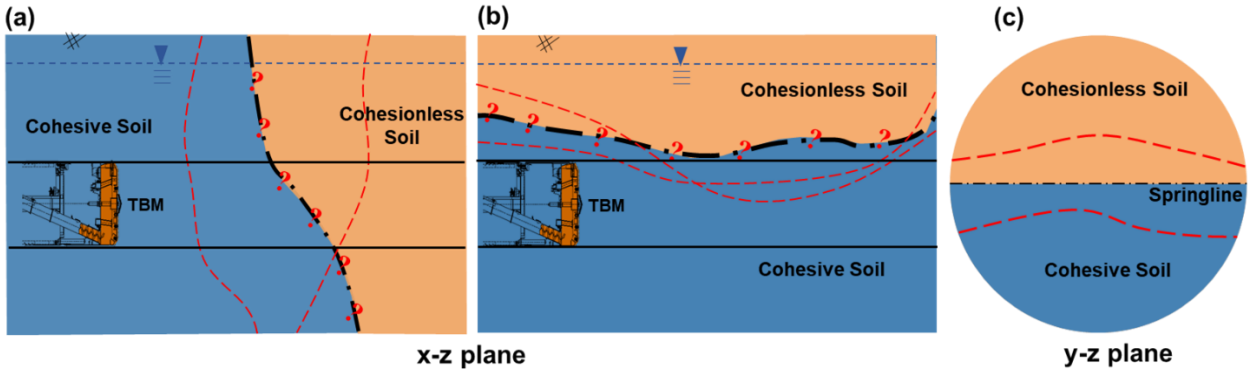

Figure 4.1 (a) and (b) A schematic representation of the qualitative interpretation ("?") of uncertainty in transitions from deterministic ground profiles in the longitudinal direction (x-z plane). (c) Representation of stratigraphic transition in the cross-sectional frame (y-z plane). Dotted red lines indicate two possible spatial locations of the stratigraphic transitions.

Probabilistic approaches exist to identify stratigraphic configurations within the borehole using cone penetration test (CPT) data (Phoon et al. 2003; Wang et al. 2014; Ching et al. 2015; Cao et al. 2016). However, these studies only identify the vertical contact points between stratigraphic units and fail to quantify the uncertainty in elevations of stratigraphic contacts. Several approaches based on interpolation methods such as geostatistics and the Markov-Chain have been developed to interpret the stratigraphic configuration at unsampled locations (Blanchin and Chilès 1993; Chilès et al. 2004; Wellmann et al. 2010). Li et al. (2016) and Wang et al. (2016) introduced a Markov random-field-based methodology to quantify the uncertainty band in stratigraphic configurations using information entropy with respect to the borehole locations. Wang et al. (2018) and Gong et al. (2020) evaluated slope stability considering the uncertainty in stratigraphic configurations using a Markov random-field-based methodology. Xiao et al. (2017) developed a probabilistic framework to characterize soil layer stratification for a construction site in Hong Kong. Hu and Wang (2020) proposed a 2D probabilistic soil classification and stratification method to quantify the vertical transition elevations between soil units using random field theory and Monte Carlo simulation on six cone penetration test (CPT) soundings. Shi et al. (2021) presented a data-driven method based on multiple-point statistics (MPS) to interpolate subsurface stratigraphy for construction site in Hong Kong. However, these studies are limited to quantifying the uncertainty in stratigraphic configurations without highlighting the uncertainty in stratigraphic

transition locations in the vertical and horizontal directions within the subsurface. To the best of the authors' knowledge, no studies in geotechnical engineering and tunneling have investigated the location uncertainty of stratigraphic transitions at unsampled locations in the longitudinal and transverse directions.

This paper focuses on quantifying stratigraphic transition location uncertainty in the longitudinal direction (Figure 4.1(a) and Figure 4.1(b)) and the elevation of the mixed-ground transition plane in a cross-sectional frame (Figure 4.1(c)) within the tunnel envelope, using a geostatistical modeling-based probabilistic approach. The probabilistic approach employs the pluri-Gaussian simulation technique (PGSIM), a stochastic geostatistical algorithm, on the geotechnical SI data from the Anacostia River Tunnel (ART) project in Washington, D.C. The stochastic geostatistical modeling technique allows for the generation of multiple realizations of equally probable ground conditions. The uncertainty in the locations of stratigraphic transitions, soil transitions in this case, at two different locations within the ART project tunnel envelope, is investigated in this paper. Individual realizations from geostatistical modeling and the probabilistic tools—empirical cumulative distribution function (ECDF) curves and confidence intervals (CI)—are used to determine the probabilistic distribution soil transition locations in the longitudinal direction of tunneling and at the TBM face. The probabilistic approach results are objectively examined with the earth-pressure balanced TBM (EPBM) operation data from the ART project and are compared to the deterministic soil profile from the GBR. The paper's motivation is to improve the understanding of where soil transitions and mixed-face conditions occur within the tunnel envelope.

The next section describes the geostatistical modeling-based probabilistic approach and the methodology to quantify the uncertainty in soil transition locations in the longitudinal direction of tunneling and at the TBM face. We then present an application of the proposed probabilistic approach to the geotechnical SI data from the ART project. Uncertainty in soil transition locations within the tunnel envelope, for the longitudinal profile and cross-section view, is quantified. Maximum dissipation of chamber pressure as recorded from EPBM operation on the ART project is examined to evaluate the probabilistic approach results in identifying soil transition locations.

4.3 Probabilistic approach

Geostatistical methods based on object-oriented models and pixel-based methods can be used for simulating spatial variability of stratigraphic units, or so-called categorical data (Chiles and Delfiner 2009). Pixel-based methods include the truncated or PGSIM modeling technique, multipoint geostatistics, and Markov chain methods such as transition probability geostatistics (Carle and Fogg 1997). Among the techniques, the PGSIM is a complete approach as geological constraints can be applied on the simulated domains. The technique overcomes most categorical simulation method limitations of not capturing the spatial changes in stratigraphic unit proportions, stratigraphic contact relationships and geological realism within realizations (Madani and Emery 2015; Madani et al. 2019).

With a stochastic modeling framework, PGSIM technique attempts to preserve and reproduce the heterogeneity of parameter of interest (Pyrcz and Deutsch 2014; Ma 2019). Application of stochastic geostatistical modeling techniques allows for generating multiple equiprobable realizations of ground conditions. Each realization from the geostatistical modeling captures the

degree of heterogeneity and spatial variability of the stratigraphic units. PGSIM modeling technique is capable of simulating multiple stratigraphic units and has been used in modeling petroleum reservoirs and environmental science problems (Emery 2007; Armstrong et al. 2011). Madani et al. (2019) presented tools to validate the reproduction of stratigraphy in individual realizations generated from PGSIM modeling technique. Madani and Emery (2015) presented a split-sample validation of the individual realizations using calibration plots, thus showing the deviation of simulated proportion of stratigraphic units from actual proportions.

In this study, a 3D grid generated along the tunnel alignment is discretized into cells, also known as voxels. Stratigraphic units are simulated within the 3D grid from the geostatistical modeling technique. Developing a 2D model does not allow to capture heterogeneities in the plane perpendicular to tunneling. Therefore, the soil transition uncertainty is evaluated in 3D. In general, for tunnel projects situated in urban environments, most often the boreholes are drilled at an offset to the tunnel alignment due to site accessibility constraints. Developing a 3D model helps use and honor the available borehole data and helps estimate the ground conditions accordingly. In other geosciences applications, like oil and gas exploration, 3D models are preferred over 2D models as 3D models offer relatively more insights on the spatial variability in reservoir shape, fault shape and engineering properties. Similarly, in tunneling applications, engineers are concerned about stratigraphic units' heterogeneity and related variability in engineering properties in the transverse direction to tunneling. Example applications could be construction of cross-passages and ground deformation profiles. Phoon et al. (2021) argues that a 2D section since the out of plane dimension to preserve the plain strain assumption cannot be spatially variable. The study discussed that no consistent 3D spatially varying soil mass that can produce a spatially varying 2D section. The results presented in the manuscript are 2D only for the presentation purposes.

One of the significant strengths of the PGSIM modeling technique is its capability to reproduce complex transitions between stratigraphic units. Factors considered in the PGSIM modeling include (a) the proportions of the stratigraphic units from geotechnical SI; (b) the spatial variability of the units; (c) the spatial connectivity of the units; and (d) the probability of the transition between units in the longitudinal and vertical directions. In this technique, the stratigraphic units' correlation is quantified using indicator variograms generated for the vertical and horizontal directions. Variograms generated in multiple directions capture the anisotropy within the available data. The variogram range, the distance beyond which no correlation exists between the data in each direction is a function of the degree of heterogeneity and the frequency of stratigraphic unit occurrence. As per the central limit theorem, each lag distance bin in a variogram must contain a minimum of 30 point pairs (Cressie 1985). In addition, the binned lags should be of equal spacing and the number of pairs should be similar across all binned lag distances. The lag distances at which the experimental variograms can be determined with an acceptable number of data pairs indicates the scale at which the spatial variation can be modelled.

In this study, an angular tolerance of 22 degrees corresponding to a 45-degree span for the data points is considered to develop the horizontal variograms. To compensate for the lack of close spacing of the boreholes, a relaxation of the angular tolerance width is required, without affecting the directionality and anisotropy of the variograms. Based on the number of data points available, a decision on the angular tolerance width and slicing height can be made to increase the precision of the horizontal variograms. Webster and Oliver (1992) discussed that practitioners should aim

to sample 150 to 200 points within a region to estimate the variograms. Vertical variograms are relatively easier to comprehend due to high data density in the vertical direction.

The stratigraphic units are transformed into Gaussian values in appropriate intervals following the indicator variogram model using the Gibbs sampler algorithm. A search neighborhood is defined, and the available Gaussian values within the neighborhood, called conditioning data, are used to simulate Gaussian values within the neighborhood. The classical conditional Gaussian simulation developed by Matheron and Journel (Chiles and Delfiner 2009) is used to simulate Gaussian values. The simulated Gaussian values are transformed back into stratigraphic units using the abovementioned factors.

Realizations generated form PGSIM modeling are constrained to the available data, therefore exhibiting realistic representations of stratigraphic configurations. The results from PGSIM modeling can be validated from investigation of indicator variograms from realizations, also called as output indicator variograms, and split-sample validation. The resemblance of the output indicator variograms to the model input variogram validates the performance of PGSIM modeling technique in reproducing stratigraphic configurations. The interpreted range for all the output indicator variograms must be similar to the range of input indicator variogram. The validation not only considers the reproduction of the average experimental indicator variogram over set of realizations, but also shows the reproduction of indicator variogram spread or fluctuations across realizations, which are key elements in geostatistical modeling of uncertainty. Such analysis validates the consistency of an interpreted stratigraphic model. A split-sample validation will help confirm that the stratigraphic sequence, as observed in the borehole data, is replicated in the individual realizations. A measure of successful classification (or misclassification) from split-sample validation will help verify the performance of the simulation technique.

Figure 4.2 presents the workflow of the geostatistical modeling-based probabilistic approach for characterizing uncertainty in stratigraphic transitions in the longitudinal and vertical directions within a tunnel envelope. The longitudinal distance along the tunnel alignment is identified and expressed in terms of ring number, ring#. A conceptual example of the ring# and realizations of stratigraphic units from PGSIM modeling is presented. The workflow consists of four distinct steps.

Step A entails building a 3D simulation grid for geostatistical modeling and discretizing available borehole data into grid voxels. Multiple realizations of stratigraphic configurations are generated. Each row of realizations within Step A in Figure 4.2 represents a single voxel of the 3D grid. Grid voxels lying within the tunnel envelope are extracted with simulated information for uncertainty quantification.

Step B involves analyzing the probability of occurrences of stratigraphic units (P_x) and the evaluation of the most-probable unit within the extracted grid voxels. From probabilistic occurrences P_x, the uncertainty (or amount of missing information) associated with each grid voxel k is obtained by calculating the normalized information entropy H_k (Shannon 1948) for a set of n stratigraphic units.

Step C involves quantifying the occurrence of transitions in the longitudinal direction of tunneling. Individual realizations from the geostatistical modeling are analyzed to quantify the proportion of

stratigraphic units (M_x) along the tunnel alignment. The voxels from the 3D simulation grid within the tunnel envelope are used to evaluate the proportion of stratigraphic units. The proportion of a stratigraphic unit *x* at ring# location *i* is calculated as shown in Eq. (4.1).

$$M_{x_i} = \frac{No.of\ observations\ of\ unit\ x\ at\ ring\#\ i}{No.of\ observations\ at\ ring\#\ i} \tag{4.1}$$

The observations discussed herein correspond to voxels from the 3D simulation grid. For each ring# *i* and from the set of *n* geostatistical realizations, the cumulative probability of occurrence of a stratigraphic unit *x* in specific proportions *t* within the tunnel envelope is evaluated as shown in Eq. (4.2).

$$F_{x_i}(t) = \frac{(No.of\ observations\ for\ M_x\ \leq t)_i}{\sum_i No.of\ observations\ for\ M_x\ \leq t} \tag{4.2}$$

A family of ECDF curves is generated for a stratigraphic unit occurring at varying proportions along the tunnel alignment. **Step D** presents a characterization of a mixed-ground transition plane and mixed-face conditions within the tunnel envelope. From individual realizations of stratigraphic configurations, transitions between stratigraphic units in the tunnel envelope's vertical plane are quantified along the alignment length. The elevation of the transition for each ring# is recorded. From *n* geostatistical realizations, a distribution of the elevation of the transition at each ring# is generated to characterize the probable elevations of the mixed-ground transition plane within the tunnel envelope. Similar to Step C, ECDF curves showing the probability of encountering mixed-face conditions with respect to elevations are generated. If E_{sp} and E_c represent the TBM springline and crown, respectively, then the cumulative probability of occurrence of the mixed-ground transition plane at elevation E_f, between E_{sp} and E_c at ring# *i* is presented as shown in Eq. (4.3).

$$F_{z_i}(E_f) = \frac{(No.of\ observations\ for\ E_c < E_f < E_{sp})_i}{\sum_i No.of\ observations\ for\ E_c < E_f < E_{sp}} \tag{4.3}$$

The probabilistic approach results aid in quantifying soil transition location uncertainty in the longitudinal direction and in the cross-sectional frame within the tunnel envelope.

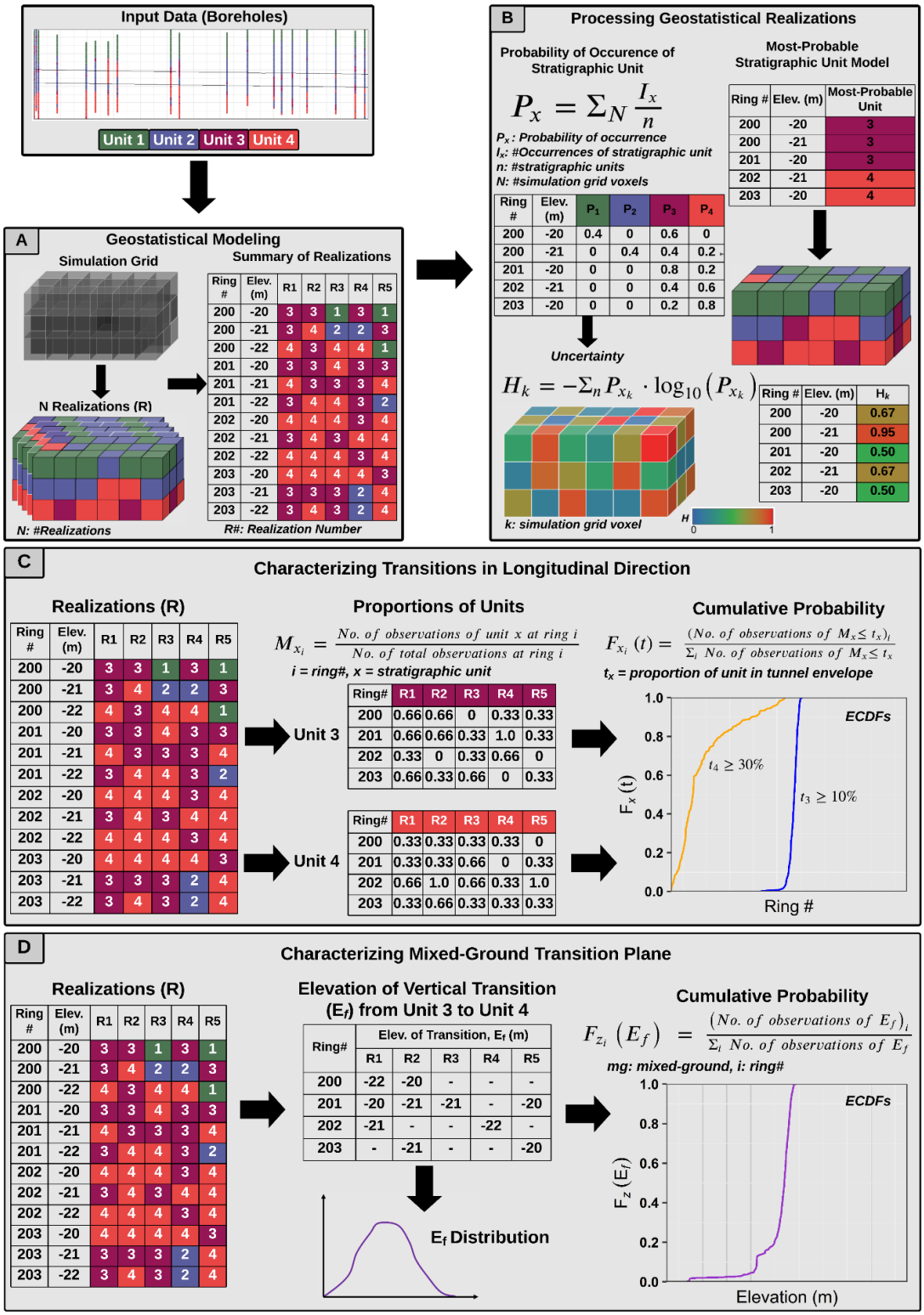

Figure 4.2 Geostatistical modeling-based probabilistic approach workflow to characterize stratigraphic transition location uncertainty.

4.4 Probabilistic assessment of soil transition location uncertainty

The proposed probabilistic approach is employed to estimate the transition location uncertainty between cohesive (G1/G2) and cohesionless (G3/G4) soils within the ART tunnel envelope. The approach uses the available geotechnical SI from the ART project site. The ART project tunnel is a 7 m diameter tunnel excavated using EPBM. The ground conditions for 2 km of the ART alignment were investigated prior to construction from 20 boreholes, which logged the soil types and extended below the tunnel invert. The mean vertical soil sampling interval within the boreholes is about 0.5 m, and the mean horizontal spacing between the boreholes is about 85 m. Soil types encountered within the boreholes show that the ART project site comprises fill, alluvium, and a thick sequence of marine sediment deposits. Highly plastic and over-consolidated clays, along with lightly over-consolidated silty/sandy clay layered with thin fine-grained sand and gravel, are predominant within the project site. Fine- to medium-grained sand and fine- to coarse-grained sandy gravel are overlaid by the over-consolidated clays. Fine- to coarse-grained sandy gravel and fine- to coarse-grained sand are interlensed with silty/clayey sand and over-consolidated clays.

The groundwater table is found to be near the ground surface. The soil types are grouped based on the Unified Soil Classification System (USCS) and are expressed in terms of engineering soil units (ESUs). Based on the ESU material descriptions, G1 and G2 are combined and identified as cohesive soils, whereas G3 and G4 are combined into cohesionless soils. Figure 4.3 presents a longitudinal profile of the boreholes in terms of ESUs, along the tunnel alignment. Table 4.1 presents a brief description of the ESUs along with the USCS classification.

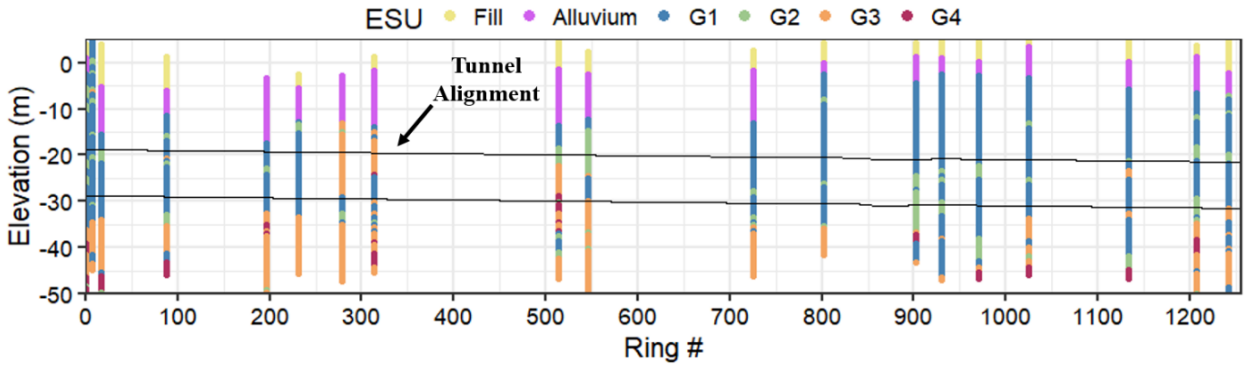

Figure 4.3 Longitudinal profile of the boreholes along 2 km ART alignment.

Table 4.1 Description of the ESUs.

ESU	Soil Type	USCS Classification	Soil Description
Fill	-	-	Fine to coarse-grained material with fragments of organic material.
Alluvium	-	-	Soft clay, loose silt, and fine sand with varying amounts of gravels, cobbles, and boulders.
G1	Cohesive	CH, MH	Highly plastic over-consolidated fine-grained soil.
G2		CL, ML	Low to medium plastic over-consolidated fine-grained soil.
G3	Cohesionless	SM, SC, SC-SM, GM, GC, GC-GM	Non-plastic silty or clayey sand and gravel, or mixtures of sand, silt, and clay.
G4		SP, SP-SM, SP-SC, GP, GP-GM, GP-GC	Fine to coarse sand with trace amounts of gravel and fines.

For geostatistical modeling, a 3D simulation grid extending to 50 m on either side of the ART alignment is generated. The borehole data is discretized into the cells, also termed as voxels, of the 3D simulation grid. Each voxel is 1.8 m x 1.8 m x 1 m in the longitudinal, transverse, and vertical direction, respectively. The longitudinal voxel length coincides with the length of each ring. A 3D model of ground conditions is required to quantify the location uncertainty of soil transitions. Developing a 3D model helps honor the borehole data, drilled at an offset to the tunnel alignment, and helps estimate the ground conditions accordingly. The results presented in the manuscript are 2D only for the presentation purposes, although the probabilistic approach is applied on the 3D grid.

The PGSIM modeling technique is applied to the borehole data, and 600 equiprobable realizations of the ground conditions are generated in terms of ESUs. ESUs are simulated at each voxel of the 3D simulation grid, considering the proportion of ESUs from the borehole data, the probability of transition between ESUs, and the spatial variability of ESUs. The number of realizations (460) was sufficient to provide results independent of the number of realizations and was determined using an information-entropy-based (Shannon 1948) approach first used by Felletti and Beretta (2009). The uncertainty (H), in terms of information entropy, at each simulation voxel (k) of the 3D simulation grid is presented in Eq. (4.4).

$$H_k = -\sum_{x=1}^{N} p_{x_k} * \log p_{x_k} \quad (4.4)$$

where p_{x_k} is the probability of outcome x out of N possible outcomes of ESUs at voxel k.

The convergence of the uncertainty measure with the increasing number of realizations is used to determine the appropriate number of realizations required for geostatistical modeling. Figure 4.4(a) presents the distribution of the uncertainty change (ΔH) in the realizations with 1 % ΔH bands. Figure 4.4(b) presents the variation of the median ΔH with geostatistical realizations and confirms that at 460 realizations, the median ΔH falls on/below the 1 % threshold. A threshold of 1% ΔH is chosen to identify the number of realizations for the probabilistic approach. A 1 % ΔH threshold indicates that for all the geostatistical realizations, there is not more than 1 % difference in the probabilistic estimates of ESUs, indicating the confidence in the repeatability of the results from the PGSIM modeling. The interpreted geostatistical model of the ground conditions and the analyses in the subsequent sections of this paper are based on the 460 realizations from the PGSIM modeling. ESU estimates from the 460 geostatistical realizations are used to quantify the probability of occurrence of ESUs at the voxels within the simulation grid. It is important to note that the uncertainty measures (expressed in terms of information entropy) do not capture the uncertainty in stratigraphic transition locations. Further discussion on this topic and results are presented in Appendix A.

ESUs with the maximum probability of occurrence (ratio of number of occurrences in all realizations to the total number of realizations) in the voxel is assigned as the most-probable ESU. We note that the available soil profile in the GBR for the ART project is presented in terms of geological formations. A longitudinal profile of ground conditions, in terms of ESUs, is developed to visualize and identify the locations of possible soil transitions. Figure 4.5 presents the most-probable ground conditions in terms of ESUs along the 2 km of the ART alignment. The voxels within the tunnel envelope are extracted from the 3D simulation grid to characterize the soil transition location uncertainty. The tunnel envelope within this study extends 0.25 times D (where D is the tunnel diameter) along the tunnel circumference. For the 7 m diameter ART tunnel, the tunnel envelope is about 10.5 m in diameter.

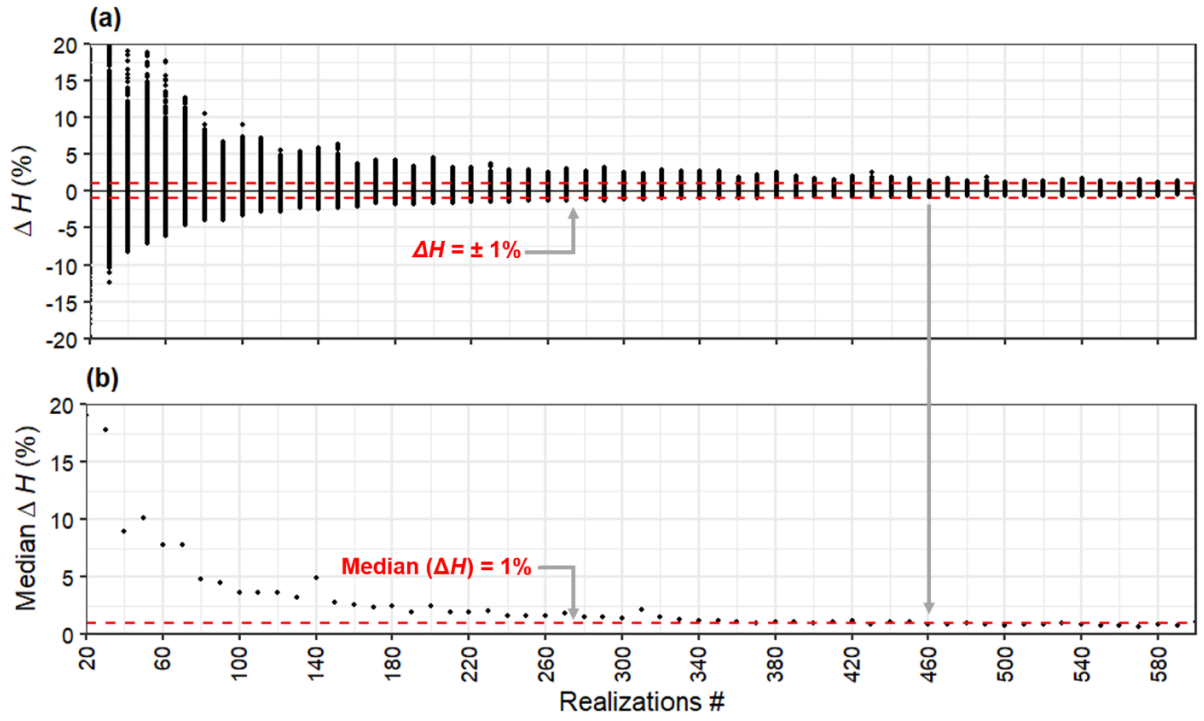

Figure 4.4 (a) Percentage distribution of uncertainty change (ΔH) and (b) median ΔH with geostatistical realizations. At 460 realizations, the distribution of ΔH and median ΔH remains within 1 %.

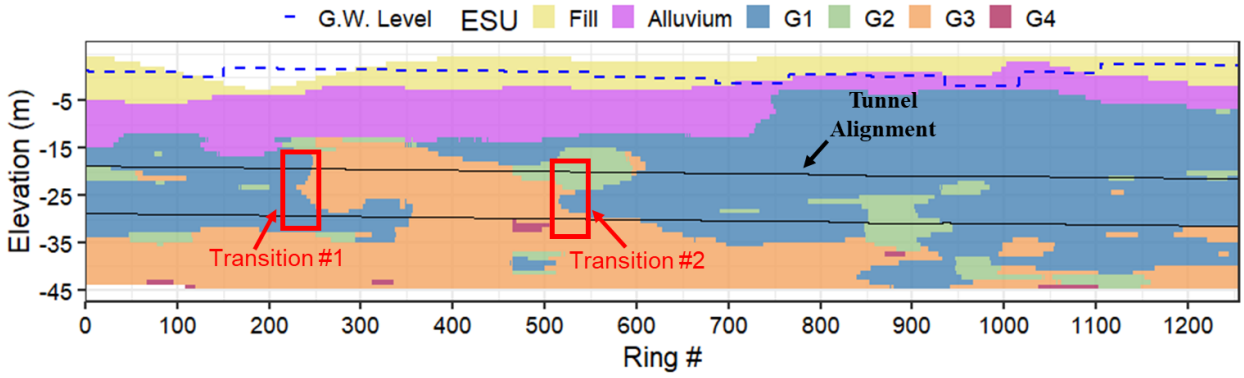

Figure 4.5 Longitudinal profile of the most-probable ground conditions with soil transitions and groundwater levels along the 2 km ART alignment.

4.4.1 Validation of geostatistical simulations

Figure 4.6 and Figure 4.7 presents the indicator variograms (from 460 PGSIM realizations) in the horizontal and vertical directions, respectively for dominant ESUs within the tunnel envelope. The magenta line represents the experimental indicator variogram derived from the borehole data for respective direction. Because the vertical sampling interval within borehole is about 1 m, vertical indicator variograms can generally be constructed easily compared to the experimental variograms in the horizontal directions. The construction of satisfactory experimental indicator variograms depends on the scale of the project. The lag distances at which the experimental indicator variograms can be determined with an acceptable number of data pairs sheds light on the scale at which the spatial variation can be modeled. The behavior of the indicator variogram at shorter lag distances (which are typically of interest) is more important than at larger distances as it relates to the modeling of boundaries between stratigraphic units (Dubrule 2017). The distance at which the indicator experimental variogram reaches the sill (correlation range) corresponds to the distance beyond which the indicator variable is independent.

Spherical and exponential models are found suitable to model Gaussian random functions as these models generally satisfy the positive definiteness for covariance and conditional positive definiteness for variograms (Chiles and Delfiner 2009). Accordingly, spherical model is used to fit the experimental variograms. Gray lines indicate the output indicator variograms from 460 realizations. Red and blue lines indicate the average of 460 output indicator variograms and average ± 2*standard deviations. The red line bears resemblance to the shape and the structure of model input indicator variogram for PGSIM modeling (black line). On average over the 460 realizations, the difference between the sill of the average output indicator variogram (red line) and the model input indicator variogram (black line) is less than 2 % for engineering soil units (ESUs) G1 and G3 and is less than 5 % for ESUs G2 and G4. This indicates that the proportions of ESUs (as observed in the borehole data) is honored in the set of 460 realizations. The interpreted range for all the output indicator variograms is similar model input indicator variogram. We note that the sill of an indicator variogram is the indicator variance and is equal to the ESU proportion multiplied by the complimentary proportion. The presented validation not only considers the reproduction of the average experimental indicator variogram over 460 realizations, but also shows the reproduction of indicator variogram spread or fluctuations across realizations, which are key elements in geostatistical modeling of uncertainty. Such analysis validates the consistency of an interpreted stratigraphic model. From Figure 4.6 and Figure *4.7*, the spatial structure of different ESUs from PGSIM modeling follow the spatial structure quantified by the input indicator variogram.

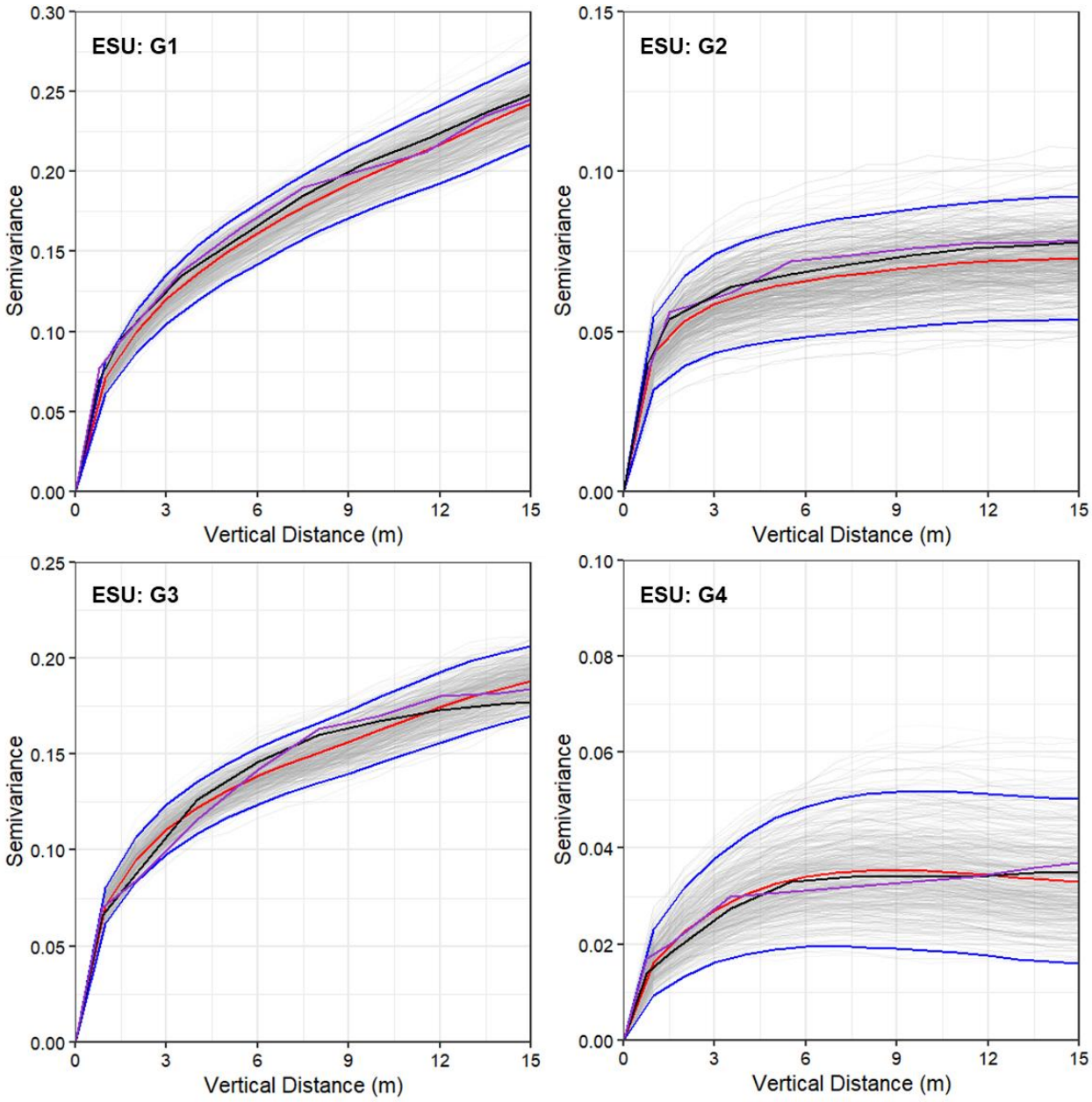

Figure 4.6 Indicator variograms in the vertical direction obtained from PGSIM realizations. Gray: output indicator variograms of 460 realizations. Red: average of 460 experimental variograms. Blue: average ± 2 standard deviations. Black: variogram model input for PGSIM.

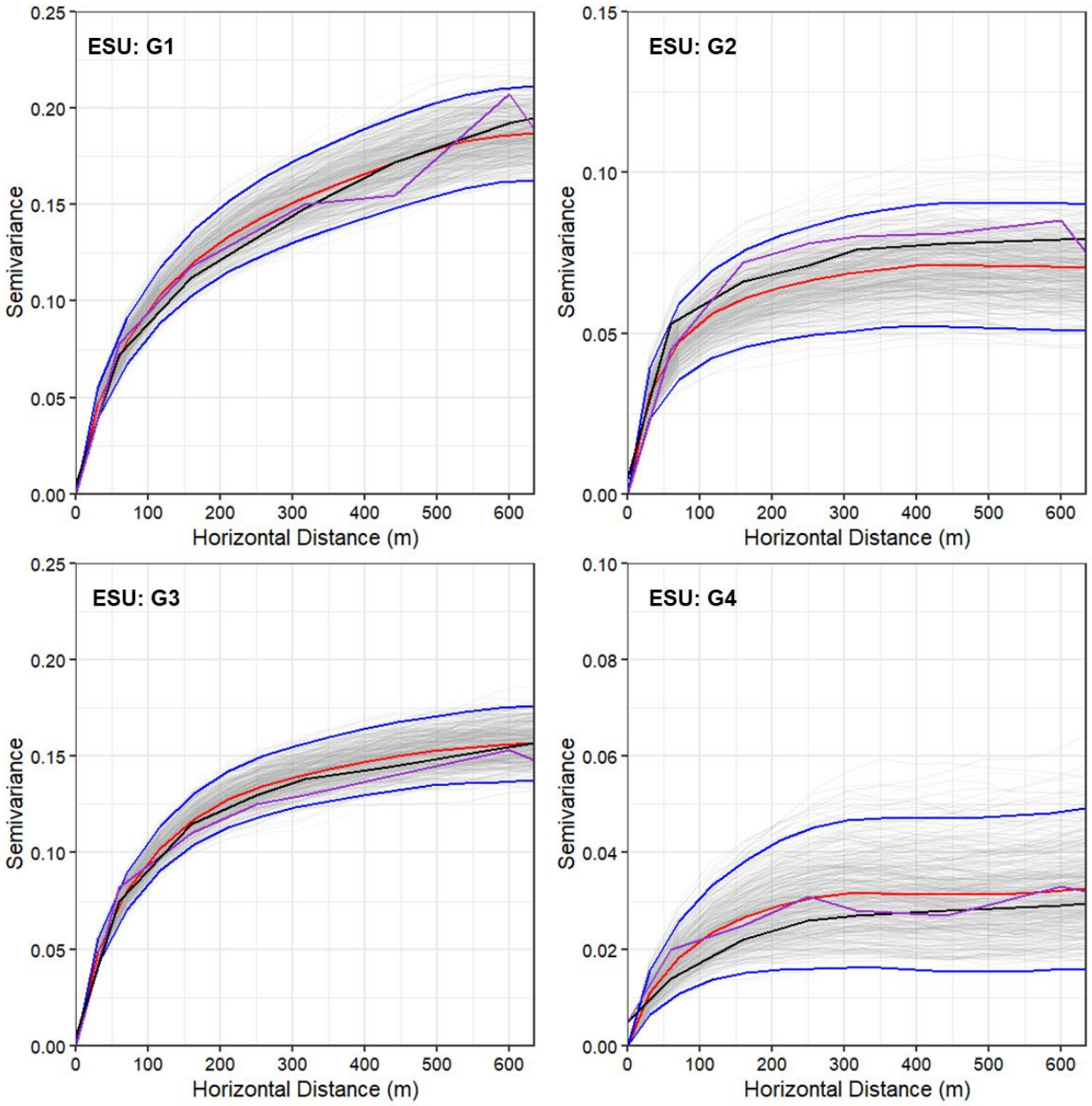

Figure 4.7 Indicator variograms in the horizontal direction obtained from PGSIM realizations. Gray: output indicator variograms of 460 realizations. Red: average of 460 experimental direct variograms. Blue: average ± 2 standard deviations. Black: variogram model input for PGSIM.

Figure 4.8 presents a five-fold cross-validation performed using 70 % and 30 % of boreholes as training and testing datasets, respectively. Each model developed from 70 % of the boreholes is validated with the remaining (30 %) borehole data. Within each fold of validation, the ensemble of 460 realizations are post-processed to identify the most-probable ESU allocation at each voxel of the simulation grid. The accuracy of the interpreted model is presented using a multi-classification confusion matrix that compares the simulated ESUs at the locations of test borehole datasets. The study uses Eq. (4.5) as a measure of geostatistical model accuracy in predicting an ESU. Accuracy, here, is a ratio of all the correct predictions to all the predictions that should have

been correct, for an ESU. Eq. (4.5) is sometimes referred to as sensitivity of the confusion matrix (Tharwat 2020).

$$Accuracy_i = \frac{N_{ij}}{\sum_{j=1}^{n} N_{ij}} \quad (4.5)$$

The results in the confusion matrix presents the percentage of simulation voxels correctly classified (or misclassified) from PGSIM modeling technique. Results reveal > 85% average accuracy of classification of all soil units. G1, G3, Alluvium (relatively high proportion ESUs) are identified with relatively high accuracy metrics. Low proportion ESUs - G2 and G4 exhibit comparatively low accuracy metrics. This is primarily due to the number of conditioning points available for the low proportion ESUs in the training data sets. Fill is identified with relatively higher accuracy than G2 despite the lower number of samples. This could be attributed to the simulation of ESUs considering the geological stratigraphic sequence at the project site.

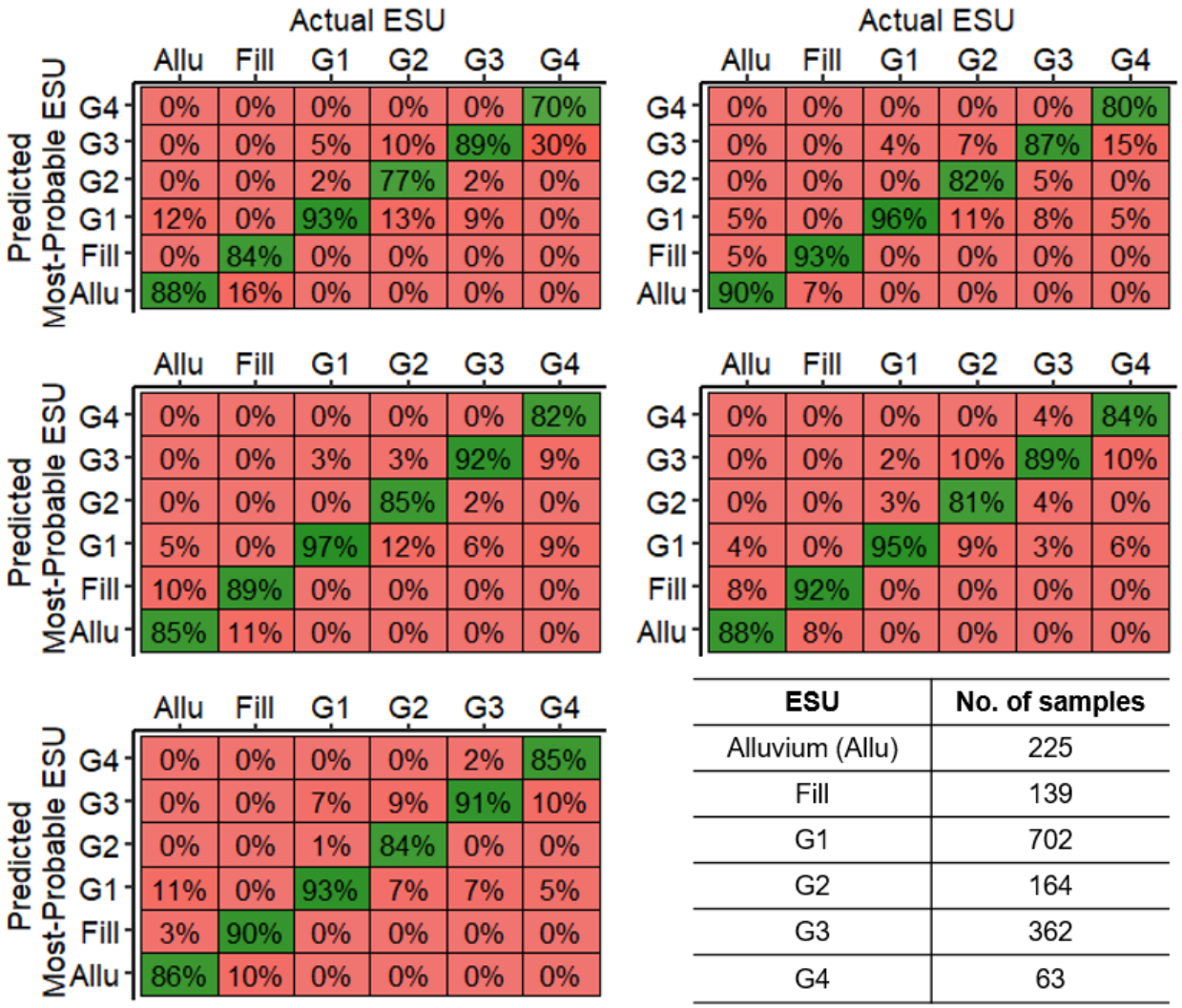

ESU	No. of samples
Alluvium (Allu)	225
Fill	139
G1	702
G2	164
G3	362
G4	63

Figure 4.8 Results from each fold of five-fold cross-validation showing accuracy of classification from PGSIM modeling technique. Number of samples for each ESU as per borehole data.

4.4.2 Soil transition location uncertainty in the longitudinal direction

This section presents a quantification of transition location uncertainty for transitions from ESUs G1/G2 to G3/G4 (transition 1) and G3/G4 to G1/G2 (transition 2) in the longitudinal direction within the tunnel envelope. From the GBR ground profile, transitions 1 and 2 are expected to occur at ring# 260 and ring# 520, respectively. Quantification of soil transition location uncertainty begins with evaluating the proportion of cohesive and cohesionless soils within the tunnel envelope over the 460 geostatistical realizations. The proportion of cohesive and cohesionless soils at each ring# is calculated from Eq. (4.1). Figure 4.9(a) highlights the distribution of the cohesive soil proportion (G1 and G2) within the tunnel envelope through sets of CI bands. As illustrated in Figure 4.9, at ring# 650 (95 % CI), the true cohesive soil proportion within the tunnel envelope lies between 50 % and 98 %. The observations indicate that there exists a possibility of the presence of cohesionless soil between ring# 600 and ring# 700. A wider band reflecting relatively higher

uncertainty in the cohesive soil proportion can be attributed to the lack of boreholes between ring# 600 and ring# 700 (see Figure 4.3). Between ring# 150 and ring# 225, the cohesive soil proportion varies between 70 % and 95 % (95 % CI). The observations indicate a quantifiable probability of encountering cohesionless soil within the tunnel envelope prior to the approximate location of transition 1 from the GBR.

Similarly, the cohesive soil proportion varies between 50 % and 95 % between ring# 530 and ring# 650, indicating the possible presence of cohesionless soil after the spatial location of transition 2 shown in the GBR. Figure 4.9(b) highlights that the cohesionless soil is expected about 100 rings before and 120 rings after the locations of transitions 1 and 2 from the GBR, respectively. The visualization of the soil proportions and the CI bands aid in interpreting the uncertainty in the soil transition locations. The results can be interpreted quantitatively as "At ring# 500, the proportion of cohesive soil (for 95 % CI) within the tunnel envelope ranges between 20 % and 50 % of the excavated soil volume." The quantitative assessment adds insights on expected ground conditions and helps characterize the soil transition location uncertainty compared to the qualitative information in the GBR.

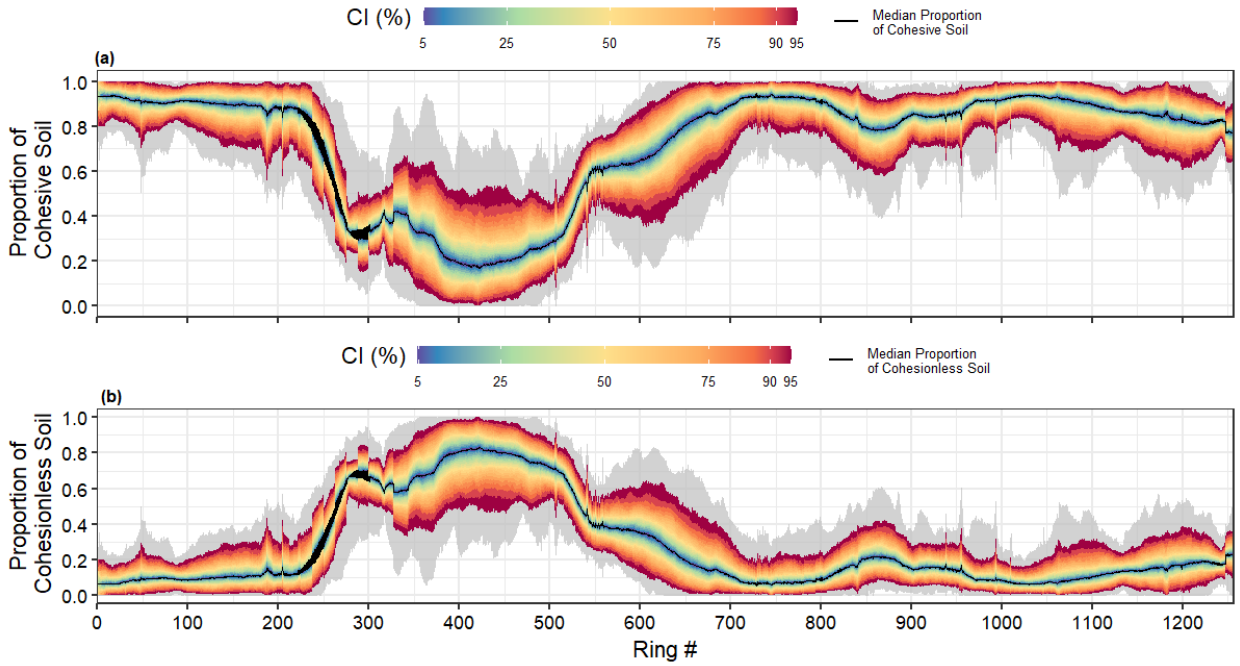

Figure 4.9 Probabilistic profile of cohesive and cohesionless soil proportions along 2 km of the ART tunnel envelope. The black line represents the median proportion of the respective soils. The gray color represents soil proportions from the 460 geostatistical realizations, and the other colors represent the CI.

Figure 4.10 presents the family of ECDF curves generated for soil transitions 1 and 2 for varying cohesive and cohesionless soil proportions encountered within the tunnel envelope. The ECDF curves display the cumulative probability of occurrence of a specific soil proportion versus ring#

and help interpret the ring# for a probability of occurrence of a specific soil proportion. The ECDF is a step function with jumps quantified as *s/S* versus the ring#, where *s* is the number of observations at the ring#, and *S* is the total observations at a spatial location. The higher the number of observations of cohesive/cohesionless soil proportions at a ring#, the higher the rate of increase of the soil's cumulative probability of occurrence. The cumulative probability of occurrence, F_x, of specific cohesive and cohesionless soil proportions is calculated from Eq. (4.2). Figure 4.10(a) shows that as the TBM approaches soil transition 1, there is a 95 % probability of occurrence (P_{95}) of a 10 % or greater proportion of cohesionless soil within the tunnel envelope at ring# 215. The observation is notable because the deterministic soil profile from the GBR does not discuss and show cohesionless soils until about ring# 260.

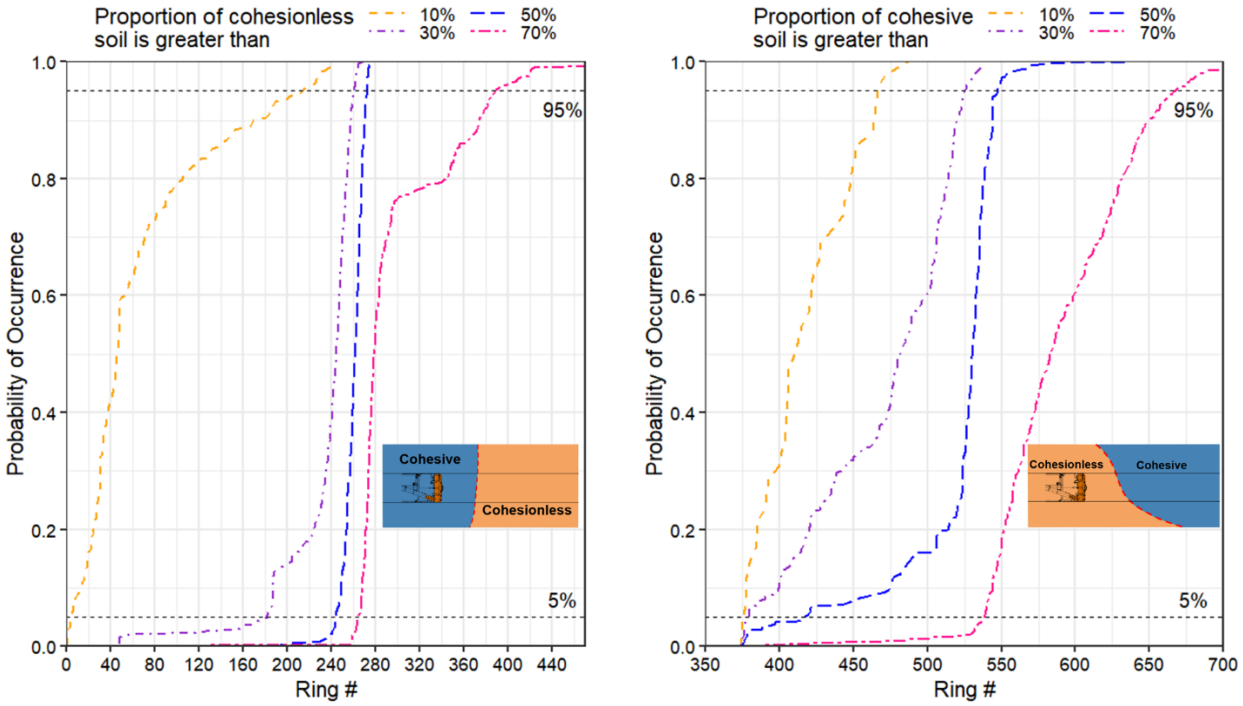

(a) Transition 1 **(b) Transition 2**

Figure 4.10 Family of empirical cumulative distribution function (ECDF) curves for varying proportions of (a) cohesionless soil for transition 1 and (b) cohesive soil for transition 2, within the tunnel envelope.

P_{95} observations from the ECDF curves for soil transition 1 indicate that the cohesionless soil proportion within the tunnel envelope increases from 10% to 50% over a longitudinal distance of approximately 60 rings (or 108 m with ring length = 1.8 m). The cohesionless soil proportion increases from 30 % to 50 % over about 20 rings. The family of ECDF curves for soil transition 1 are clustered, reflecting the increased cohesionless soil proportion over short longitudinal

distances. In comparison, the family of ECDF curves for soil transition 2 are relatively more spaced out, indicating a slow and gradual transition from cohesionless to cohesive soil. P_{95} observations from the ECDF curves for soil transition 2 indicate that the cohesive soil proportion within the tunnel envelope increases from 10 % to 50 % over a longitudinal distance of approximately 80 rings (about 160 m). A key observation from Figure 4.10(b) is that at ring# 550, the probability of encountering a proportion of cohesive soil greater than 70 % is only about 20 %, highlighting the possible presence of cohesionless soil within the tunnel envelope. However, the GBR profile does not show cohesionless soil within the tunnel envelope after ring# 520. The uncertainty in soil transition location for varying CI, expressed in terms of longitudinal distances, can be extracted from the ECDF curves. Soil transition location uncertainty for a specific CI, denoted as U_{CI}, and for a proportion of cohesive/cohesionless soil can be evaluated as shown in Eq. (4.6).

$$U_{CI} = (Ring\#)_{P_{\left(\frac{100+CI}{2}\right)}} - (Ring\#)_{P_{\left(\frac{100-CI}{2}\right)}} \tag{4.6}$$

where CI is the confidence interval, and $(Ring\#)_{Px}$ is the ring# for a probability of occurrence for a proportion of cohesive/cohesionless soil from the ECDF curves. Table 4.2 summarizes the uncertainty in the locations of soil transitions 1 and 2 for 90 % CI, U_{90}, using the ECDF curve showing a greater than 50 % proportion of cohesive/cohesionless soil from Figure 4.10.

Table 4.2 U_{90} in the location of soil transitions 1 and 2 for the ECDF curve showing a 50 % proportion of cohesive/cohesionless soil.

	Ring# for P_5	**Ring# for P_{95}**	**Transition Ring# from GBR**	***U_{90}* (#Rings)**	***U_{90}* (distance, m)**
Transition 1	247	275	260	28	50
Transition 2	420	550	520	130	234

Note: *P = Probability of occurrence; Longitudinal length of the ring = 1.8 m.*

A key observation from Table 4.2 is the difference in the location uncertainty of soil transitions 1 and 2. The width of the uncertainty band, U_{90}, for soil transition 2 is almost five times that of soil transition 1. A broader uncertainty in the proximity of soil transition 2 is possibly due to the lack of boreholes and knowledge of the ground conditions. Figure 4.11 presents locations with a greater than 10 % and 50 % proportion of cohesive/cohesionless soil (P_{95}), in terms of ring# superimposed on the most-probable ground conditions along with the deterministic interpretation from the GBR. The black line in Figure 4.11 represents the transitions between cohesionless and cohesive material, as interpreted in the soil profile in the GBR. Investigation of the uncertainty results for soil transition 1 reveals that cohesionless soil greater than 10% of total soil volume is expected to occur at ring# 215 (P_{95}), about 50 rings before the transition suggested in the GBR. For soil

transition 2, a cohesive soil proportion greater than 10 % and 50 % (P_{95}) is expected to occur at ring# 470 and ring# 550, respectively, approximately 50 rings before and 70 rings after the GBR suggested transition location.

The probabilistic approach offers superior and quantitative insights into the expected ground conditions within the tunnel envelope compared to the deterministic soil profile from the GBR. Key outcomes of the probabilistic approach include (a) knowledge of the spatial locations and (b) quantification of the probability of varying cohesive/cohesionless soil proportions within the tunnel envelope. The results aid in quantifying the soil transition location uncertainty expressed in terms of CI. As typically observed on tunneling projects, any additional information about the ground conditions improves the success rate of mechanized tunneling. The knowledge of the spatial extent of U_{90} for soil transitions provides insights into the priority locations for additional geotechnical investigations to improve the understanding of the ground conditions within the tunnel envelope. Relatively large variability in the cohesive soil proportion between ring# 400 and ring# 550 within the tunnel envelope and a wider band of U_{90} for soil transition 2 indicates the need for additional geotechnical investigations. The results from the probabilistic approach can help evaluate the uncertainty in the excavation volume of soils. The probabilistic approach results indicate that the excavated volume of cohesionless soil between ring# 215 and ring# 275 varies from 2500 m^3 to 7700 m^3 (for 154 m^2 full face excavation). The geostatistical modeling-based probabilistic approach can be applied during the tunnel project's procurement stage to estimate the volume of a soil type to be excavated, an important element in planning the management of the excavated material.

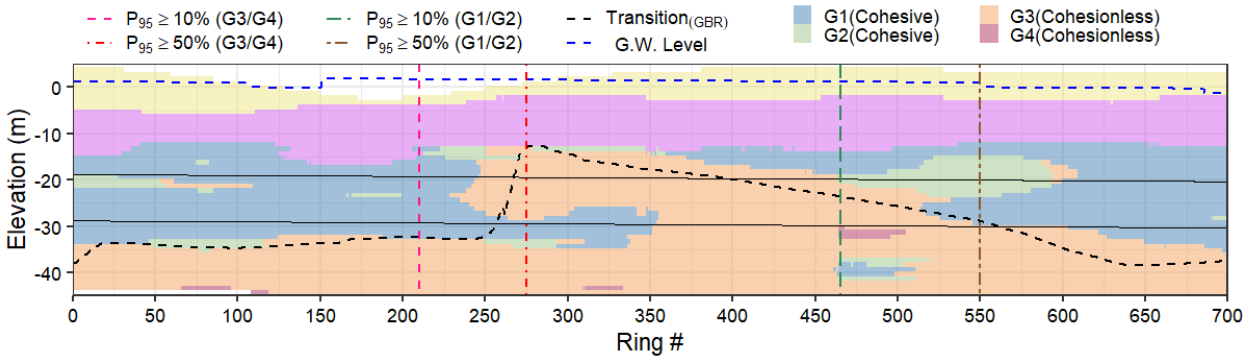

Figure 4.11 The spatial location of transitions (P_{95}) for varying cohesive and cohesionless soil proportions, superimposed on the most-probable model from geostatistical modeling. The black line shows the deterministic interpretation of the boundary between two materials from the GBR.

4.4.3 Soil transition location uncertainty at the TBM face

Soil transitions occurring within the tunnel envelope in the vertical plane parallel to TBM tunneling are also referred to as mixed-face conditions. The current tunneling practice lacks an understanding of the probability of encountering mixed-face conditions along the tunnel alignment. Consequently, the expected elevation of the mixed-ground transition plane within the tunnel envelope is not characterized. The proposed probabilistic approach is applied to quantify

the probability of occurrence of mixed-face conditions and the mixed-ground transition plane elevation uncertainty within the tunnel envelope. The example in this paper focuses on the critical scenario in TBM tunneling of cohesionless soil overlying cohesive soil within the tunnel envelope. For each ring# and each of the 460 geostatistical realizations, the elevations of transition from cohesionless to cohesive material are recorded to generate a distribution of transition elevations.

ECDF curves are generated for each ring# using Eq. (4.3) to quantify the probability of mixed-face conditions for corresponding transition elevations. ECDF curves for mixed-face conditions thus quantify the probability of encountering mixed-face conditions and the probabilistic distribution of the mixed-ground transition plane's elevations. Figure 4.12 presents the example ECDF curves generated for ring# 325 and ring# 1100 for mixed-face conditions where cohesionless soil lies above the cohesive soil within the tunnel envelope. Elevation of the tunnel springline, crown, and invert at each ring# is extracted from the available design tunnel alignment (DTA) for the ART project. For each ring#, the intersection of the ECDF curve with the elevation of the TBM crown, invert, and springline is used to interpret the respective probability of occurrence of mixed-face conditions. The probability of occurrence of mixed-face conditions between certain elevations is calculated as the difference in the probabilities of mixed-ground occurring at the respective elevations. Figure 4.12(a) shows that the probability of encountering mixed-face conditions between the TBM springline and crown is about 13 %, whereas that between the TBM springline and invert is about 80 %. Similarly, in Figure 4.12(b), the probability of encountering mixed-face conditions between the TBM springline and crown is higher (about 83%) than that between the TBM springline and invert (17 %).

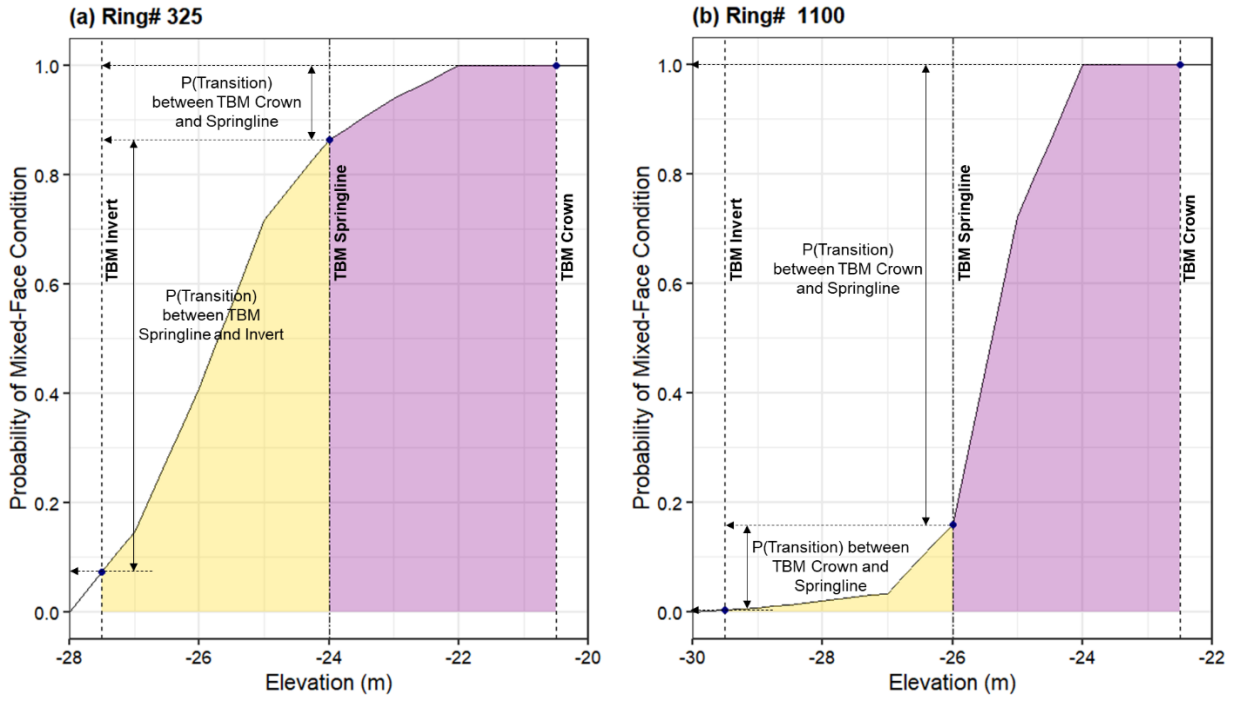

Figure 4.12 Empirical cumulative distribution curves for the elevation of transition from cohesionless to cohesive material within the ART tunnel envelope for (a) ring# 325 and (b) ring# 1100.

Figure 4.13(a) presents the probability of occurrence of mixed-face conditions within the tunnel envelope for the longitudinal length of tunnel alignment. As shown between ring# 200 and ring# 400, the probability of mixed-face conditions occurring between the TBM springline and invert is higher than between the TBM crown and springline. Between ring# 400 and ring# 600, the proximity of the probability curves indicates the possibility of mixed-face conditions along the TBM springline. This observation can be confirmed from Figure 4.13(b), which illustrates a probabilistic distribution of the mixed-ground transition plane's elevations within the tunnel envelope. The elevations presented herein are with respect to the TBM crown. Figure 4.13(b) illustrates the case of mixed-face transition from cohesionless to cohesive soil along with the median elevation of the mixed-face transition. The uncertainty in the mixed-ground transition plane elevations is expressed in terms of CI bands for different probability intervals. The transparency of the CI bands represents the uncertainty in the elevation of the transition plane. Relatively wider bands (higher uncertainty) are observed at locations with a low density of investigations or no investigations (see Figure 4.3). Figure 4.13(c) presents the percentage of geostatistical realizations indicating the occurrence of mixed-face conditions along the tunnel alignment. Results show that more than 50 % of 460 geostatistical realizations indicate mixed-face conditions between ring intervals 50 and 100, 200 and 400, and 500 and 600. The percentage of realizations exhibiting mixed-face transition remains consistently below 40 % between ring# 600 and ring# 1100, indicating a low probability of mixed-ground occurrence at the tunnel face.

An integrated review of the results from the framework provides quantitative insights in understanding the occurrence of mixed-face conditions and the tunnel excavation environment compared to the ground profiles from the GBR. For example, the results from the probabilistic approach in Figure 4.10 and Figure 4.13 can be interpreted as: "Between ring# 200 and ring# 300, the probability of occurrence of mixed-face conditions varies between 60 % and 90 %. The mixed-face conditions are expected to occur between the TBM springline and the invert with the transition plane occurring between 3 m and 5 m (elevations with respect to TBM crown) for 50 % CI." The probabilistic approach results help identify the spatial locations where mixed-face conditions are expected to occur, the probability of occurrence of mixed-face conditions, and the mixed-ground transition plane elevation uncertainty along the tunnel alignment.

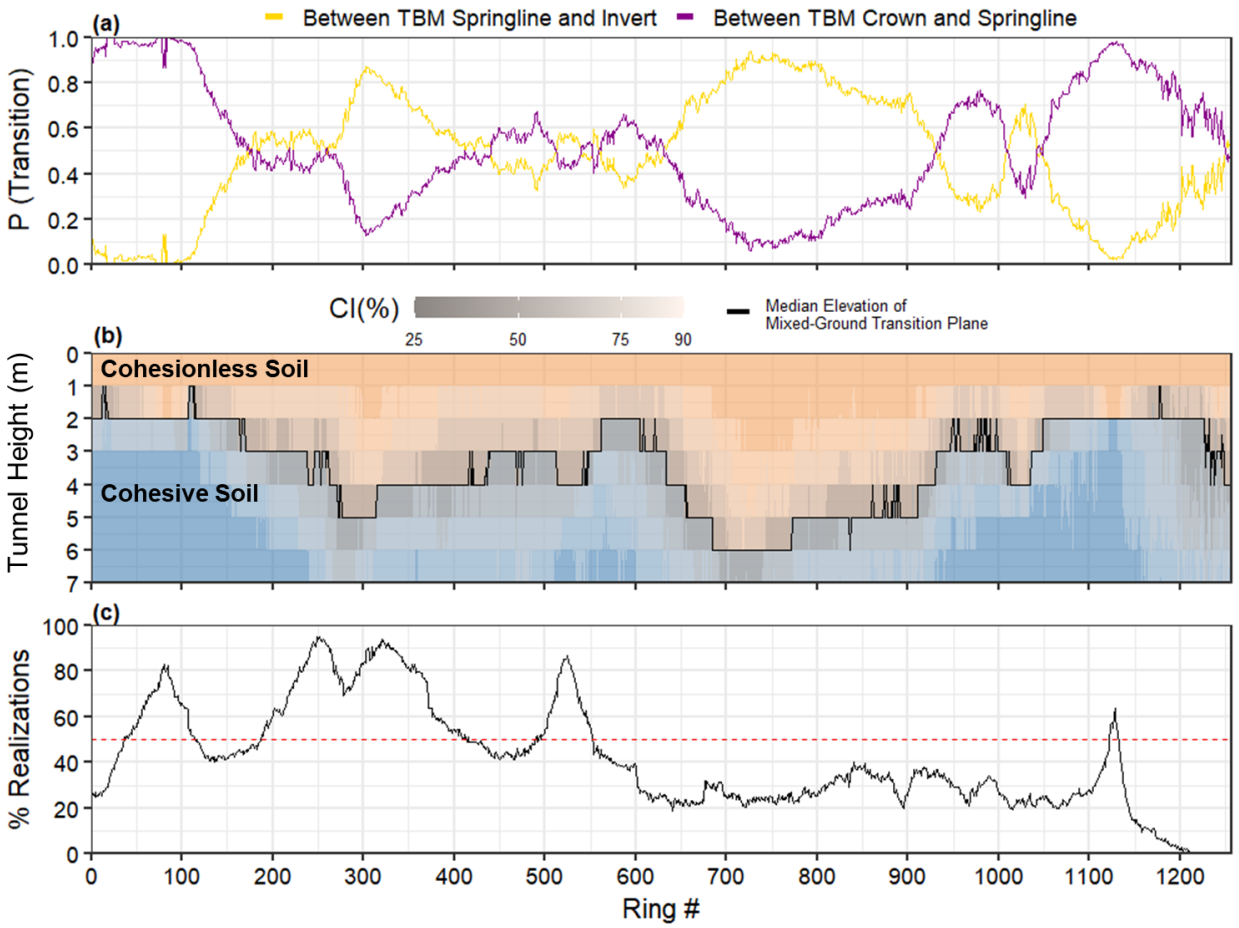

Figure 4.13 (a) The probability of vertical transition from cohesionless to cohesive soil within the ART tunnel envelope. (b) The distribution of elevation (normalized to TBM crown) of the mixed-ground transition plane. The black line indicates the median elevation of the transition plane. (c) The percentage of geostatistical realizations showing the mixed-ground conditions.

4.5 Field validation of probabilistic assessment

4.5.1 Using EPBM operation data

The efficacy of the probabilistic approach in characterizing the uncertainty in soil transition locations is examined using the EPBM operation data from the ART project. Specifically, we use the rate of chamber pressure dissipation at the tunnel springline to identify the occurrence of soil transitions. Bezuijen and Dias (2017) showed that earth pressure balance tunneling in saturated sand with foam conditioning would generally exhibit a reduction in chamber pressure during standstill. During standstill, the soil-foam mixture in the chamber will have a higher pressure than the pore water pressure in the formation soil at the EPBM face. The resulting dissipation of chamber pressure is strongly influenced by the hydraulic conductivity of the soil immediately in front of the cutterhead. Yu et al. (2020) further advanced the model proposed by Bezuijen (2002) and discussed the seepage rate at the excavation face of the EPBM. Eq. (4.7) presents the analytical solution for the chamber pressure dissipation as presented by Bezuijen and Dias (2017).

$$y = y_o + (y_o - y_f)e^{-\alpha t} \tag{4.7}$$

where y_f is the pore water pressure far from the tunnel, y_o is the absolute pressure in the mixing chamber, α is the rate of dissipation, and t is time in minutes. The rate of dissipation (α) is directly proportional to the permeability (k) of the material at the tunnel face. From Bezuijen and Dias (2017), rate of dissipation (α) is presented as shown in Eq. (4.8).

$$\alpha = \frac{\pi R k {y_o}^2}{c \rho g} \tag{4.8}$$

where, R is the tunnel radius in meters (m), k is the permeability of soil at the tunnel face (m/sec), y_o is the absolute pressure in the mixing chamber, c is a constant, ρ is the density of water in kN/m^3, and g is the gravity in m/sec^2.

From the ART project GBR, the baseline permeability of (G1/G2) cohesive soils is considered to be, $k_c \in$ [1E-9 to 1E-6] m/s, and the permeability of (G3/G4) cohesionless soils is considered to be, $k_s \in$ [1E-6 to 1E-3] m/s. As per the model proposed by Bezuijen and Dias (2017), a higher proportion of cohesionless soil at the EPBM face will lead to a faster dissipation of chamber pressure during EPBM standstill. It is to be noted that Bezuijen's model considers permeability of uniform soil type at the tunnel face. For this study, interpretation of chamber pressure decay from Bezuijen's model is used only to validate the dominant soil type at the tunnel face, as derived from the probabilistic assessment. The analytical model presented in Eq. (4.7) is fit to the EPBM chamber pressure dissipation observed in the ART project to determine the rate of dissipation (α). Figure 4.14 presents an example fit of analytical model to pressure dissipation observed at the end of excavation of ring# 312. The goodness of the fit is presented in terms of residual sum of squares (RSS) that measures the level of variance in the residuals. The rate of dissipation (α) is used to

obtain the permeability of soil (k_{soil}) at the tunnel face from Eq. *(4.8)*. For ring #312, the derived k_{soil} = 2.2E-4 m/s falls within the permeability baseline values k_s, indicating that cohesionless soils (G3/G4) is the predominant soil type at ring# 312. Similarly, k_{soil} = 5.3E-7 m/s at ring# 585 indicates presence of high proportion of cohesive soils (G1/G2) at the tunnel face. Figure 4.15 shows the maximum dissipation of EPBM chamber pressure during standstill at the tunnel springline for sections of the ART alignment in the proximity of the soil transitions. Locations of transition suggested in the GBR and from the probabilistic approach (for P_{95}) are presented.

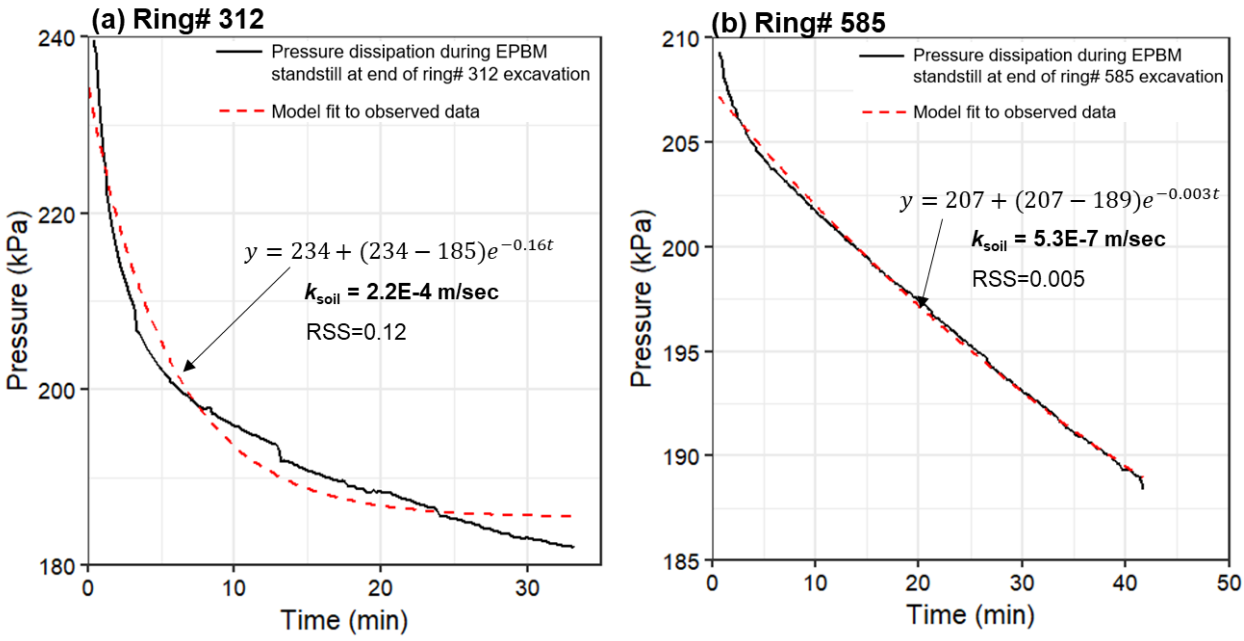

Figure 4.14 Analytical fit to the pressure reduction in EPBM chamber at end of excavation of (a) ring# 312, and (b) ring# 585.

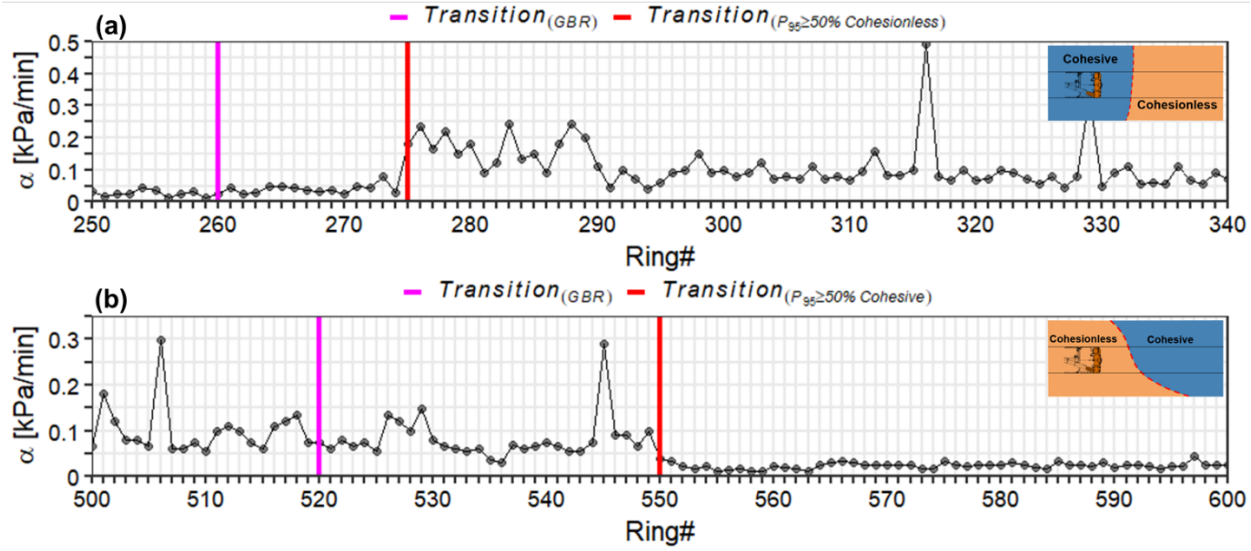

Figure 4.15 Rate of dissipation of EPBM chamber pressure as determined from the analytical fit to chamber pressure drop during EPBM standstill, in proximity of (a) soil transition 1 and (b) soil transition 2. Pink and red lines indicate the soil transition from GBR and probabilistic approach, respectively.

Figure 4.15(a) shows that the maximum EPBM chamber pressure dissipation rate between ring# 250 and ring# 274 is between zero and 0.05 kPa/min, except at ring# 273, where rate of dissipation is relatively high. A sharp increase in the rate of dissipation of chamber pressure up to about 0.25 kPa/min is observed from ring #275 onwards. It is important to note that the groundwater level within the soil transitions' tunnel sections is consistent (see Figure 4.11). Given no change in the overburden and geostatic groundwater conditions, the observed increase in chamber pressure decay rate is very likely a result of formation soil permeability increase at the face.

From ring# 275, the observed relatively high rates of maximum chamber pressure dissipation indicate the presence of highly permeable cohesionless soil in relatively high proportions at the EPBM face. Rate of chamber pressure dissipation ≤ 0.05 kPa/min, between ring# 250 and ring#273 indicate the presence of relatively high proportion of low permeability cohesive soil at the EPBM face. The observations reveal that the transition from cohesive to cohesionless soil, within the tunnel envelope, does not occur at or near ring# 260, as indicated in the GBR. An analysis of locations of longitudinal soil transitions and mixed-face conditions from the probabilistic approach shows a higher proportion of cohesionless soil at the EPBM face from ring# 275 (see Figure 4.10 and Figure 4.13 (b)).

Figure 4.13(b) shows that the proportion of cohesionless soil within the tunnel envelope increases as the mixed-ground transition plane between cohesionless and cohesive soil is predicted to occur between the EPBM springline and invert. Relatively high pressure rates of chamber pressure dissipation, between -0.05 and 0.5 kPa/min, in the tunnel section from ring# 275 to ring# 340 correspond with the increased proportion of cohesionless soil at the EPBM face. An investigation of the maximum chamber pressure dissipation in the proximity of soil transition 1 confirms that

the transition from cohesive to cohesionless soil occurs (P_{95} for a 50 % or greater proportion of cohesionless soil at the EPBM face) at ring# 275, as interpreted from the probabilistic approach.

Figure 4.15(b) presents the maximum chamber pressure decrease during standstill within the tunnel section in the proximity of soil transition 2. The maximum chamber pressure dissipation at the tunnel springline during EPBM standstill, between ring# 500 and ring# 540, varies between 0.05 and 0.3 kPa/min. From ring# 550, the maximum dissipation of chamber pressure decreases and is observed to be less than 0.05 kPa/min, indicating a change in the soil type at the EPBM face. The observed large decrease in chamber pressure between ring# 500 and ring# 550 indicates the presence of highly permeable cohesionless soil at the EPBM face in relatively large proportions. The dip in maximum chamber pressure dissipation beyond ring# 550 indicates the presence of cohesive soil in equal or relatively higher proportions as compared to cohesionless soil at the EPBM face. The variation in the rate of chamber pressure dissipation beyond ring# 550 is possibly due to a longer EPBM standstill period. The probabilistic approach shows that the transition from cohesionless to cohesive soil (P_{95} for 50 % or greater proportion of cohesive soil at the EPBM face) occurs at about ring# 550. The probabilistic approach results are found to correspond to the observations of maximum chamber pressure dissipation from recorded EPBM data.

4.5.2 Data-driven model for as-encountered ground conditions

In another validation approach, the results from the geostatistical modeling-based probabilistic approach were validated with the as-encountered ground conditions derived from a data-driven model. To proceed with the validation, a representation of the actual ground conditions within the tunnel envelope is required. However, excavation using closed-face mechanized shield machines do not allow for a continuous inspection of the ground conditions at the tunnel face. To overcome this limitation, Yu and Mooney (2021) utilized earth pressure balanced machine (EPBM) operation and reaction data while tunneling to characterize the as-encountered ground type. Their approach involved using supervised learning (SL) and semi-supervised learning (SSL) methods to interpret the occurrence probability of soils at each ring along the tunnel alignment. The work concluded that both data-driven models could generate trustworthy inferences of ground conditions using EPBM data; however, the SSL model agreed better with the geologist's interpretation of ground conditions.

To characterize the as-encountered ground conditions within the Anacostia River Tunnel (ART) project, soil fractions within the tunnel envelope were extracted from 43 boreholes by associating the boreholes to the nearest ring. From the EPBM operational data, Yu and Mooney (2021) utilized thrust force, advance rate, cutterhead rotation speed, cutterhead torque, chamber pressure at springline and its vertical gradient, screw conveyor rotation speed, screw conveyor torque, and excavated soil mass were used for training the SSL model. Therefore, each ring was represented by the aforementioned EPBM operation parameters and the estimated soil fractions within the tunnel envelope for the SSL model training. The data-driven models thus utilize the ring-level TBM data rather than only the sparse boreholes for prediction. Therefore, the results from the SSL model can be considered reliable to validate the occurrence of transitions at a finer resolution. For a comprehensive understanding of SSL model construction and its performance, the reader is referred to Yu and Mooney (2021). Figure 4.16 presents the longitudinal profile of the as-encountered ground conditions within the tunnel envelope inferred from the SSL model. Table 4.3

compares the soil transition locations from the probabilistic assessment, geotechnical baseline report (GBR), and the SSL model.

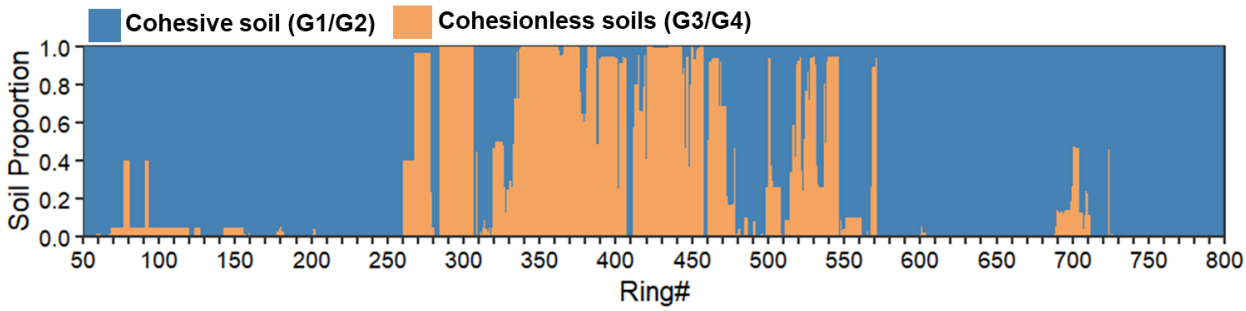

Figure 4.16 Inferred geological profile within the tunneling envelope of ART project as per the SSL model (after Yu and Mooney 2021).

Table 4.3 Comparison of soil transition locations (longitudinal direction) from the probabilistic approach, data-driven model (Yu and Mooney 2021), and GBR.

Soil Transition	**Ring# (P_{95}) from the Probabilistic approach**	**Ring# from SSL model (Yu and Mooney 2021)***	**Ring# from GBR**
Transition 1 (cohesive to cohesionless)	275	268	260
Transition 2 (cohesionless to cohesive)	550	547	520

**Transition is considered to occur when cohesive/cohesionless soil proportion within tunnel envelope is ≥ 50 %.*

The presented field evaluation using EPBM operation data demonstrates the capability of the proposed probabilistic approach in identifying soil transitions within the tunnel envelope. The probabilistic approach results provide an improved understanding and quantifiable characterization of soil transition locations compared to the interpretations from the GBR. The practical benefits of the proposed probabilistic approach include (i) estimating the maximum dissipation of chamber pressure during prolonged EPBM standstill, (ii) estimating the volume of soil excavated for better management of excavated material, and (iii) identifying locations for additional geotechnical investigations and laboratory testing.

The efficacy of the geostatistical modeling-based approach in capturing soil transition locations in a tunnel project situated in a glacial geological environment (relatively more heterogeneous geological setting) and validation with the data-driven is presented in Appendix B. The assessment presented above is based on the results from the PGSIM technique. It is acknowledged that the

results from the probabilistic approach are sensitive to the applied geostatistical modeling technique. TPROGS modeling technique is applied to simulate the soil conditions within the ART tunnel envelope. A comparison of the TPROGS technique with the PGSIM technique and field validation from rate of EPBM chamber pressure dissipation is documented in Appendix C.

4.6 Conclusions

Lack of characterization of uncertainty in transitions between stratigraphic units with different compositions and different geological and mechanical properties within the tunnel envelope prior to tunnel construction remains a challenging issue for successful and safe mechanized tunneling. For tunnels or any other large-scale geotechnical projects where infrastructure is installed into the subsurface, the owner, contractor, and involved stakeholders generally prefer to work with a quantitative rather than a qualitative assessment of stratigraphic transition uncertainty. To address this problem, this study presents a geostatistical modeling-based probabilistic approach to characterize the stratigraphic transition location uncertainty within the tunnel envelope. The geostatistical modeling method adopted herein utilizes the PGSIM modeling technique, a transition probability, and a variogram-based geostatistical method for modeling soil units.

The proposed probabilistic approach is applied to geotechnical SI from a 2 km section of the ART project. In terms of ESUs, the available borehole data is used to generate multiple equiprobable realizations of ground conditions. The realizations are post-processed using probabilistic tools—ECDF curves and CI. The proportions of soils within the tunnel envelope are visually characterized using CI and are quantified using ECDF curves. The interpretations are used to characterize the probability of occurrence of stratigraphic units, soil units in this case, along the longitudinal length and vertical plane of the tunnel envelope. The realizations are further used to characterize the soil transition location uncertainty and mixed-ground transition plane elevation uncertainty within the tunnel envelope. The results from the proposed probabilistic approach are examined with EPBM operation data from the ART project and are quantitatively compared to the deterministic soil profile from the GBR. The main conclusions of this study are as follows:

i. The geostatistical modeling-based probabilistic approach allows for an intuitive visualization and a quantitative interpretation of the expected soil proportion within the tunnel envelope. For example, the results may be interpreted as follows: “At ring# 500, the proportion of cohesive soil (for 95 % CI) is expected to be between 20 % and 50 % of the excavated soil volume.”
ii. ECDF curves serve as a robust tool to quantify the probability of occurrence of varying soil proportions within the tunnel envelope. The difference in probabilities from the ECDF curves helps evaluate the uncertainty in the soil transition locations in terms of CI, offering quantitative insights into the expected ground conditions compared to the deterministic evaluations from the GBR.
iii. A key outcome of the probabilistic approach is quantifying the probability of occurrence of mixed-face conditions and the mixed-ground transition plane elevation uncertainty. For example, the study results indicate that between ring# 200 and ring# 300, the probability of occurrence of mixed-face conditions (cohesionless soil overlying cohesive soil) at the EPBM face varies between 60 % and 90 %. The mixed-face conditions are expected to occur between the EPBM springline and the invert, with the transition plane occurring between 3 m and 5 m (elevations with respect to EPBM crown) for 50 % CI.

iv. It is feasible to use EPBM operation data to identify the soil transition locations within the tunnel envelope. Locations of soil transitions at ring# 275 and ring# 550, as interpreted from the probabilistic approach, agree with locations where chamber pressure's maximum dissipation at tunnel springline changes. The probabilistic approach results present an improved characterization of soil transition locations within the tunnel envelope when compared to the deterministic interpretations in the GBR.

With the growth in the number of tunnel projects in the urban environment, it is evident that tunnels will be placed in complex ground conditions facing stricter construction constraints. It is worth emphasizing that tunnel risks and failures due to unforeseen ground conditions can be mitigated with a focus on evaluating and quantifying the stratigraphic transition location uncertainty within the tunnel envelope. The improved knowledge of the tunnel excavation environment from this probabilistic approach will help the tunnel designer and contractor to (a) understand the pressure drops during prolonged standstill periods to mitigate the possibility of a tunnel face collapse, (b) identify locations of future TBM interventions, (c) estimate the volume of excavated soils, and (d) identify locations of additional geotechnical SI, laboratory testing, and instrumentation and monitoring. This work is developed with a vision to be used as a tool by tunneling contractors and involved stakeholders to improve overall ground awareness prior to starting construction for safe and efficient tunnel construction performance.

CHAPTER 5- PROBABILISTIC ASSESSMENT OF VOID RISK AND GROUTING VOLUME FOR TUNNELING APPLICATIONS

5.1 Abstract

Tunneling in karstic geology confronts numerous challenges due to unpredictable occurrence of voids. The current approach of karstic void risk assessment is qualitative or semi-quantitative and lacks consideration of the spatial variability and distribution of voids. This often influences the pricing strategies, and design and construction activities on tunnel projects. This paper presents a geostatistical modeling-based methodology to develop a quantitative assessment of karstic void risk for a tunnel project in a karstic geological setting. The methodology is applied on an actual mixed-ground tunnel project situated in a karstic geological environment in Malaysia. The geology at the tunnel project site consists of sedimentary rock formations with limestone as the predominant rock type overlain by weak sedimentary residual soils. Pluri-Gaussian simulation (PGSIM) technique, a stochastic geostatistical–modeling algorithm, is applied to characterize the spatial distribution of voids in 3D along tunnel alignment. PGSIM realizations take into consideration the anisotropic distribution of voids on the tunnel project site. PGSIM utilizes void data from borehole investigations to model different void sizes (V_s) as categorical variables. The variability in multiple realizations from PGSIM technique is used to quantify the uncertainty in occurrence probabilities, number, and frequency of karstic voids. The proposed methodology demonstrates the ability to develop probabilistic estimates of occurrence frequency of different void sizes. Probabilistic assessments indicating 95 % confidence interval (CI) on number of voids and respective occurrence probabilities are presented. The probabilistic assessment results are applied to estimate the grout quantity required for void treatment, while considering uncertainty in void occurrence. A minimum, mean, and maximum cumulative grout volume of about 2,000 m^3, 4,000 m^3, and 8,000 m^3 (for 95 % CI), respectively, is estimated along the alignment.

5.2 Introduction

5.2.1 Context and Motivation

For any tunnel project, the largest technical and financial risk element usually lies in the ground, predominantly due to the spatial variability in ground conditions and specific ground features that affect tunneling. The spatial variability and the associated uncertainty, especially of critical ground features, need to be carefully assessed and considered in the planning, design, and construction phases of tunnel projects. One such ground feature affecting tunneling is the solution cavities and voids formed due to the dissolution of limestone or gypsum in karstic geological environments. For tunnel projects planned in geological formations exhibiting karstic features, the detection of voids in the driving path of the tunnel boring machine (TBM) has always been a critical issue. Tunnel excavation in a karstic geological setting can induce severe geotechnical hazards leading to high construction costs and schedule delays (Yau et al. 2020). Ren et al. (2016), Zarei et al. (2010), Shahriar et al. (2008), Day (2004), and Xeidakis et al. (2004) presented a summary of the karst-related geotechnical hazards from tunneling in a karstic geological setting for multiple tunnels in Iran and the adopted mitigation measures. Zabidi and De Freitas (2013), Boon et al. (2020), Cui et al. (2015), and Wang et al. (2020) discussed the design and construction problems due to karstic features in Kuala Lumpur and China. These case studies from Kuala Lumpur and

China indicate that unpreparedness in estimating karstic features has been an influencing factor in geotechnical hazards due to karstic feature presence.

Eskesen et al. (2004) determined that geotechnical hazards due to tunneling predominantly result from an inadequate level of site investigations or failure to comprehend the information from site investigations. Typically, with limited and sparse geotechnical site investigations on tunnel projects, there exists significant uncertainty regarding the location and occurrence frequency estimates of karstic voids. Irregular distribution of the karstic voids and their various shapes and sizes compounds the problem of evaluating the void fraction within the tunnel envelope. Like any other tunnel risk, karstic risk assessments are included in the geotechnical baseline report (GBR). Interestingly, although GBRs are used increasingly to demarcate risk allocation and resolve any financial disputes, the karstic risk evaluation incorporated in GBRs is qualitative or semi-quantitative (Yau et al. 2020). More importantly, the GBR assessments lack consideration of the spatial variability and distribution of the karstic voids. The qualitative or semi-quantitative risk assessments from the GBR may result in overbidding or underbidding on the project, depending on the tunnel contractor's perspective. Tunnel design and construction decisions based on GBR assessments can influence the project pricing and construction means and methods and can potentially result in an increased number of differing site condition (DSC) claims.

5.2.2 Background

Karstic features are formed by the dissolution of sedimentary formations of soluble carbonate rock, such as limestone or dolomite. These features can also develop in other rock types, such as gypsums/ salt-rich formations, or less commonly in quartzite formations (Piccini and Mecchia 2009). Interaction of the mildly acidic water with weakly soluble carbonate rocks results into development of karstic features. Duringer et al. (2012) discussed a two-stage process – (i) rain water interacting with carbon dioxide to form carbonic acid, and (ii) percolation of acidic water through soil to dissolve the carbonate rocks. The rate of dissolution depends on the strength of the acidic water and the presence of pre-existing fractures, joints, bedding planes, and discontinuities in carbonate rocks.

Over time, the openings in rock increase in size, and intersect the groundwater regime, resulting into a significant construction risk of water inflow in underground construction and tunneling projects. In tunnel construction, typically watertight segmental concrete liners are installed around the tunnel opening to arrest the water ingress. However, the performance of the segmental liners can be affected due to unevenly applied ground stress in void-filled ground. A lack of knowledge of the karstic feature distribution can lead to unforeseen changes in hydraulic pressures, resulting in face stability issues, tunneling-induced settlement, subsidence, and sinkhole formations during shield tunneling.

A number of studies have attempted to examine the spatial variability of karstic features. Paraskevopoulou and Benardos (2013) determined that the spatial variability and the associated risk of uncertainty need to be carefully considered and assessed prior to tunnel design and construction as encountering unforeseen conditions could lead to catastrophic delays and cost overruns. Ford and Williams (2013) highlighted the uncertainty arising from the spatial variability of karstic voids. Zabidi and De Freitas (2013) developed a geospatial analysis-based methodology to generate deterministic estimates of karst void fraction in the ground from volumetric analysis

of the boreholes drilled for a tunnel in Kuala Lumpur. Li et al. (2015) quantified the risk of water inrush in tunnels situated in karstic geological setting using fuzzy mathematics and analytical hierarchy process (AHP). Cheng et al. (2017) proposed a fractal analysis model describing the relationship between drilled boreholes and karst caverns' diameters to predict the grouting volume for treating karst caverns along a tunnel alignment. Yau et al. (2020) used a random distribution of karstic voids and developed a numerical model to quantify the impact of karstic voids of water pressure expected and the structural capacity of the tunnel liners. Kovačević et al. (2020) presented a customized neural network (NN) model, trained to learn the complex non-linear relationship between rock mass parameters in karstic environment and tunnel design parameters. However, the study is limited to using empirical correlations to determine reduced rock stiffness in presence of karstic features.

5.2.3 Scope of Work

It is evident from the abovementioned geotechnical hazards that a quantified knowledge of karstic void size, occurrence frequency, and locations of occurrence within tunnel envelope would be beneficial for active risk management and decision-making on tunnel projects. Probabilistic approaches capable of characterizing the spatial variability and the associated uncertainty of subsurface features could be implemented for a comprehensive quantitative assessment. Application and inclusion of probabilistic assessments into the GBR can provide insights into the expected tunnel excavation environment and facilitate improved risk estimation and allocation. In tunneling applications, Grasmick (2019) and Gangrade et al. (2020) employed geostatistical techniques to quantify spatial uncertainties in geotechnical conditions within the tunneling envelope. Grasmick et al. (2020b) used geostatistical simulations to quantify uncertainties and confidence intervals for geotechnical properties relevant to tunneling risks. Gangrade and Mooney (2020) interpreted the geostatistical modeling results to quantify the uncertainty in soil transition locations in the longitudinal and transverse directions to tunneling. Grasmick et al. (2020a) and Gangrade and Mooney (2020) discussed and proposed the incorporation of probabilistic assessments into the GBRs. The study by van der Pouw Kraan (2014) discussed the risk-sharing mechanism on tunnel projects and presented a strong case for incorporating probabilistic assessments and geotechnical uncertainty in tunnel project GBRs. The existing studies on karstic voids are limited in characterizing a qualitative and/or semi-quantitative distribution only.

This paper presents a quantitative assessment of karstic void risk within the tunnel envelope using a geostatistical modeling-based probabilistic approach. The probabilistic assessment applies the pluri-Gaussian simulation (PGSIM) technique, a stochastic geostatistical algorithm, on borehole data from a tunnel project situated in a karstic geological environment. Multiple realizations from stochastic modeling are post-processed to quantify the locations, the sizes, the number, and the occurrence frequency of karstic voids within the tunnel excavation envelope. The paper's motivation is to implement a probabilistic approach to characterize karstic void spatial variability and develop quantitative evaluations for GBR baseline statements such as, "There is a 40 % probability of encountering at least three voids, with a maximum size of approximately 0.5 m between tunnel length X and Y." The study attempts to contribute to the applicability of probabilistic methods towards an elaborate risk assessment of encountering karstic voids within a tunnel envelope, which is currently not taken into account in tunnel projects. The quantitative assessment of karstic voids is utilized to estimate the grout volume required as a part of pre-excavation grouting for treating karstic voids. The improved probabilistic knowledge of voids

would allow the tunnel contractors to better target the required pre-excavation grouting quantities and respective costs.

The next section describes the methodology of the geostatistical modeling-based probabilistic approach to generate quantitative assessments of karstic voids within the tunnel excavation envelope. We then present an application of the proposed methodology on geotechnical site investigations from a tunnel project situated in karstic geology. The probability of occurrence, the expected number, and the occurrence frequency of karstic voids of multiple sizes are quantified and presented.

5.3 Overview of Project Dataset

This study considers a 3 km tunnel section of a 5.8 m diameter tunnel project set in a karstic geological environment and excavated using a shield machine. The exact location and name of the tunnel project cannot be disclosed as authors are bound by a non-disclosure agreement (NDA) with the project owner and involved stakeholders. The geology at the tunnel project site consists of sedimentary rock formations with limestone as the predominant rock type. Based on the borehole investigations, the bedrock consists of limestone, with highly folded and faulted sandstone and shale overlying the limestone. The sedimentary rocks have been regionally metamorphosed to form metasediments. The degree of metamorphism varies across the region. Under low grade metamorphism, quartzites (from sandstone) and phyllite (from shales) have evolved. On the other hand, schist (from shales) has evolved under high grade of metamorphism.

Weak alluvium material, deposited by the major rivers in the region, is found at the surface. The material comprises of loose, unconsolidated soil or sediments. Due to natural sedimentation process, alluvium is typically found to consist of a mixture of clay, silt, sand, and gravels. The bedrock is overlain by sedimentary residual soils that covers most parts of the land in Malaysia. The residual soils in the area are composite soils of sand, silt and clay in varied proportions depending on the geological setting of the soil. For the purpose of this study, weak alluvium and the residual soils are grouped into soil. Various rock types encountered within the tunnel project site are grouped and denoted by rock in the borehole profile. The tunnel alignment is expected to traverse predominantly through soil/limestone interface with intrusions of granite, quartize, phyllite and schist. Interaction of soil water and rainwater with limestone, especially at the soil-rock interface, causes the formation and enlargement of voids.

Waltham and Fookes (2003) discussed that the upper part of the rock mass is more fissured and are progressively isolated from the neighboring rock mass. This leads to formation of isolated, undercut pinnacles of limestone surrounded by soil. Between the remnant pinnacles of limestone, fissures are enlarged and are filled with soil or remain open. Narrow vertical, soil-filled sections are particularly common in porous limestone. At the project site, the karstic voids are typically found to occur within isolated limestone blocks that are left as dissolution remnants within the soil. For simplicity, this study does not account for the void fillings of cohesive or non-cohesive material, and groundwater. Geohazards associated with the karstic limestone on this project include the pinnacle zone (i.e., highly irregular rock head profile, pinnacles alternating with deep troughs) and collapsed weak soil zones or slumped material near the soil rock contact zone. The high variability of the ground conditions within several meters of tunneling is a major issue of

tunneling in karstic limestone on this project. No fault zones exist in the tunnel section discussed in this study.

Historical and recent geotechnical investigations on the tunnel section consisted of 115 continuous-core boreholes drilled vertically at least 20 m to 30 m below the tunnel springline. However, a few boreholes were terminated just about at or above the tunnel springline. Figure 5.1 presents a plan layout of the boreholes vis-à-vis tunnel alignment. Three to four clusters of closely drilled boreholes are observed along the tunnel alignment. The rock quality designation (RQD) of cores ranged between 11 % and 100 %, with a mean, median, and standard deviation of 55 %, 60 %, and 22 %, respectively. The horizontal spacing between the drilled boreholes ranges from 8 m to 150 m with a mean and standard deviation of 35 m and 28 m, respectively. The mean vertical sampling interval within the boreholes for the soil samples is about 1.3 m, whereas the rock cores were continuously logged. This study considers the tunnel envelope to be about 0.2 times the tunnel diameter above and below the tunnel crown and invert, to account for karstic voids present just outside the excavation envelope. For the 5.8 m diameter tunnel, the tunnel envelope is 8.0 m. Figure 5.2 shows a distribution of the horizontal spacing between the nearest-neighbor boreholes and vertical sampling, as observed from investigations. Figure 5.3 shows the boreholes' longitudinal profile and the groundwater level along the tunnel alignment. The groundwater level is consistently found to be near the ground surface.

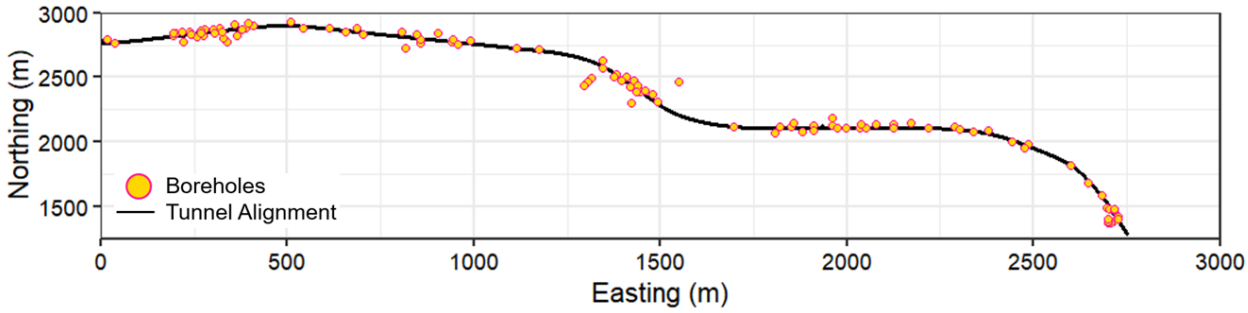

Figure 5.1 Plan view of the tunnel alignment with borehole locations.

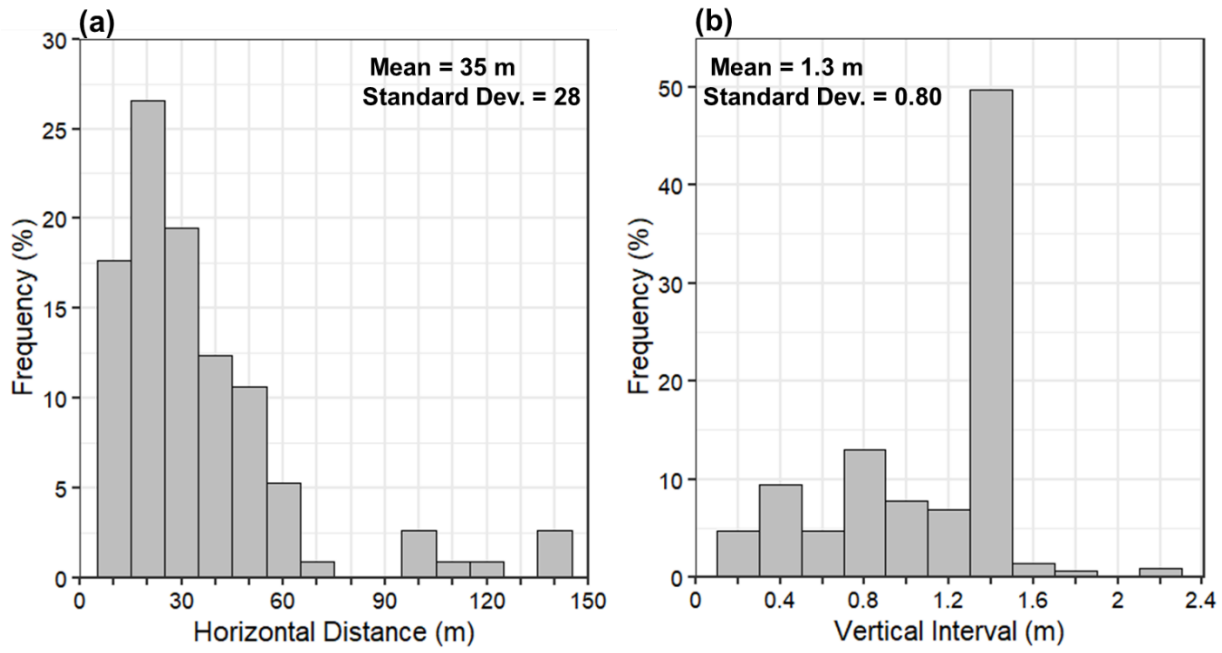

Figure 5.2 Distribution of nearest-neighbor horizontal spacing between the boreholes and vertical sampling within boreholes.

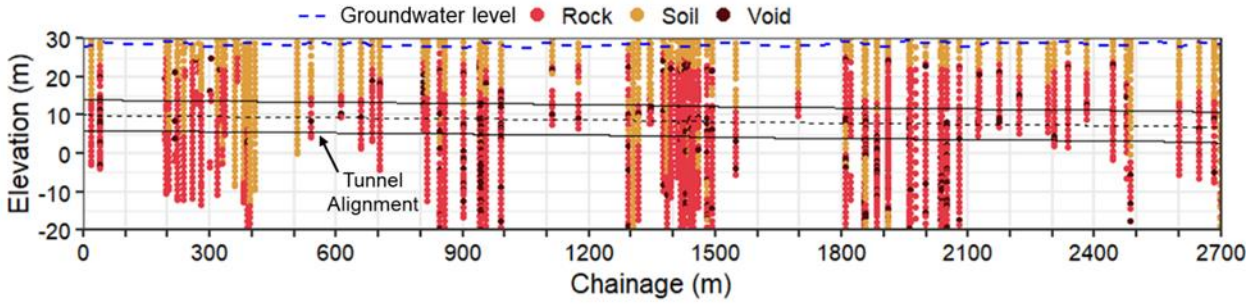

Figure 5.3 Longitudinal profile of the boreholes along tunnel alignment in terms of samples observed during investigations.

The karstic voids are predominantly found at the contact zone of soil and rock formation and within the rock formation. However, a few karstic voids are observed to occur within the soil formation. Tunneling-induced ground settlement or sinkhole development is highly likely to occur, given the weak alluvium material overlying the limestone with karstic voids. Figure 5.4 presents the rock head profile from a karst site in Malaysia and shows presence of voids in isolated limestone blocks surrounded by soil. For the data in the study, we have observed that karstic voids typically occur within isolated limestone blocks that are left as dissolution remnants within the soil.

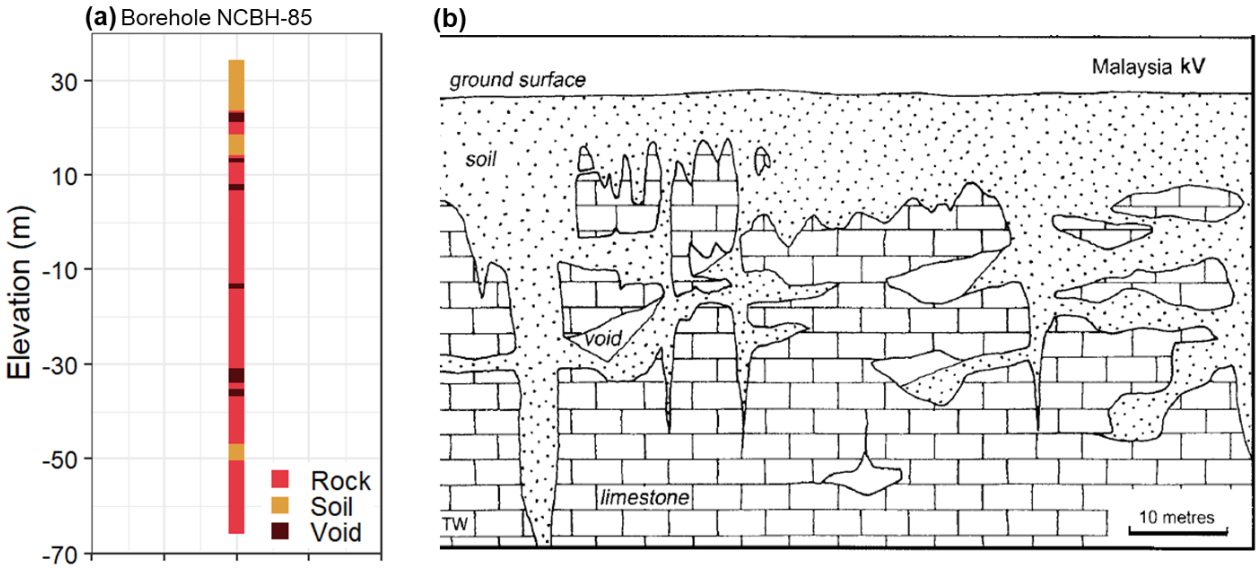

Figure 5.4 Stick log of borehole NCBH-85 (borehole from project data), (b) rock head profile of a typical karst site in Malaysia (Waltham and Fookes 2013).

As illustrated in Figure 5.3, there exists significant variability in the number of voids within the tunnel excavation envelope. A relatively higher density of voids is observed from Chainage 800 m to 1000 m, Chainage 1300 m to 1500 m, and Chainage 1800 m to 2000 m. Figure 5.5 presents the proportion of investigation samples categorized as rock, soil, and voids, and the distribution of void sizes encountered during investigations. The investigations revealed the karstic void size (V_s) to range between 0.1 m and 1.5 m. It is to be noted that void sizes reported and recorded from the drilled boreholes are based on only vertical dimensions. For this study, the voids have been subdivided into three categories based on the void length intercepted by the vertical boreholes: (1) category V1 voids with a maximum size between 0.10 m and 0.25 m inclusive ($0.10\ m \leq V_s \leq 0.25\ m$), (2) category V2 voids with a maximum size between 0.25 m and 0.75 m ($0.25\ m < V_s < 0.75\ m$), and (3) category V3 voids with a maximum size equal to or larger than 0.75 m ($V_s \geq 0.75\ m$). The void grouping is based on data analysis V_s from borehole investigations. Mean (μ) and standard deviation (σ) of V_s are 0.55 m and 0.25, respectively. Half-standard deviation from mean value ($\mu \pm 0.5*\sigma$) was used for size categorization. This comes out to 0.30 m and 0.80 m. The demarcations for void categories were decided to be at 0.25 m and 0.75 m. About 48 % of the voids identified belong to category V2. Category V1 and V3 account for 30 % and 22 %, respectively, of the voids identified during investigations.

The voids are assumed to have a spherical shape, and the void diameter is considered equal to the length of the void intercepted by the borehole. We note that the void's recorded size represents only a certain length of the void intercepted by the vertical borehole. This size is rarely expected to represent the largest dimension of the void, i.e., the diameter in the case of spherical voids. Hence, the measured sizes are likely underestimates of void sizes. Prior work on probabilistic assessment of karstic voids includes applying a randomly generated distribution of spherical-shaped karstic cavities for liner stability assessment and water inflow (Yau et al. 2020). Medley (2002), and Tang et al. (1986) previously investigated the estimation of boulder size in 3D from the 1D measurement of intercepted borehole lengths. The statistically rigorous techniques

identified boulder shapes, boulder orientation, and volumetric proportions as the most important factors in accounting for statistical uncertainty. Felletti and Beretta (2009) assumed spherical boulders and considered the length intercepted by the vertical borehole as its maximum size. The methodology was applied to characterize the boulder occurrence frequency for a tunnel project in glacial till. Figure 5.6 shows a schematic representation considering the intercepted void length as the spherical void diameter. In this study, a void size equal to the void diameter has been used for setting up the 3D grid for geostatistical simulations and probabilistic assessment of the void occurrence frequency. Though the probabilistic modeling approach presented herein is limited to the assumption of a spherical shape for the karstic voids; the approach is not limited to a specific void shape and can be applied to any void geometry.

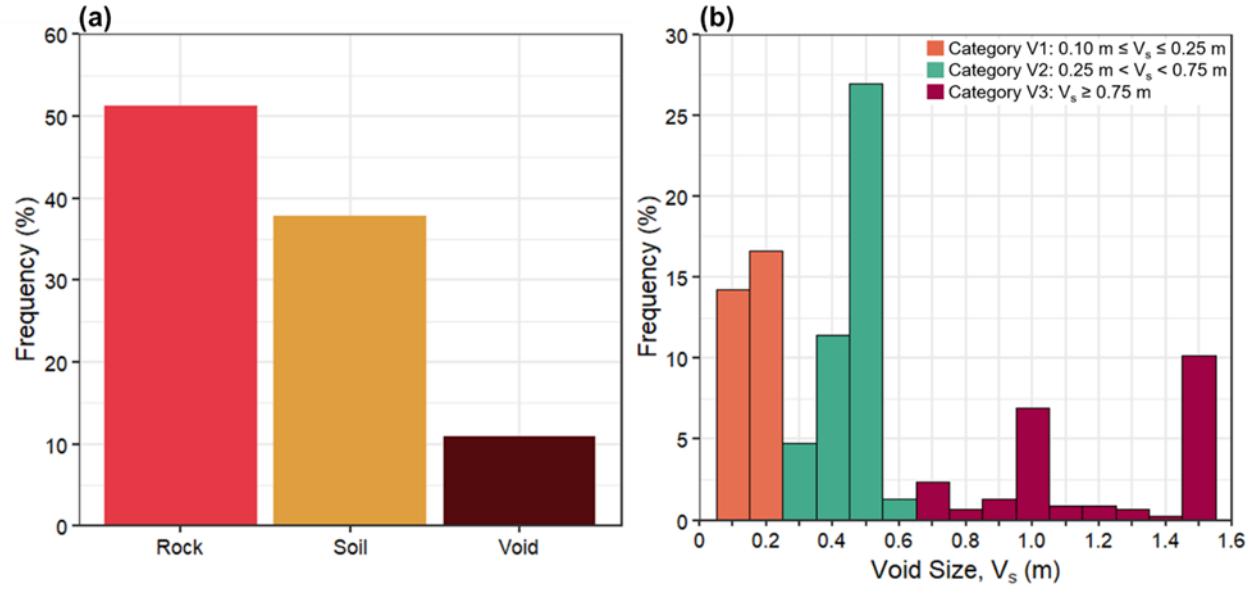

Figure 5.5 Distribution of (a) samples observed during investigations and (b) void sizes encountered within boreholes.

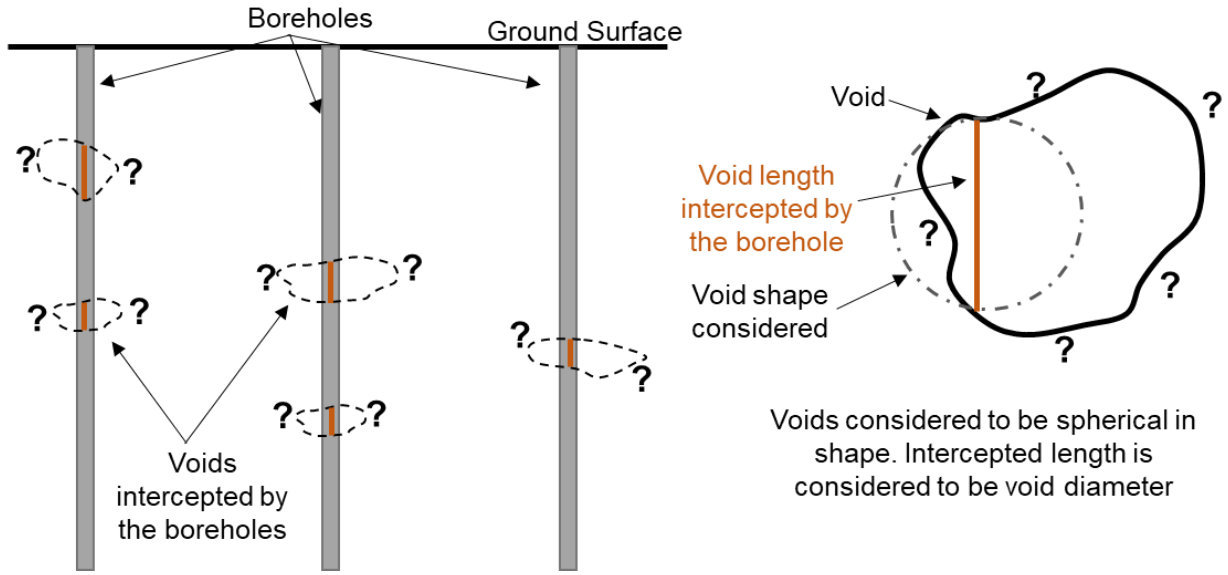

Figure 5.6 Void geometry considered for the probabilistic estimation of void number and occurrence frequency.

Figure 5.7 presents the voids' longitudinal profile, subdivided into the three abovementioned categories, vis-à-vis tunnel alignment. Category V1 and V2 voids are observed in the initial 100 m of the tunnel envelope (tunneling left to right). Category V3 voids are frequently observed for the next 800 m of the tunnel envelope. A higher density of all three void categories is observed from Chainage 800 m to 1500 m and from Chainage 1800 m to 2200 m. All three void categories are observed in the borehole cluster from Chainage 800 m to 1000 m and from Chainage 1800 m to 2200 m. The borehole cluster between Chainage 1200 m and 1500 m exhibits category V2 and V3 voids in dominant proportions. From Chainage 2200 m onwards, the number of observed voids decreases up to about Chainage 2600 m. This could be due to the lower density of boreholes within the section. A cluster of voids is observed after Chainage 2600 m. The high density of logged boreholes within the project site provides an excellent opportunity to assess the karstic void occurrence quantitatively. However, as observed in Figure 5.3 and Figure 5.7, there are gaps in the void occurrence data due to the absence of dense boreholes from Chainage 400 m to 800 m, Chainage 1000 m to 1300 m, and Chainage 1500 m to 1800 m.

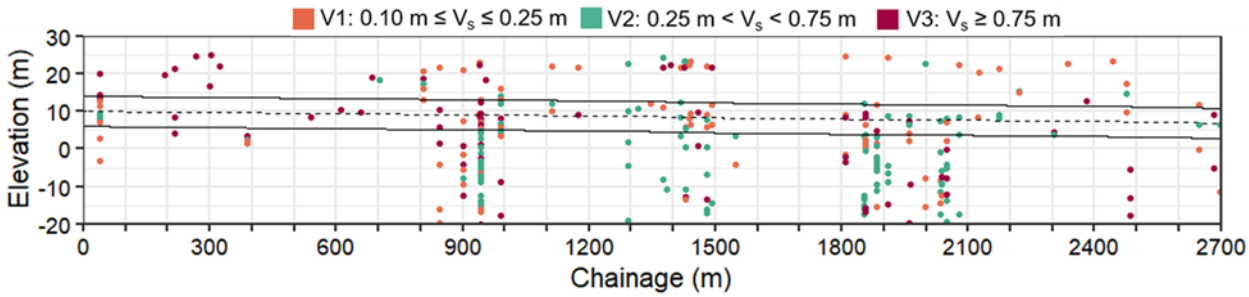

Figure 5.7 Longitudinal profile of the voids along the tunnel alignment. Voids are categorized based on the sizes observed during investigations.

5.4 Methodology

The methodology begins with exploratory data analysis of the geotechnical investigations on the project site. The data analysis aims to identify the range of karstic void sizes to set up a 3D simulation grid for geostatistical modeling. The decision on the resolution of the 3D grid in the longitudinal (*x*-*y* plane), transverse, and vertical (*y*-*z* plane) directions is based on the karstic void sizes. Karstic voids encountered within boreholes are subdivided into categories based on the void sizes encountered during investigations. The aim of categorizing the voids is to comprehend the occurrence frequency of different sizes of karstic voids. The methodology assumes a void shape and size based on the intercepted length of void within a borehole. Conversion of the intercepted borehole length to void size is discussed in the previous section.

Next, the borehole data is discretized into the 3D simulation grid cells, also known as voxels. The karstic voids are coded as geological–geotechnical units or categorical variables for stochastic geostatistical modeling. The methodology employs the PGSIM technique, a stochastic geostatistical modeling method to simulate the spatial variability of the geological–geotechnical units. Chiles and Delfiner (2009) discussed the pixel-based methods – truncated or pluri-Gaussian simulation technique (Armstrong et al. 2011) , multipoint geostatistics, and Markov chain methods such as T-PROGS (Carle and Fogg 1997) to simulate the spatial variability stratigraphic units, or so-called categorical variables. Among the techniques, the PGSIM technique is a complete approach as geological constraints can be applied on the simulated domains. The technique overcomes most categorical simulation method limitations of not capturing the spatial changes in stratigraphic unit proportions, stratigraphic contact relationships and geological realism within realizations (Madani and Emery 2015; Madani et al. 2019). PGSIM technique is used due to its advantages of better characterizing spatial transitions and contact relationships between stratigraphic units.

With a stochastic modeling framework, the PGSIM technique attempts to preserve and reproduce the heterogeneity of parameter of interest (Pyrcz and Deutsch 2014; Ma 2019). Application of stochastic geostatistical modeling techniques allows for generating multiple equiprobable realizations of ground conditions. Each realization from the geostatistical modeling captures the degree of heterogeneity and spatial variability of the stratigraphic units. Madani and Emery (2015) presented a split-sample validation of the individual realizations using calibration plots, thus showing the deviation of simulated proportion of stratigraphic units from actual proportions.

Next, the tunnel envelope is digitized to a cylindrical volume to extract the tunnel envelope voxels from the 3D grid. The voxels' information from the realizations is post-processed to evaluate the occurrence probability of the geological–geotechnical units, the most probable ground conditions, and the uncertainty in the units' occurrence. The number of voxels belonging to each geological–geotechnical unit along the tunnel alignment's longitudinal length is identified and segregated for every realization generated from the geostatistical modeling. The number of voids within the tunnel envelope are calculated from the number of voxels belonging to the respective void categories and the void category area. The number of occurrences of each void category is recorded from the individual realizations to estimate uncertainty in the occurrence probability of the void category. The total volume of karstic voids is calculated to estimate the required pre-excavation grout volume to treat the karstic voids. Factors such as the presence of loose infill material within voids, grouting methodologies, and specifics of the grouting material are beyond this study's

scope. The steps to estimate the void number for each void category and the volume of pre-excavation grouting required within the tunnel excavation envelope are outlined below.

Step 1: Observe the minimum size of the karstic voids. Set up the 3D grid resolution to be the same as the minimum karstic void size in the longitudinal, transverse, and vertical directions.

Step 2: Model the karstic voids as a geological–geotechnical unit, or so-called categorical data, and generate multiple realizations of ground conditions using a stochastic geostatistical modeling algorithm.

Step 3: Extract the voxels and the associated simulations within the tunnel envelope volume.

Step 4: Post-process the realizations from the geostatistical modeling to estimate the occurrence probabilities of the voids.

Step 5: Find the number of voids for each void category as shown in Eq. (5.1).

$$V_{i_c} = (Number\ of\ simulation\ voxels\ with\ i)_c * \Delta x * \Delta y * \Delta z, \quad (5.1)$$

where V denotes the volume, i is the void category, c denotes the longitudinal ID length of tunnel alignment (chainage, in this case), and Δx, Δy, and Δz represent the resolution of the 3D grid in the longitudinal, transverse, and vertical directions, respectively.

$$A_i = \pi * r^2, \quad (5.2)$$

where r is the mean radius, and A is the area of the void category. The methodology assumes a spherical void shape.

Step 6: Find the number of voids (5.3) expected along the tunnel alignment and within the tunnel envelope.

$$N_i = {V_i}/{A_i}, \quad (5.3)$$

where N_i denotes the number of voids for void category i.

Step 7: Calculate the volume of pre-excavation grouting (V_g) (5.4) required from the volume of karstic voids along the tunnel alignment.

$$V_{g_c} = \sum_{c=1}^{c} V_{i_c} = \sum_{c=1}^{c} N_{i_c} * A_i \quad (5.4)$$

5.5 Geostatistical Modeling

In this study, the 3D reconstruction of geological–geotechnical conditions and karstic void distribution was simulated using the PGSIM technique. The PGSIM requires the definition of (i) geological–geotechnical units for simulations, (ii) the simulation grid, (iii) the relative proportions of units and the transition probability matrix, (iv) the spatial variability characterization, and (v) the number of simulations. In this technique, the correlation of the geological–geotechnical units is quantified using indicator variograms generated for the vertical and horizontal directions. Variograms generated in multiple directions capture the anisotropy within the available data. The variogram range, the distance beyond which no correlation exists between the data in each direction and sill, is the maximum value of the variogram and defines it. The range of a stratigraphic unit indicator variogram is a function of heterogeneity and stratigraphic unit occurrence frequency. Dubrule (2017) provided an overview of indicator variograms for geostatistical modeling in three dimensions. Maleki et al. (2017) discussed that indicator variograms convey valuable information on proportions of geological-geotechnical units, spatial correlation structure and contact relationships between the units. Indicator variograms can also be used to validate the consistency of the interpreted geostatistical model (Madani et al. 2019).

As per the central limit theorem, each lag distance bin in a variogram must contain a minimum of 30 point pairs (Cressie 1985). In addition, the binned lags should be of equal spacing and the number of pairs should be similar across all binned lag distances. The lag distances at which the experimental variograms can be determined with an acceptable number of data pairs indicates the scale at which the spatial variation can be modelled. For horizontal variograms, a decision on the angular tolerance and the slicing height is made to achieve the balance between the number of data points available and number of pairs found in the variogram search. In this study, an angular tolerance of 15 degrees corresponding to a 30-degree span for the data points is considered to develop the horizontal variograms. To compensate for the lack of close spacing of the boreholes, a relaxation of the angular tolerance width is required, without affecting the directionality and anisotropy of the variograms. Based on the number of data points available, a decision on the angular tolerance width and slicing height can be made to increase the precision of the horizontal variograms. Webster and Oliver (1992) discussed that practitioners should aim to sample 150 to 200 points within a region to estimate the variograms. Due to higher density of data points in the vertical direction, vertical variograms are relatively easier to comprehend. Spherical and exponential models are found suitable to model Gaussian random functions as these models generally satisfy the positive definiteness for covariance and conditional positive definiteness for variograms (Chiles and Delfiner 2009). Accordingly, spherical model is used to fit the experimental variograms.

Following the indicator variogram model, the geological–geotechnical units are transformed into Gaussian values in appropriate intervals using the Gibbs sampler algorithm. A search neighborhood is defined, and the available Gaussian values within the neighborhood, called conditioning data, are used to simulate Gaussian values within the neighborhood. The simulated Gaussian values are transformed back into geological–geotechnical units using the above-mentioned factors. The realizations generated from the PGSIM technique therefore exhibiting realistic representations of ground configurations. The geostatistical analyses in this study were performed through Isatis, a geostatistical toolkit by Geovariances software (https://www.geovariances.com/en/software/isatis-geostatistics-software/).

The three void categories—V1, V2, and V3—and soil and rock were considered the geological–geotechnical units in the PGSIM realizations. Since the study's interest was to characterize the distribution of karstic voids larger than 0.10 m, a 3D simulation grid of resolution 0.10 m in the longitudinal, transverse, and vertical directions was generated. The 3D simulation grid extended to about 50 m on either side of the tunnel alignment. About 150 million voxels were generated in the 3D simulation grid enclosing the complete tunnel alignment. The boreholes were discretized and digitized into voxels, such that voxels along the borehole length were identified with a geological–geotechnical unit. Due to computational capacity constraints, the tunnel alignment was divided into seven subsections, and a 3D grid was generated for each subsection. Within PGSIM modeling, units are modeled by random fields that incorporate the geological–geotechnical knowledge from information on the probability of finding a specific unit in a specific proportion at any given location. This information is converted into conditioning data to ensure that each unit's spatial variation within the modeling domain is reproduced.

Figure *5.8* (a) presents the global vertical proportion curve (VPC) of the geological–geotechnical units from all the boreholes within the tunnel project site. The tunnel envelope's minimum and maximum elevations are presented to quantify each unit's proportion within the tunnel envelope. VPCs are a simple tool for quantifying the proportions of geological–geotechnical units present as a function of elevation or depth (Huber et al. 2015). The VPCs are computed along the lines vertical to a chosen reference level. The tunnel alignment is subdivided into multiple sections, and within each section, multiple VPCs are generated to capture the lateral variation in the unit's proportions for geostatistical modeling. Figure *5.8* (b) represents an interpretation of the available borehole data and conceptual geological–geotechnical model. The rule derived from the available boreholes controls the permissible and forbidden contacts between pairs of units and reproduces the units' ordering. Relative proportions presented in Figure *5.8* (c) indicate the proportions of borehole samples belonging to each unit within the tunnel envelope. Total 200 equally probable realizations of the ground conditions were generated in terms of the coded geological–geotechnical units within the seven 3D grids. Each simulation differs from the others within a specific range of variation. The quantification of the variation indicates the uncertainty of the simulation results. For this study, at about 200 realizations, the uncertainty difference of the simulation results was within 1 %, indicating that 200 realizations were sufficient for geostatistical modeling. A similar methodology for identifying the number of simulations has been applied by Gangrade and Mooney (2020) to characterize the location uncertainty in soil transition boundaries within the tunnel excavation envelope.

The simulation of geological–geotechnical units proceeds as follows:

i. Gaussian fields are iteratively co-simulated at points within the modeling domain that contain sampled borehole data. Within each iteration, a random point among the borehole samples is selected, and the Gaussian fields are updated based on the values taken by the Gaussian fields at other sampled locations. Gibbs sampler, an optimization algorithm, is used to perform the Gaussian fields' iteration and modeling.
ii. Next, the Gaussian fields are simulated at the unsampled locations. Since the Gaussian fields are independent, each field is conditioned to its previously simulated values. In this study, the turning bands algorithm is used to simulate the Gaussian fields.

iii. The regionalized VPCs and the geological–geotechnical unit rule (see Figure 5.8) are applied to the simulated Gaussian fields to convert Gaussian variables to the actual geological–geotechnical unit.
iv. The process is repeated multiple types leading to the generation of multiple realizations of the ground conditions.

It is to be noted that the realizations are only equally probable mathematically for a given modeling method and the given inputs, and not equally probable physically (Ma 2019).

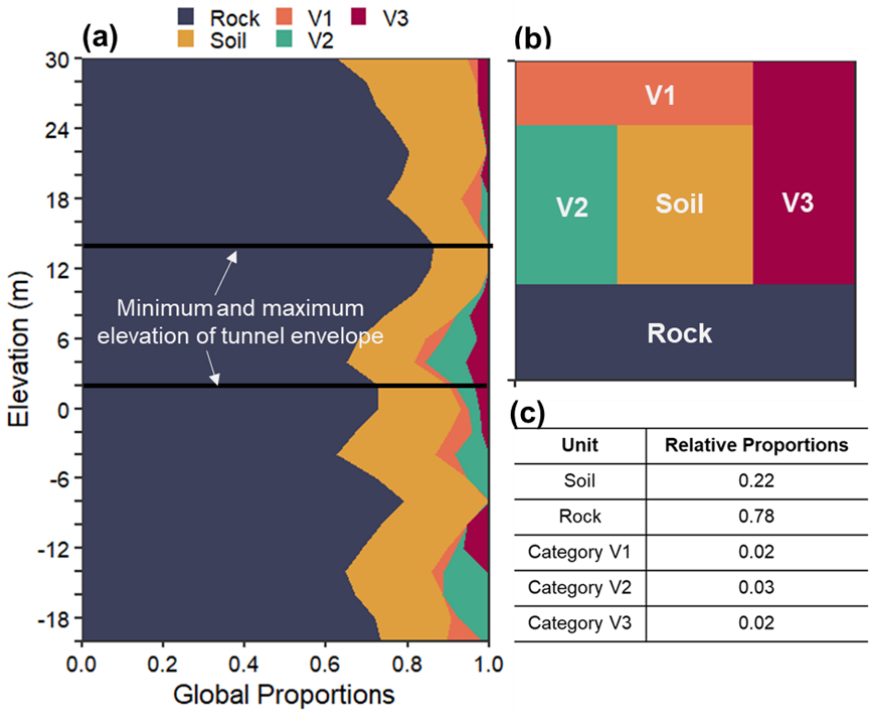

Unit	Relative Proportions
Soil	0.22
Rock	0.78
Category V1	0.02
Category V2	0.03
Category V3	0.02

Figure 5.8 (a) Global proportions of the geological–geotechnical units considering all the boreholes along the tunnel alignment, (b) geological–geotechnical unit modeling rule generated based on the probability of transition and juxtaposition tendency between units from boreholes, and (c) relative proportions of the units as observed from boreholes.

5.6 Results and Discussion

5.6.1 Quantitative assessments

The set of 200 realizations from PGSIM modeling is utilized to determine the occurrence probability of the units and identify the most frequently occurring unit at each simulation grid's voxel. The simulations of the geological–geotechnical units within the 3D tunnel envelope are presented using 2D profiles developed through the center of the tunnel alignment. The longitudinal 2D profile of an example realization and the most frequently occurring unit (i.e., the most probable unit within each simulation voxel) is presented in Figure 5.9. The elevations within the tunnel

envelope are normalized with respect to the tunnel invert level. As shown in Figure 5.9, category V1 voids are expected to occur at the start of the tunnel alignment below, at, and above the tunnel springline level. The model predicts the presence of category V1 voids at about Chainage 2050 m at the springline level. Category V2 voids are expected to occur at about Chainage 2050 m just above and at the tunnel springline level. Individual realization shows that category V2 voids predominantly occur from Chainage 1500 m to 1600 m and from Chainage 1900 m to 2100 m. Category V3 voids are expected to occur between Chainage 500 m and 600 m, just about at the tunnel springline level. The individual realization shows the presence of category V3 voids from about Chainage 900 m to 1000 m.

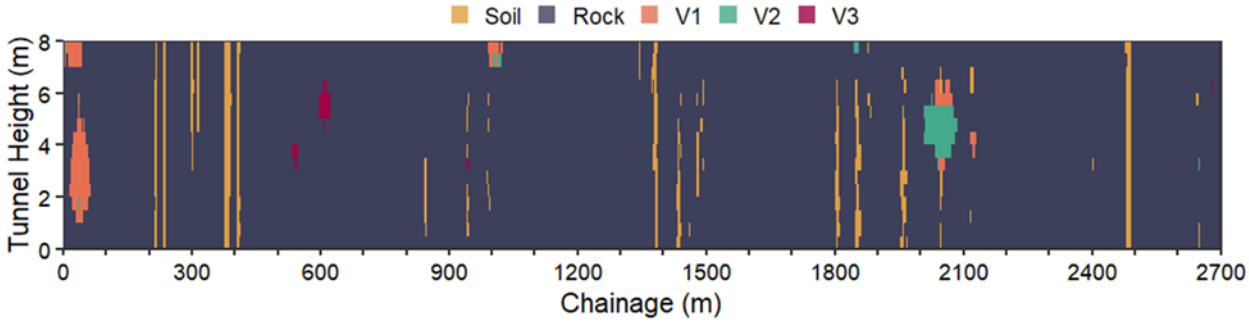

Figure 5.9 Longitudinal profile the most frequently occurring unit within the tunnel envelope.

Figure 5.10 presents, for each void size category, the occurrence probabilities and the number of voids expected spatially within the tunnel excavation envelope. The occurrence probabilities are calculated as the ratio of the number of occurrences of the void category, at each simulation voxel, to the total number of geostatistical realizations. It is noted that the occurrence probabilities shown in Figure 5.10 are along the tunnel centerline only. The number of voids is calculated using Eq. (5.1) – (5.3), where the volume of the simulation grid is normalized with the mean void area of the respective void category. The results in Figure 5.10 are for the most probable ground conditions within the 3D tunnel envelope. Contour plots are used to represent the expected number of voids within the 3D tunnel envelope. The contour plots provide a 2D profile view in which tunnel sections with the same number of voids are connected to produce contour lines. The gaps between each pair of neighboring contour lines are filled with color to make it easier to identify the number of voids.

As shown in Figure 5.10 (a), the occurrence probability of category V1 voids, P (V1), ranges between 35 % and 80 % from Chainage 0 to 50 m. Two to five category V1 voids are expected within the 50 m interval. Two to four category V1 voids are expected with 40 % < P (V1) < 80 %, between Chainage 2000 m and 2200 m. P (V1) is relatively low between Chainage 900 m and 1800 m. From Figure 5.10 (b), P (V2) > 40 % at the start of the tunnel alignment and between Chainage 900 m and 1800 m. At Chainage 2050 m, category V2 are expected with 50 % < P (V2) < 80 %. Two to eight category V2 voids are expected at or below the tunnel springline between Chainage 600 m and 1300 m. Results reveal that a relatively high number of category V2 voids are expected to be encountered between tunnel springline and invert. Figure 5.10 (c) shows that 40 % < P (V3) < 90 %, between Chainage 500 m and 700 m. For the rest of tunnel alignment,

P(V3) is relatively low. Between one and four category V3 voids are expected within the tunnel envelope, with maximum expected between Chainage 600 m and 900.

Individual realizations are utilized to capture the uncertainty in the occurrence probability of void categories from equally probable ground conditions. This study's probabilistic approach highlights significant variations in the inferred probability of encountering voids during tunneling. Confidence interval (CI) bands are a robust measurement of the uncertainty estimates. Figure 5.11 presents a distribution of occurrence probabilities within the 3D tunnel envelope from 200 realizations through CI band sets. The black line indicates the median occurrence probability of the void categories as extracted from 200 realizations. The most extensive band reflects the 95 % CI, i.e., a 95 % probability that the void category's actual occurrence probability within the tunnel envelope is captured within the band. As an example, in Figure 5.11 (a) at Chainage 50 m (95 % CI), the occurrence probability of category V1 voids within the tunnel envelope lies between 0 % and 80 % with a median value of about 20 %.

Similar significant variations in the occurrence probabilities of category V2 and V3 voids are observed in a few sections along the tunnel alignment. A wider CI band reflects relatively higher uncertainty in the occurrence probability of the void categories. The visualization of the occurrence probabilities and the CI bands help interpret the uncertainty in the void occurrence within the tunnel envelope. As illustrated, all three void categories show higher uncertainty at chainage locations with a low density of boreholes (see Figure 5.3 and Figure 5.7), resulting in fewer available data points to condition the geostatistical realizations. The results can be interpreted quantitatively as, "At Chainage 1000 m, the occurrence probability for category V2 voids (for 95 % CI) within the tunnel envelope ranges between 0 % to 60 %." The observations indicate a quantifiable occurrence probability for the three void categories within the tunnel envelope rather than the qualitative or semi-quantitative assessments indicated in the GBR.

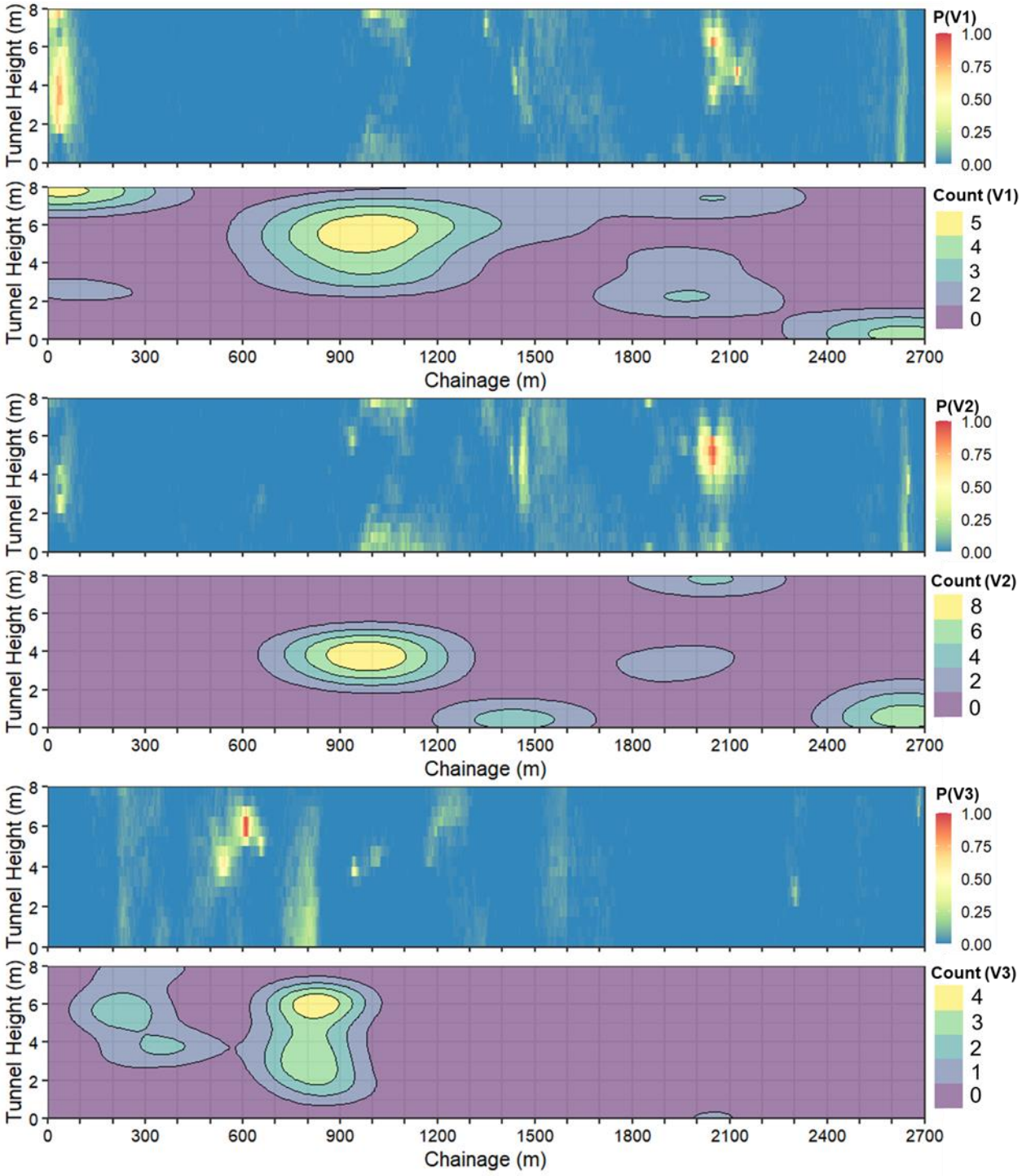

Figure 5.10 Longitudinal profile of occurrence probability and contours indicating void number for each void category within the tunnel envelope. Occurrence probability and number of voids from 200 geostatistical realizations within the 3D tunnel envelope are presented in 2D profiles.

Figure 5.12 presents the variability in the number of voids expected within the tunnel envelope in terms of a 95 % probability interval (PI) band. From the set of 200 geostatistical realizations, the minimum, the mean, and the maximum number of voids expected for every 100 m of longitudinal tunnel excavation is calculated from Eq. (3). The results quantify the variability in the number of voids for about 5300 m^3 of tunnel excavation (every 100 m of longitudinal length and full-face excavation of 53 m^2). The abscissa in Figure 5.12 indicates the length of the longitudinal tunnel excavation. Discussion on the number of voids for each category is provided below.

Category V1 voids: Geostatistical modeling predicts that up to about 40 category V1 voids could be expected in the first 100 m of tunneling. About the same number of category V1 voids is expected at the end of the tunnel alignment. The maximum concentration of category V1 voids is expected to be between Chainage 1000 m and 1600 m, where the maximum expected number ranges between 20 and 40. The mean and the maximum cumulative count of category V1 voids expected within the tunnel envelope is about 200 and 500, respectively.

Category V2 voids: Results from geostatistical modeling indicate a maximum concentration of category V2 voids between Chainage 1000 m and 1500 m and at the end of the tunnel alignment. In contrast, the expected number of category V2 voids ranges between zero and four for the rest of the tunnel alignment. A cumulative maximum of 140 voids of category V2 is expected to be encountered within the tunnel envelope for the complete tunnel excavation.

Category V3 voids: Compared to the number of category V1 and V2 voids, fewer category V3 voids are expected. A cumulative maximum of about 55 category V3 voids are predicted to be encountered within the tunnel envelope. Results indicate that two to three category V3 voids are expected within every 100 m of tunneling from the start of tunneling up to about Chainage 1700 m. Less than two voids of this category are expected between Chainage 1700 m and 2500 m, with three to four voids expected for the last 200 m of tunneling.

An integrated review of the probabilistic assessment results provides quantitative insights to understanding the void occurrence and the tunnel excavation environment, which cannot be obtained from the ground profiles and assessments from the GBR. For example, the results from the probabilistic approach in Figure 5.11 and Figure 5.12 can be interpreted as, “Between Chainage 2000 m and 2100 m, about six category V2 voids are expected with an occurrence probability between 0 % and 80 % (for 95 % CI). A total of about 40 category V2 voids are expected in 2100 m of longitudinal tunneling.” The probabilistic assessment results help interpret the spatial locations where voids are expected to be encountered, the occurrence probability of void categories, the occurrence frequency, and the cumulative number of voids within the 3D tunnel envelope.

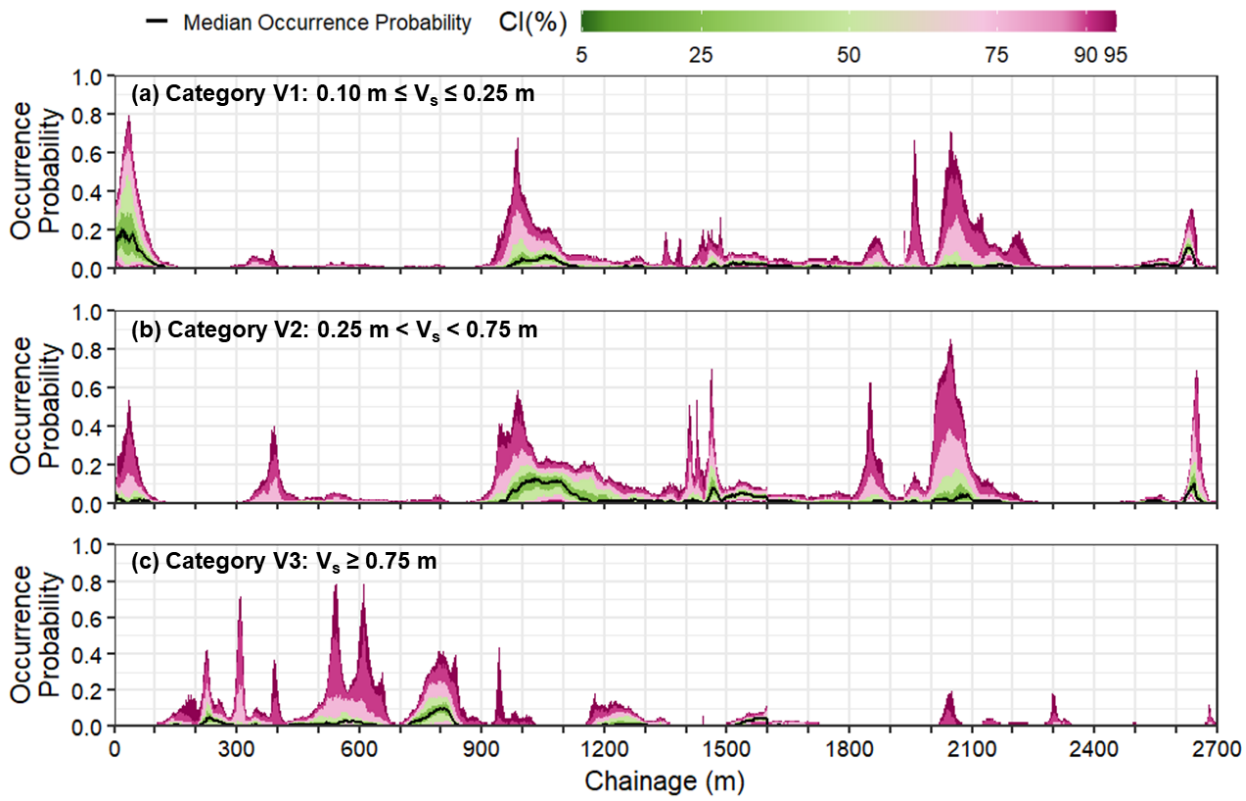

Figure 5.11 Confidence interval **(**CI) profile of occurrence probability of void categories within the 3D tunnel envelope using 200 geostatistical realizations.

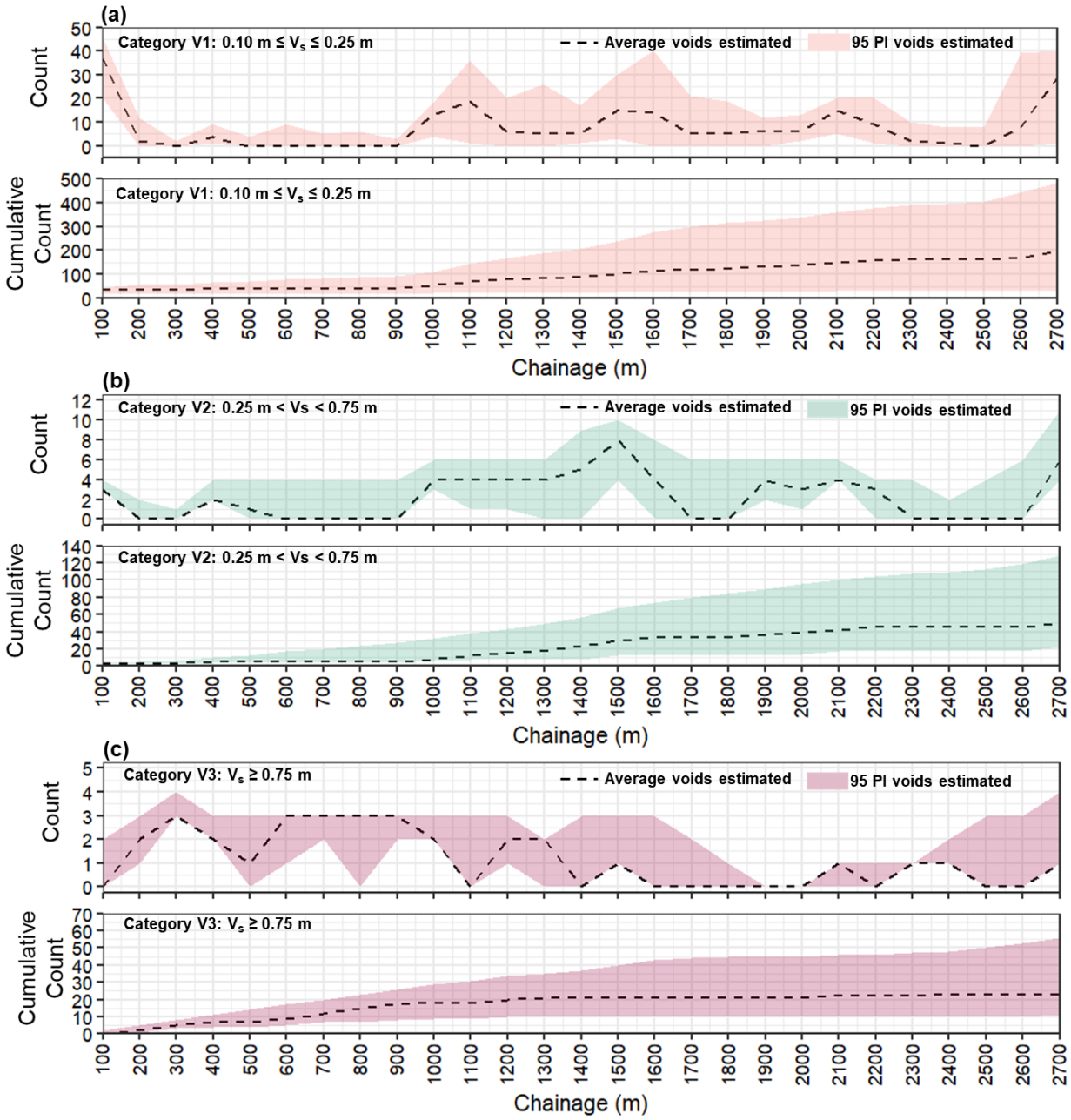

Figure 5.12 Number of voids expected within tunnel envelope for every 100 m of tunnel excavation. These values have been obtained using the 200 individual geostatistical realizations and a tunnel excavation area of 53 m^2 (for an 8 m diameter tunnel).

5.6.2 Application of Probabilistic Assessment

Figure 5.13 presents the volumetric fraction of voids within the tunnel envelope for every 50 m of tunnel excavation. The volumetric void fraction is evaluated from the total volume of each void category and volume of excavation for 50 m longitudinal distance. For most of the tunnel

alignment, the average void fraction within the tunnel envelope remains at or below 6% with an exception between Chainage 1400 m and 1600 m and around Chainage 2600 m. The 95 % probability interval of expected void fraction shows a maximum value of about 12% at Chainage 1500 m. The expected void fraction from Chainage 2300 m to 2600 m remains about 3% and increases to about 9% at the end of the tunnel section. The results from probabilistic assessment aid in quantifying the occurrence probability, void count, and void fraction within the tunnel envelope.

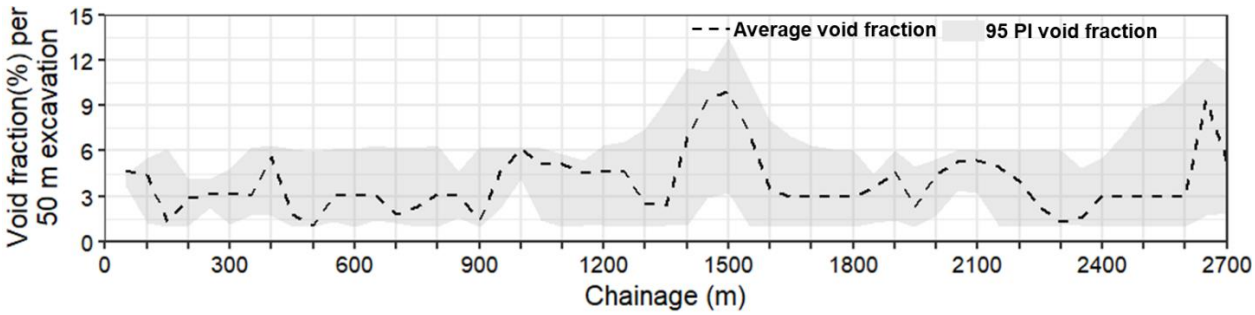

Figure 5.13 Longitudinal profile of the void fraction for every 50 m of tunnel excavation with tunnel excavation area of 50 m^2 (for an 8 m diameter tunnel).

In a karstic geological setting, pre-excavation grouting can be utilized as an effective measure to mitigate the geohazards of water ingress and face collapse during tunneling. Within pre-excavation grouting, the grout is typically injected in front of the shield machine to improve water tightness and stiffness at the excavation face. This is to avoid any geohazards and maintain an optimal rate of tunneling without lengthy stoppages. Cui et al. (2015) and Yang et al. (2020) discussed the pre-excavation grouting methodologies for tunnels in karstic geological environments. The methodologies involve injecting the grouting slurry from the ground surface into the karstic cavities and voids within a specific transverse distance from the tunnel alignment. This study only estimates the grouting volume required to fill the karstic voids prior to tunnel construction. The quantity of grout volume required for voids within the 3D tunnel envelope is calculated using Eq. (5.4). The void number estimates presented in Figure 5.11 are used for grout volume calculations. Figure 5.14(a) presents the minimum, the mean, and the maximum grout volume estimates for every 50 m of longitudinal tunnel excavation (about 2650 m^3 of tunnel volume) and filling karstic voids within the tunnel envelope. The increase in the estimated grout volume between Chainage 1400 m and Chainage 1500 m is due to the possible presence of category V1 and V2 voids within the tunnel section. A higher estimated concentration of category V2 and V3 voids from Chainage 2300 m onwards leads to an increase in the estimated grout volume required within the tunnel section. Figure 5.14(b) presents an estimate of the cumulative volume of grout required to fill the karstic voids within the tunnel envelope. The gradient of the cumulative grout volume curve is indicative of the tunnel sections with relatively higher void concentrations. A consideration of spherical void shape and the mean dimension of the void are the predominant limiting factors for grout volume estimations.

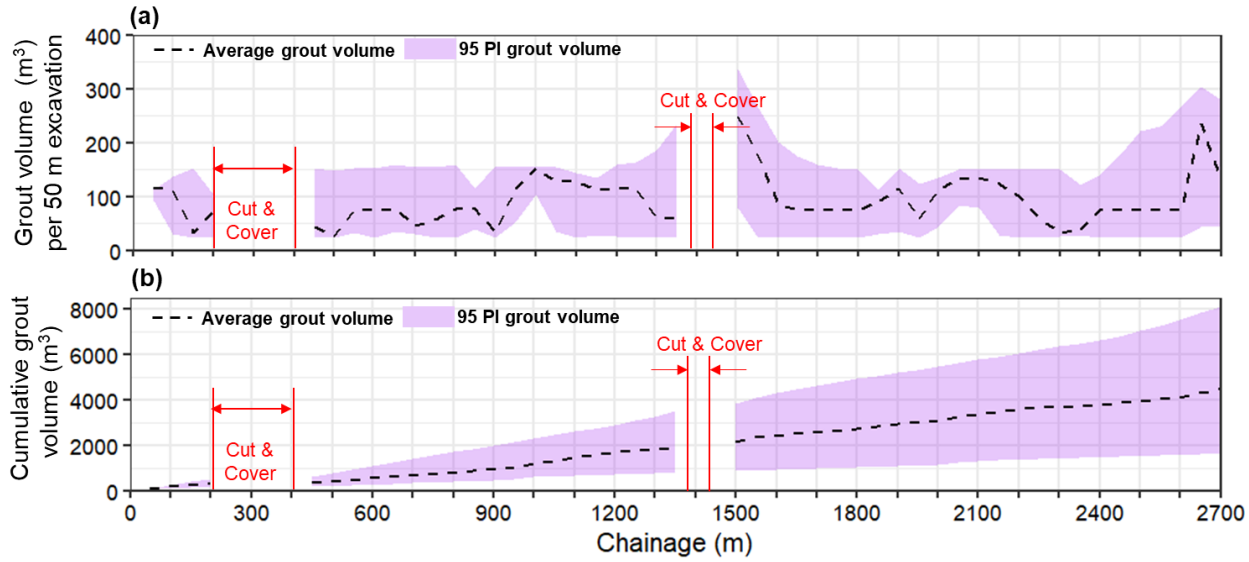

Figure 5.14 Pre-excavation grouting volume estimates of karstic voids treatment within the tunnel envelope. The grout volume required for every 50 m of longitudinal excavation and the cumulative grout volume are estimated using 200 geostatistical realizations.

No empirical studies or rule of thumb estimate the extra time and cost of risk mitigation strategies, such as pre-excavation grouting requirements, on a tunnel project. Since each tunnel project is unique, very few statistical data is readily available concerning the occurrence probability and consequences of unexpected subsurface features, such as karstic voids. A number of decision–support tools such as Decision Aids in Tunneling (DAT) (Einstein et al. 1987), Successive Method (Lichtenberg 1990), and Isaksson (2002) developed probabilistic estimates of tunnel construction time and costs whilst planning and bidding for a tunnel project. The results from the probabilistic approach discussed in the manuscript can be fed into the available decision–support tools to get improved estimates of tunnel construction cost. An improved quantitative probabilistic assessment of voids would allow tunnel contractors to better target the pre-excavation grouting quantities, avoid over-use, and optimize costs towards the risk mitigation strategy.

Conclusions

A geostatistical modeling-based probabilistic approach is proposed and is applied to geotechnical site investigations from a 3 km section of a tunnel project situated in karstic geology. Karstic voids observed within the project site are classified into three size categories (V1, V2, and V3). The PGSIM technique, a stochastic geostatistical algorithm, is applied to develop multiple realizations of the ground conditions, including the karstic voids. The realizations are used to characterize the occurrence probability, the number, and the frequency of karstic voids within the 3D tunnel envelope. Confidence intervals (CI) and contour plots characterize the occurrence probability and void number within the tunnel envelope. The study then uses the probabilistic assessment results to develop estimates of the pre-excavation grout volume required to treat karstic voids. This study's results contribute to the applicability of probabilistic methods towards a quantitative risk assessment and compensation/mitigation of karstic features for tunneling applications. The conclusions from this study are as follows:

i. The geostatistical modeling-based probabilistic assessment allowed for developing assessments of occurrence probabilities and the number of expected voids for each void category. The results also aided in identifying the spatial locations of the occurrence of karstic voids within the tunnel envelope.
ii. Quantitative interpretations of the results were given in the following format: "Between Chainage 2000 m and 2100 m, about six category V2 voids are expected with an occurrence probability between 0 % and 80 % (for 95 % CI). A total of about 40 category V2 voids are expected within 2100 m of longitudinal tunneling."
iii. Contour plots, providing a 2D profile view of the 3D tunnel envelope, were generated to identify voids' number and spatial locations with respect to the shield machine cutterhead.
iv. Interpretations of the results of contour plots were given in the following format: "Just below and at the tunnel springline elevation, four to six category V2 voids are expected between Chainage 600 m and 1300 m. Category V2 voids ranging between two and six in number are expected to occur along the rest of the tunnel alignment."
v. Probabilistic assessment results are used to evaluate the expected volumetric fraction of voids within the tunnel envelope. For every 50 m of tunnel excavation, an average volumetric void fraction between 2 % and 6 % is expected in the tunnel section. A 95 % probability interval indicates about 12 % volumetric void fraction at Chainage 1500 m and at end of the tunnel section. For the remaining alignment, the maximum volumetric void fraction remains at about 6 %.
vi. A cumulative number of voids for each category were used to generate estimates of pre-excavation grouting volume for void treatment. Absolute grout volume required for every 50 m of longitudinal excavation (about 2650 m^3 of tunnel volume) was calculated. Estimates of cumulative grout volume indicated that an average of 4000 m^3 and a maximum possible value of 8000 m^3 would be required for karstic void treatment along the complete tunnel alignment.

Application of the proposed probabilistic approach can help develop baseline statements in the GBR for karstic risk assessment. Tunnel contractors can utilize the improved knowledge of the tunnel excavation envelope to (1) plan additional geotechnical investigations, (2) identify grouting locations and techniques, (3) develop appropriate financial and technical bids, and (4) allocate risk and resolve contractual disputes. The work presented herein was developed to be applied by tunnel designers, contractors, and involved stakeholders to evaluate karstic feature risk and improve ground awareness prior to tunnel project procurement and construction.

CHAPTER 6- RISK-BASED METHODOLOGY TO OPTIMIZE GEOTECHNICAL SITE INVESTIGATIONS FOR TUNNEL PROJECTS

6.1 Abstract

The scope of geotechnical investigations in tunnel projects is generally driven by the allocated resources rather than the expected variability in the ground conditions. Uncertainties in ground conditions may lead to poor decisions in project planning and active risk management. This paper presents a systematic and rational methodology to identify priority locations of additional geotechnical investigations for soft ground tunneling applications based on tunnel risks, site conditions, and project-related constraints. The methodology is applied to the cutter tool wear risk and quantifies the uncertainty in soil abrasivity index (SAI), the relevant geotechnical parameter. Preliminary geotechnical investigation data and site conditions from an actual tunnel project in an urban environment are used to illustrate the proposed methodology and demonstrate its effectiveness. Pluri-Gaussian simulation and sequential Gaussian simulation are used to characterize the 3D spatial variability in soil units and soil abrasivity, respectively, along the tunnel alignment. The study integrates geospatial assessments of SAI uncertainty and consequences of tool wear to develop an *R* index map that delineates the impact of uncertainty in tool wear rate. Project constraints of drilling accessibility and budget are incorporated in the *R* index map to find locations of additional geotechnical investigations. The study simulates a virtual sampling of additional boreholes and quantifies the reduction in uncertainty in tool wear rate and tunnel boring machine (TBM) intervention locations. Additional investigation at priority locations is found to reduce cutterhead intervention location uncertainty by approximately 90 rings (160 m). Further, integrating the uncertainty in tool travel distance is found to influence the cutterhead intervention location uncertainty by approximately 40 rings.

6.2 Introduction

In soft ground tunneling, abrasive soils elevate tool wear rate. Periodic inspection and maintenance stop of tunnel boring machine (TBM) to replace tools, called interventions, is time-consuming, risky, and expensive (Gharahbagh 2013). Optimizing intervention locations for cutter tool wear inspection can significantly improve the overall production rate of the tunnel construction. Too infrequent inspections can lead to cutterhead damage resulting in prolonged intervention for significant repair. Conversely, unnecessary interventions result in lost time that could otherwise have been used to continue excavation. The uncertainty in tool wear rate translates to uncertainty in cutterhead intervention locations. An evaluation of cutterhead intervention is critical (Farrokh and Kim 2018) as the cost of interventions is about 30 % of tunnel construction cost (Wang et al. 2017). The uncertainty in ground conditions, specifically soil abrasivity, resulting from insufficient knowledge of ground variability and the TBM operational parameters, influences the uncertainty in the rate of tool wear.

While FHWA (2009) recommends an average spacing of 100-150 m to determine the number and locations of boreholes for tunnel geotechnical SI, the effect of limited and sparse geotechnical site investigation (SI) on the uncertainty in tool wear rate and cutterhead intervention locations is not known. The disputes and claims reported in the tunnel and geotechnical engineering projects (National Research Council 1984; Tonks et al. 2017), due to flawed interpretation of ground conditions from low-quality SI, imply that the prevailing practice of locating boreholes does not

necessarily capture the ground variability. The scope of limited and sparse SI on tunnel projects is driven by the budget constraints and subjective engineering experience rather than '*where to drill*' approach to characterize the expected variability in the ground conditions. For tunnel projects, generally, the allocated budget for SI (involves fieldwork, data collection, interpretation, and baseline preparation) is about 0.75% of the project budget (Walters et al., 2011) and recover less than 1 % of the ground compared to excavated tunnel volume.

The tunnel engineering community has gradually realized that ground spatial variability and uncertainty are significant challenges and need to be addressed (Dong et al. 2016; Sotiropoulos et al. 2016; Xia et al. 2017). Uzielli et al. (2006) suggested improving the overall quality of SI to reduce uncertainty in ground conditions and associated risks. The motivation to improve the investigation quality leads to the question – *how to identify priority additional investigation locations, considering limitations on allocated time and budget, and ground variability to minimize the uncertainty in active risk assessment and decision-making for tunnel projects?* For tunnel applications, a number of studies have developed geotechnical SI methodologies driven by locating boreholes at high uncertainty locations (Gong et al. 2014; Pinheiro et al. 2017) and investigated the economic justification for drilling boreholes at high uncertainty locations (Gong et al. 2017; Karam et al. 2007a, 2007b; Sousa et al. 2016; Zetterlund et al. 2015). For broader geotechnical engineering applications such as slope stability, liquefaction assessment, pile design – the value of information is applied to find optimal locations of geotechnical SI (Crisp et al. 2020; Hu et al. 2021; Jiang et al. 2020; Yoshida et al. 2018; Zhao and Wang 2019). However, none of these studies investigates prioritizing geotechnical SI to minimize the uncertainty in one or more geotechnical risks while accounting for true ground variability and actual site conditions.

This paper focuses on improving SI quality to minimize the uncertainty in tool wear rate and cutterhead intervention locations while explicitly accounting for ground uncertainty. Further, the paper discusses the extension of the methodology to incorporate other relevant tunnel risks. Risks created by tool wear rate include unplanned interventions, cutterhead damage, and impacts to overlying facilities having cost, time, and safety implications. Therefore, optimizing intervention locations based on maximizing the reduction in uncertainty in tool wear rate from additional SI will result in significant cost and time savings and better risk control/reduction. The paper quantifies the uncertainty in soil abrasivity index (SAI), a geotechnical parameter related to tool wear rate, and prioritizes additional investigation locations considering SAI uncertainty and tunnel site conditions. Geotechnical investigation and tunnel site conditions from North-East Boundary Tunnel (NEBT) in Washington, DC, are used to demonstrate the effectiveness of the methodology. Geospatial assessments of SAI uncertainty, consequences related to an unplanned cutterhead intervention, and project constraints are developed to identify the priority investigation locations. A comparison of uncertainty in cutterhead intervention locations from initial and virtually sampled additional investigations is presented. The paper is organized as follows: Section 6.2 presents the method to estimate SAI and cutterhead intervention location. Section 6.3 discusses the proposed methodology. Section 6.4 presents the NEBT project as an illustrative example to demonstrate the proposed, followed by conclusions in Section 6.5.

6.3 Evaluating tool wear rate

This study considers uncertainty in tool wear rates (resulting in cutterhead interventions) as a tunnel risk due to the time and cost implications and possible impact on overlying structures. The

study defines that uncertainty in tool wear rates is a risk only when a continuous measurement of tool wear rate is not available. Köppl and Thuro (2013) listed abrasivity of the soil components, stress at the contact force between soil and cutting tool, and shape parameter of soil components as the critical factors influencing the rate of cutter tool wear. From field data of more than ten slurry tunnel boring machines, Köppl (2014) introduced a soil abrasivity index (SAI), a combined index of equivalent quartz content (EQC), soil shear strength, and soil gradation size at 60 % passing (D_{60}) to predict the rate of cutter tool wear.

$$SAI = \frac{EQC}{100} * (\tau_c) * D_{60} \tag{6.1}$$

This study uses geotechnical parameters in Eq. (6.1) to quantify SAI and associated uncertainty along the tunnel to capture the uncertainty in tool wear rate and intervention locations. Any similar models for estimating SAI conditions can also be used. The cutterhead intervention location uncertainty is derived from the empirical estimates of allowable and actual cutting distances for disc cutters and rippers from the model proposed by Köppl (2014). Table 6.1 summarizes the empirical relationships. The study herein considers that a cutterhead intervention shall occur when cumulative e_{wear} is greater than equal to 50 % for greater than equal to 50 % of tools on the cutterhead. Tunneling contractor preferred criteria could also be integrated to estimate the cutterhead intervention location uncertainty.

Table 6.1 Travel distances for disc cutters and rippers for soft ground TBMs and expected tool wear rate (Köppl 2014, Köppl and Thuro 2013).

Terminology	Equation	Comment
Allowable travel distance for disc cutter ($S_{c,disc}$)	$S_{c,disc} = 312 + \exp[-0.0048 * (SAI - 1400)]$	
Allowable travel distance for ripper ($S_{c,ripper}$)	$S_{c,ripper} = 281 + \exp[-0.0050 * (SAI - 1300)]$	
Actual cutting distance	$S_{actual} = \frac{L_d * 2 * \pi * r_s}{p_r * 1000}$	L_d is the ring length, r_s is the radial distance of the cutting tool, p_r is the average penetration rate (PR) of the ring.
Expected tool wear rate	$e_{wear} = \frac{S_{actual}}{S_c}$	This study considers tool replacement at cumulative $e_{wear} \geq 50$ %.

6.4 Methodology

6.4.1 Locating additional investigations

The methodology to find optimal investigation locations begins with identifying one or more tunnel risks and the relevant geological-geotechnical parameter(s) influencing the risk. The methodology applies pluri-Gaussian simulation (PGSIM) and sequential Gaussian simulation (SGSIM) on preliminary SI data to generate 3D spatial variability and uncertainty models of geological-geotechnical parameters relevant to the target risk(s). Next, geospatial quantification of geotechnical parameter uncertainty, accessibility, and tunnel risk consequences are developed and superimposed on the tunnel alignment's geospatial location. Geometries/extent of ground uncertainties is different for each tunnel risk. For uncertainty in tool wear rate, consideration of geotechnical uncertainty encountered within tunnel envelope is critical; however, for tunneling induced-ground deformation, geotechnical uncertainties between the tunnel invert and ground surface are critical. The decision on the extent of *z* (vertical direction) of geotechnical uncertainty is related to the tunnel risk of interest. In this study, for the risk created by tool wear, geotechnical uncertainties within 3D tunnel envelope are averaged along *z* at each *(x, y)* (coordinates in longitudinal and transverse directions) to develop a 2D geospatial assessment of geotechnical parameter uncertainty *(U)*.

The framework then entails developing a 2D assessment of tunnel risk consequences (*C*) from observations of project site characteristics. The consequence geospatial assessment delineates the severity of consequences on project site conditions for a tunnel risk. The probability of occurrence of the risk with intervention beneath existing structures and utilities is relatively higher than at locations without existing facilities (e.g., open park spaces, parking lot). For example, forced cutterhead intervention beneath a critical structure can result in building damage if the tunnel face is not supported by sufficient pressurized air. Here, building damage and the cost associated with the damage is the risk related to tool wear and cutterhead intervention. The consequences geospatial assessment considers the risk of (a) cutterhead damage as tools are entirely worn out, resulting in prolonged repair time and requiring shaft excavation and ground improvement; (b) forced intervention due to reduced tunneling efficiency. The anticipated severity of the consequences at locations along tunnel alignment is categorized as low, medium, and high. A quantitative metric is assigned to the consequence severity categories to prioritize locations of investigations.

The next step of the framework involves developing a 2D geospatial assessment of site accessibility (*A*), dictating where boreholes can be drilled, based on available permissions from multiple agencies and private property owners. *U* and *C* assessments can drive the prioritized effort of obtaining permissions for investigations, only to optimize the effort of gaining access and investigating in the critical regions. The framework then includes the investigation budget constraint through the number of boreholes drilled within the investigation phase. We note that geospatial assessments for accessibility and tunnel risk consequences severity will require input and an update from the project owner/engineer and the involved stakeholders. The framework integrates 2D assessments of *U* and *C* to generate an *R* index assessment that shows the uncertainty in geotechnical parameters related to tunnel risk and consequences of tunnel risk on site conditions. *R* index utilizes normalized geotechnical uncertainty for the index to range from 0 to 1. Table 6.2 summarizes the different geospatial assessments developed within the proposed framework.

Table 6.2 Summary of geospatial assessments developed within the proposed framework.

Geospatial assessments	Equation	Comment
Geotechnical uncertainty (U)	$U_{(x,y)} = \sum_{(x,y)} U_{n_{(x,y,z)}}$	Assessment developed from the 3D geostatistical model. n: number of simulation voxels within tunnel envelope; x, y, z: spatial coordinates in the longitudinal, transverse, and vertical direction of tunneling, respectively.
Consequences (C)	$C_{(x,y)} = \begin{cases} Low \\ Medium \\ High \end{cases}$	It can be developed in consultation with the project owner/engineer and involved stakeholders.
Drilling accessibility (A)	$A_{(x,y)} = \begin{cases} 1, & accesible\ to\ drilling, \\ 0, & otherwise \end{cases}$	It can be developed and updated based on permissions from multiple agencies and private property owners.
R index	$R_{(x,y)} = (U_{(x,y)}, C_{(x,y)})$	

The framework identifies the additional investigation locations (L_{SI}), for a specific threshold of uncertainty in tunnel risk (T_R), from the project domain (D) using Eq. (6.2)

$$L_{SI_{(x,y)}} = D_{(x,y)} \in [R_{(x,y)} > T_R\ , A_{(x,y)} = 1] \tag{6.2}$$

The framework can be extended to identify additional investigation locations from multiple tunnel risks. Individual assessments of geotechnical uncertainty and consequences for each tunnel risk can be integrated to identify the locations of additional investigations. For example, we consider that ground deformation, uncertain tool wear rate, and TBM clogging are risks on a tunnel project situated in an urban environment. We understand the respective consequences (time, cost, personnel injury, and impact to the community) of each of these risks. R index assessments for respective tunnel risk can be combined to develop a holistic R index map to identify the priority locations of investigations using Eq. (6.3).

$$R = (R_{ground\ deformation}, R_{tool\ wear}, R_{clogging}) \tag{6.3}$$

The holistic R index assessment for tunnel site (Eq. (6.3)) can then be used to identify L_{SI} (Eq. (6.2)). Weights can also be assigned to different risks based on the severity when multiple risks are assessed. In this sense, the proposed framework is flexible in finding applications to optimize additional investigations for tunnel projects with multiple tunnel risks situated in different geological depositional environments and different project settings.

6.4.2 Geostatistical modeling

The study employs PGSIM and SGSIM to estimate soil conditions (categorical data) and related geotechnical parameters (continuous data) between sampled locations. The spatial correlation structure of geotechnical parameters is defined for each soil type using variogram analysis. The

variogram, $\gamma(h)$, measures the average dissimilarity between two variables—for example, between the values of a parameter ($\boldsymbol{x}$) at location u and location $u+h$ (6.4).

$$\gamma(h) = \frac{1}{2N(h)} \sum_{N(h)} [z(u) - z(u+h)]^2 \tag{6.4}$$

$z(u)$ is the parameter value at location u, and $N(h)$ is the number of data pairs separated by h.

PGSIM characterizes the soil type configuration using two or more Gaussian variables honoring the proportions, spatial contacts, probability of transition, and the spatial structure of the soil types (Armstrong et al. 2011; Chiles and Delfiner 2009). The PGSIM realizations capture the vertical variability in soil proportions through vertical proportion curves (VPCs). The spatial contacts between soil types and transition probability from one type to another are integrated into the realizations using the *lithotype* rule. Next, the indicator variograms are used to convey valuable information on the spatial correlation structure (geometry, variability) of soil types. Following the indicator variogram modeling, the soil types are transformed to Gaussian values using the Gibbs sampler algorithm, and the simulated Gaussian values are back-transformed to soil types. Gangrade et al. (2021) provided a detailed description of the critical steps in the PGSIM technique.

In SGSIM, the spatial structure of the geotechnical parameter is modeled using variograms for the longitudinal, transverse, and vertical directions of the simulation domain. Experimental variograms, whose data are usually scattered and discrete, are modeled with analytical or model variograms that filter the noise due to measurement error or lack of data in experimental variograms. In SGSIM, the previously simulated cells are used as data points for subsequent simulations. The combination of random path and simulated values as new data points makes the overall simulation honor the input statistics of the modeling parameter (Ma 2019). This includes the mean, variance, and variogram structure of the modeling parameter.

A 3D simulation grid extending to 50 m on either side of the NEBT alignment is generated for geostatistical modeling. The center of each voxel of the 3D grid is identified with the coordinates (x, y, z) denoting easting (longitudinal direction), northing (transverse direction), and elevation (vertical direction), defined from the start of the tunnel alignment at a resolution of 5 m, 5 m, and 1 m, respectively. Developing a 3D model allows capturing and honoring data from boreholes drilled offset to the tunnel alignment. Soil types are simulated at each simulation voxel using the PGSIM technique. The most occurring soil type at each voxel is identified to generate the most probable soil conditions model. The occurrence probability of soil types at each voxel is used to estimate the uncertainty in terms of information entropy. This study uses the methodology adopted by Felletti and Beretta (2009) and Gangrade and Mooney (2020) to decide the number of realizations for geostatistical modeling. The study uses the *local simulation approach* discussed by Grasmick et al. (2020), where 100 realizations of geotechnical parameters are simulated within each soil type realization, resulting in 20,000 realizations of geotechnical parameters. All geotechnical parameter realizations are post-processed to estimate uncertainty in terms of variance.

6.5 Illustrative Example

6.5.1 NEBT project overview and geotechnical conditions

The NEBT project in Washington, DC, is an 8 km long 8 m diameter single tunnel excavated using an earth pressure balance machine (EPBM). This study considers a 6.5 km stretch of the NEBT alignment in congested urban settings starting at ring# 1600. Initial geotechnical investigations on the 6.5 km tunnel stretch consist of 30 boreholes with soil sampling, in situ testing, and laboratory tests to determine geotechnical parameters. Standard penetration test (SPT) blow counts, among other in situ tests, and soil types were recorded within each borehole at a vertical sampling interval of 0.5 m to 1 m. Other relevant geotechnical parameters such as grain size distributions, Atterberg limits, natural moisture content, unit weight, strength, and chemical properties were measured from laboratory tests. Soil samples were classified according to the Unified Soil Classification System (USCS) and grouped into engineering soil units (ESUs). Figure 6.1 presents a longitudinal profile of the boreholes, SPT blow counts corrected for hammer efficiency and overburden stress ($N_{1-(60)}$), and grain size distribution test results at sampled locations used to determine D_{60} along the NEBT alignment.

Table 6.3 provides a description of the ESUs identified on the NEBT project. The tunnel envelope passes predominantly through CH and Sands with CL and Gravels deposits in relatively lower proportions. The tunnel envelope transitions between ESUs, $N_{1-(60)}$ ranges from 0-100, and D_{60} varies by orders of magnitude up to 8 mm. The observed variability in geotechnical parameters highlights the limitation of relying on a deterministic interpretation of geological/geotechnical conditions from the geotechnical baseline reports (GBR) for active risk management and decision-making.

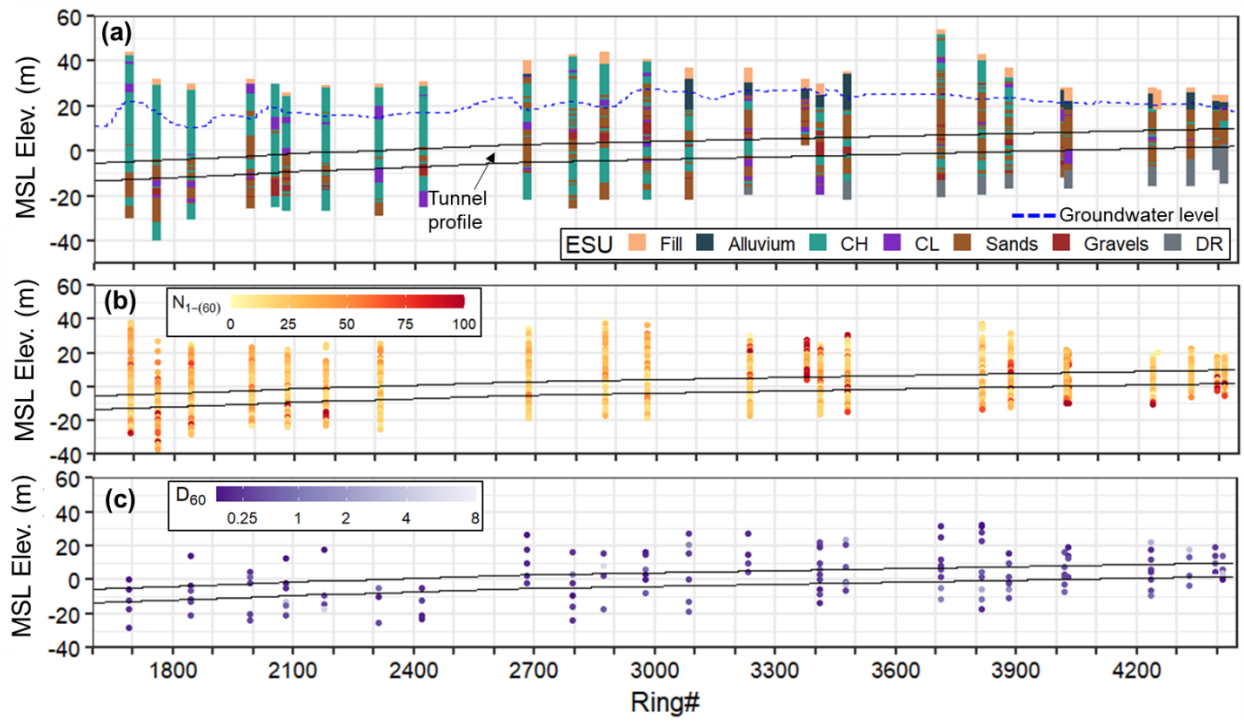

Figure 6.1 Longitudinal profile of (a) boreholes in terms of ESUs, (b) Normalized standard penetration test blow counts $N_{1-(60)}$ [1318 samples], and (c) soil particle size that 60 % of soil is smaller than D_{60} [220 samples].

Table 6.3 Description of engineering soil units (ESUs) encountered on the NEBT project.

ESU	USCS	Description
Fill		Fine to coarse-grained soil with fragments of organic material.
Alluvium		Mixtures of variably dense silt, clay, sand, gravel, and organics.
CH	CH, MH	Highly plastic over-consolidated fine-grained soil.
CL	CL, ML	Low to medium plastic over-consolidated fine-grained soil.
Sands	SP-SC, SP-SM, SC, SM	Very dense non-plastic silty/clayey sand with silt and low plasticity clay
Gravels	GP-GC, GC GP-GM, GM	Fine to coarse sand with trace amounts of coarse gravel, cobbles, and fines

DR		Decomposed rock

For 3D geostatistical modeling of soil conditions and geotechnical parameters relevant to cutter tool wear rate, data from all the available 106 boreholes and laboratory tests are utilized. All drilled boreholes contain ESU information but do not necessarily contain $N_{1-(60)}$ and D_{60} sample information. The voxels within the 3D tunnel envelope *(x, y, tunnel invert elevation ≤ z ≤ tunnel crown elevation)* are extracted from the whole simulation grid *(x, y, z)*. From here onwards, *z* represents the elevation of voxels within the tunnel envelope.

Geotechnical parameters ESU, $N_{1-(60)}$, and D_{60} are modeled stochastically, where initial investigation data is utilized to develop multiple equally probable realizations from PGSIM and SGSIM techniques. Geostatistical models of ESU, $N_{1-(60)}$, and D_{60} are transformed to estimate SAI conditions (Eq. (6.5–(6.8) within the tunnel envelope. The empirical relationship presented in Eq. (6.5) proposed by Hatanaka and Uchida (1996) was adopted to estimate effective friction angle (φ') [°] for shear strength (τ_c) calculations. While the relationship applies to sandy soils, it was found to produce φ' values for other ESUs on the NEBT project comparable to the baseline values. For effective vertical stress estimates at any simulation voxel ($\sigma'_{(x,y,z)}$), groundwater levels (h_w) shown in Figure 6.1 is adopted. Table 6.4 presents the variability in the geotechnical parameters EQC and unit weight (γ) from the GBR. No variability was observed in effective cohesion (c') due to the limited number of tests. The variability in EQC is incorporated into SAI estimates using the Monte Carlo simulation technique (MCS), where a normal distribution with mean and 20 % standard deviation of mean EQC is generated. Deterministic values of γ and c' values are considered in estimating SAI, primarily due to limited samples to infer any correlations. Grasmick and Mooney (2021) have discussed the minimal impact of considering deterministic values of geotechnical parameters on SAI calculations. SAI conditions at each simulation voxel are modeled using the relationship proposed by Köppl (2014) presented in Eq. (6.8) where EQC is in %, D_{60} is in mm and τ_c is in kN/m^2. Theoretically, the dimension of SAI is N/m, however Köppl (2014) suggests that index should be regarded as dimensionless due to its empirical character.

$$\varphi'_{(x,y,z)} = \sqrt{15.4 * N_{1-(60)_{(x,y,z)}}} + 20 \tag{6.5}$$

$$\sigma'_{(x,y,z)} = \sum \left(\gamma_{ESU_{(x,y,z)}} * h_{ESU_{(x,y,z)}}\right) - \gamma_w * h_{w_{(x,y,z)}} \tag{6.6}$$

$$\tau_{c_{(x,y,z)}} = c'_{ESU_{(x,y,z)}} + \sigma'_{(x,y,z)} * \tan \varphi'_{(x,y,z)} \tag{6.7}$$

$$SAI_{(x,y,z)} = \frac{EQC_{ESU_{(x,y,z)}}}{100} * \tau_{c_{(x,y,z)}} * D_{60_{(x,y,z)}} \tag{6.8}$$

Table 6.4 Geotechnical parameter values for ESUs in tunnel envelope, as reported in the GBR.

ESU	EQC [Min-Max] (%)	Mean EQC (%)	γ [Min-Max] (kN/m^3)	Mean unit weight (γ) (kN/m^3)	c' (kN/m^2)
CH	[34–58]	46	[18-20]	19	5
CL	[36–57]	48	[18-20]	19	5
Sands	[65-75]	70	[19-22]	20	-
Gravels	[88-91]	89	[20-21]	21	-

Figure 6.2(a) and (b) present a longitudinal profile of the average SAI and standard deviation of SAI (σ_{SAI}) from mean values along the tunnel centerline *(x, y=0, z)* and within the tunneling envelope. Since Sands and Gravels exhibit higher EQC and relatively higher $N_{1-(60)}$ and D_{60} values, the tunnel alignment section with these ESUs exhibits a relatively higher mean SAI. SAI variability observed within the tunnel envelope translates to the variability anticipated in the rate of cutter tool wear. Individual realizations of SAI at voxels within tunnel envelope *(x, y, z)* are utilized to capture the uncertainty in terms of confidence interval (CI) (Figure 6.2(c)). At each ring#, the most extensive band reflects the 95 % CI, i.e., 95 % probability that the true SAI lies within the CI band. Locations lacking geotechnical investigations exhibit a wider CI indicating a higher uncertainty in the SAI estimates.

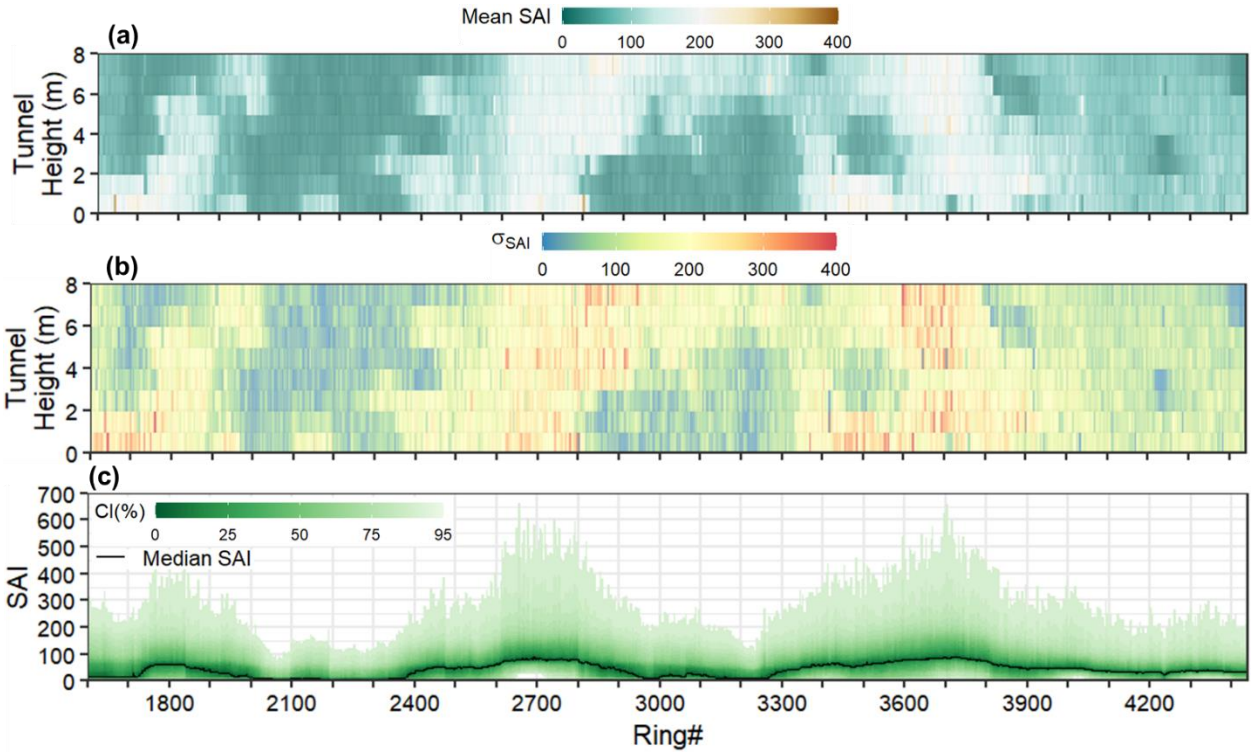

Figure 6.2 Results of transformation to SAI conditions (a) average $_{(x, y=0, z)}$; (b) uncertainty$_{(x, y=0, z)}$ as standard deviation; and (c) uncertainty$_{(x, y, z)}$ as CI.

6.5.2 Geospatial assessments

Figure 6.3 and Figure 6.4 present the geospatial assessment of SAI uncertainty, consequences of cutterhead interventions, and investigation accessibility superimposed on the NEBT alignment. The visualizations extend to +/- 50 m from the tunnel centerline to consider the tunneling zone of influence and locate additional boreholes within 50 m from tunnel alignment. The geospatial surface assessments are developed using equations in Table 6.2 specific to NEBT project site conditions. Figure 6.3(a) presents a plan layout of the normalized spatial uncertainty in SAI conditions within the tunnel envelope. Relatively high (≥ 50 %) uncertainty measures are primarily related to the variability in the ESU conditions and the associated geotechnical parameters of $N_{1-(60)}$ and D_{60}. Figure 6.3(b) presents a conceptual assessment of the severity of consequences from forced cutterhead interventions arising from uncertainty in the rate of tool wear. As illustrated in Figure 6.3(b), the consequence severity is high in regions with overlying structures and facilities within distance of three tunnel diameters from tunnel alignment, whereas critical structures within distance of three to six tunnel diameters away from the tunnel alignment fall into the medium category. Table 6.5 summarizes the metric range for consequence severity categories and a brief description of the surface location characteristics within each category. We note that the consequence metric presented in Table 6.5 is subjective and is based on engineering judgment. As discussed earlier, the severity of consequences can be decided in consultation with the project owner/engineer.

Table 6.5 Summary of consequence severity categories for tunnel risk related to tool wear.

Category	Spatial location characteristics	Metric
Low	Locations without any overlying structures	$0.25 \leq C < 0.5$
Medium	Locations between and near existing structures/utilities within three to six tunnel diameters from tunnel.	$0.5 \leq C < 0.75$
High	Locations with overlying structures/utilities within three tunnel diameters from tunnel.	$C \geq 0.75$

Figure 6.4(a) presents a geospatial assessment of drilling accessibility superimposed on the NEBT alignment. For this study, the conceptual accessibility assessment is developed by estimating the accessibility to investigations in urban settings. Surface features such as railway tracks, railway yards, metro bridges, and residential and commercial structures are considered inaccessible to investigations. Parking lots near and between structures, open park spaces, main streets, road intersections, and the spaces between residential and commercial structures are considered accessible to investigations. Figure 6.4(b) presents an integrated assessment of SAI uncertainty and consequences severity that delineates uncertainty in tool wear rate and consequences of forced cutterhead intervention, damaged cutterhead using an R index from 0 to 1.0. In this study, R index ≥ 0.5 is considered the threshold (T_R) to identify priority locations of additional investigations.

This study simulates an additional phase of geotechnical investigation and considers that the allowable budget for the investigation phase is about 30 % of the initial geotechnical investigations (i.e., ten additional boreholes can be drilled). Locations of additional investigations (L_{SI}) are identified using Eq.(6.3) for an R index threshold (T_R) ≥ 0.5 and accessibility to drilling ($A_{(x,y)}$=1). The proposed methodology enables the optimization of investigation efforts at the periphery of regions inaccessible to drilling but show high uncertainty in tool wear rate. Since all (T_R) ≥ 0.5 locations are treated equally, locations of L_{SI} identified along the alignment (Figure 6.4(b)) are grouped into polygons for a coarse discretization, and specific locations of additional investigations are obtained at the centroid of the polygons. Figure 6.4b) shows the L_{SI}, specific locations of additional boreholes, and the initial phase investigation boreholes, superimposed on the R index map along the NEBT alignment.

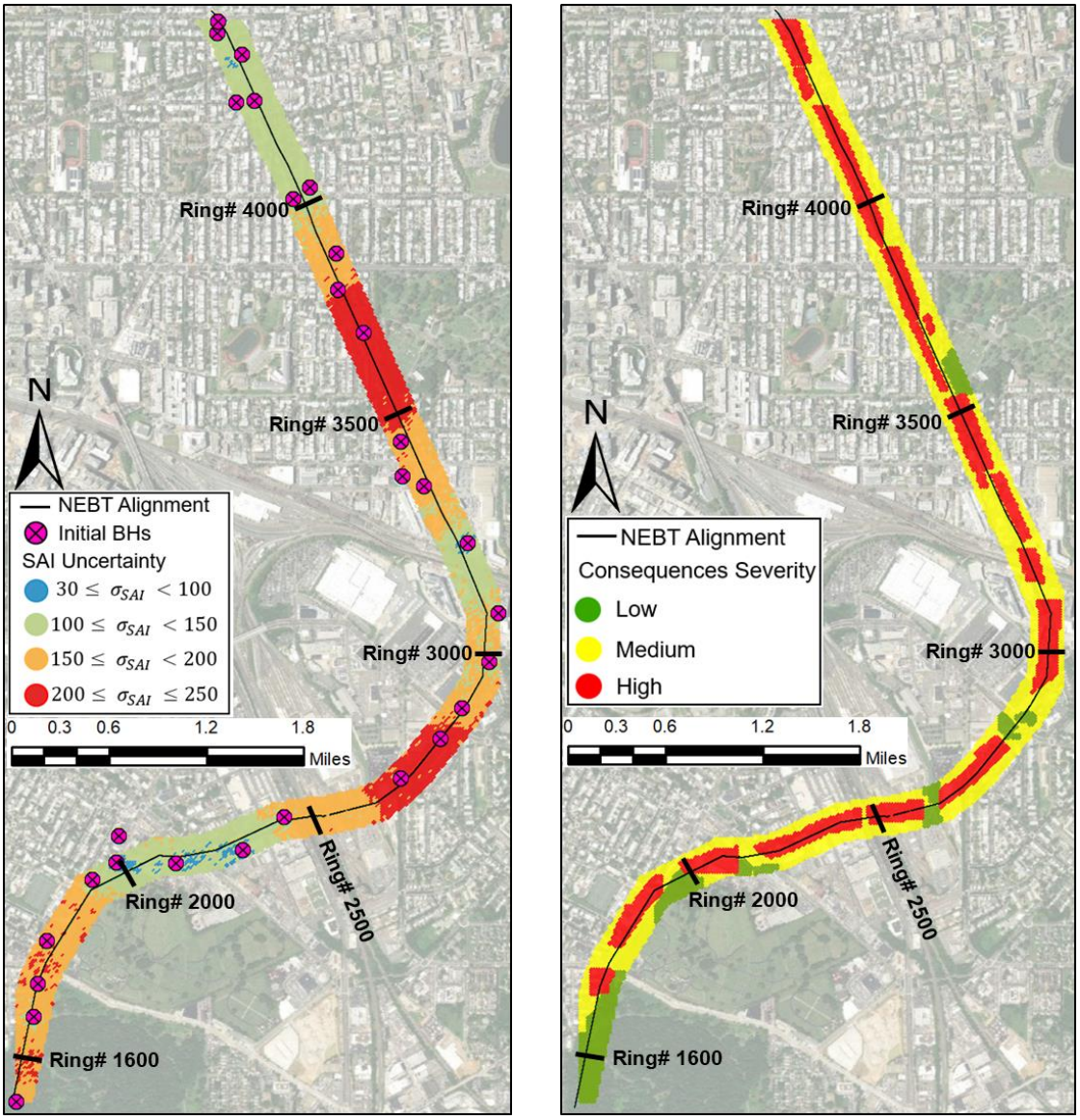

(a) **(b)**

Figure 6.3 Plan layout of (a) geotechnical parameter SAI uncertainty map (U); (b) a conceptual consequence severity map (C) for building damage, shaft excavation, and ground improvement in the vicinity of existing structures superimposed on the 6.5 km section of the NEBT alignment.

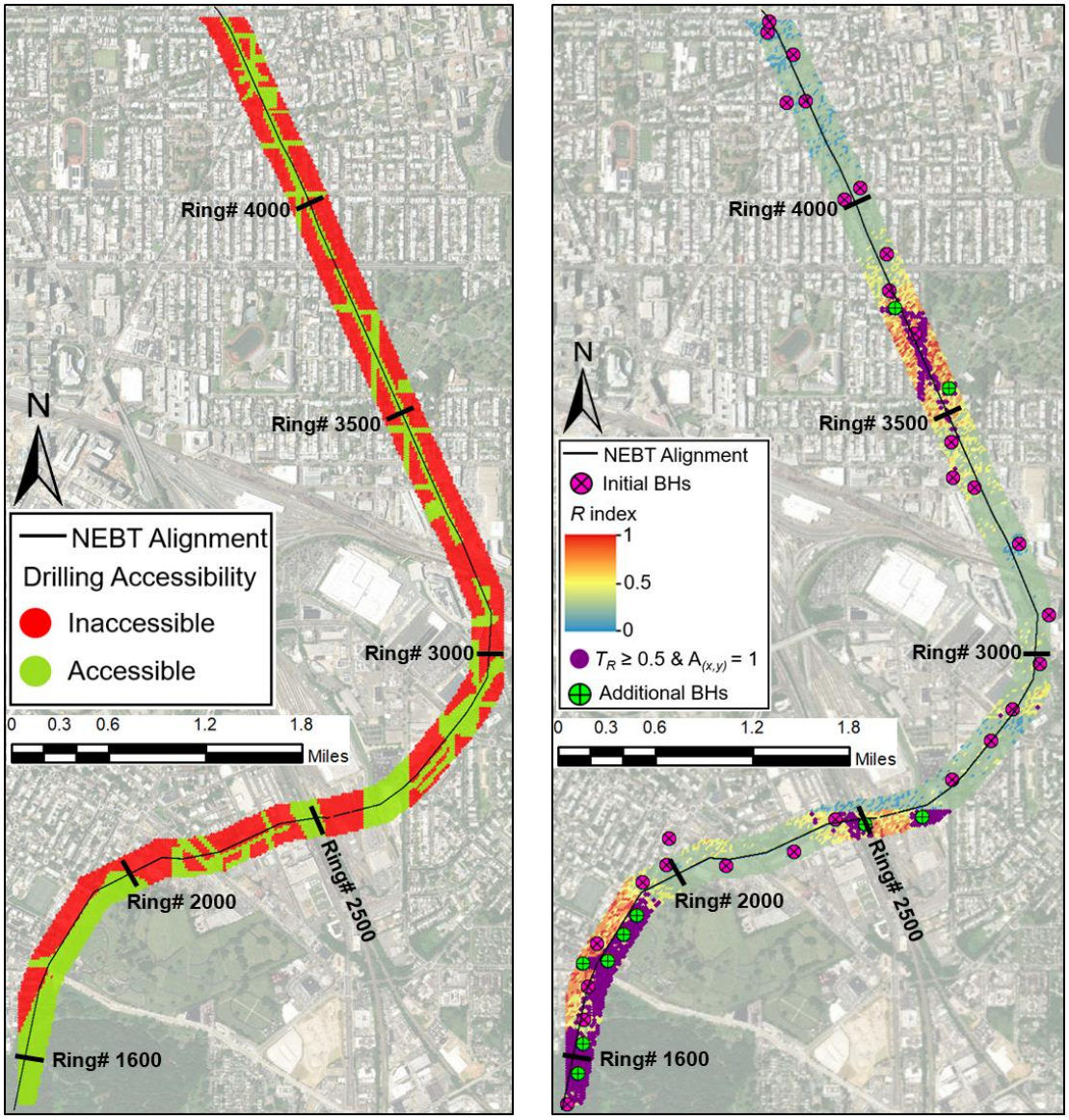

(a) **(b)**

Figure 6.4 Plan layout of (a) a conceptual investigation accessibility (A) map for a specific phase of geotechnical investigation, and (b) R index map delineating priority locations of investigations and additional boreholes sampled, superimposed on the 6.5 km section of the NEBT alignment.

6.5.3 Evaluating cutterhead intervention location uncertainty

The SAI uncertainty within the tunnel envelope (in longitudinal, transverse, and vertical directions of the 3D simulation grid) is used to evaluate the cutterhead intervention location uncertainty for the first two interventions on the NEBT project. Note that while SAI uncertainty within the tunnel

envelope is averaged for geospatial assessments to identify additional borehole locations, SAI uncertainty for all voxels within the tunnel envelope is utilized for the evaluation of tool wear rates and cutterhead interventions. Uncertainty in cumulative tool wear involves the integration of uncertainty in tool wear rate, which varies along the alignment. Evaluation of uncertainty in cutterhead intervention location captures the integrative effect of uncertainty in tool wear rate.

This study evaluates six disc cutters and eight ripper tools at varying radial distances, which were installed at a prior intervention at ring #1600. The cutterhead intervention location uncertainty is derived from the empirical estimates of allowable and actual cutting distances for disc cutters and rippers from the model proposed by Köppl (2014) and summarized in Table 6.1. This study considers a constant p_r of 30 mm/rev to estimate the cutterhead intervention location uncertainty. Sensitivity analyses of p_r on cutterhead intervention location are discussed further. This study checks cumulative e_{wear} for 5 % quantiles, mean, and 95 % quantiles from SAI uncertainty within the 3D tunnel envelope for cutterhead intervention location assessment. As discussed earlier, the study considers that a cutterhead intervention shall occur when cumulative e_{wear} is greater than equal to 50 % for at least 50 % of tools on the cutterhead.

As per the specified criteria, ring# for the occurrence of ≥ 50 % wear of (a) ≥ 50 % rippers, (b) ≥ 50 % disc cutters, and (c) ≥ 50 % of all tools (rippers and disc cutters) are recorded for different levels of SAI. The earliest occurrence (ring#) for (a), (b), and (c) are used to locate cutterhead interventions. Figure 6.5(a) presents the uncertainty, expressed as 90 % CI, in the cutterhead intervention locations for the first two interventions. As observed, SAI from initial investigations results in a 330 ring (595 m) uncertainty in the first cutterhead intervention location. Assuming that all tools on the cutterhead are replaced at the mean ring# from the first intervention, Figure 6.5(b) shows that the location uncertainty for the second cutterhead intervention is about 250 rings (450 m). Table 6.6 summarizes the ring# for tool replacements/inspection for minimum (5 % CI), mean, and maximum (95 % CI) of SAI uncertainty. The uncertainty in the location of cutterhead interventions reflects the SAI uncertainty within the tunnel envelope, as the TBM advance is assumed constant.

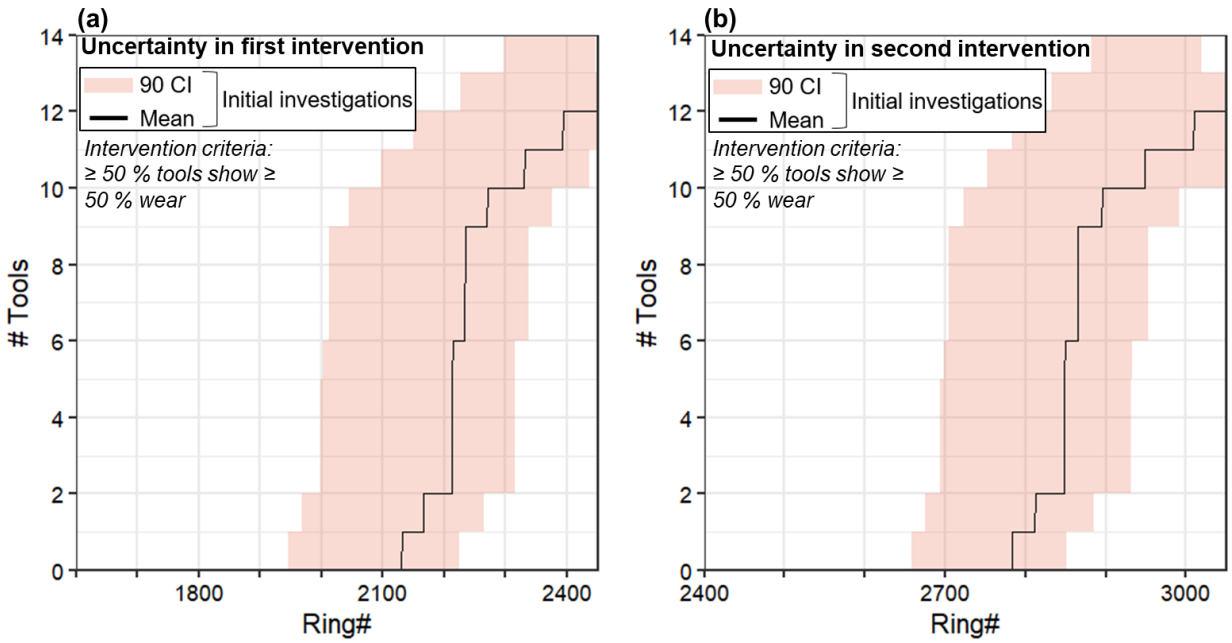

Figure 6.5 Uncertainty in cutterhead intervention locations for (a) first intervention and (b) second intervention.

Table 6.6 Summary of ring# for first and second cutterhead interventions considering SAI uncertainty from initial geotechnical investigations on NEBT project.

SAI	First intervention (Ring#)	Second intervention (Ring#)*
Low SAI [5 % quantile]	2010	2700
Mean SAI	2130	3670
High SAI [95 % quantile]	2340	2950

*Note: The study considers that the tools are replaced at mean ring# from the first intervention.

6.5.4 Effect of additional investigations

Virtual boreholes are sampled at the additional investigation locations identified in Figure 6.4(b). Since tool wear accumulates over the distance traveled by the tool and the abrasivity conditions encountered (TBM operation not considered here), it is logical to locate additional boreholes in the region that affect cumulative tool wear. Sampling data for the ten additional boreholes were obtained from one geostatistical realization randomly selected (realization #57) from an ensemble of realizations available for ESU, $N_{1\text{-}(60)}$, and D_{60}. Since all the realizations are constrained to the variograms, sampling data from any other realization would be expected to be within a specific

deviation from realization# 57 and associated with the uncertainty in the variance of the geotechnical parameter. Sampling from a random realization allows respecting the true heterogeneities of the modeled ground conditions. A similar approach was adopted by Koppe et al. (2011) to simulate the addition of boreholes for a mining project. PGSIM and SGSIM techniques were applied to evaluate the updated SAI uncertainty.

The update in the SAI uncertainty from additional investigation boreholes is presented in Figure 6.6. Results indicate relatively less variation in the SAI values, primarily between ring# 2400 and ring# 2900 and between ring# 3500 and ring# 4000. A comparison of uncertainty distributions from initial and additional investigations for ESU, $N_{1-(60)}$, D_{60}, and SAI is presented in Figure 6.7(a)-(d). All three geotechnical parameters contribute to SAI uncertainty reduction; however, the uncertainty reduction in ESU dominates the uncertainty reduction in SAI uncertainty. This is primarily due to the uncertainty reduction in EQC and geotechnical parameters modeled on ESU realizations. Figure 6.8 compares the *R* index map from initial investigations and an update from adding ten boreholes to the initial investigations. Since the consequences and accessibility conditions are kept the same from the initial investigation phase, the reduction in the *R* index reflects the reduction in the SAI uncertainty from additional investigations. Figure 6.9 presents the updated uncertainty in the cutterhead intervention locations (Table 6.6) with updated SAI uncertainty. Results indicate that with the SAI uncertainty reduction from additional investigations, the uncertainty in intervention locations (90% CI) is reduced by 80 and 90 rings for the first and second cutterhead interventions. Table 6.7 summarizes the ring intervals for 90% CI and the uncertainty reduction in cutterhead intervention locations from additional investigations.

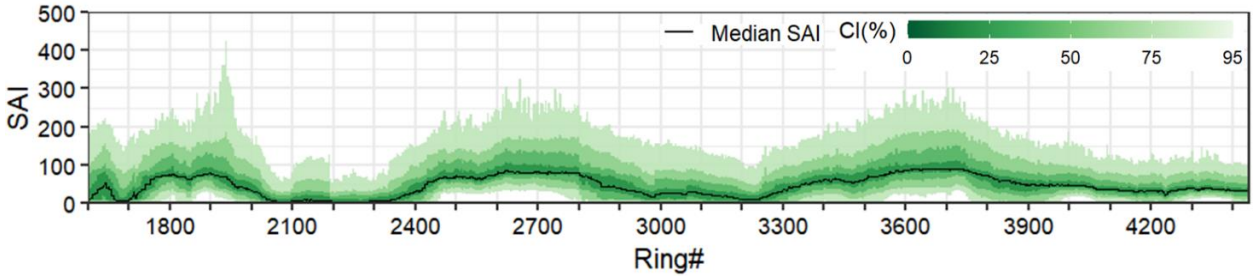

Figure 6.6 Updated SAI uncertainty (expressed as CI) from additional investigations.

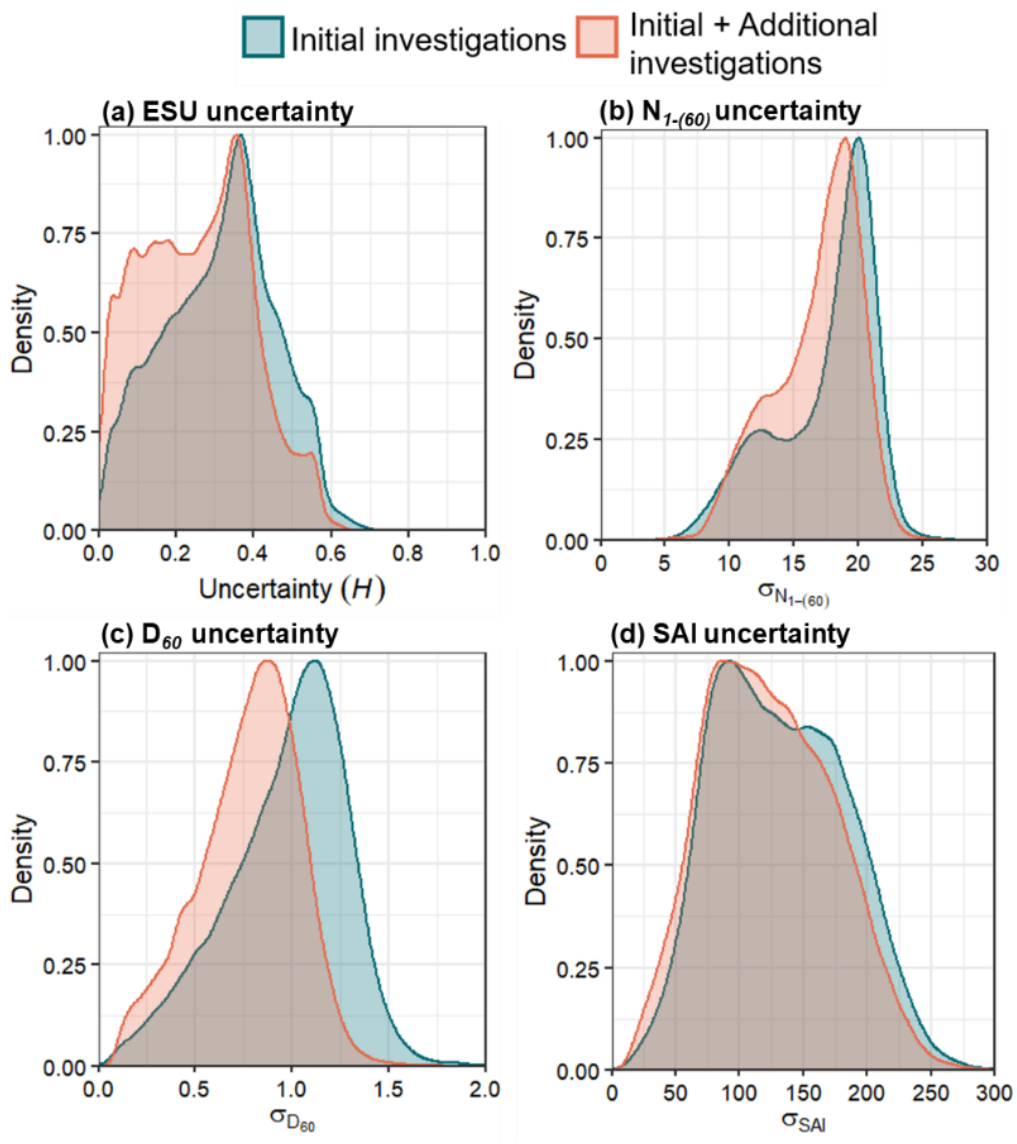

Figure 6.7 Uncertainty distribution comparison for ESU, $N_{1-(60)}$, D_{60}, and SAI conditions from initial and the additional geotechnical investigations.

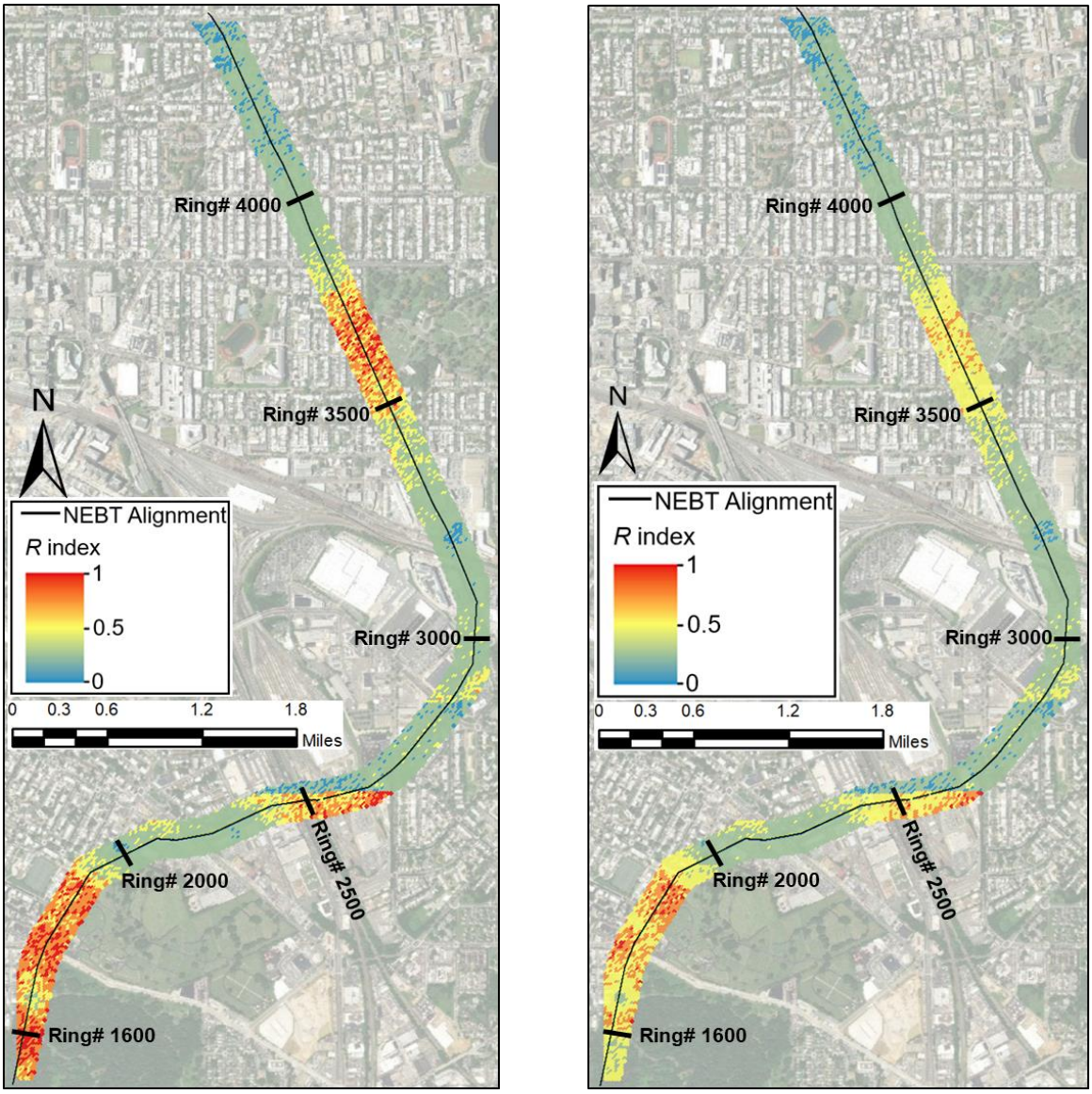

Figure 6.8 Plan layout of (a) R index map from initial geotechnical investigations, and (b) updated R index from the addition of boreholes at the priority locations along the NEBT alignment.

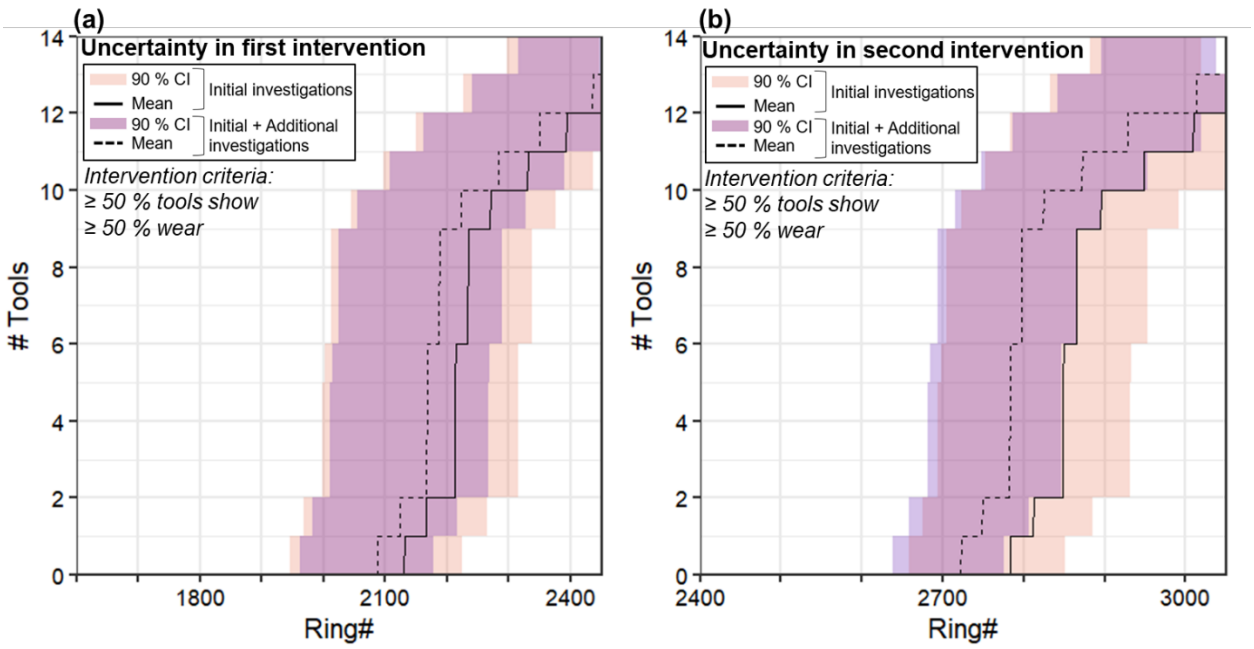

Figure 6.9 Comparison of cutterhead intervention location uncertainty from initial and initial + additional investigations for (a) first intervention, (b) second intervention.

Table 6.7 Uncertainty reduction in the first and second cutterhead intervention locations from the updated SAI uncertainty.

Intervention	90 % CI [initial investigations]	90 % CI [initial + additional investigations]	% Uncertainty reduction
First intervention	330	250	24
Second intervention	250	160	36

Note: Ring length = 1.8 m.

Since it is imperative to understand and compare the influence of the borehole locations on the geotechnical uncertainty reduction, Gangrade et al. (2020) characterized the geotechnical uncertainty reduction from different approaches of locating boreholes along NEBT alignment. Results from the study by Gangrade et al. (2020) showed that locating the boreholes with informed guidance of geotechnical uncertainty led to an additional 25 % reduction in geotechnical uncertainty compared to locating boreholes with conventional practice (without uncertainty knowledge). The findings from the study are document in Appendix D.

6.5.5 Integrating uncertainty in tool travel distance

To assess the influence of uncertainty in tool travel distance, this study considers a normal distribution of p_r with mean (μ_{PR}) of 30 mm/rev and a standard deviation (σ_{PR}) of 10 (30 % of mean), as shown in Figure 6.10(a). p_r values lower than 10 mm/rev are filtered out to consider realistic TBM p_r values within the study. Due to the skewness in the distribution, p_r values < 30 mm/rev are larger in proportion than the p_r values > 30 mm/rev. Using the MCS technique, 10,000 p_r values are randomly drawn from the distribution to simulate p_r values at every ring.

The uncertainty in p_r is integrated into the empirical tool wear assessment model discussed in Table 1, such that 10,000 possible intervention locations are determined for 5 % and 95 % quantiles for SAI uncertainty from initial + additional investigations. Figure 6.10(b) compares the 90% CI for a constant p_r of 30 mm/rev and variable p_r as drawn from the distribution. The results illustrate that incorporating the uncertainty in p_r reduces the uncertainty (90% CI) in the first cutterhead intervention location by about 40 rings (16 %) compared to a constant p_r = 30 mm/rev. For a relatively large proportion of p_r values < 30 mm/rev within the distribution, the actual tool travel distance of disc cutters and rippers increases resulting in cutterhead intervention relatively earlier than for constant p_r = 30 mm/rev. With increased travel distance for 5% and 95% quantiles of SAI, the uncertainty in cutterhead intervention decreases for the p_r distribution used herein. The proposed methodology serves as a robust tool to capture the uncertainty in cutterhead intervention locations considering the uncertainty in tool travel distance.

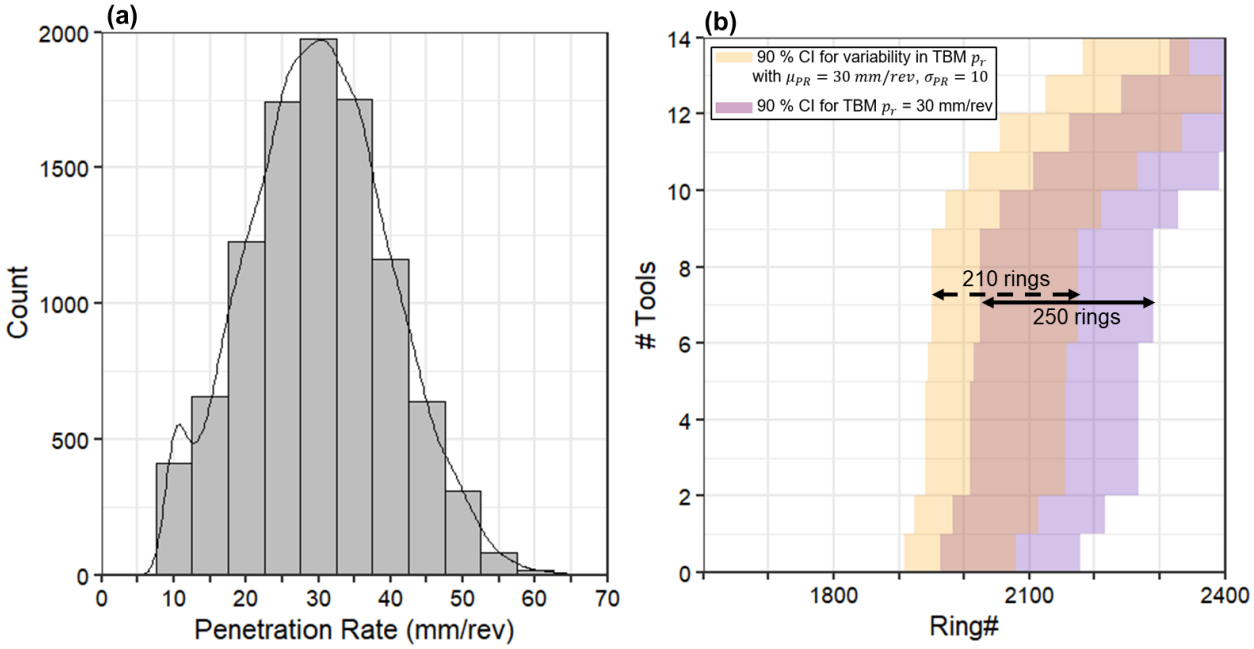

Figure 6.10 (a) Distribution of p_r, (b) uncertainty in the location of the first cutterhead intervention considering uncertainty in SAI and TBM p_r.

In this study, the location of additional investigations is optimized using knowledge of geotechnical uncertainty and tunnel site conditions. The empirical model to estimate tool wear rate used in this study does not account for any additional/excessive wear from tools interacting with cobbles and boulders (as no cobbles and boulders were encountered on the NEBT project site). However, probabilistic analysis to estimate boulder/cobble size, frequency, and location of occurrence within tunnel envelope can be integrated within the proposed methodology. In addition, the proposed methodology can be extended to include more than one tunnel risk to optimize construction means and methods, TBM operation, and risk mitigation strategies. The methodology can be extended to provide a dynamic update of geospatial assessments with every additional borehole to identify the optimal borehole configuration and sequence of drilling along the tunnel alignment. A probabilistic cost-benefit analysis of additional investigations, effective risk mitigation measures, and the reduction in geotechnical variability can be integrated for informed decision-making on geotechnical investigations.

6.6 Conclusions

This paper presents a methodology to optimize geotechnical investigations based on one or more tunnel risks, tunnel site conditions, and project-related constraints. Based on the results presented, the following conclusions are made:

i. The proposed geostatistical modeling-based methodology is practical and significant in identifying additional investigation locations to improve knowledge of geotechnical conditions for tunnel risk assessment. The methodology is demonstrated with actual site conditions and geotechnical investigation data from a 6.5 km stretch of the NEBT alignment in an urban setting in Washington, DC.
ii. Geospatial assessments of geotechnical uncertainty, tunnel site conditions, and project constraints for one or more tunnel risks allow effective communication of project and ground conditions and serves as a robust approach in deciding locations of additional geotechnical investigations.
iii. In the illustrated example, ten additional boreholes (30 % of initial investigations) virtually sampled at priority locations are found to reduce the uncertainty in tool wear rates and the resulting intervention location uncertainty by about 90 rings (~160 m) for the first two cutterhead interventions. A deviation of 30 % from the mean penetration rate (p_r) of 30 mm/rev reduces the uncertainty in the location of the first cutterhead intervention by 40 rings.
iv. The methodology serves as a practical tool to quantify the uncertainty reduction from additional investigations, evaluate the investigation effectiveness and reliability, and perform a probabilistic cost-benefit analysis before investing time and effort in actual investigations.

This work is developed with a vision to be used as a tool by the tunnel project owner, owner's engineer, and involved stakeholders for informed guidance on selecting priority locations of geotechnical investigations considering relevant tunnel risks and project site conditions.

CHAPTER 7- EVALUATION OF GEOSTATISTICAL MODEL ACCURACY IN PREDICTING SOIL TYPE TRANSITIONS FOR TUNNEL PROEJCTS

7.1 Abstract

This study deals with the evaluation of geostatistical model accuracy in predicting soil profiles for tunneling applications, with an emphasis on the accuracy of predicting soil transitions. Over the past decade, interpretations of soil profiles from geostatistical modeling have been applied towards characterizing risks, optimizing design and construction activities, and predicting tunneling performance. Such application of geostatistical models raises questions – *how accurate are developed geostatistical models, how do we investigate the accuracy of models, and what is the influence of geotechnical site investigation (SI) density on geostatistical model accuracy?* The study presents a methodology for quantitative evaluation of geostatistical model accuracy in predicting soil transitions and compares the influence of SI density on accuracy for two soft ground tunnel projects in different geological environments. Actual geotechnical SI data, encoded in terms of soil categories, are utilized to generate multiple possibilities of ground conditions from the pluri-Gaussian modeling technique. A comprehensive discussion on the validation of geostatistical models using indicator variogram reproduction and the soil type proportions is presented herein. The study uses a multi-classification confusion matrix to report the geostatistical model accuracy in predicting the soil conditions. The geostatistical model accuracy is derived from the deviation of soil type predictions from the actual ground conditions. The probabilistic estimates of soil types are examined to evaluate the geostatistical model accuracy at a finer resolution of the project domain. For a tunnel project situated in a well-stratified and sedimentary geological setting, the mean geostatistical model accuracy in predicting soil transitions is about 60 % for 100 m mean horizontal borehole spacing. The geostatistical model accuracy in predicting soil transitions in a highly variable and heterogeneous glacial setting is about 50 % for 100 m mean horizontal borehole spacing.

7.2 Introduction

Accurate interpretation of soil profiles is paramount for the planning, design, and construction of tunnel projects. The soil profiles help understand the nature of heterogeneity, help evaluate uncertainty and risks for tunneling applications. Inadequate interpretation of subsurface conditions has led to tunnel failures resulting in construction delays, cost overruns, and even injury or loss of life (Soldo et al. 2019; Sousa, 2010). Geostatistical techniques are one of the main techniques for estimating soil profiles. Geostatistical techniques produce multiple equiprobable soil profile simulations enabling spatial variability quantification of the subsurface conditions (Chiles and Delfiner, 2012). Over the past decade, there has been an increased application of geostatistical techniques in tunneling works to estimate the subsurface conditions, evaluate tunnel risks, and predict tunneling performance. Several publications have interpreted soil and rock profiles using geostatistical techniques for tunneling applications (Huang et al. 2017, Felletti and Beretta 2009, Grasmick 2020, Boyd 2019, Pinheiro 2016, Gangrade et al. 2021, Chen et al. 2017).

Geostatistical models offer a probabilistic interpretation of subsurface conditions and help quantify uncertainty. These ground conditions estimated from geostatistical modeling are utilized for decision-making in tunnel and geotechnical engineering projects. Therefore, it is imperative to

assess the accuracy of geostatistical models in predicting the ground conditions. Among the two different geostatistical models – categorical geostatistical models (for geologic units, soil/rock type) and continuous parameter geostatistical models (SPT, PI) – this paper focuses on evaluating the accuracy of categorical geostatistical models. Grasmick et al. (2020) discussed the *local* simulation approach in which soil profiles were utilized to simulate geotechnical parameters for tunnel risk assessment. The logical sequence of developing a categorical (or soil type) geostatistical model first to generate a model of geotechnical parameters makes a strong case for the accuracy evaluation of categorical geostatistical model. The use of such geostatistical models for tunnel risk assessment and decision-making raises the question: *how accurate are the geostatistical models in characterizing ground conditions, and how does typical geotechnical SI density adopted for tunnel works influence the accuracy of the models in different geological settings?*

In previous works discussing the accuracy of geostatistical models, in the field of soil sciences, Kravchenko (2003) evaluated the effect of sampling density on mapping the accuracy of soil properties with different spatial structures and variability. The study used cross-validation techniques to evaluate the accuracy of the interpreted geostatistical model. In traditional geostatistics, Goovaerts (2001) and Leuangthong et al. (2004) presented techniques such as cross-validation, jack-knife, histogram reproduction, and variograms reproduction to evaluate the geostatistical models. The cross-validation techniques give a measure of variability expected by withholding data but do not provide an accuracy measure of the suite of categorical geostatistical models. Leaving out a set of boreholes may not necessarily offer insights on model performance in capturing the soil transitions, one of the significant risks in geotechnical and tunnel applications.

Accuracy plots, an alternative method to evaluate geostatistical model accuracy, is inadequate in evaluating the accuracy of categorical geostatistical models. For models with disproportionate categories, the accuracy plots skew the accuracy metric in favor of high proportion categories, thus showing inadequacies in assessing the prediction accuracy of low proportion categories (Deutsch and Deutsch, 2012). Grasmick et al. (2020) developed geostatistical models from continuous geotechnical parameters such as moisture content, standard penetration tests (SPT), plasticity index (PI) for tunnel risk assessment and evaluated the accuracy of models for *global* and *local simulation approaches*. The study used accuracy plots (also known as reliability diagrams) as a diagnostic tool to evaluate the geostatistical models and revealed the significance of evaluating models of uncertainty in selecting the appropriate modeling approach. Boyd et al. (2019) used a synthetic dataset and evaluated the performance of 2D categorical geostatistical models from seven boreholes, for varying variogram parameters, by comparing them to a geologist's interpretation of subsurface conditions. The study used accuracy plots and R^2 values to evaluate the prediction performance of geostatistical models. However, global accuracy evaluation of a geostatistical model through R^2 values and accuracy plots is insufficient, as it does not guarantee that model is valid everywhere in its domain. For a quantitative assessment of the categorical geostatistical models, there exists a need for a diagnostic tool that captures the presence/absence of all categories and does not skew the accuracy results in favor of high proportion categories.

In the current practice, no specific guidelines, techniques, or procedures exist that provide a category wise quantitative evaluation of the categorical geostatistical model accuracy. The expected growth in the number of tunnel projects, especially in an urban environment, and the increased awareness about applying geostatistical techniques to estimate soil profiles needs a

discussion on the accuracy of the interpreted geostatistical models. An assessment of the categorical geostatistical model accuracy over the complete domain, also called as global accuracy, could be insufficient as it does not the guarantee that the model is accurate everywhere in its domain. An assessment of the categorical geostatistical models in predicting transitions between categorical units is warranted, especially for tunneling applications. It is acknowledged that the underlying stochastic algorithms are designed to reproduce distributions and spatial covariance; unlike the kriging solution, they are not meant to minimize the average prediction error.

This paper presents a quantitative evaluation of geostatistical model accuracy in predicting soil types, emphasizing the accuracy of predicting the soil transitions. Further, the paper investigates the influence of SI density and geological environment on geostatistical model accuracy in predicting soil transitions. This study extends the concept of a multi-class confusion matrix to quantitatively assess the classification (or misclassification) of predicted soil types and evaluate the accuracy. Geotechnical SI data collected on Northgate Extension Link (N125) tunnel project in Seattle, Washington, USA, and Anacostia River Tunnel (ART) project in Washington, DC, USA is used in this study. The research offers contributions towards presenting a methodology and metric to evaluate the geostatistical model accuracy of soil transitions. The remainder of the paper is organized as follows: In Section 7.3, we introduce the proposed methodology. A discussion of the tunnel project sites and modeling ground-truth conditions is presented in Section 7.4. Section 7.5 presents the accuracy evaluation of geostatistical models in predicting soil conditions within the tunnel envelope and predicting two soil transitions from each tunnel project. Conclusions are presented in Section 7.5.

7.3 Proposed methodology

The proposed methodology involves developing geostatistical models using varying SI densities and comparing modeled soil profiles to ground-truth conditions. To proceed with the proposed methodology, a representation of the ground-truth conditions within the tunnel project is required. Since boreholes are typically drilled at an offset from the tunnel alignment, a 3D representation of the ground-truth conditions is preferred over the 2D conditions presented in the geotechnical baseline report (GBR). Further, the soil transition presented in the GBR are subjective and generally do not represent the actual soil transition locations. Therefore, a virtual sampling of the boreholes is not possible using the deterministic 2D ground profiles in the GBR. To overcome this limitation, 3D geostatistical models representing soil types were created from two comprehensive sets of borehole logs from the respective project. Actual borehole logs from the projects were used to avoid the complexity of generating artificial 3D ground-truth models for each tunnel project and to capture the effect of the geological depositional environment.

To develop these ground-truth models, soil types encountered in the borehole logs of each project were compiled from the respective geotechnical data report (GDR). The pluri-Gaussian simulation (PGSIM) technique, a stochastic geostatistical modeling technique capable of modeling soil data, was utilized to generate 3D geostatistical models of soil types. Multiple possible realizations of ground-truth conditions generated from the PGSIM technique were processed to develop a single most likely ground-truth model for each tunnel project. The most likely representation of soil conditions in 3D is used to represent the ground-truth (G) models. The G models are used to represent a deterministic interpretation of the ground conditions for each tunnel project.

To evaluate the influence of geotechnical SI density on geostatistical model accuracy, boreholes with three different mean horizontal spacing (S_h) were virtually sampled from the G models of each tunnel project. S_h is selected based on the typical mean horizontal borehole spacing observed in the geotechnical SI campaigns in tunnel projects. For each S_h multiple unique borehole configurations (B_i, *where i=1,2, 3,…n; n=number of borehole configurations*) were generated to account for the borehole location uncertainty along the tunnel alignment. From each borehole configuration, soil types at the borehole locations were extracted from the G models of respective tunnel projects at a vertical resolution of 1 m. The virtually sampled boreholes are extended to two tunnel diameters below the tunnel invert. The choice of sampling resolution in the vertical direction and extents of the borehole is based on typical tunneling practice. Soil samples within the boreholes (of each borehole configuration) were extracted and utilized to generate a 3D ground conditions model for the borehole configuration. The extracted soil types for each tunnel project were discretized into a 3D random field of the same resolution as the respective G models. Using the sampled borehole data, multiple equally possible realizations of ground conditions, in terms of soil types, were generated utilizing the pluri-Gaussian modeling (PGSIM) technique. These equally possible realizations were post-processed to identify the most probable soil type and the occurrence probability of soil types in all simulation cells for a given set of borehole configurations and each S_h. The process was repeated until the total number of borehole configurations (B_n) generated were utilized.

The ground conditions modeled from each virtually sampled borehole configuration (B_i), also called the predicted model, were compared to the respective G model. For each B_i, the virtually sampled boreholes are used to develop a single predicted model (post-processing multiple equally possible predicted models), which is compared then compared to the G model. The deviation of the soil type predictions from the G model is quantified using a multi-classification confusion matrix. For a soil type, classification accuracy (A) is defined as the ratio of the sum of correct predictions to the sum of predictions that should have been correct, as shown in Eq.(7.2). The relationship is sometimes referred to as *sensitivity* of the confusion matrix (Tharwat 2020) and is used to measure geostatistical model accuracy in predicting soil type. The accuracy (A) of the geostatistical model in predicting soil type is reported as shown in Eq. (7.1).

$$A_k = \sum_{U} \frac{N_{kk}}{\sum_j^U N_{kj}} \tag{7.1}$$

where k is the soil type, N_{kj} represents the number of simulation voxels belonging to soil type k but classified as soil type j, U is the total number of soil types.

The accuracy of the soil transition is derived from the soil type probabilities of predicting the ground-truth conditions for each borehole density. The accuracy of soil transitions (A_{st}) in terms of occurrence probabilities of ground-truth soil k, p is calculated as shown in Eq. (7.2).

$$A_{st} = \frac{1}{n} \sum_{n} p_k \tag{7.2}$$

where *n* is the number of simulation voxels within a certain distance of the soil transition location. In summary, we note that the accuracy of probabilistic predictions is based on the knowledge of (a) soil type from the ground-truth conditions and (b) the occurrence probability of soil type from an ensemble of realizations for each borehole density.

7.4 Illustrative Example

7.4.1 Project overview

The Anacostia River Tunnel (ART) project in Washington, DC, is a 3.8 km long 8 m diameter single tunnel situated in a well-stratified sedimentary and marine deposit environment. This study considers a 2 km stretch of the ART alignment consisting of 20 boreholes, with an average borehole spacing of about 80 m. The boreholes were drilled at an average offset distance of about 30 m from the tunnel alignment. The subsurface conditions and the ART project primarily consist of a thick sequence of sediments deposited by streams in various onshore, fluvial, estuarine, and deltaic marine environments. As illustrated by the ESU logs in Figure 7.1, the subsurface is stratified with about 20 m to 30 m thick upper formation consisting of silty, sandy clay-dominated soil types and the 15 m to 30 m thick lower formation consisting of sand and gravel-dominated soil types (Southworth and Denenney, 2006). Standard penetration test (SPT) blow counts and soil types were recorded within each borehole at a vertical sampling interval of 0.5 m to 1 m. The soil types encountered along the ART alignment were grouped into engineering soil units (ESUs) based on the Unified Soil Classification System (USCS). Table 7.1 presents a brief description of the ESUs along with the USCS soil types. From the available borehole data, about 67 %, 15 %, and 18 % of the soil samples within the tunnel envelope were classified as G1, G2, and G3, respectively.

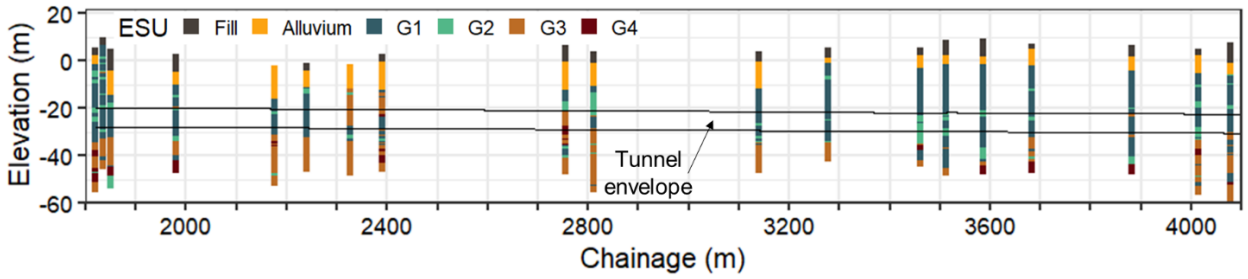

Figure 7.1 Longitudinal profile of boreholes along the 2 km section of the ART alignment.

Table 7.1 Description of ESUs encountered on 2 km ART alignment section.

ESU	**USCS Soil Classification**	**Description**
Fill	-	Fine to coarse-grained material with fragments of organic material.

Alluvium	-	Soft clay, loose silt, and fine sand with varying amounts of gravels, cobbles, and boulders.
G1	CH, MH	Highly plastic over-consolidated fine-grained soil.
G2	CL, ML	Low to medium plastic over-consolidated fine-grained soil.
G3	SM, SC, SC-SM, GM, GC, GC-GM	Non-plastic silty or clayey sand and gravel, or mixtures of sand, silt, and clay.
G4	SP, SP-SM, SP-SC, GP, GP-GM, GP-GC	Fine to coarse sand with trace amounts of gravel and fines.

The N125 project in Seattle, Washington, consists of 5.6 km long twin tunnels of 7 m diameter. This study considers a 1 km section of the northbound tunnel alignment consisting of 17 boreholes, with an average borehole spacing of about 110 m. The boreholes were drilled at an average offset distance of about 40 m from the tunnel alignment. The geological setting within the N125 project comprises sediments deposited by glacial processes. These glacial sediments consist of till, till-like deposits, advance outwash, glaciomarine and glaciolacustrine deposits. The soil types vary in thickness and lateral extent with a high degree of horizontal stratification, in some instances grading laterally, vertically, or both, into the adjacent soil type. Figure 7.2 presents a longitudinal profile of the drilled boreholes in terms of the ESUs for 1 km N125 alignment. Table 7.2 presents a description of the ESUs encountered within the 1 km of N125 alignment. From the available borehole samples, about 31 %, 25 %, 31 %, and 13 % of the soil samples within the tunnel envelope were classified as CCS, CSF, CSG, and TLD, respectively.

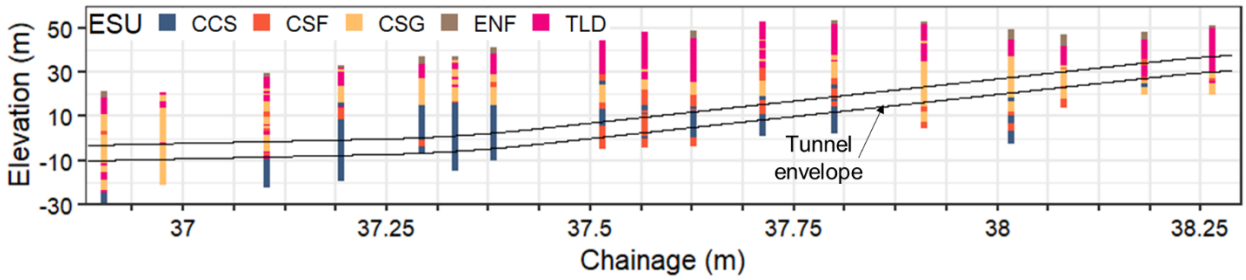

Figure 7.2 Longitudinal profile of boreholes along the 1 km section of the N125 alignment.

Table 7.2 Summary of the ESUs encountered along 1 km N125 alignment.

ESU	**Description**

CCS	Hard, interbedded silt and clay with lenses of silt, sand, and gravel.
CSF	Fine-grained soil consisting of fine, very dense silt and silty fine sand.
CSG	Dense to very dense silty sand to sandy gravel with lenses of clay and silt.
ENF	Very loose to very dense sand with varying amounts of silt and gravel.
TLD	Changes from a mixture of gravel, sand, silt, and clay to a mixture of silt, sand, and gravel to clean or relatively clean sand and gravel.

7.4.2 Modeling ground-truth conditions

A 3D simulation grid extending to 50 m on either side of the tunnel alignment of each project is generated for developing G models. The center of each voxel of the 3D grid is identified with the coordinates *(x, y, z)* denoting easting (longitudinal direction), northing (transverse direction), and elevation (vertical direction), defined from the start of the tunnel alignment at a resolution of 5 m, 5 m, and 1 m, respectively. Using the available geotechnical SI data, multiple equally possible scenarios of 3D ground conditions, also known as realizations, are developed. A set of 500 realizations is generated for each tunnel project site. Within these individual realizations, each voxel of the 3D grid is simulated with an ESU category based on the conditioning data, transition probabilities between ESUs, and the ESUs' spatial structure conveyed through indicator variograms. A 2D longitudinal representation of the most likely ground-truth conditions for the two tunnel projects established using the PGSIM technique are presented in Figure 7.3**Error! Reference source not found.**.

PGSIM characterizes the soil type configuration using two or more Gaussian variables honoring the proportions, spatial contacts, probability of transition, and the spatial structure of the soil types (Armstrong et al. 2011; Chiles and Delfiner 2009). The PGSIM realizations capture the vertical variability in soil proportions through vertical proportion curves (VPCs). The spatial contacts between soil types and transition probability from one type to another are integrated into the realizations using the *lithotype* rule. Next, the indicator variograms convey valuable information on the spatial correlation structure (geometry, variability) of soil types. Following the indicator variogram modeling, the soil types are transformed to Gaussian values using the Gibbs sampler algorithm, and the simulated Gaussian values are back-transformed to soil types. Gangrade et al. (2021) provided a detailed description of the critical steps in the PGSIM technique.

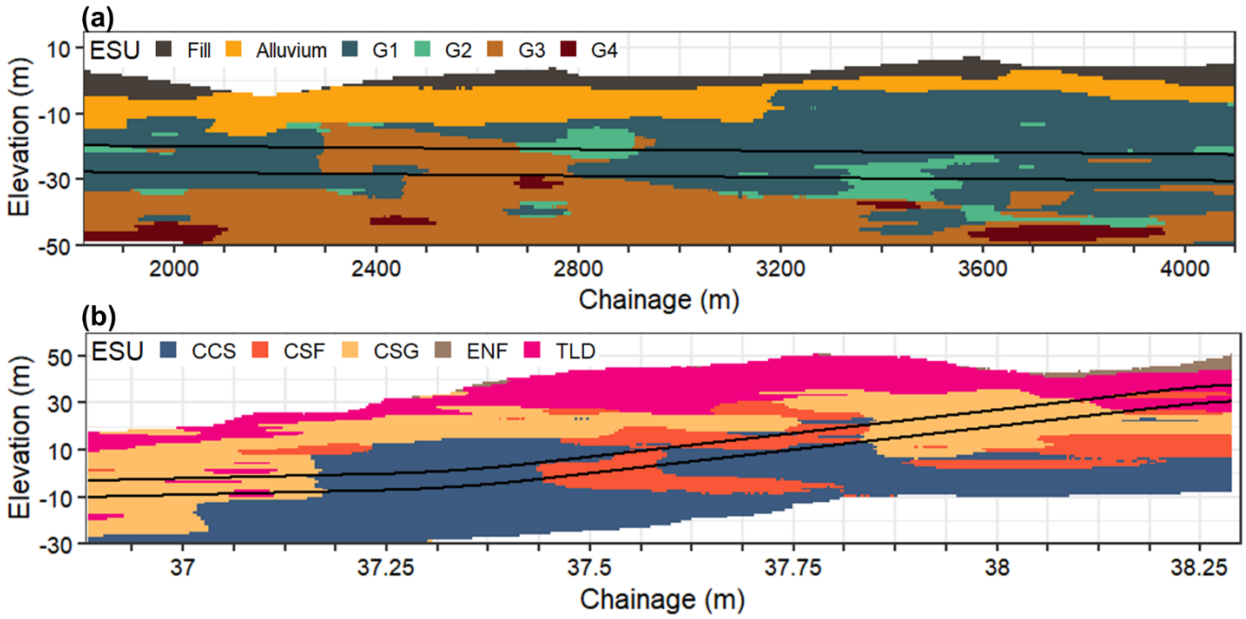

Figure 7.3 Longitudinal profile (x, y = 0, z) of ground-truth conditions for (a) ART project, and (b) N125 project generated using PGSIM technique.

Most depositional processes impart spatial correlation to geologic units (ESUs, in this case) that can be quantified and conveyed through indicator variograms (Maleki et al. 2017; Emery and Maleki 2019). Figure 7.4(a)-(d) presents the experimental and model indicator variograms for each ESU of the respective projects along the *x*, *y*, and *z* directions of the tunnel project site. The experimental indicator variograms are calculated from the borehole data and represent the probability of a different ESU as a function of distance. As observed, the experimental indicator variograms increase monotonically, reflecting that the correlation between the two locations decreases up to a certain distance. Therefore, the rate of increase of the semivariance represents the degree of dissimilarity between the data points. The distance at which correlation becomes equal to the sill is the range of the indicator random variable. The physical meaning of the variogram range is that the data point pairs that are range distance or greater apart are not spatially correlated.

Comparing the two project sites, the correlation between ESUs from the N125 project decreases at shorter distances than for the ART project, reflecting the heterogeneity of the N125 project. In addition, the rate of increase of the indicator variograms (horizontal and vertical) for N125 project ESUs than the ART project ESUs indicating a higher degree of dissimilarity between the data points. The correlation range observed for N125 project ESUs is less than the ART project ESUs indicating a higher degree of heterogeneity. Since geostatistical simulations require a positive definite model of spatial variability, the experimental indicator variograms cannot be used directly. Instead, parametric models are fit to the experimental data to describe the spatial variability as a function of lag distance. Within the PGSIM technique, the generated realizations are constrained to spatial structure quantified through indicator variograms. Multiple such realizations are generated and are post-processed to quantify the occurrence probability and the most likely ESU

at each voxel of the 3D simulation grid. For visualization purposes, ground conditions expected along the tunnel centerline ($x, y = 0, z$) are presented for the two tunnel projects in Figure 7.4.

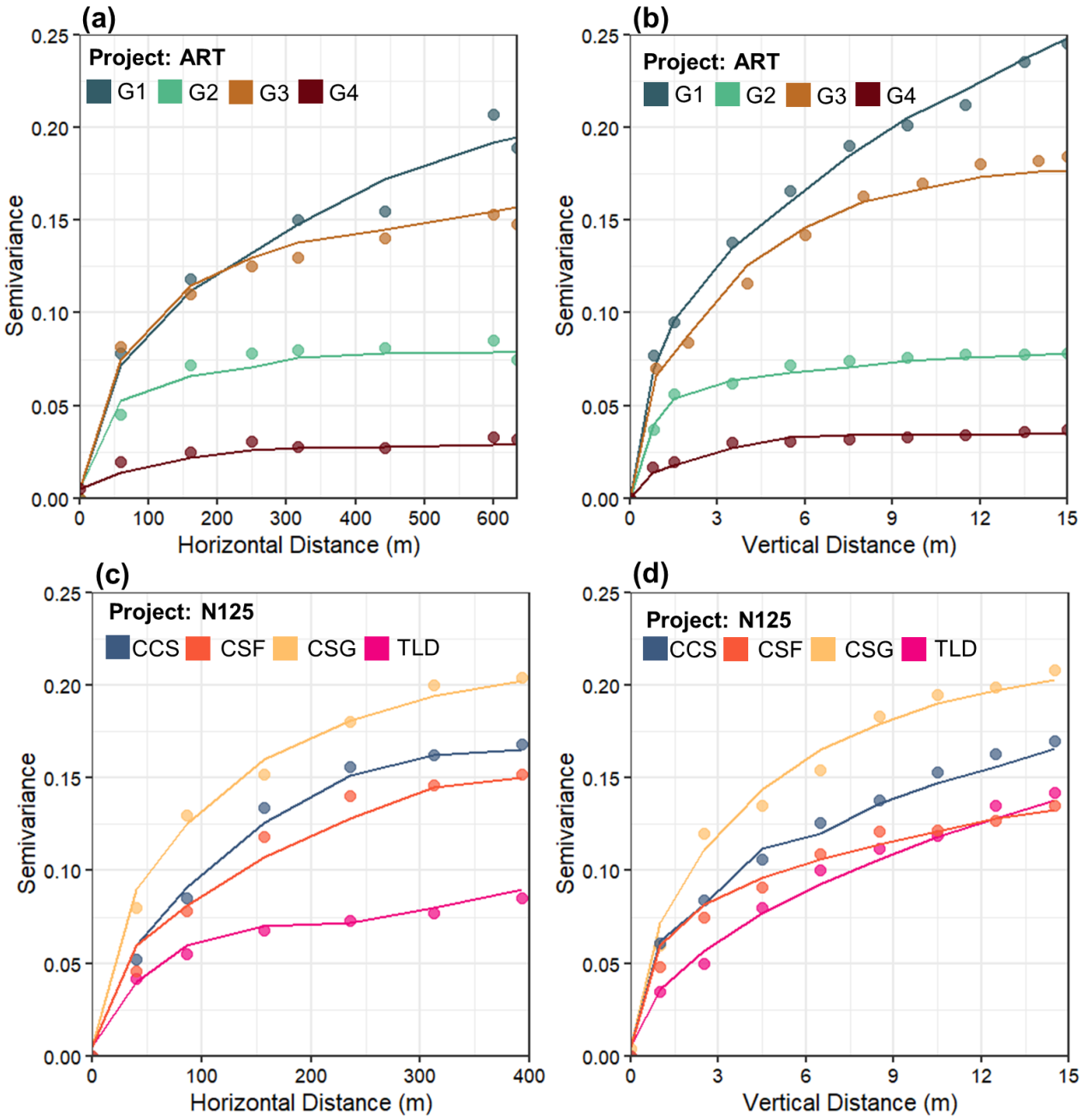

Figure 7.4 Directional indicator variograms for ESUs in ART project tunnel envelope (**a, b**) and N125 project tunnel envelope (**c, d**). Dotted lines correspond to experimental indicator variograms, and solid lines correspond to model indicator variograms.

7.5 Accuracy evaluation of geostatistical models

To quantify the influence of geotechnical SI density on geostatistical model accuracy, the boreholes were located at S_h = 100 m, 70 m, and 40 m along each tunnel alignment. For the ART project, 17, 25, and 42 boreholes were located along the tunnel alignment within one borehole configuration for S_h = 100 m, 70 m, and 40 m, respectively. For the N125 project, 10, 16, and 33 boreholes were located within one borehole configuration for the respective S_h. The boreholes were staggered one diameter away from the tunnel alignment and at a maximum offset distance of 30 m using. Ten unique borehole configurations were generated for each S_h and for each tunnel project. Each borehole was sampled from the respective G model to generate the SI ESU data set. The resolution of vertical ESU sampling was kept to 1 m, as typically observed in tunnel projects. These virtually sampled boreholes were then utilized to generate geostatistical ESU models. Within the PGSIM technique, the ESU proportions were updated for each borehole configuration. The lithotype rule and the indicator variograms, the same as utilized to generate the ground-truth model, were utilized to generate realizations from each borehole configuration. The resolution of the ESU simulation grid for each borehole configuration and spacing was consistent with the resolution of the G model (5 m x 5 m x 1 m). The ESUs predicted by the geostatistical model for each borehole configuration was compared to the ESUs from the G model. A voxel-based comparison allowed developing a multi-classification confusion matrix to quantify the correct classifications (or misclassification) of ESU.

7.5.1 Validation of geostatistical realizations

Geostatistical realizations generated from each borehole spacing are validated with the variogram reproduction from the realizations. The variogram reproduction is checked by calculating directional variograms from multiple realizations and comparing against the input model variogram (and experimental variogram) for the same directions. In this study, 50 randomly chosen realizations (10 % of generated realizations) are extracted from each borehole configuration associated with the borehole spacing. For example, 50 randomly chosen realizations each are extracted from the ten borehole configurations generated for S_h = 100 m, resulting in 500 realizations for validation of variogram reproduction. The process is repeated for each S_h and for each tunnel project. The resulting indicator variograms are validated with the input variogram model in terms of structure, resemblance, and other variogram parameters. The validation considers the reproduction of the input indicator variogram model over 500 realizations and shows the reproduction of indicator variogram spread or fluctuations across realizations, which are critical elements in geostatistical modeling of uncertainty.

Figure 7.6 and Figure 7.6 show that the spatial structure of ART tunnel envelope ESUs from randomly chosen 500 realizations follow the spatial structure quantified by the input indicator variogram model. The magenta line represents the experimental indicator variogram derived from the borehole data. Gray lines indicate the output indicator variograms from realizations. Red and blue lines indicate the average of 500 output indicator variograms and average ± two standard deviations. The red line bears a resemblance to the shape and the structure of the model input indicator variogram model (black line). The difference between the sill of the average output indicator variogram (red line) and the input model (black line) is less than 2 % for G1 and G3 and is less than 5 % for G2 and G4. This indicates that the proportions of ESUs (as observed in the borehole data) are honored in the set of 500 realizations. The interpreted range for all the output

indicator variograms is similar to the model input indicator variogram. Similar observations are made from the indicator variograms for N125 tunnel envelope ESUs, as shown *Figure 7.7* and *Figure* 7.8Figure 4.7. The difference between the sill of the average output indicator variogram (red line) and the input model (black line) is less than 1 % for CSF, CSG, and TLD and is about 7 % for CSF. The results indicate that the ESU proportions and the interpreted range from all the output indicator variograms are honored in the set of 500 realizations. Such analysis helps validate the consistency of an interpreted stratigraphic model.

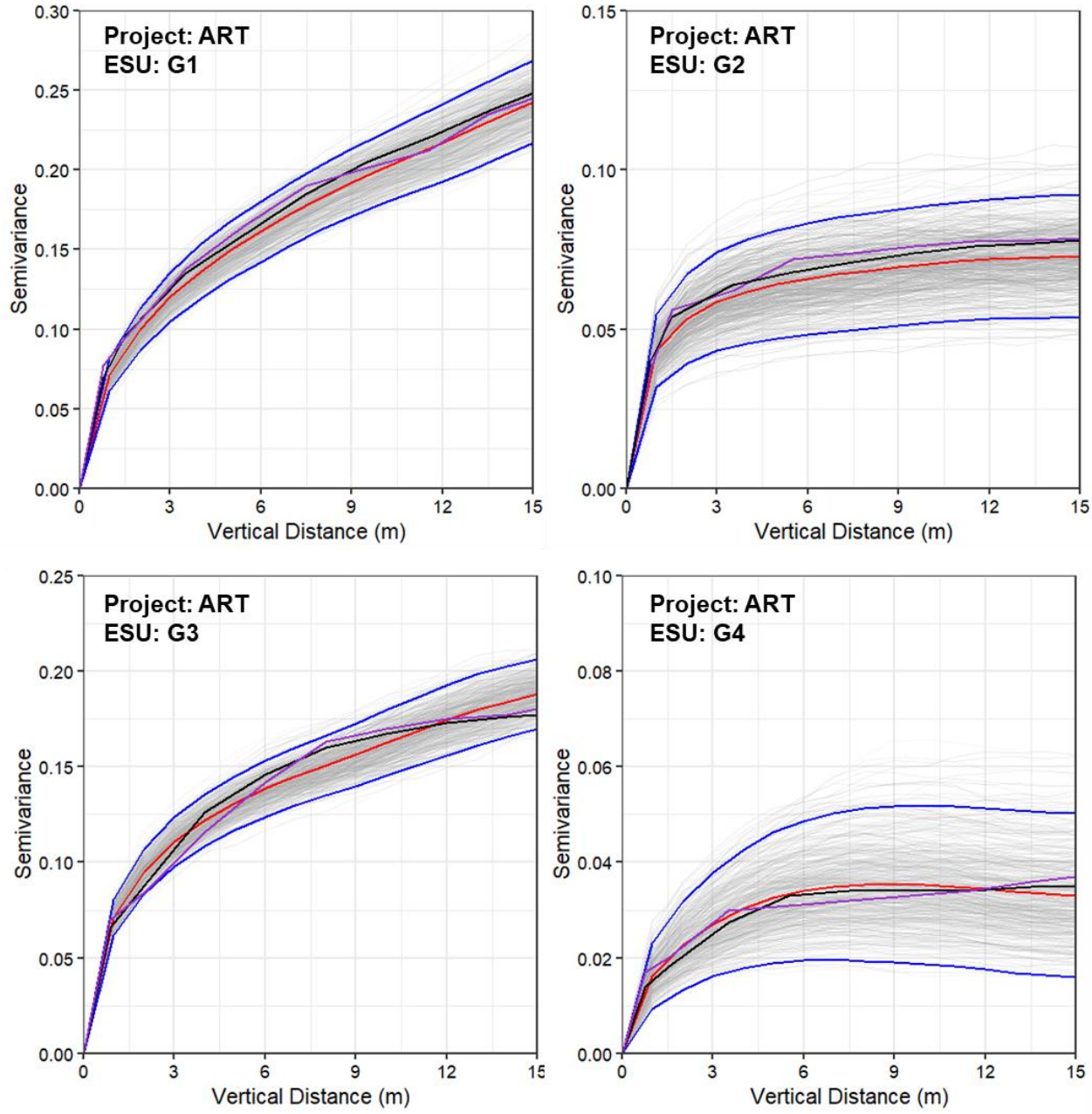

Figure 7.5 ART project indicator variograms in the vertical direction obtained from 500 randomly chosen realizations. Gray: output indicator variograms of 500 realizations. Red: average of output

indicator variograms. Blue: average ± two standard deviations. Black: variogram model input. Magenta: experimental indicator variogram from borehole data.

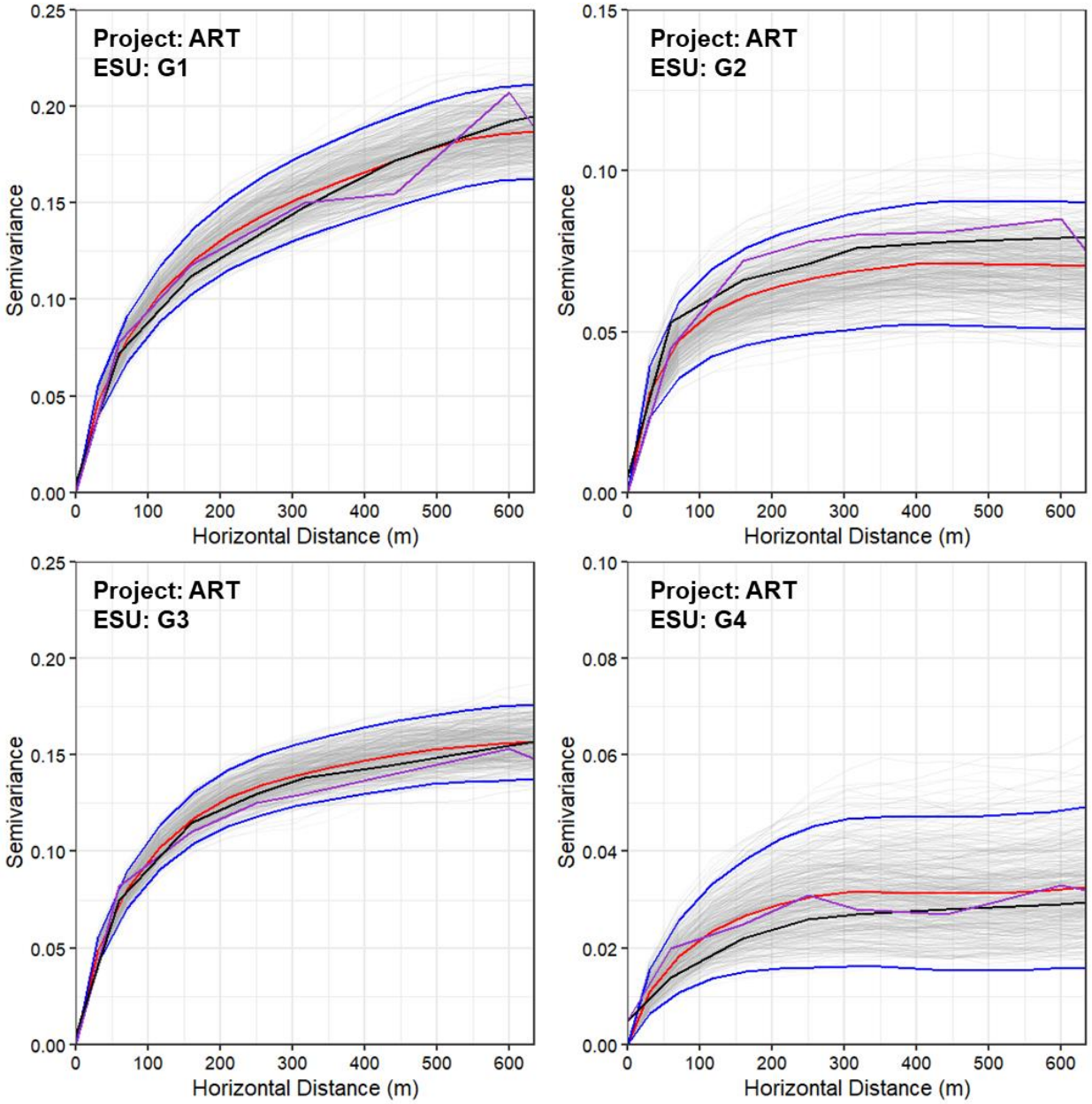

Figure 7.6 ART project indicator variograms in the horizontal direction obtained from 500 randomly chosen realizations. Gray: output indicator variograms of 500 realizations. Red: average of output indicator variograms. Blue: average ± two standard deviations. Black: variogram model input. Magenta: experimental indicator variogram from borehole data.

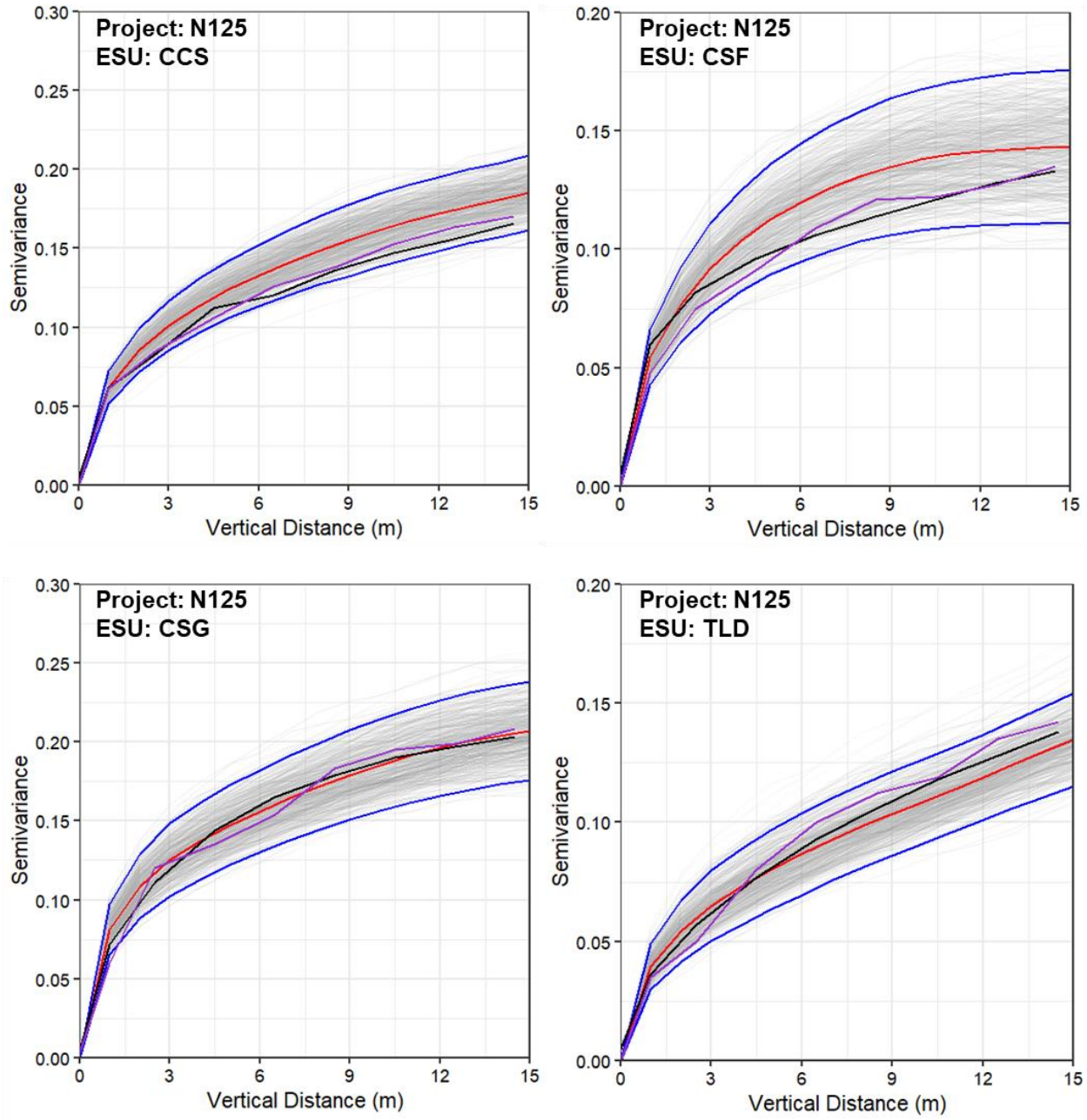

Figure 7.7 N125 project indicator variograms in the vertical direction obtained from 500 randomly chosen realizations. Gray: output indicator variograms of 500 realizations. Red: average of output indicator variograms. Blue: average ± two standard deviations. Black: variogram model input. Magenta: experimental indicator variogram from borehole data.

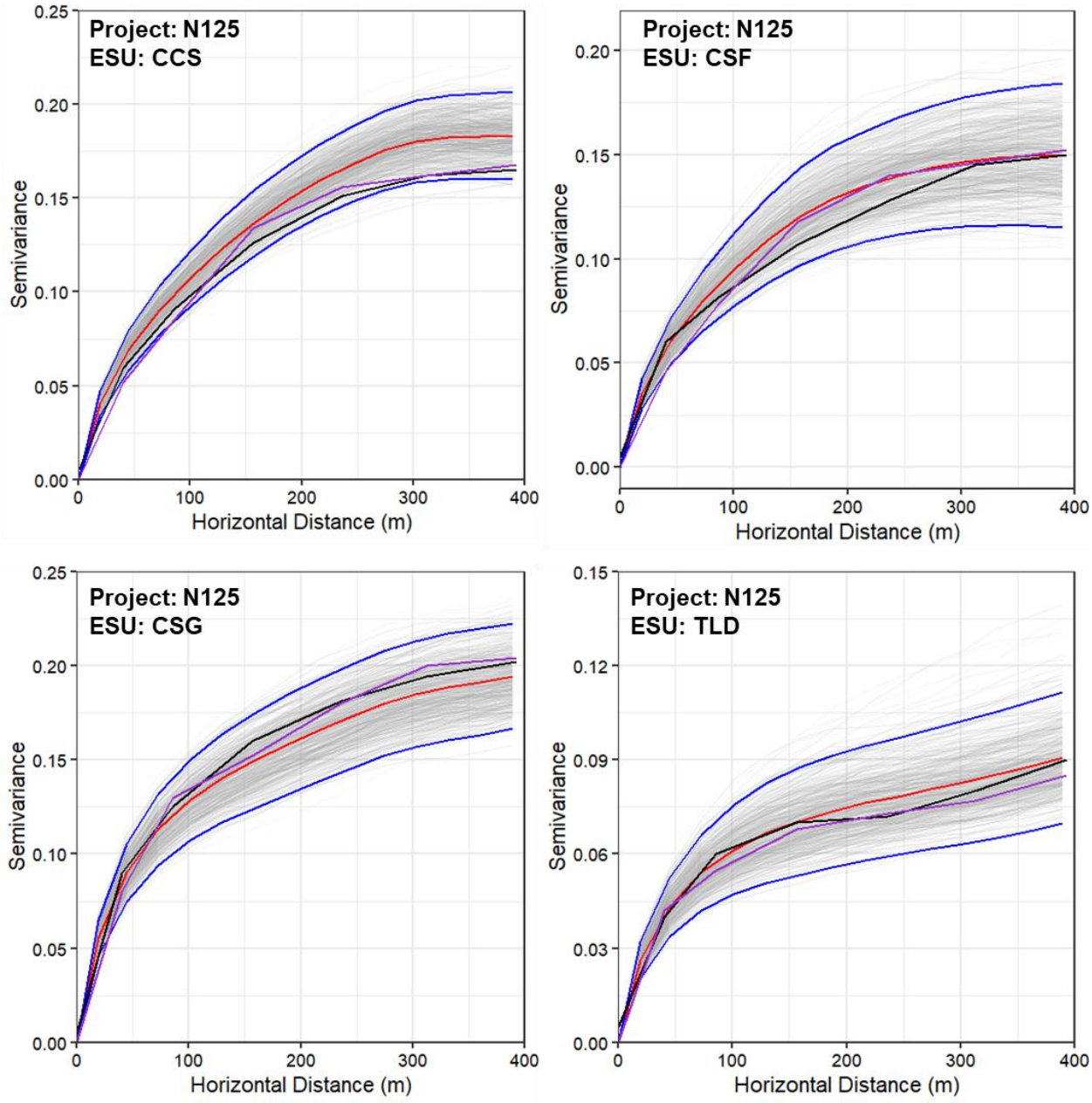

Figure 7.8 N125 project indicator variograms in the horizontal direction obtained from 500 randomly chosen realizations. Gray: output indicator variograms of 500 realizations. Red: average of output indicator variograms. Blue: average ± two standard deviations. Black: variogram model input. Magenta: experimental indicator variogram from borehole data.

One of the essential steps in analyzing the geostatistical model is to validate if the input ESU proportions (from boreholes) are reproduced within the realizations. It is evident that if the ESU proportions are reproduced, the probability of spatial structure reproduction of indicator variograms would be high. One of the reasons for better spatial structure reproduction from realizations honoring the input proportions is that, in indicator variograms, the sill is a function of the category proportion, i.e. $s_k = f_k(1 - f_k)$, for category *k.* Moreover, the category proportions

influence the near-origin slopes of the spatial structure models. For indicator variograms, Maleki et al. (2017) conveyed that the modeling of categorical boundaries in the PGSIM technique is related to the second-order derivative of indicator variogram at the origin, which relates to the category proportion within the modeling domain. As a result, better reproduction of the input proportions leads to an improved reproduction of the sills and the near origin slopes of indicator variograms, thus validating the consistency of the interpreted model. Table 7.3 presents the input and output ESU proportions for each borehole spacing and project site derived from the randomly chosen 500 realizations.

Table 7.3 Input and output proportions of ESUs for each borehole spacing (derived from ten unique borehole configurations) and project site, expressed as mean ± standard deviation over an ensemble of randomly chosen 500 realizations.

	S_h = 100 m		S_h = 70 m		S_h = 40 m	
ESU	*Input*	*Output*	*Input*	*Output*	*Input*	*Output*
ART Project						
G1	69.1 ± 3.9	71.5 ± 1.6	72.0 ± 3.9	73.5 ± 1.8	70.8 ± 4.0	71.2 ± 1.2
G2	11.3 ± 3.0	7.2 ± 1.2	8.6 ± 3.5	7.1 ± 1.5	10.0 ± 3.8	8.9 ± 0.5
G3	19.6 ± 2.7	21.3 ± 1.6	19.4 ± 2.3	19.4 ± 1.8	19.2 ± 5.2	19.9 ± 1.0
N125 Project						
CCS	36.0 ± 8.8	37.3 ± 2.9	38.3 ± 7.8	32.6 ± 3.4	35.8 ± 5.2	32.0 ± 1.6
CSF	17.3 ± 8.3	14.5 ± 2.6	19.0 ± 7.5	17.3 ± 4.3	18.5 ± 6.8	19.4 ± 1.5
CSG	39.2 ± 3.9	39.0 ± 4.2	39.9 ± 2.5	44.9 ± 2.5	38.7 ± 2.4	39.9 ± 1.4
TLD	7.5 ± 4.0	9.2 ± 1.0	2.8 ± 1.4	5.2 ± 1.0	7.0 ± 3.1	8.7 ± 0.5

7.5.2 Tunneling envelope accuracy

For each S_h and each unique borehole configuration, voxels within the 3D tunnel envelope are extracted and compared to the voxels from the G model. An ESU category-wise assessment of the geostatistical model predictions within the tunnel envelope for each borehole spacing is quantified

using a multi-classification confusion matrix. The elements of the multi-classification confusion matrix represent the percentage of the most probable ESU category predicted correctly/incorrectly (along with the number of simulation voxels) compared to the G model. The diagonal elements of the confusion matrix illustrate the percentage of correct predictions of ESU categories, whereas the non-diagonal elements of the matrix illustrate the misclassifications (or incorrect predictions). A multi-classification confusion matrix is derived for each unique configuration indicating the number of voxels correctly classified (or misclassified) within the tunnel envelope. The results from each unique confusion matrix are processed to derive the mean number of voxels with correct classification and misclassification of the ESUs.

Figure 7.9 presents the multi-classification confusion matrix for ESUs within the ART tunnel envelope and each S_h . The numbers reflect the mean number of voxels that are correctly classified (or misclassified), as derived from ten unique borehole configurations for each S_h . The percentage of classification and misclassification is derived as the ratio of the number of voxels predicted as an ESU category and the number of voxels with the ESU category in the G model. As an example from Figure 7.9, the tunnel envelope of ART G model contains 9960 voxels of G1 (adding simulation voxels along the G1 column) from which a mean of 9485 voxels have been identified correctly over ten borehole configurations for S_h = 100 m. It is interesting to note that the G2, ESU with the lowest proportion within the tunnel envelope is identified with an accuracy of less than 60 % for S_h = 100 m and 70 m. High proportion ESUs , G1 and G3, are identified with relatively the same level of accuracy for the two borehole densities. A 14 % increase in the accuracy of G2 classification, as S_h is reduced to 40 m, indicates that larger number of conditioning points helps the geostatistical realizations better capture the presence/absence of low proportion ESU. Results indicate that the accuracy of the geostatistical model in capturing high proportion ESUs, G1 and G3, is consistently greater than about 87 % for all S_h , whereas the accuracy in capturing G2, low proportion ESU, increases with the borehole density and number of conditioning points.

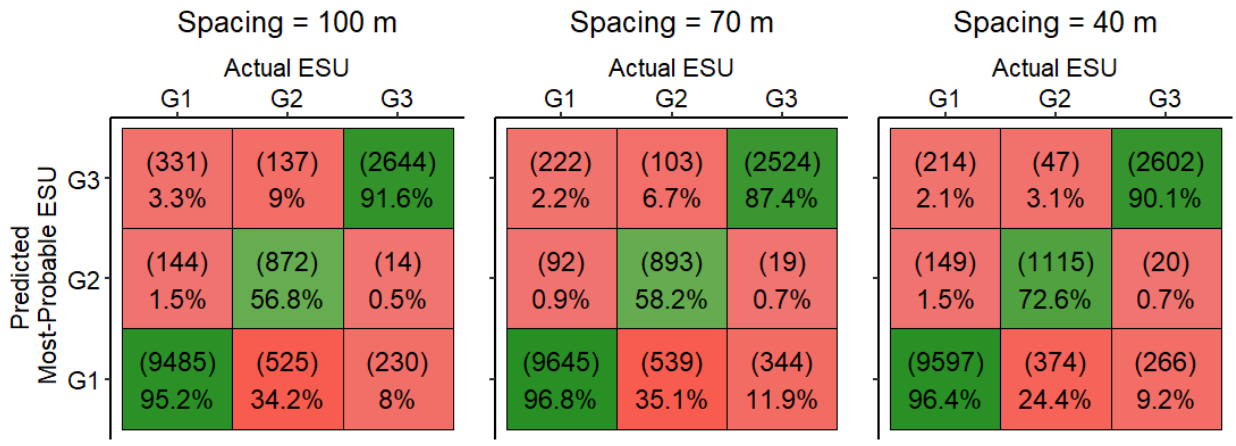

Figure 7.9 Multi-classification confusion matrix, expressed as the mean number of voxels (or percentage) correctly classified and misclassified for ESUs in ART tunnel envelope and each borehole density.

Figure 7.10 presents the multi-classification confusion matrix with the mean percentage of classification and misclassification for the N125 tunnel envelope. As observed earlier, the mean accuracy of CSG and CCS classification remains consistently above 87 % in the geostatistical models developed for each borehole spacing. However, lower proportion ESUs – TLD and CSF are captured with relatively less accuracy for all S_h . However, with the increase in the number of conditioning points, the percentage accuracy of TLD and CSF increases by about 7 % and 26 %, respectively as S_h is reduced from 100 m to 40 m. The significant difference in the percentage accuracy increase of TLD and CSF could be attributed to the respective proportions and range from indicator variograms.

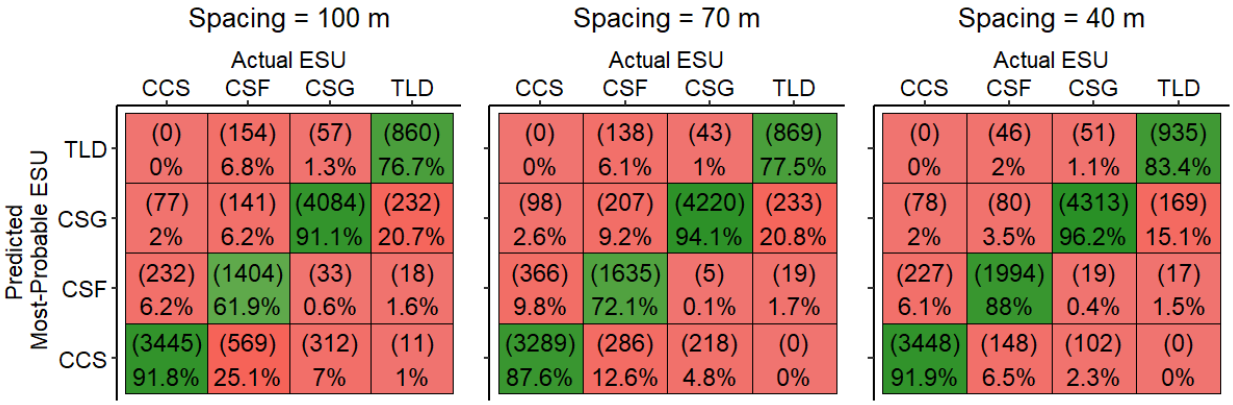

Figure 7.10 Multi-classification confusion matrix, expressed as the mean number of voxels (or percentage) correctly classified and misclassified for ESUs in N125 tunnel envelope and each borehole density.

7.5.3 Soil transition accuracy

The geostatistical model accuracy in predicting soil transitions is evaluated using Eq. (7.2). ESU probabilities in the voxels within the longitudinal and transverse distance of two tunnel diameters from the soil transition boundary in G models are utilized to derive the soil transition accuracy. It is to be noted that the extent window of voxels that can be considered for soil transition accuracy can be subjective.

Figure 7.11(a) shows the longitudinal profile of the 55 m stretch of ground-truth conditions within the ART tunnel envelope at the location of transition between G1 and G3. The probabilistic predictions of ground-truth ESUs for each borehole density are presented in Figure 7.11(b)-(d). For ART soil transition 1 within the 3D tunnel envelope, the A_{st} measures for S_h = 100 m, 70 m, and 40 m are 0.62, 0.70, and 0.80, respectively. Figure 7.11(e-h) shows the longitudinal profile of ART soil transition 2 ground-truth conditions and the mean probabilities of ground-truth ESUs over a longitudinal distance of 160 m. Considering probabilistic measurements from voxels within the 3D tunnel envelope in the proximity of soil transition 2, the A_{st} measures for S_h = 100 m, 70 m, and 40 m are 0.60, 0.64, and 0.76. Results indicate that soil transitions for ART tunnel project situated in a sedimentary and marine geological environment are effectively captured with an accuracy of 55 % to 80 % for borehole density as per S_h = 100 m and 40 m, respectively. It is

important to note that the accuracy of geostatistical model in capturing soil transition also depends on the location and the number of conditioning points, i.e., the number and locations of ESU samples in the proximity of the soil transitions. It is evident that drilling multiple boreholes within a short distance of soil transition location may help characterize the soil transitions from geostatistical modeling with relatively higher accuracy. This is assuming that the location of soil transition is estimated from preliminary investigations.

The multi-classification matrices presented in Figure 7.12 provide evidence on how ESU proportions play a significant role in geostatistical simulations. For ART soil transition 1, G1 classification accuracy consistently remains greater than 75 % for each S_h. However, for ART soil transition 2, the G1 classification accuracy is less than 70 % for the highest borehole density. The contrast accuracies are primarily due to the difference in the local proportions of G1, the number of available conditioning points in the proximity of the respective soil transitions, and the indicator variograms. Interestingly, the classification accuracy of G2, low proportion ESU, in soil transition 2 increases by about 20 % with the increase in the borehole density, as observed in the accuracy metrics for the ART tunnel envelope.

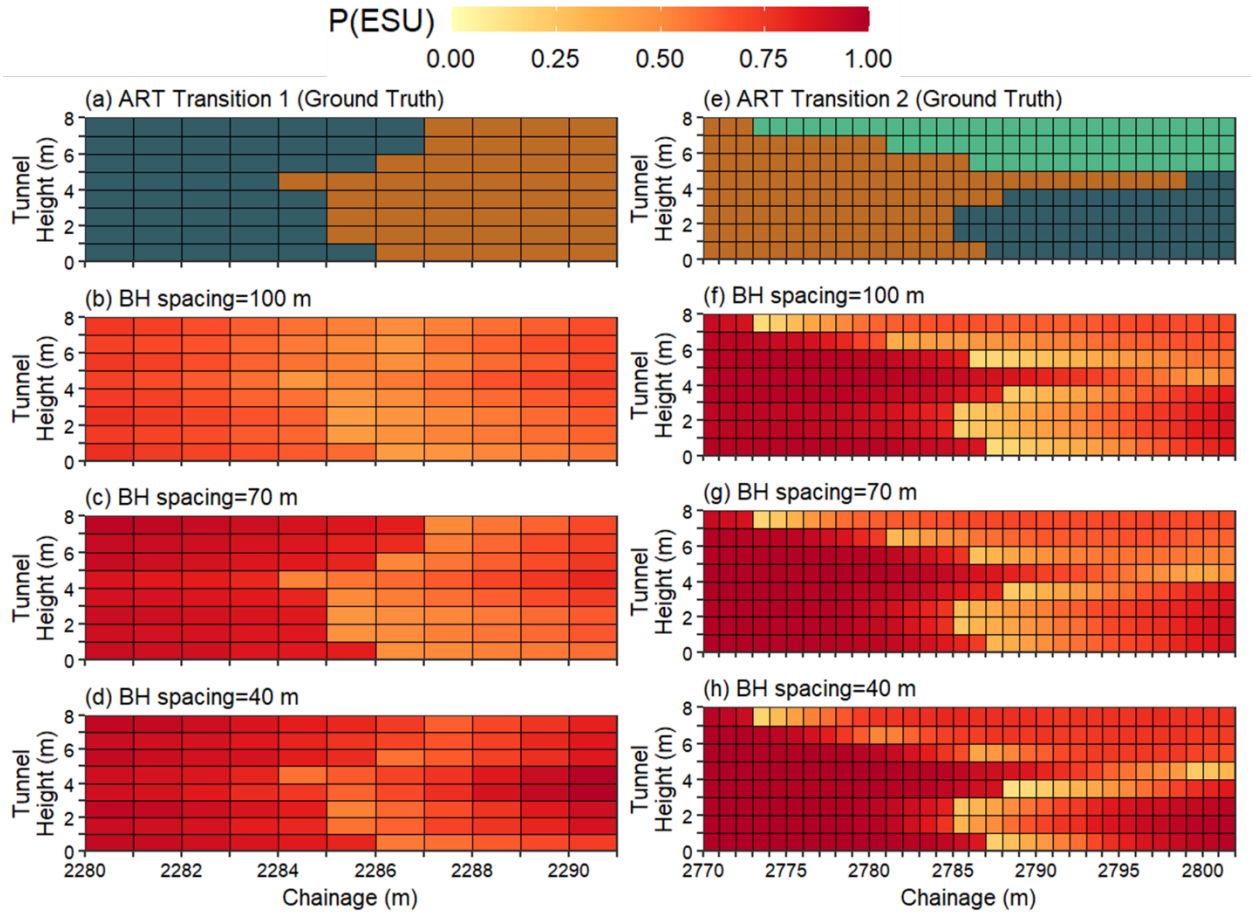

Figure 7.11 (a, e) Longitudinal profile (x, y = 0, z) of soil transitions within the ART tunneling envelope; (b)-(h) indicate the mean occurrence probability of ground-truth ESU for all borehole density.

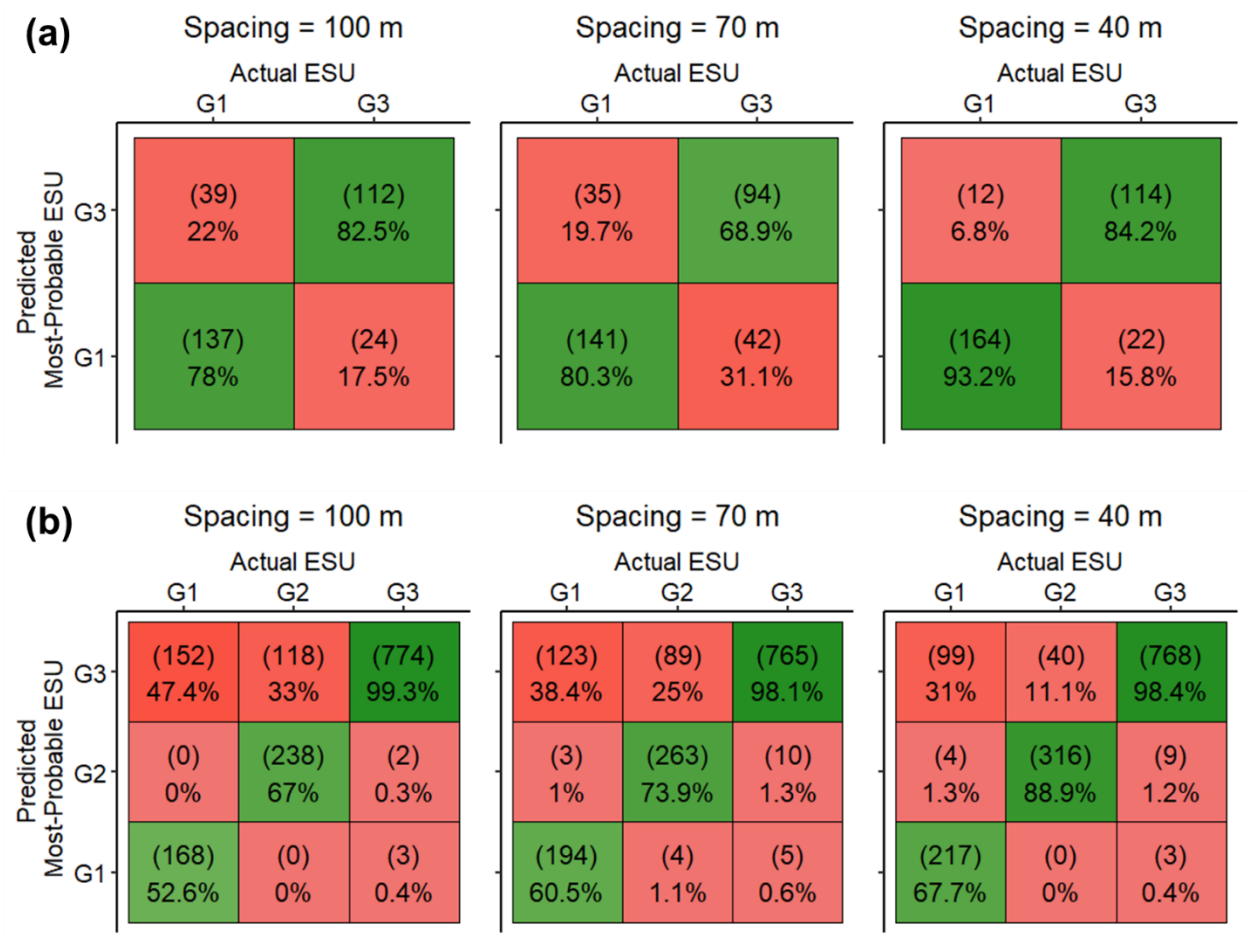

Figure 7.12 Multi-classification confusion matrix, expressed as the mean number of voxels (or percentage) correctly classified and misclassified for (a) soil transition 1 and (b) soil transition 2 within the ART tunnel envelope and for each borehole density.

Figure 7.13(a) shows the longitudinal profile of 50 m stretch of ground-truth conditions within the N125 tunnel envelope at the location of transition between CSG and CCS. The probabilistic predictions of ground-truth ESUs for each borehole density are presented in Figure 7.13(b)-(d). Considering the voxels within the 3D tunnel envelope in the proximity of N125 soil transition 1, the A_{st} measures for S_h = 100 m, 70 m, and 40 m are 0.55, 0.61, and 0.68, respectively. As illustrated, CSG is simulated with relatively low probabilities for S_h = 100 m and 70 m, thus reducing the geostatistical model accuracy in capturing the soil transition. Relatively poor prediction of CSG could be attributed to the spatial correlation structure at shorter distances and the proportion of CCS and CSG in the proximity of the transition. For N125 soil transition 2 presented in Figure 7.13(e) – (h), the A_{st} measures for S_h = 100 m, 70 m, and 40 m are 0.50, 0.61, and 0.71. Results indicate that soil transitions for N125 tunnel project situated in a glacial geological environment are effectively captured with an accuracy of 50 % to 70 % for borehole density as per S_h = 100 m and 40 m, respectively.

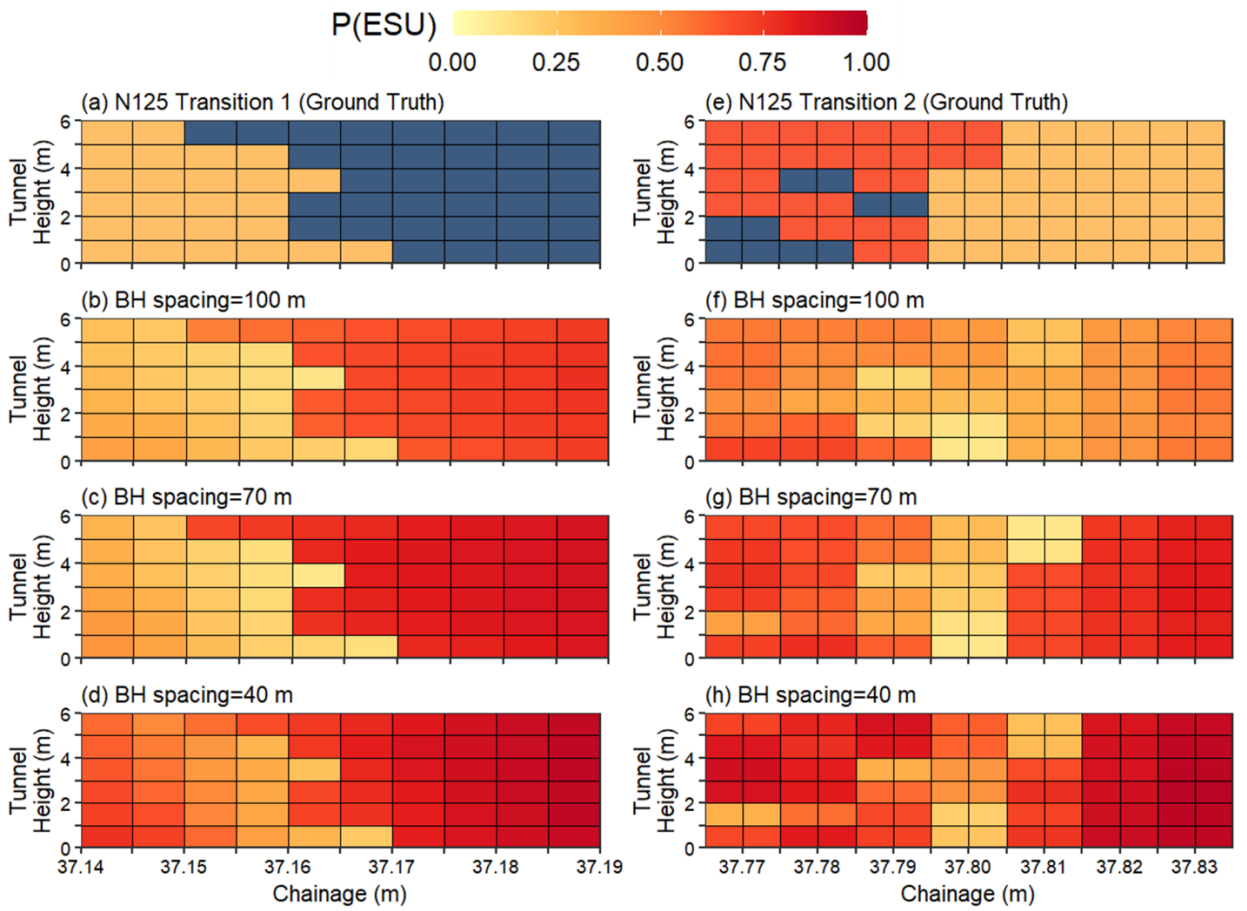

Figure 7.13 (a, e) Longitudinal profile (x, y = 0, z) of soil transition within the N125 tunneling envelope; (b)-(h) indicate the mean occurrence probability of ground-truth ESU for all borehole density.

Figure 7.14 presents the ESU confusion matrix for N125 soil transitions 1 and 2 for all the voxels in the proximity of the transitions and within the 3D tunnel envelope. For the N125 soil transitions, the mean percentage accuracy of ESUs is low compared to the ART soil transitions. For soil transition 2, although high proportion ESUs CCS and CSG are predicted with nearly 80 % accuracy for S_h = 100 m, the overall accuracy of the soil transition remains at about 0.50. The mean percentage accuracy metrics of ESUs are low compared to the accuracy of the geostatistical model in predicting the ESUs within the complete tunnel envelope.

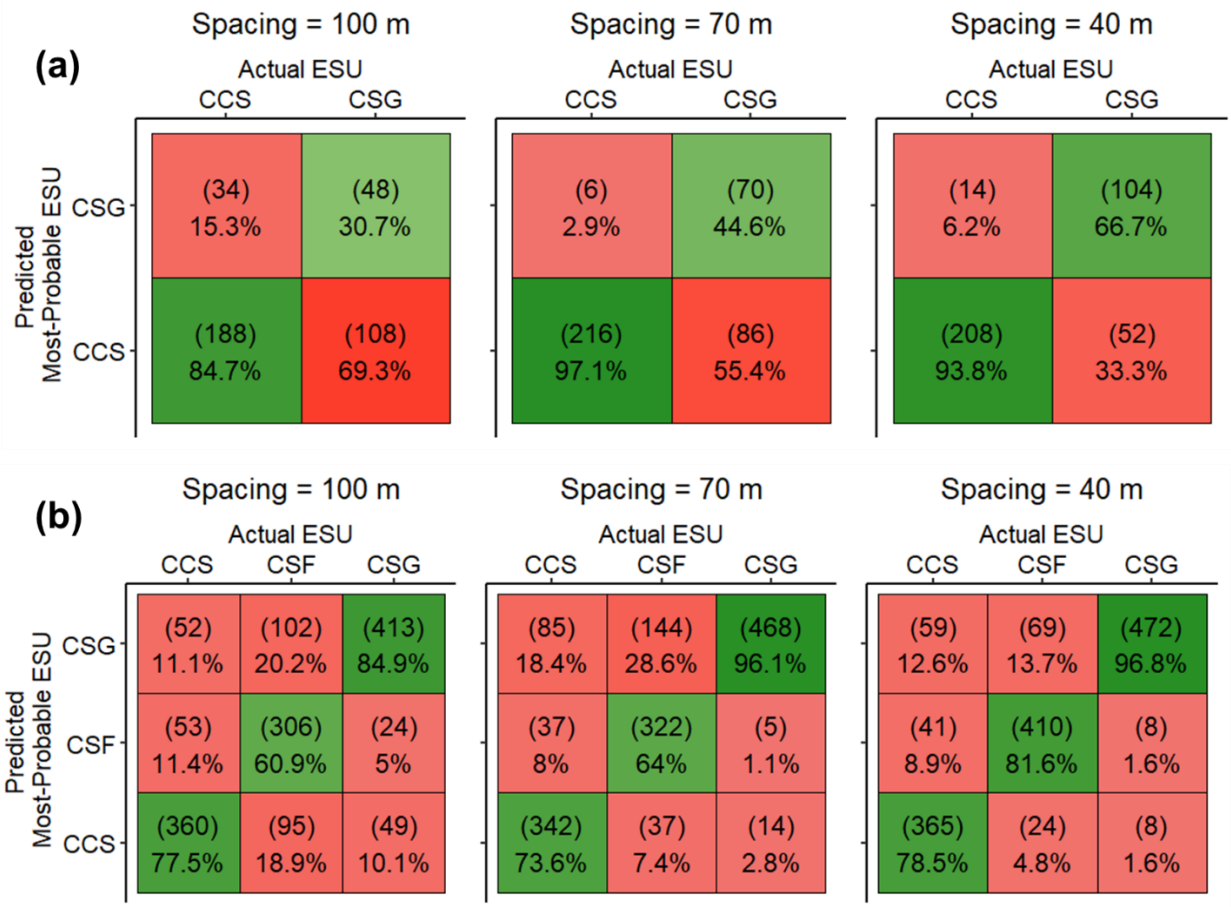

Figure 7.14 Multi-classification confusion matrix, expressed as the mean number of voxels (or percentage) correctly classified and misclassified for (a) soil transition 1 and (b) soil transition 2 within the N125 tunnel envelope and for each borehole density.

Following are a few possible applications of evaluating geostatistical model accuracy for tunnel projects:

- Future tunnel projects could benefit from the accuracy evaluation of geostatistical models from previous tunnel projects in the same geological setting. The knowledge of the geotechnical SI density on previous projects and the resulting geostatistical model accuracy could be utilized to plan SI for future projects and improve the understanding of model accuracy in predicting critical ground features, such as transitions.
- A comparison of the geostatistical model accuracy for multiple borehole densities in a specific geological setting could guide estimating the accuracy of interpreted ground conditions for completely different borehole densities in a similar geological setting.
- A quantitative assessment of the geostatistical model's accuracy in predicting soil transitions could guide drilling additional boreholes in the proximity of the soil transitions to enhance the ground awareness.
- The accuracy of the geostatistical models could be presented along with their application in tunnel risk assessment and decision-making.

7.6 Conclusions

This paper presents a quantitative assessment of the geostatistical model accuracy in predicting the soil conditions for two soil tunnel projects, emphasizing the accuracy of predicting the soil transitions. Further, the paper investigates the influence of geotechnical SI density on geostatistical model accuracy in predicting the ground conditions and soil transitions. The paper presents a quantitative comparison of geostatistical model accuracy in two different geological settings for chosen geotechnical SI density. For this study, geotechnical SI data, in terms of engineering soil units (ESUs), from Anacostia River Tunnel (ART) project in Washington DC, USA, and Northgate Extension Link (N125) project in Seattle, Washington, USA. Boreholes are virtually placed along the respective tunnel alignment at three different mean horizontal borehole spacing (S_h) of 100 m, 70 m, and 40 m to assess the influence of SI density on geostatistical model accuracy. Quantitative results of geostatistical model accuracy are conveyed using a multi-classification confusion matrix and probabilistic estimates of ESUs are presented for the conditions within the tunnel envelope of each project. The following conclusions are reached based on the results of this study:

i. The use of a multi-classification confusion matrix allows a quantitative evaluation of geostatistical model accuracy. The study presents a novel approach of evaluating categorical geostatistical model accuracy with imbalanced category proportions, thus preventing the skewness in accuracy metrics due to the high accuracy of high proportion categories. Since the confusion matrix highlights the voxel-based accuracy of each category, it serves as a suitable diagnostic tool to evaluate the geostatistical model accuracy. Along with the multi-classification confusion matrix, probabilistic estimates of simulated categories help evaluate the accuracy at a finer resolution of the project domain.

ii. For the complete tunnel envelope of the ART project situated in a well-stratified and sedimentary geological environment, the mean percentage accuracy of G1 and G3 (high proportion ESUs) consistently remained > 90 %; however, the mean percentage accuracy of G2 (low proportion ESU) remained < 60 % for S_h = 100 m and 70 m. From the probabilistic estimates of simulated ESUs, the geostatistical model accuracy in capturing the ART tunnel project soil transitions varied between 55-62 % to 75-80 % for S_h = 100 m and 40 m, respectively. The geostatistical model accuracy in predicting ART soil transition 2 was about 5- 8 % less than the accuracy in predicting ART soil transition 1. The difference in the results could be attributed to the increased complexity of ART soil transition 2. Results indicate that, in a sedimentary environment, a geostatistical model of ground conditions developed from boreholes with mean S_h ~ 100 m may capture the soil transitions with about 60 % accuracy.

iii. For the tunnel envelope of the N125 project situated in a highly variable and heterogeneous geological setting, the mean percentage accuracy of CSF and TLD (low proportion ESUs) remained between 60 % and 75 %, and that for CSG and CCS (high proportion ESUs) was > 90 % for S_h = 100 m. The geostatistical model accuracy in predicting N125 soil transitions varied between 50 % and 70 %, with the variation in S_h between 100 m and 40 m. Results indicate that for a tunnel project situated in a complex and heterogeneous geological setting, the geostatistical model developed with boreholes drilled at mean $S_h \geq$ 100 m may capture the soil transition locations with < 50 % accuracy.

An evaluation of the geostatistical model accuracy is imperative with an increased effort towards applying geostatistical techniques to characterize ground conditions before design and construction activities in tunnel projects. This work is developed with a vision to increase the discussion of geostatistical model accuracy before using the developed geostatistical models for tunnel risk assessment and decision-making. The work is expected to help the tunneling community with decisions on the acceptable geostatistical model accuracy for a project, given the scale, complexity of ground conditions, and the consequences of accepting the developed model.

CHAPTER 8- CONCLUSIONS AND RECOMMENDATIONS FOR FUTURE RESEARCH

8.1 Conclusions

The research in this report demonstrates how geostatistics-based methodologies can aid the tunneling community in advancing the practice of tunneling risk assessment and guide informed decision-making on tunnel projects. The methodologies outlined in this report show the success and advantages of geostatistical techniques in developing a probabilistic characterization of ground conditions instead of the deterministic interpretation from conventional practice. The research outcomes show that geostatistical-based methodologies could be successfully adapted for unique challenges in the tunnel and geotechnical projects to improve ground awareness. The results derived from the methodologies are exclusively tied to tunnel risk assessment and decision-making problems for the tunneling community to relate to the advantages of geostatistical modeling.

The following paragraphs summarize the findings of the research.

A probabilistic geostatistical approach was developed to quantify the soil transition location uncertainty (in the longitudinal and transverse direction) (Chapter 4). A parameter variable was defined for longitudinal and transverse directions to capture the occurrence probability and proportions of soil types within the tunnel envelope. The parameter variables aided in capturing the occurrence probability of varied proportions of soil type along the tunnel length and mixed-ground transition plane (vis-à-vis TBM cutterhead). 95 % occurrence probability (P_{95}) for $\geq$ 50 % proportion of soil type within tunnel envelope was used to validate the results of the probabilistic approach.

The developed probabilistic geostatistical approach was applied to the Anacostia River Tunnel (ART) project, where the soil transition location uncertainty at two different locations along the tunnel alignment was quantified. It was found that the P_{95} estimates of soil transition location agree reasonably well with the ground truth transition, estimated via the difference in the rates of chamber pressure dissipation at the tunnel springline observed on the ART project. In another validation approach, the results from the developed approach were found to concur with the soil transition locations identified from the data-driven model developed to characterize as-encountered ground conditions. From the results obtained, it can be concluded that the developed approach's P_{95} estimates of soil transition location were within three to eight rings of the soil transition locations identified from the data-driven model. The developed approach was also applied on a section of the Northgate Extension Link (N125) tunnel project, situated in a relatively heterogeneous and highly variable geological setting, and uncertainty in the location of two soil transitions was quantified. Transition location captured from the data-driven model for each soil transition was found within ± one standard deviation of the probabilistic distribution of location for each soil transition as interpreted from the developed approach.

A geostatistics-based methodology was developed to advance the qualitative/semi-quantitative assessments (from conventional practice) of karstic feature occurrence within the tunnel envelope (Chapter 5). The methodology involved modeling karstic features of different radii as a geological unit that captured the volume of karstic features within the tunnel envelope. The outcome of the

methodology aided in developing quantitative estimates – the size, number, occurrence probability, and occurrence location of karstic features within the tunnel envelope.

The geostatistics-based methodology was applied to a mixed-ground tunnel project in Malaysia to develop probabilistic estimates of the void fraction within the tunnel envelope. It was found that the average volumetric void fraction between 2 % and 6 % was expected for every 50 m tunnel excavation. Results from the quantitative assessment of void occurrence were utilized to estimate the grout volume required for void treatment. An average cumulative grout volume of 4000 m^3 was estimated for the complete tunnel section.

A risk-based methodology to optimize geotechnical SI from geotechnical parameter uncertainty modeling was introduced in Chapter 6. The methodology introduced a geospatial quantification of the geotechnical parameter uncertainty, tunnel risk consequences, and investigation accessibility. The geospatial assessments were effective in communicating the project site conditions and geotechnical uncertainty along the tunnel alignment. An index that integrated the geotechnical parameter uncertainty and tunnel site conditions was defined to identify priority locations of additional investigations based on a tunnel risk.

The developed methodology was applied to the 5 km section of the North-East Boundary Tunnel (NEBT) project for the risk of cutter tool wear. The uncertainty in soil abrasivity index (SAI) was quantified from realizations of soil types and relevant geotechnical parameters. Additional investigations at priority locations reduced SAI uncertainty by about 30 % to 40 %. It was found that the reduction in the soil type uncertainty (due to additional investigations) had a relatively stronger influence on the SAI uncertainty reduction. Additional investigations at priority locations of relatively high SAI uncertainty and high consequences from tool wear were found to reduce the uncertainty in the location of the first two cutterhead interventions by about 90 rings (~160 m). The methodology was found capable of evaluating the investigation effectiveness in reducing the uncertainty associated with the occurrence of tunnel risk.

Lastly, a methodology for quantitative evaluation of geostatistical model accuracy in predicting the soil conditions within the tunnel envelope with an emphasis on predicting soil transitions was developed (Chapter 7). The methodology introduced the use of a multi-class confusion matrix to quantify the accuracy of the geostatistical model in predicting each soil type. The methodology was extended to identify the influence of typical geotechnical SI density on tunnel projects situated in different geological environments. The results from the methodology aided in comparing geostatistical model accuracy for two tunnel project sites and different densities of investigations.

The methodology was applied to the ART project and N125 project situated in two different geological settings and for varied borehole spacing. It was found that the multi-class confusion matrix highlights the voxel-based accuracy of each soil type and prevents the skewness in accuracy metrics due to the high accuracy of high proportion soil types. The probabilistic estimates of soil types were found appropriate to quantify the accuracy at the finer resolution of soil transitions. From the results obtained, it can be concluded that a geostatistical model developed for a tunnel project in a sedimentary environment (ART project) with 100 m mean borehole spacing may capture soil transitions with about 60 % accuracy. However, the accuracy of the geostatistical model in capturing soil transition reduces to less than 50 % in a heterogeneous glacial environment (N125 project) with the same mean borehole spacing.

This report has shown that effective geostatistics-based methodologies can be developed for unique challenges in tunneling and geotechnical engineering applications. In the research discussed, it was critical to understand the geostatistical modeling intricacies for different tunnel projects and apply the derived results for risk management in underground construction and tunneling. The research outcomes have shown that geostatistics-based methodologies improve ground assessments and guide decision-making for improved tunneling performance. The work has exclusively shown that geostatistics serves as a powerful tool to quantify and communicate ground spatial variability and uncertainty, although a sound knowledge of geostatistical modeling algorithms and parameters is warranted.

8.2 Potential and limitations of geostatistics in tunnel applications

Tunnel design is traditionally based on a deterministic interpretation of ground conditions. While traditional practice does not explicitly account for ground spatial variability, engineering interpretations of ground conditions often lack realism. Probabilistic assessment is not novel to the tunnel design and construction practice. Fluctuations of various loads, groundwater levels, material quantities, muck disposal, cost and time estimates, and other factors are incorporated into design and construction decisions. However, there is a need to incorporate the variability in ground properties and uncertainty quantification into the geotechnical baseline reports (GBR) and sophisticated models that capture the ground structure interaction.

Geostatistics is a powerful and versatile tool for investigating the influence of ground uncertainties on a given geotechnical problem. However, it is essential to remember that the results derived from geostatistics are based on the given input of limited geotechnical SI data. Decisions concerning the geostatistical model parameters (e.g., variogram parameters, simulation grid resolution) will influence the model outcomes and interpretations. These factors channel down to tunnel risk assessment and decision-making strategies. Of course, there is a need to conduct a more extensive geotechnical SI campaign than the state-of-the-art because more input data are needed to derive statistical distributions and parameters describing spatial variability.

Is it worth investing in quantifying ground spatial variability?

Geostatistics offers the capability to enrich subjective engineering judgment by providing the framework for uncertainty quantification and incorporate soil variability. The uncertainty quantification framework offers an opportunity to consider uncertainties/errors within the geotechnical design of tunnels. More importantly, the framework offers an opportunity to evaluate the impact of uncertainties on tunnel risk assessment. As shown in Chapter 4, the uncertainty in soil transition locations could potentially impact TBM operation and project environment. Chapter 5 offers a unique case study discussing the probabilistic occurrence of void risk in a tunnel project in Malaysia. Improved awareness of the tunnel excavation environment will lead to efficient construction performance and help resolve any disputes and claims on the project. Example project illustrated in Chapter 6 highlights the potential cost and effort savings in additional SI decision-making on tunnel projects in a complex urban environment.

To what extent do we need to know the ground spatial variability?

Geotechnical SI strategies are key in detecting ground variability. Chapters 4, 5, and 6 indicate that geotechnical SI in typical tunnel practice is sufficient to derive initial ground variability and uncertainty estimates. However, it is just not possible to sample 100 % of the ground. As shown in Chapter 6, optimal geotechnical SI schemes can be derived from ground uncertainty knowledge. In addition to the geotechnical SI boreholes, data from other field investigations could be integrated into the geostatistical interpretations to improve the characterization of ground conditions and engineering properties.

What are the possible avenues to evaluate ground spatial variability?

The quantification of ground spatial variability is probably one of the most critical issues in tunnel design and construction. In addition to the variogram-based geostatistical analyses, Markov Chain methodologies, such as Markov Chain Random Field (MCRF), Markov Chain Monte Carlo (MCMC), offer ground spatial variability modeling capabilities. Radial basis functions (RBFs), used in LeapFrog by Seequent, offer the capability to estimate unknown data points to create surfaces using the knowledge of the known data points.

What resources are used to evaluate ground spatial variability?

Open-source software packages and libraries in R and Python are readily available to visualize and process the geotechnical SI data. The Stanford Geostatistical Modeling Software (SGeMS), SaTScan, Spatial Analysis and Decision Assistance (SADA), Geostatistical Software Library (GSLIB), Variogram Estimation, and Spatial Prediction Plus Error (VESPER) are a few free software available to analyze the point cloud data. The open-source and free software provides an opportunity to gain experience in ground spatial variability modeling before investing in licensed tools such as Geovariances Isatis, LeapFrog, Surfer, Geostokos toolkit, and ArcGIS toolkit.

8.3 Recommendations for future research

The research conducted as a part of the report contributed to the knowledge and the understanding of (a) locations of soil transitions within tunnel envelope, (b) quantitative assessments of critical features such as karstic voids, (c) optimal SI scheme based on tunnel risk and project site conditions, and (d) accuracy of geostatistical models for typical sampling density in tunnel projects. At the same time, the research highlighted a few aspects that require further research. Following aspects are recommended for future research:

- A real-time updating of soil transition locations could be integrated with the progress of the TBM. The knowledge of the as-encountered ground conditions at each ring could be utilized to periodically update the geostatistical models to update the soil transition locations and compare with the interpretations prior to construction. Additionally, the difference in the approach of the TBM operator in driving the TBM, with and without the knowledge of soil transition location could be quantified.
- The quantitative assessments of void occurrence within the tunnel envelope could be validated with the TBM operational data. While this was initially intended as a key part of the validation methodology for the project in Malaysia, the TBM operational data from the project site were found not to be sufficient and applicable for validation. Also, the actual

grout quantities required for void treatment could compared to the estimated grout quantities. The capabilities of the geostatistics-based approach could be compared to the capabilities of ground penetrating radar (GPR) in detecting voids behind the tunnel segmental linings and in front of the TBM.

- The work on optimizing geotechnical SI could be expanded to include multiple tunnel risks and probabilistic cost analysis of the proposed approach. Identifying the optimal sequence of borehole drilling while prioritizing the tunnel site conditions and ground uncertainty is a potential avenue for future research. The value of information (VOI) from adding a borehole could be quantified prior to future decision-making.
- The uncertainty from geostatistical modeling could be integrated into 3D Finite Difference Analysis (FDA) numerical models to quantify uncertainty in the risk of tunneling-induced ground deformation and identify the optimal TBM face support pressure and grouting pressures for efficient tunnel construction.
- For the accuracy of geostatistical models, results obtained from the analysis could be compared to the traditional Markov Chain approach, which uses the transiograms instead of the indicator variograms. Further, the proposed methodology could be expanded to include multiple geological settings for accuracy assessment.

REFERENCES

Armstrong M, Galli A, Beucher H, et al (2011) Plurigaussian Simulations in Geosciences. Springer-Verlag Berlin Heidelberg

Baecher GB, Christian JT (2005) Reliability and statistics in geotechnical engineering. John Wiley & Sons

Bezuijen A (2002) The influence of soil permeability on the properties of a foam mixture in a TBM. Tunnelling A Decad Progress GeoDelft 1995-2005 35–41. https://doi.org/10.1201/9781439834268.ch6

Bezuijen A, Dias TGS (2017) EPB, chamber pressure dissipation during standstill. EUROTUN 2017 - 4th Int Conf Comput Methods Tunneling Subsurf Eng

Bianchi M, Kearsey T, Kingdon A (2015) Integrating deterministic lithostratigraphic models in stochastic realizations of subsurface heterogeneity. Impact on predictions of lithology, hydraulic heads and groundwater fluxes. J Hydrol 531:557–573. https://doi.org/10.1016/j.jhydrol.2015.10.072

Bivand Roger, Rundel Colin (2020) rgeos

Blanchin R, Chilès J-P (1993) The Channel Tunnel: Geostatistical prediction of the geological conditions and its validation by the reality. Math Geol 25:963–974

Boon CW, Ooi LH, Tan JG, Goh CY (2020) Deep excavation of an underground metro station in karstic limestone: a case history in the Klang Valley SSP Line. Springer Singapore

Bossé MC (2005) Performance of EPB-TBM in mixed face conditions: City of Edmonton South LRT Extension, University Station to Health Sciences Station

Boyd DL (2019) Application of Geostatistical Methods for the Quantification of Multiple-scale Uncertainty due to Aleatory Geologic Variability. Colorado School of Mines

Boyd DL, Walton G, Trainor-Guitton W (2019) Quantifying spatial uncertainty in rock through geostatistical integration of borehole data and a geologist's cross-section. Eng Geol 260:105246. https://doi.org/10.1016/j.enggeo.2019.105246

Boyd L, Walton G, Trainor-Guitton W (2020) Geostatistical estimation of Ground Class prior to and during excavation for the Caldecott Tunnel Fourth Bore project. Tunn Undergr Sp Technol 100:103391. https://doi.org/10.1016/j.tust.2020.103391

British Tunneling Society (2005) Closed-Face Tunnelling Machines and Ground Stability. Thomas Telford Publishing, London

Caers JK, Srinivasan S, Journel AG (2007) Geostatistical Quantification of Geological Information for a Fluvial-Type North Sea Reservoir. SPE Reserv Eval Eng 3:457–467.

https://doi.org/10.2118/66310-pa

Cao Z, Wang Y, Li D (2016) Quantification of prior knowledge in geotechnical site characterization. Eng Geol 203:107–116. https://doi.org/10.1016/j.enggeo.2015.08.018

Carle SF (1999) T-PROGS: Transition probability geostatistical software. Univ California, Davis, CA 1–78

Carle SF, Fogg GE (1997) Modeling Spatial Variability with One and Multidimensional Continuous-Lag Markov Chains. Math Geol 29:891–918. https://doi.org/10.1023/A:1022303706942

Carle SF, Fogg GE (2020) Integration of Soft Data Into Geostatistical Simulation of Categorical Variables. Front Earth Sci 8:1–28. https://doi.org/10.3389/feart.2020.565707

Carle SF, Fogg GE (1996) Transition probability-based indicator geostatistics. Math Geol 28:453–476. https://doi.org/10.1007/BF02083656

Chen J, Li X, Zhu H, Rubin Y (2017) Geostatistical method for inferring RMR ahead of tunnel face excavation using dynamically exposed geological information. Eng Geol 228:214–223. https://doi.org/10.1016/j.enggeo.2017.08.004

Cheng WC, Cui QL, Shen JSL, et al (2017) Fractal prediction of grouting volume for treating karst caverns along a shield tunneling alignment. Appl Sci 7:. https://doi.org/10.3390/app7070652

Chilès J-P, Aug C, Guillen A, Lees T (2004) Modelling the geometry of geological units and its uncertainty in 3D from structural data: the potential-field method. In: Proceedings of international symposium on orebody modelling and strategic mine planning, Perth, Australia. p 24

Chiles J-P, Delfiner P (2009) Geostatistics: modeling spatial uncertainty. John Wiley & Sons

Ching J, Wang JS, Juang CH, Ku CS (2015) Cone penetration test (CPT)-based stratigraphic profiling using the wavelet transform modulus maxima method. Can Geotech J 52:1993–2007. https://doi.org/10.1139/cgj-2015-0027

Clough GW, Leca E (1993) EPB shield tunneling in mixed face conditions. J Geotech Eng 119:1640–1656. https://doi.org/10.1061/(ASCE)0733-9410(1993)119:10(1640)

Cressie N (1985) Fitting variogram models by weighted least squares. J Int Assoc Math Geol 17:563–586. https://doi.org/10.1007/BF01032109

Cromer M V (1996) Geostatistics for environmental and geotechnical applications: a technology transferred. In: Geostatistics for Environmental and Geotechnical Applications. ASTM International

Cui QL, Wu HN, Shen SL, et al (2015) Chinese karst geology and measures to prevent geohazards during shield tunnelling in karst region with caves. Nat Hazards 77:129–152.

https://doi.org/10.1007/s11069-014-1585-6

Davis JA (2021) Geotechnical Baseline Reports - ground models you can just make up? Q J Eng Geol Hydrogeol 54:. https://doi.org/10.1144/qjegh2020-019/5102966/qjegh2020-019.pdf

Day MJ (2004) Karstic problems in the construction of Milwaukee's Deep Tunnels. Environ Geol 45:859–863. https://doi.org/10.1007/s00254-003-0945-4

de Marsily G, Delay F, Gonçalvès J, et al (2005) Dealing with spatial heterogeneity. Hydrogeol J 13:161–183. https://doi.org/10.1007/s10040-004-0432-3

DeGroot DJ, Baecher GB (1994) Estimating autocovariance of in situ soil properties. J Geotech Eng 120:1455–1457. https://doi.org/10.1061/(ASCE)0733-9410(1994)120:8(1455)

dell'Arciprete D, Bersezio R, Felletti F, et al (2012) Comparison of three geostatistical methods for hydrofacies simulation: A test on alluvial sediments. Hydrogeol J 20:299–311. https://doi.org/10.1007/s10040-011-0808-0

Deutsch C V, Journel AG (1992) Gslib Geostatistical Software Library And User's Guide Pdf

Dubrule O (2017) Indicator Variogram Models: Do We Have Much Choice? Math Geosci 49:441–465. https://doi.org/10.1007/s11004-017-9678-x

Duringer P, Bacon AM, Sayavongkhamdy T, Nguyen TKT (2012) Karst development, breccias history, and mammalian assemblages in Southeast Asia: A brief review. Comptes Rendus - Palevol 11:133–157. https://doi.org/10.1016/j.crpv.2011.07.003

Einstein HH, Labreche DA, Markow MJ, Baecher GB (1978) Decision analysis applied to rock tunnel exploration. Eng Geol 12:143–161. https://doi.org/10.1016/0013-7952(78)90008-X

Einstein HH, Salazar GF, Kim YW, Ioannou PG (1987) Computer based decision support systems for underground construction. In: Proc., Rapid Excavation Tunneling Conference. pp 1287–1307

El Gonnouni M, Riou Y, Hicher PY (2006) Geostatistical method for analysing soil displacement from underground urban construction. Risk Var Geotech Eng Inst Civ Eng 185–196. https://doi.org/10.1680/ravige.34860.0019

Emery X (2007) Simulation of geological domains using the plurigaussian model: New developments and computer programs. Comput Geosci 33:1189–1201. https://doi.org/10.1016/j.cageo.2007.01.006

Emery X, Lantuéjoul C (2014) Can a training image be a substitute for a random field model? Math Geosci 46:133–147

Eskesen SD, Tengborg P, Kampmann J, Holst Veicherts T (2004) Guidelines for tunnelling risk management: International Tunnelling Association, Working Group No. 2. Tunn Undergr Sp Technol 19:217–237. https://doi.org/10.1016/j.tust.2004.01.001

Essex R (2007) Geotechnical Baseline Reports for Underground Construction. American Society of Civil Engineers, Virginia

Felletti F, Beretta G Pietro (2009) Expectation of boulder frequency when tunneling in glacial till: A statistical approach based on transition probability. Eng Geol 108:43–53. https://doi.org/10.1016/j.enggeo.2009.06.006

Ford D, Williams PD (2013) Karst hydrogeology and geomorphology. John Wiley & Sons

Gangrade R, Mooney M, Trainor-Guitton W (2020a) Quantification of Stratigraphic Transition Location Uncertainty for Tunneling Projects. J Geotech Geoenvironmental Eng In Review:

Gangrade R, Mooney M, Trainor-Guitton W (2020b) Incorporating Spatial Uncertainty into Site Investigations for Tunneling Applications. In: Geo-Congress 2020: Engineering, Monitoring, and Management of Geotechnical Infrastructure. ASCE, Reston, VA, USA. pp 345–354

Gangrade RM, Grasmick JG, Mooney MA (2021a) Probabilistic Assessment of Void Risk and Grouting Volume for Tunneling Applications. Rock Mech Rock Eng 54:. https://doi.org/10.1007/s00603-021-02528-6

Gangrade RM, Grasmick JG, Mooney MA (2021b) Probabilistic Assessment of Void Risk and Grouting Volume for Tunneling Applications. Rock Mech Rock Eng 1–16

Gao M, Zhang R, Wang M (2013) The mechanism of ground subsidence induced by EPB tunneling in sand and cobble stratum. In: IACGE 2013: Challenges and Recent Advances in Geotechnical and Seismic Research and Practices. pp 447–454

Gong W, Juang CH, Martin JR, et al (2018) Probabilistic analysis of tunnel longitudinal performance based upon conditional random field simulation of soil properties. Tunn Undergr Sp Technol 73:1–14. https://doi.org/10.1016/j.tust.2017.11.026

Gong W, Luo Z, Juang CH, et al (2014) Optimization of site exploration program for improved prediction of tunneling-induced ground settlement in clays. Comput Geotech 56:69–79. https://doi.org/10.1016/j.compgeo.2013.10.008

Gong W, Zhao C, Juang CH, et al (2020) Stratigraphic uncertainty modelling with random field approach. Comput Geotech 125:103681. https://doi.org/10.1016/j.compgeo.2020.103681

Goovaerts P (2001) Geostatistical modelling of uncertainty in soil science. Geoderma 103:3–26. https://doi.org/10.1016/S0016-7061(01)00067-2

Goovaerts P (1998) Geostatistical tools for characterizing the spatial variability of microbiological and physico-chemical soil properties. Biol Fertil Soils 27:315–334. https://doi.org/10.1007/s003740050439

Grasmick J, Mooney M, Trainor-Guitton W (2018) Incorporating Geological and Geotechnical Spatial Variability into TBM and Ground Settlement Risk Assessment. North Am Tunneling 2018 Proc

Grasmick JG (2019) Modeling Spatial Geotechnical Parameters Uncertainty and Quantitative Tunneling Risks

Grasmick JG, Maxwell A, Gangrade R, Mooney MA (2020a) Probabilistic Subsurface Modelling in Tunnelling Applications: Suggestions for Use in Practice. In: ITA-AITES World Tunnel Congress, WTC 2020 and 46th General Assembly, Kuala Lumpur, Malaysia, September 2020

Grasmick JG, Mooney MA (2021) A Probabilistic Geostatistics Based Approach to Tunnel Boring Machine Cutter Tool Wear and Cutterhead Clogging Prediction. J Geotech Geoenvironmental Eng In Review:

Grasmick JG, Mooney MA (2020) Risk maps for cutter tool wear assessment and intervention planning. Tunnels Undergr Cities Eng Innov Meet Archaeol Archit Art Vol 3 Geol Geotech Knowl Requir Proj Implement 856

Grasmick JG, Mooney MA, Trainor-Guitton WJ, Walton G (2020b) Global versus Local Simulation of Geotechnical Parameters for Tunneling Projects. J Geotech Geoenvironmental Eng 146:04020048. https://doi.org/10.1061/(asce)gt.1943-5606.0002262

Griffiths D V, Fenton GA (2008) Risk assessment in geotechnical engineering. John wiley&Sons, Inc 381–400

Hammah RE, Curran JH (2006) Geostatistics in geotechnical engineering: Fad or empowering? GeoCongress 2006 Geotech Eng Inf Technol Age 2006:102. https://doi.org/10.1061/40803(187)102

He C, Jiang Y, Fang Y, et al (2013) Impact of shield tunneling on adjacent pile foundation in sandy cobble strata. Adv Struct Eng 16:1457–1467

Hu Y, Wang Y (2020) Probabilistic soil classification and stratification in a vertical cross-section from limited cone penetration tests using random field and Monte Carlo simulation. Comput Geotech 124:103634. https://doi.org/10.1016/j.compgeo.2020.103634

Huang HW, Xiao L, Zhang DM, Zhang J (2017) Influence of spatial variability of soil Young's modulus on tunnel convergence in soft soils. Eng Geol 228:357–370. https://doi.org/10.1016/j.enggeo.2017.09.011

Huber M, Marconi F, Moscatelli M (2015) Risk-based characterisation of an urban building site. Georisk 9:49–56. https://doi.org/10.1080/17499518.2015.1015574

Isaksson T (2002) Model for estimation of time and cost based on risk evaluation applied on tunnel projects. Byggvetenskap

Jacobs A (2013) Northgate Link Extension Light Rail Project Contract N125: TBM Tunnels (UW to Maple Leaf Portal) Geotechnical Baseline Report. Seattle, Washington

Jaksa M, Fenton G (2002) Assessment of fractal behavior of soils

Jaksa MB (2007) Modeling the natural variability of over-consolidated clay in Adelaide, South Australia. Characterisation Nat Prop Nat Soils 2721–2751

Jaksa MB (2014) Experimental evaluation of the scale of fluctuation of a stiff clay

Jaksa MB (1995) The influence of spatial variability on the geotechnical design properties of a stiff, overconsolidated clay.

Kaewkongkaew K, Phien-wej N, Kham-ai D (2015) Prediction of rock mass along tunnels by geostatistics. KSCE J Civ Eng 19:81–90. https://doi.org/10.1007/s12205-014-0505-3

Karacan CÖ, Olea RA, Goodman G (2012) Geostatistical modeling of the gas emission zone and its in-place gas content for Pittsburgh-seam mines using sequential Gaussian simulation. Int J Coal Geol 90–91:50–71. https://doi.org/10.1016/j.coal.2011.10.010

Karam KS, Karam JS, Einstein HH (2007a) Decision Analysis Applied to Tunnel Exploration Planning. I: Principles and Case Study. J Constr Eng Manag 133:344–353. https://doi.org/10.1061/(ASCE)0733-9364(2007)133:5(344)

Karam KS, Karam JS, Einstein HH (2007b) Decision Analysis Applied to Tunnel Exploration Planning. II: Consideration of Uncertainty. J Constr Eng Manag 133:354–363. https://doi.org/10.1061/(asce)0733-9364(2007)133:5(354)

Köppl F (2014) Abbauwerkzeugverschleiß und empirische Verschleißprognose beim Vortrieb mit Hydroschild TVM in Lockergesteinen

Köppl F, Thuro K (2013) Cutting tool wear prognosis and management of wear-related risks for mix-shield TBM in soft ground. 18th Int Conf Soil Mech Geotech Eng Challenges Innov Geotech ICSMGE 2013 2:1739–1742

Kovačević MS, Bačić M, Gavin K (2020) Application of neural networks for the reliability design of a tunnel in karst rock mass. Can Geotech J 467:1–13. https://doi.org/10.1139/cgj-2019-0693

Kravchenko AN (2003) Influence of Spatial Structure on Accuracy of Interpolation Methods. Soil Sci Soc Am J 67:1564–1571. https://doi.org/10.2136/sssaj2003.1564

Lark RM (2012) Towards soil geostatistics. Spat Stat 1:92–99

Lark RM, Cullis BR, Welham SJ (2006) On spatial prediction of soil properties in the presence of a spatial trend: the empirical best linear unbiased predictor (E-BLUP) with REML. Eur J Soil Sci 57:787–799

Lark RM, Webster R (2006) Geostatistical mapping of geomorphic variables in the presence of trend. Earth Surf Process Landforms J Br Geomorphol Res Gr 31:862–874

Lee SY, Carle SF, Fogg GE (2007) Geologic heterogeneity and a comparison of two geostatistical models: Sequential Gaussian and transition probability-based geostatistical simulation. Adv

Water Resour 30:1914–1932. https://doi.org/10.1016/j.advwatres.2007.03.005

Leuangthong O, McLennan JA, Deutsch C V. (2004) Minimum acceptance criteria for geostatistical realizations. Nat Resour Res 13:131–141. https://doi.org/10.1023/B:NARR.0000046916.91703.bb

Li J, Cassidy MJ, Huang J, et al (2016a) Probabilistic identification of soil stratification. Geotechnique 66:16–26. https://doi.org/10.1680/jgeot.14.P.242

Li L, Lei T, Li S, et al (2015) Risk assessment of water inrush in karst tunnels and software development. Arab J Geosci 8:1843–1854. https://doi.org/10.1007/s12517-014-1365-3

Li W, Zhang C (2007) A Random-Path Markov Chain Algorithm for Simulating Categorical Soil Variables from Random Point Samples. Soil Sci Soc Am J 71:656. https://doi.org/10.2136/sssaj2006.0173

Li Z, Wang X, Wang H, Liang RY (2016b) Quantifying stratigraphic uncertainties by stochastic simulation techniques based on Markov random field. Eng Geol 201:106–122. https://doi.org/10.1016/j.enggeo.2015.12.017

Lichtenberg S (1990) Projekt Planlaegning–i en foranderlig verden. Polyteknisk Forlag, Denmark. Polyteknisk Forlag, Denmark

Loganathan N, Poulos HG (1998) Analytical prediction for tunneling-induced ground movements in clays. J Geotech geoenvironmental Eng 124:846–856

Ma H, Yin L, Gong Q, Wang J (2015) TBM tunneling in mixed-face ground: Problems and solutions. Int J Min Sci Technol 25:641–647. https://doi.org/10.1016/j.ijmst.2015.05.019

Ma Z (2019) Quantitative Geosciences: Data Analytics, Geostatistics, Reservoir Characterization and Modeling

Madani N, Emery X (2017) Plurigaussian modeling of geological domains based on the truncation of non-stationary Gaussian random fields. Stoch Environ Res Risk Assess 31:893–913. https://doi.org/10.1007/s00477-016-1365-9

Madani N, Emery X (2015) Simulation of geo-domains accounting for chronology and contact relationships: application to the Río Blanco copper deposit. Stoch Environ Res Risk Assess 29:2173–2191. https://doi.org/10.1007/s00477-014-0997-x

Madani N, Maleki M, Emery X (2019) Nonparametric Geostatistical Simulation of Subsurface Facies: Tools for Validating the Reproduction of, and Uncertainty in, Facies Geometry. Nat Resour Res 28:1163–1182. https://doi.org/10.1007/s11053-018-9444-x

Mahmoudi E, Stepien M, König M (2021) Optimisation of geotechnical surveys using a BIM-based geostatistical analysis. Smart Sustain Built Environ

Maleki M, Emery X, Mery N (2017) Indicator Variograms as an Aid for Geological Interpretation

and Modeling of Ore Deposits. Minerals 7:241. https://doi.org/10.3390/min7120241

Marache A, Breysse D, Piette C, Thierry P (2009) Geotechnical modeling at the city scale using statistical and geostatistical tools: The Pessac case (France). Eng Geol 107:67–76. https://doi.org/10.1016/j.enggeo.2009.04.003

Matheron G (1971) The Theory of Regionalized Variables and Its Applications. École national supérieure des mines

Medley EW (2002) Estimating block size distributions of melanges and similar block-in-matrix rocks (bimrocks). In: Proc. 5th North American Rock Mechanics Symposium, Toronto, Canada

Nadim F, Einstein H, Roberds W (2005) Probabilistic stability analysis for individual slopes in soil and rock. In: Landslide risk management. CRC Press, pp 73–108

Nebbia D, Mooney M, Gangrade R, et al (2021) NEBT Project: The Application of Artificial Intelligence (AI) to Improve TBM Operations. In: Rapid Excavation Tunneling Conference. Society for Mining, Metallurgy & Exploration, Las Vegas, Nevada, USA, pp 822–836

Oliver MA, Webster R (2014) A tutorial guide to geostatistics: Computing and modelling variograms and kriging. Catena 113:56–69

Ozturk CA, Simdi E (2014) Geostatistical investigation of geotechnical and constructional properties in Kadikoy-Kartal subway, Turkey. Tunn Undergr Sp Technol 41:35–45. https://doi.org/10.1016/j.tust.2013.11.002

Paraskevopoulou C, Benardos A (2013) Assessing the construction cost of Greek transportation tunnel projects. Tunn Undergr Sp Technol 38:497–505. https://doi.org/10.1016/j.tust.2013.08.005

Phoon K-K, Ching J (2014) Risk and reliability in geotechnical engineering. CRC Press

Phoon K-K, Kulhawy FH (1999a) Characterization of geotechnical variability. Can Geotech J 36:612–624

Phoon K-K, Kulhawy FH (1999b) Evaluation of geotechnical property variability. Can Geotech J 36:625–639

Phoon K-K, Quek S-T, An P (2004) Geostatistical analysis of cone penetration test (CPT) sounding using the modified Bartlett test. Can Geotech J 41:356–365

Phoon KK, Ching J, Shuku T (2021) Challenges in data-driven site characterization. Georisk 0:1–13. https://doi.org/10.1080/17499518.2021.1896005

Phoon KK, Quek ST, An P (2003) Identification of statistically homogeneous soil layers using modified bartlett statistics. J Geotech Geoenvironmental Eng 129:649–659. https://doi.org/10.1061/(ASCE)1090-0241(2003)129:7(649)

Piccini L, Mecchia M (2009) Solution weathering rate and origin of karst landforms and caves in the quartzite of Auyan-tepui (Gran Sabana, Venezuela). Geomorphology 106:15–25. https://doi.org/10.1016/j.geomorph.2008.09.019

Pinheiro M, Emery X, Rocha AMAC, et al (2017) Boreholes plans optimization methodology combining geostatistical simulation and simulated annealing. Tunn Undergr Sp Technol 70:65–75. https://doi.org/10.1016/j.tust.2017.07.003

Pinheiro M, Vallejos J, Miranda T, Emery X (2016) Geostatistical simulation to map the spatial heterogeneity of geomechanical parameters: A case study with rock mass rating. Eng Geol 205:93–103. https://doi.org/10.1016/j.enggeo.2016.03.003

Pyrcz MJ, Deutsch C V (2014) Geostatistical reservoir modeling. Oxford university press

Rackwitz R (2000) Reviewing probabilistic soils modelling. Comput Geotech 26:199–223

Reiner H (2011) Developments in the tunneling industry following introduction of the tunneling code of practice. In: IMIA Annual Conference, Amsterdam

Ren DJ, Shen SL, Cheng WC, et al (2016) Geological formation and geo-hazards during subway construction in Guangzhou. Environ Earth Sci 75:1–14. https://doi.org/10.1007/s12665-016-5710-6

Sánchez Rodríguez S, Sampedro G, Fernández JD, López JD (2020) Predicting rock mass conditions ahead of tunnel face and the use of geostatistical methods. A comparative study. In: ISRM International Symposium-EUROCK 2020. OnePetro

Sartore L (2013) spMC: Modelling Spatial Random Fields with Continuous Lag Markov Chains. A peer-reviewed, open-access Publ R … XX:1–15

Seidenfuss T (2006) Collapses in tunnelling. Master Degree Found Eng Tunnelling Stuttgart, Ger 194:

Shahriar K, Sharifzadeh M, Hamidi JK (2008) Geotechnical risk assessment based approach for rock TBM selection in difficult ground conditions. Tunn Undergr Sp Technol 23:318–325. https://doi.org/10.1016/j.tust.2007.06.012

Shannon CE (1948) A mathematical theory of communication. Bell Syst Tech J 27:379–423

Shi C, Wang Y (2021) Nonparametric and data-driven interpolation of subsurface soil stratigraphy from limited data using multiple point statistics. Can Geotech J 58:261–280. https://doi.org/10.1139/cgj-2019-0843

Shirlaw JN (2016) Pressurised TBM tunnelling in mixed face conditions resulting from tropical weathering of igneous rock. Tunn Undergr Sp Technol 57:225–240. https://doi.org/10.1016/j.tust.2016.01.018

Sousa R, Karam KS, Costa AL, Einstein HH (2016) Exploration and decision-making in

geotechnical engineering – a case study. Georisk Assess Manag Risk Eng Syst Geohazards 0:1–17. https://doi.org/10.1080/17499518.2016.1250916

Sousa RL (2010a) Risk analysis for tunneling projects (Doctoral report, MIT, Boston)

Sousa RL (2010b) Risk Analysis for Tunneling Projects. Environ Eng

Spyridis P, Proske D (2021) Revised Comparison of Tunnel Collapse Frequencies and Tunnel Failure Probabilities. ASCE-ASME J Risk Uncertain Eng Syst Part A Civ Eng 7:4021004

Stavropoulou M, Xiroudakis G, Exadaktylos G (2010) Spatial estimation of geotechnical parameters for numerical tunneling simulations and TBM performance models. Acta Geotech 5:139–150. https://doi.org/10.1007/s11440-010-0118-z

Tang BW, Asce M, Quek ST (1986) Statistical model of boulder size and fraction. J Geotech Geoenvironmental Eng 112:79–90

Tharwat A (2020) Classification assessment methods. Appl Comput Informatics 17:168–192. https://doi.org/10.1016/j.aci.2018.08.003

Uzielli M, Lacasse S, Nadim F, Phoon K (2006) Soil variability analysis for geotechnical practice. In: Characterisation and Engineering Properties of Natural Soils

Uzielli M, Vannucchi G, Phoon KK (2005) Random field characterisation of stress-nomalised cone penetration testing parameters. Geotechnique 55:3–20

van der Pouw Kraan M (2014) Rockmass Behavioural Uncertainty : Implications for Hard Rock Tunnel

Vanarelli MJ (2021) A Geostatistical Solution to Estimating Groundwater Inflows in Deep Rock Tunnels with Validation Through Case Studies. Mining, Metall Explor 38:347–357

Vanmarcke E (2010) Random fields: analysis and synreport. World Scientific

Waltham AC, Fookes PG (2003) Engineering classification of karst ground conditions. Q J Eng Geol Hydrogeol 36:101–118. https://doi.org/10.1144/1470-9236/2002-33

Wang C, Chen Q, Shen M, Juang CH (2017) On the spatial variability of CPT-based geotechnical parameters for regional liquefaction evaluation. Soil Dyn Earthq Eng 95:153–166. https://doi.org/10.1016/j.soildyn.2017.02.001

Wang CH, Harken B, Osorio-Murillo CA, et al (2016a) Bayesian approach for probabilistic site characterization assimilating borehole experiments and Cone Penetration Tests. Eng Geol 207:1–13. https://doi.org/10.1016/j.enggeo.2016.04.002

Wang X, Lai J, He S, et al (2020) Karst geology and mitigation measures for hazards during metro system construction in Wuhan, China. Nat Hazards 103:2905–2927. https://doi.org/10.1007/s11069-020-04108-3

Wang X, Li Z, Wang H, et al (2016b) Probabilistic analysis of shield-driven tunnel in multiple strata considering stratigraphic uncertainty. Struct Saf 62:88–100. https://doi.org/10.1016/j.strusafe.2016.06.007

Wang X, Wang H, Liang RY (2018) A method for slope stability analysis considering subsurface stratigraphic uncertainty. Landslides 15:925–936. https://doi.org/10.1007/s10346-017-0925-5

Wang Y, Huang K, Cao Z (2014) Bayesian identification of soil strata in London clay. Geotechnique 64:239–246. https://doi.org/10.1680/geot.13.T.018

Webster, R., Oliver MA (1992) Sample adequately to estimate variograms of soil properties. Eur J Soil Sci 43:177–192. https://doi.org/10.5771/0038-6073-2013-1-2-191

Wellmann JF, Horowitz FG, Schill E, Regenauer-Lieb K (2010) Towards incorporating uncertainty of structural data in 3D geological inversion. Tectonophysics 490:141–151

Xeidakis GS, Torok A, Skias S, Kleb B (2004) Engineering Geological Problems Associated With Karst Terrains: Their Investigation. Monitoring, and Mitigation and Design of Engineering Structures on Karst Terrains. Bull Geol Soc Greece 36:1932. https://doi.org/10.12681/bgsg.16679

Xiao T, Zhang LM, Li XY, Li DQ (2017) Probabilistic stratification modeling in geotechnical site characterization. ASCE-ASME J Risk Uncertain Eng Syst Part A Civ Eng 3:1–10. https://doi.org/10.1061/AJRUA6.0000924

Yamamoto JK (2005) Correcting the smoothing effect of ordinary kriging estimates. Math Geol 37:69–94

Yang J, Zhang C, Fu J, et al (2020) Pre-grouting reinforcement of underwater karst area for shield tunneling passing through Xiangjiang River in Changsha, China. Tunn Undergr Sp Technol 100:103380. https://doi.org/10.1016/j.tust.2020.103380

Yau K, Paraskevopoulou C, Konstantis S (2020) Spatial variability of karst and effect on tunnel lining and water inflow. A probabilistic approach. Tunn Undergr Sp Technol 97:. https://doi.org/10.1016/j.tust.2019.103248

Yu H, Mooney M (2021) Logging the as-encountered ground condition with EPBM data using supervised and semi-supervised learning. Autom Constr In Review:

Yu H, Mooney M, Bezuijen A (2020) A simplified excavation chamber pressure model for EPBM tunneling. Tunn Undergr Sp Technol 103:103457. https://doi.org/10.1016/j.tust.2020.103457

Zabidi H, De Freitas MH (2013) Geospatial analysis in identifying karst cavity distribution: The SMART Tunnel, Malaysia. Carbonates and Evaporites 28:125–133

Zarei HR, Uromeihy A, Sharifzadeh M (2010) Identifying geological hazards related to tunneling in carbonate karstic rocks - Zagros, Iran. Arab J Geosci 5:457–464.

https://doi.org/10.1007/s12517-010-0218-y

Zetterlund MS, Norberg T, Ericsson LO, et al (2015) Value of information analysis in rock engineering: a case study of a tunnel project in Äspö Hard Rock Laboratory. Georisk 9:9–24. https://doi.org/10.1080/17499518.2014.1001401

Zhang G-H, Jiao Y-Y, Chen L-B, et al (2015) Analytical model for assessing collapse risk during mountain tunnel construction. Can Geotech J 53:326–342

Zhang P, Chen RP, Wu HN, Liu Y (2020) Ground settlement induced by tunneling crossing interface of water-bearing mixed ground: A lesson from Changsha, China. Tunn Undergr Sp Technol 96:103224. https://doi.org/10.1016/j.tust.2019.103224

Zhao J, Gong QM, Eisensten Z (2007) Tunnelling through a frequently changing and mixed ground: A case history in Singapore. Tunn Undergr Sp Technol 22:388–400. https://doi.org/10.1016/j.tust.2006.10.002

Zhao LI (2009) Statistics of tunnel collapse accidents and its assessment based on case reasoning. J Railw Sci Eng 4:

Zhu H, Zhang LM (2013) Characterizing geotechnical anisotropic spatial variations using random field theory. Can Geotech J 50:723–734. https://doi.org/10.1139/cgj-2012-0345

APPENDIX A – CAN INFORMATION ENTROPY CAPTURE SOIL TRANSITION UNCERTAINTY?

A.1 Information entropy measures for Anacostia River Tunnel project

Several researchers have focused on generating soil stratigraphy realizations from Markov Random Field (MRF) approach and have quantified the uncertainty in stratigraphic configurations (Li et al. 2016b; Wang et al. 2018; Gong et al. 2020; Shi and Wang 2021). However, the uncertainty in stratigraphic configurations does not capture the uncertainty in stratigraphic transition locations. In this study, uncertainty measures (expressed in terms of information entropy) were analyzed to verify if these measures convey the uncertainty in soil transition locations. The study uses the geotechnical site investigation (SI) data from 20 boreholes drilled along the 2 km stretch of the Anacostia River Tunnel (ART) alignment.

Figure 0.1 presents a longitudinal profile of the boreholes along the alignment, the most likely stratigraphic configuration, the associated uncertainty (H) (expressed in terms of information entropy), and median uncertainty within the tunnel envelope. As shown in Figure 0.1 (c) and (d), the uncertainty at transition 1 (transition from cohesive to cohesionless soils) and transition 2 (transition from cohesionless to cohesive soils) is between 0.3 and 0.6, with a median uncertainty of about 0.4. These uncertainty measures do not quantify or indicate the uncertainty in locations of stratigraphic transitions, which are critical for the efficient operation of the tunnel boring machine (TBM). It is noted that relatively higher uncertainty measures are observed at locations of transitions between stratigraphic units; however, the stratigraphic transitions may not be captured without setting a threshold on the acceptable uncertainty measures.

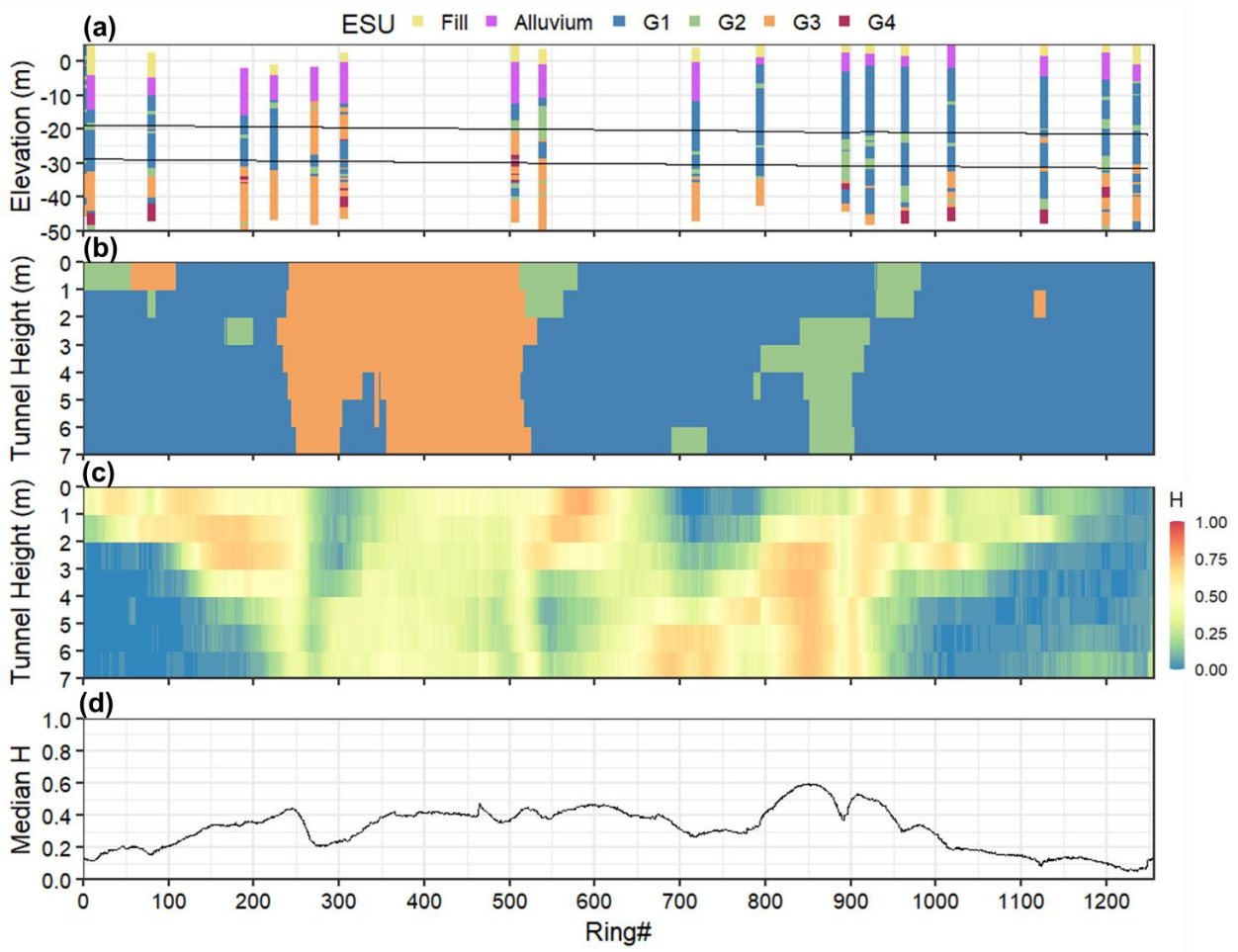

Figure 0.1 (a) Longitudinal borehole profile, (b) most-probable stratigraphic configuration along tunnel centerline, (c) uncertainty (H) expressed in terms of information entropy, and (d) median uncertainty within tunnel envelope.

Along with the longitudinal (*x-z* plane) direction, the study analyzed the uncertainty measures in the transverse (*y-z* plane) direction. **Error! Reference source not found.** presents uncertainty measures for rings # 311 and #520 in the *y-z* plane. As illustrated, for ring# 311, the uncertainty in the vertical soil profile increased between the TBM axis (4 m elevation) and invert level (7 m elevation), indicating a transition between two stratigraphic units. Again, the information entropy is misleading as almost 90 % of realizations show transition between cohesionless and cohesive soils (see Figure 3.13 in Chapter 3). For ring# 520, the uncertainty in the *y-z* plane almost remains the same, indicating no transition. This is misleading as about 80 % of the individual realizations from PGSIM modeling show transition between cohesionless and cohesive soils at TBM axis elevation. The most likely soil conditions at ring# 520 are presented for comparison. The results from information entropy are based only on the most likely stratigraphic configuration and provide only a definite elevation of transition without quantification of the possible fluctuation in the transition elevation.

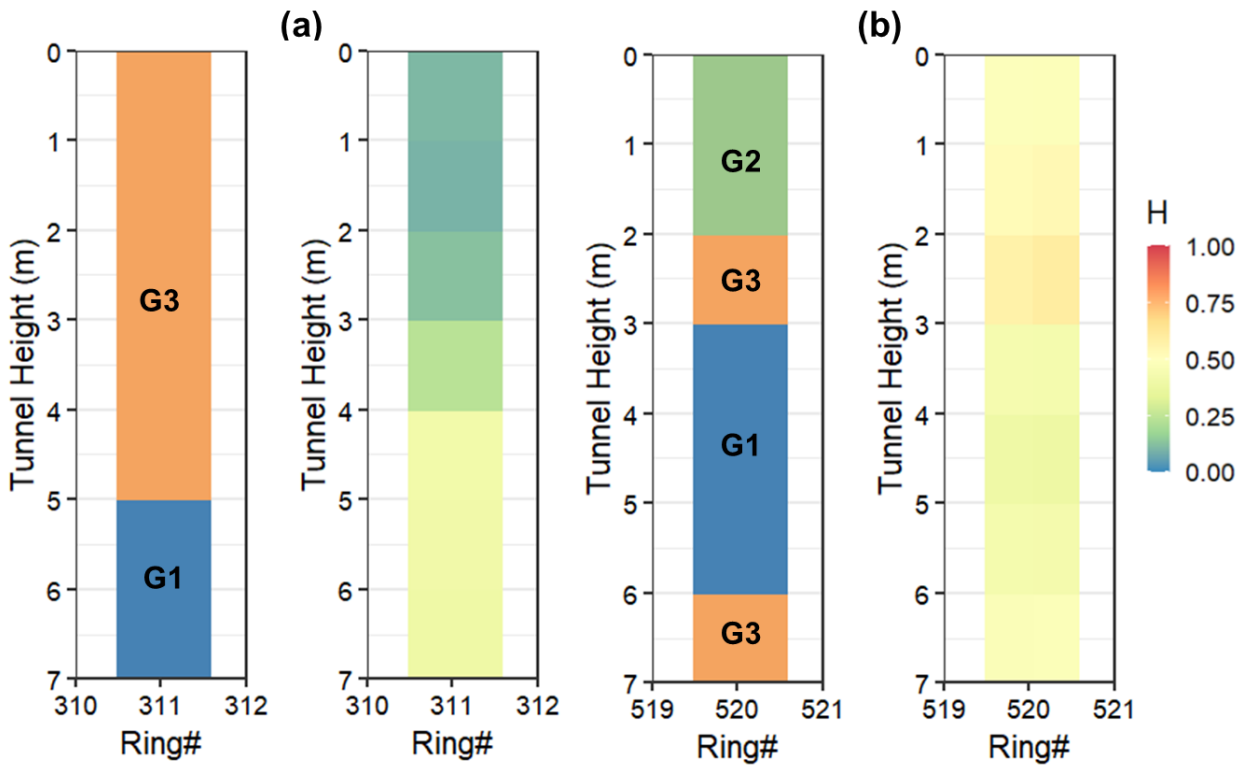

Figure 0.2 Uncertainty (H) expressed as information entropy for transverse cross-section (y-z plane) for ring# 311 and #520.

The study concludes that although information entropy can quantify uncertainty in stratigraphic configurations, the approach cannot be applied to obtain a quantitative assessment of stratigraphic transition location uncertainty in the longitudinal (*x-y* plane) transverse (*y-z* plane) direction within the tunnel envelope.

APPENDIX B – VALIDATION OF PROBABILISTIC ASSESSMENT WITH SEMI-SUPERVISED LEARNING AS-ENCOUNTERED GROUND CONDITION DETECTION MODEL

B.1 Validation of probabilistic assessment for Northgate Link Extension project

This study considers about 850 m (560 rings) section Northgate Link Extension (N125) tunnel project in Seattle, Washington. The tunnel section of N125 consists of 5.6 km long twin tunnels excavated using EPBMs. Geotechnical site investigation (SI) campaign for the 850 m section involved drilling 13 boreholes at a mean horizontal spacing of 120 m. Based on SI, five major soil types were identified: (1) engineering fill (Fill); (2) till and till-like deposit (TLD); (3) cohesionless sand and gravel (CSG); (4) cohesionless silt and fine sand (CSF); (5) cohesive clay and silt (CCS). The validation study is simplified as the CSG and CSF are grouped into cohesionless soils, and CCS and TLD are grouped into cohesive soils. In terms of soil types, the SI data is utilized to generate 500 realizations of ground conditions using the PGSIM technique. The resolution of the 3D simulation grid is kept to 1.5 m x 1.5 m x 1 m in the *x* (longitudinal), *y* (transverse), and *z* (vertical) directions. Within the probabilistic approach, individual realizations of ground conditions for voxels within the tunnel envelope are extracted and are used to characterize the soil transition uncertainty. Figure 0.1 shows the longitudinal profile of the boreholes and the most likely ground conditions within the tunnel envelope developed from the PGSIM technique.

For the SSL model of the N125 project, soil fractions within the tunneling envelope were extracted from 83 boring logs by associating the boreholes to the nearest ring. From the 600 parameters automatically measured by the EPBM, Yu and Mooney (2021) utilized thrust force, advance rate, cutterhead rotation speed, cutterhead torque, chamber pressure at springline and its vertical gradient, screw conveyor rotation speed, screw conveyor torque, and excavated soil mass were used for training the SSL model. Therefore, each ring was represented by the aforementioned EPBM operation parameters and the estimated soil fractions within the tunnel envelope for the SSL model training. Figure 0.2 presents the longitudinal profile of the as-encountered ground conditions within the tunnel envelope inferred from the SSL model.

Figure 0.3 presents the probability distribution function (PDF) of soil transitions in the longitudinal direction, as derived from the geostatistical modeling-based probabilistic approach. From the SSL model interpretation, transitions between cohesive and cohesionless soils are considered to occur, as the proportion of either soil type ≥ 50 %. As illustrated in Figure 0.3, from the SSL model, transition #1 from cohesionless to cohesive soils occurs between ring# 3300 and ring# 3100, and transition #2 from cohesive to cohesionless soils occurs at about ring# 3490. The inferred as-encountered ground conditions from the SSL model are utilized to validate the soil transition locations in the longitudinal direction. Results indicate that the soil transition locations identified from the SSL model fall within one standard deviation from the mean of the probability distribution, as derived from the geostatistical modeling approach. The validation indicates the efficacy of the geostatistical modeling-based probabilistic approach in quantifying the soil transition location uncertainty.

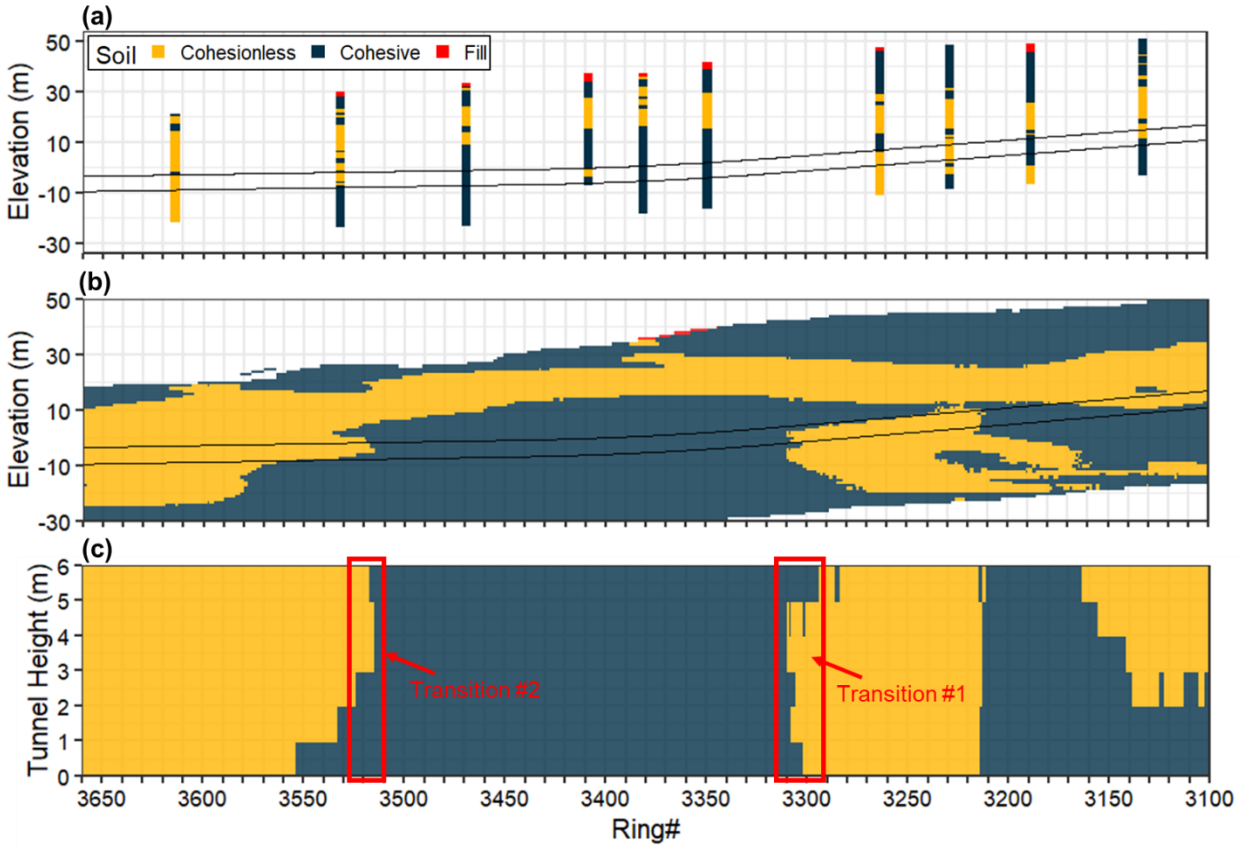

Figure 0.1 (a) Longitudinal profile of the boreholes, (b) most likely ground conditions along tunnel alignment centerline (x, y = 0, z), and (c) most likely ground conditions along tunnel alignment centerline and within the tunnel envelope (x, y = 0, tunnel crown ≤ z ≤ tunnel invert).

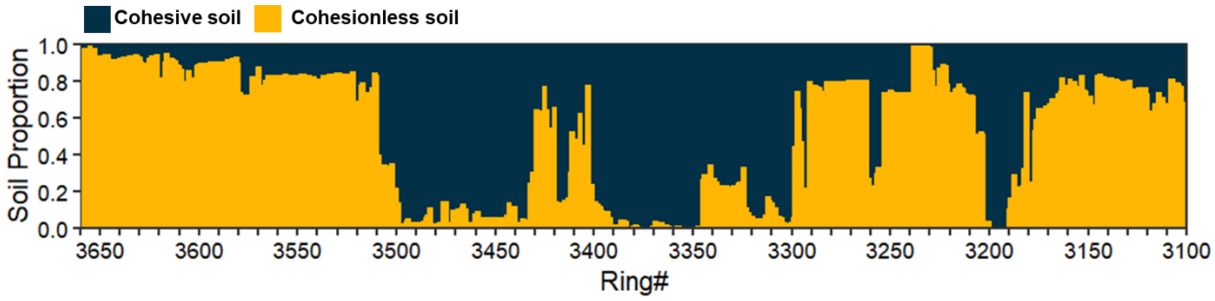

Figure 0.2 Inferred geological profile within the tunneling envelope of N125 project as per the SSL model (after Yu and Mooney 2021).

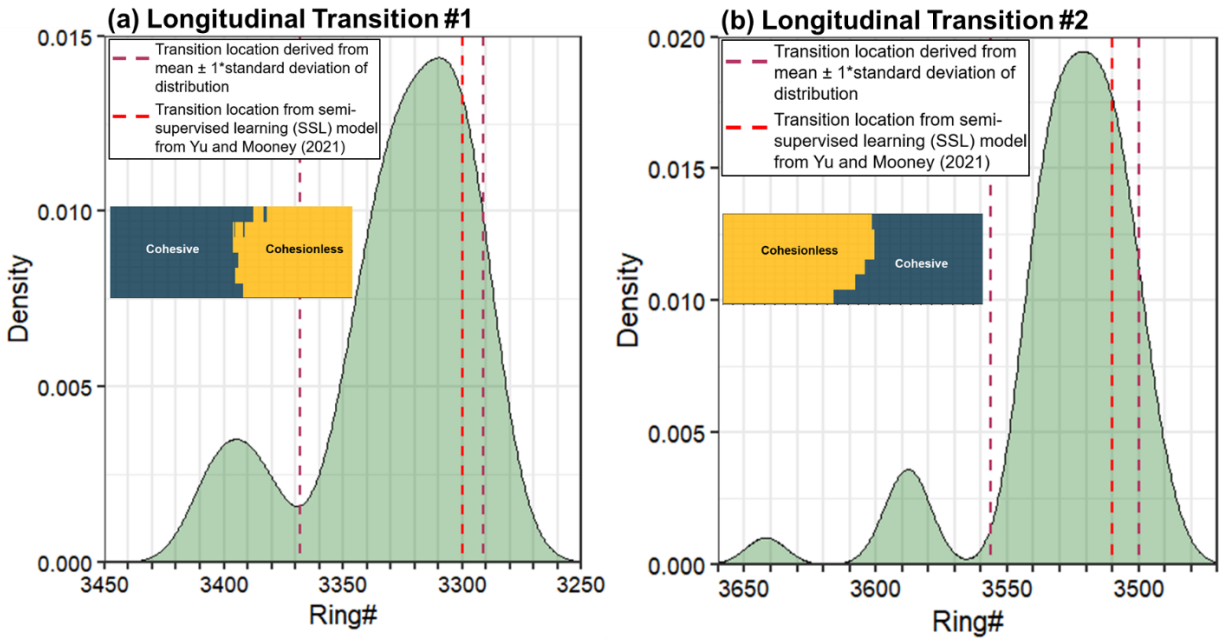

Figure 0.3 Probabilistic distribution of spatial locations of (a) transition 1 – from cohesive to cohesionless material, and (b) transition 2 – from cohesionless to cohesive material occurring in the x (longitudinal) direction in N125 project. The red line indicates the spatial location of soil transition from the SSL model developed by (Yu and Mooney 2021).

B.2 Conclusion

Soil transition locations (P_{95}) identified from the geostatistical modeling-based probabilistic approach are validated with the semi-supervised learning (SSL) model that considers the EPBM operational data and geotechnical site investigations. Since the SSL model captures the EPBM operational behavior at ring resolution, it is a robust tool for validating the soil transition locations. Validation from two actual soil tunnel projects situated in the different geological environments is discussed. For the N125 project situated in a heterogeneous glacial environment, the soil transition locations from the geostatistical modeling-based probabilistic approach fall within ten rings of the transition location identified in the SSL model.

APPENDIX C – COMPARISON OF TPROGS AND PGSIM IN CAPTURING SOIL TRANSITIONS

C.1 Modeling soil conditions using TPROGS technique

Different geostatistical simulation methods are available to achieve the goal of modeling geological conditions using borehole data. TPROGS and PGSIM have been previously utilized to model soil and rock conditions in tunneling applications (Felletti and Beretta 2009; Grasmick et al. 2020b; Gangrade et al. 2021a) and hence are selected for comparison from a variety of other techniques. The aim of the work is to compare the performance of TPROGS and PGSIM techniques in modeling soil conditions within tunnel envelope. The work is extended to compare the consistency of modeling results with the soil condition interpretation within the tunnel envelope. The logical sequence of developing a soil type geostatistical model first, to generate a model of geotechnical parameters makes a strong case to validate the performance of PGSIM and TPROGS.

Here, the analysis is focused on the characterization of soil transition location uncertainty to improve the knowledge of tunnel excavation environment. Geotechnical site investigation (SI) data from Anacostia River Tunnel (ART) project is utilized to quantify the soil transition location uncertainty between two geological units. Since the modeled soil types are classified as per the Unified Soil Classification System (USCS), it is not straightforward to make direct comparison with the geological formation based interpretations in the geotechnical baseline report (GBR). The geostatistical methods were compared and ranked based on how closely they honored the input data and geological realism of the soil conditions within tunnel envelope as derived from tunnel boring machine (TBM) data. A brief description and summary of the conditioning data required to quantify the soil transition location uncertainty, as taken from the geotechnical SI of ART project, is presented in Chapter 4. Locations of transition between cohesionless and cohesive soils for 95 % occurrence probability (P_{95}), as derived from the PGSIM technique, are presented in Chapter 4.

TPROGS methodology is based on modeling of transition probabilities between different categorical classes (or geologic units) with Markov Chains (Carle 1999; dell'Arciprete et al. 2012). The methodology incorporates interclass dependencies in effectively modeling the spatial distribution of categorical classes. The spatial variation between categorical classes is modeled using transiograms that serve as the spatial measures for Markov Chain geostatistics (Carle and Fogg 1996, 1997). The transiograms convey the transition probabilities, proportions, mean lateral extent, vertical thickness, connectivity, and juxtaposition tendencies for each categorical class. Equiprobable realizations of categorical class configuration generated are conditional to the abovementioned factors from transiograms. Markov Chain models draw needed transition probabilities with different lags from continuous transiogram models fitting the experimental transiograms.

The transiograms can be expressed as a two-point transition probability function over a distance lag $\boldsymbol{h}$ (Carle and Fogg 1997) as shown in Eq. (0.1).

$$p_{jk}(\boldsymbol{h}) = P\{Z(\boldsymbol{v}+\boldsymbol{h}) = k \mid Z(\boldsymbol{v}) = j\} \tag{0.1}$$

where $\boldsymbol{v}$ and $\boldsymbol{h}$ are lag distance vectors, respectively. This is considered a Markov Chain approach since the occurrence of class k at location $\boldsymbol{v}+\boldsymbol{h}$ is only dependent on the occurrence of class j at location $\boldsymbol{v}$. An auto-transiogram $p_{jj}(\boldsymbol{h})$ represents the self- dependence (i.e., auto-correlation) of single class j, and a cross-transiogram $p_{jk}(\boldsymbol{h})$ ($j \neq k$) represents the cross-dependence of class k on class j. Because of the asymmetric property of transition probabilities, we always have cross-transiogram $p_{jk}(\boldsymbol{h})$ (h) $\neq p_{kj}(\boldsymbol{h})$, irrespective of the directionality of transiograms. The transiograms have three basic properties that are constraint conditions in transiogram modeling: (a) no nuggets for multinomial classes, which are exclusive of each other; (b) nonnegative; and (c) at any lag $\boldsymbol{h}$, values of transiograms headed by the same class sum to 1. Because of property (a), the start point (0, 0) is always counted into cross-transiograms and the start point (0, 1) is always counted into auto-transiograms.

Figure 0.1 presents the transition probabilities of ESUs from geotechnical SI data of ART project and the fitted transiogram models in the horizontal and vertical directions. For the calculation of conditional probabilities according to the SI data, a lag distance spacing of 10 m and 1.5 m were used in the horizontal and vertical direction, respectively. The models represent the conditional occurrence probabilities of same or different ESU at a certain lag distance and direction from a known ESU at a point. For example, if location of G1 is known, 5 m vertically from that location there is a 55 % probability of encountering G1, 10 % probability of encountering Alluvium and Fill, 7 % probability of encountering G2, 16 % probability of encountering G3, and 2 % probability of encountering G4. TPROGS modeling methodology is applied to the ART SI data, and 460 equiprobable realizations of ground conditions are generated in terms of ESUs. The resolution and extents of the 3D simulation grid is kept the same as described in Chapter 3. For a one-to-one comparison between PGSIM and TPROGS, the random path of individual realizations is kept the same using the same seed number.

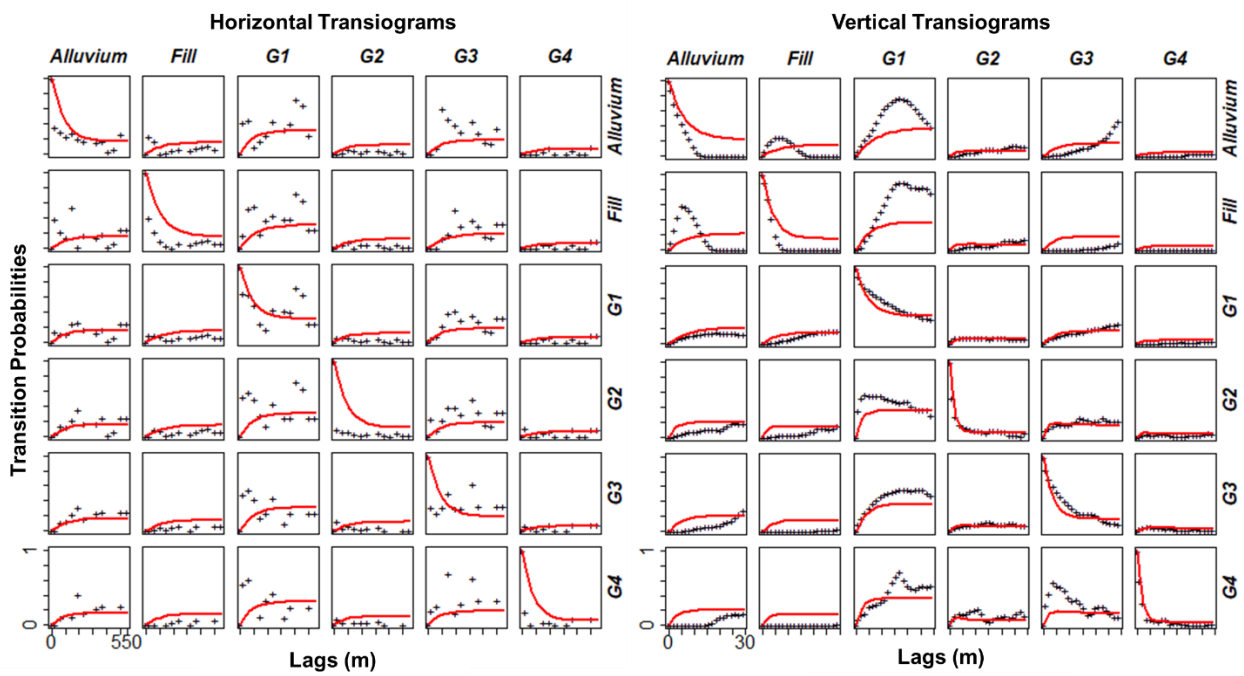

Figure 0.1 Horizontal and vertical transiograms for ESU simulation. The black points represent the conditional probabilities calculated from Eq. (0.1) and the red lines are the fitted Markov chain model.

One of the essential steps in analyzing the geostatistical model is to validate if the input proportions of categories are reproduced within the individual realizations. It is evident if the category proportions are reproduced within the realizations, the probability of spatial structure reproduction, i.e., indicator variograms in PGSIM and transiograms in TPROGS would be high. One of the reasons for better spatial structure reproduction from realizations honoring the input proportions is that, in indicator variograms, the sill is a function of the category proportion, i.e. $s_k = f_k(1 - f_k)$, for category *k*. It is also known that the sill of transiogram $p_{jk}(\boldsymbol{h})$ approaches p_k, the proportion of category *k*, whether $j = k \; or \; j \neq k$ (Carle and Fogg 1996). Moreover, the category proportions have an influence on the near origin slopes of the spatial structure models. For indicator variograms, Maleki et al. (2017) conveyed that the modeling of categorical boundaries in PGSIM technique is related to the second-order derivative of indicator variogram at the origin which in turn relates to the category proportion within the modeling domain. For transiograms, it is open knowledge that larger the mean length of a category, larger is the proportion of the category. Carle and Fogg (1996) showed that the mean length of the categories is inversely proportional to the near origin slopes in auto-transiograms. Therefore, it could be suggested that the near origin slopes should be larger in auto-transiograms of categories with small proportions and vice-versa. This is confirmed from Figure 0.1 where near origin slope for G2 and G4 (lowest proportion) is greater than the near origin slopes of G1 (highest proportion). As a result, a better reproduction of the input proportions leads to an improved reproduction of the sills of indicator variograms and transiograms and the near origin slopes of transiograms. Hence, the selection of better proportions-reproducing realizations would be an important progress in screening

techniques with better fulfillment of spatial variability structure reproduction and the other minimum required acceptance criteria.

From Chapter 3, since G1, G2, and G3 occur within the ART tunnel envelope, a comparison of input proportions (from borehole data) and output proportions from individual realizations of TPROGS and PGSIM are presented in Table 0.1. The ESU proportions in the simulations from two techniques are slightly different from the input proportions due to the averaging effect between the conditions imposed by different modeling parameters such as transiograms and indicator variograms.

Table 0.1 Input and output proportions for TPROGS and PGSIM techniques, expressed as mean ± standard deviation over an ensemble of 460 realizations.

ESU	Input proportion (%)	Output proportion (%)	
		TPROGS	PGSIM
G1	68	65.7 ± 1.2	66.2 ± 1.0
G2	14	10.3 ± 1.1	13.3 ± 1.3
G3	18	24.1 ± 2.4	20.5 ± 1.0

The conditional realizations are generated in the TPROGS approach through a two-step procedure

1. Generating an ‘initial configuration’ using a cokriging-based version of sequential indicator simulation (SISIM).
2. Iteratively improving the conditional realizations in terms of matching simulated and modeled transition probabilities by applying simulated annealing algorithm.

The two steps are mutually dependent because the SISIM step alone will not yield stochastic realizations that adequately honor the model of spatial variability, and the optimization step will not succeed without a rudimentary initial configuration.

C.2 Probabilistic assessment of soil transition location and field validation

Individual realizations from PGSIM and TPROGS technique are utilized to generate a family of empirical cumulative distribution function (ECDF) curves for soil transition 1 (Figure 0.2) and soil transition 2 (Figure 0.3) for varying cohesive and cohesionless soil proportions within the tunnel envelope. It is interesting to note the similarity in the P_{95} observations for greater than 50 % proportion of cohesionless soil in soil transition 1 ECDFs, from two techniques. PGSIM suggests transition at ring# 275, whereas TPROGS suggests transition at ring# 272. However, the longitudinal distance over which cohesionless soil proportion increases from 30 % to 50 % is 20 rings from PGSIM technique and 3 rings from TPROGS technique. The individual realizations of

TPROGS suggest a four times wider 90 % confidence interval (CI) band (200 rings) compared to the PGSIM technique (50 rings).

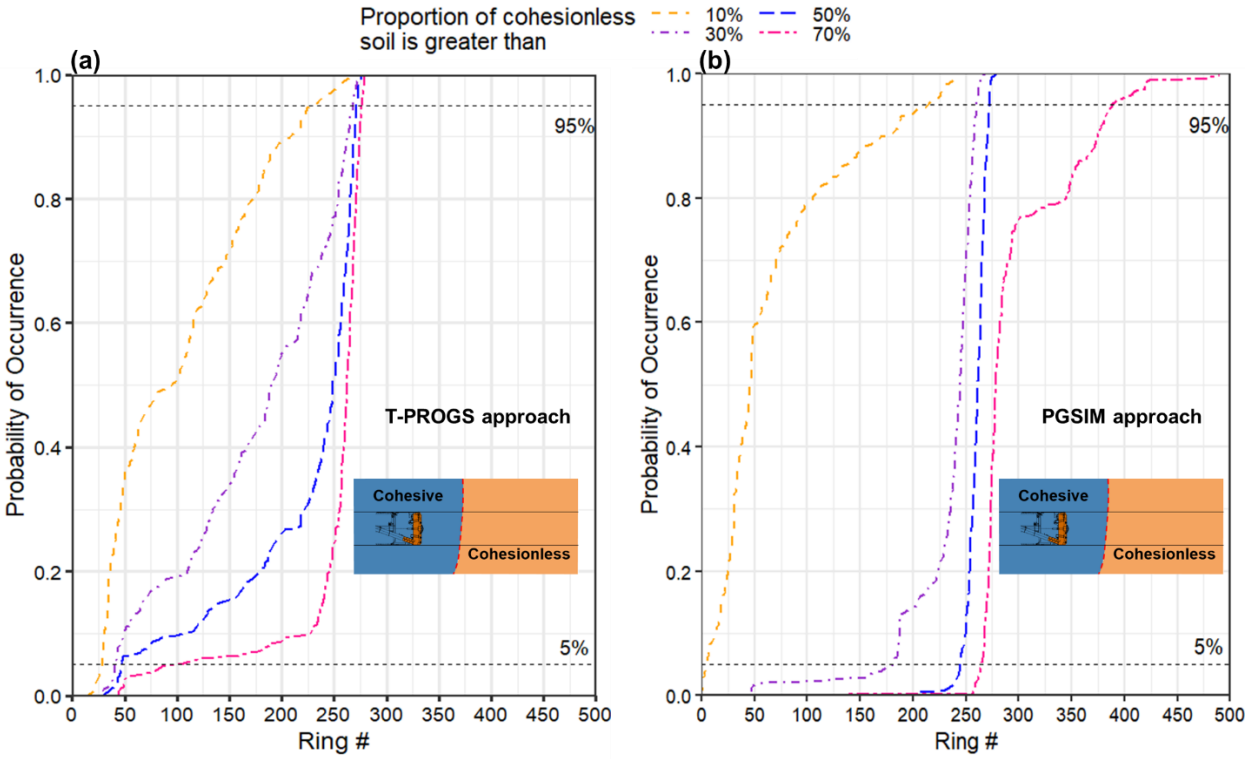

Figure 0.2 Family of empirical cumulative distribution function (ECDF) curves for varying proportions of cohesionless soil for transition 1 within the tunnel envelope as evaluated from (a) TPROGS approach and (b) PGSIM approach.

For soil transition 2, ECDFs generated from TPROGS reflect 10-20 ring difference in P_{95} observations of cohesive soil proportion, compared to ECDFs from PGSIM. A majority of the 500 TPROGS realizations show presence of cohesive soil proportion greater than 10 % and 30 % transition at around ring# 375 and #380, resulting into a vertical ECDF line. As illustrated, greater than 50 % proportion of cohesive soil occurs at about ring# 540 from TPROGS methodology, compared to ring# 550 from PGSIM. It is interesting to note that, although the difference in P_{95} observations is minimal (in context of size of tunnel projects), the difference in the occurrence probabilities of cohesive soil at each ring are drastically different. In addition, the 90 % CI band obtained from TPROGS indicates higher uncertainty in soil transition location compared to the results from PGSIM. The difference in the results from TPROGS and PGSIM is primarily due to the difference in (a) spatial structure of ESUs, (b) difference in the near slope origins of the spatial structure, and (c) additional constraints imposed in PGSIM modeling from the *lithotype* rule.

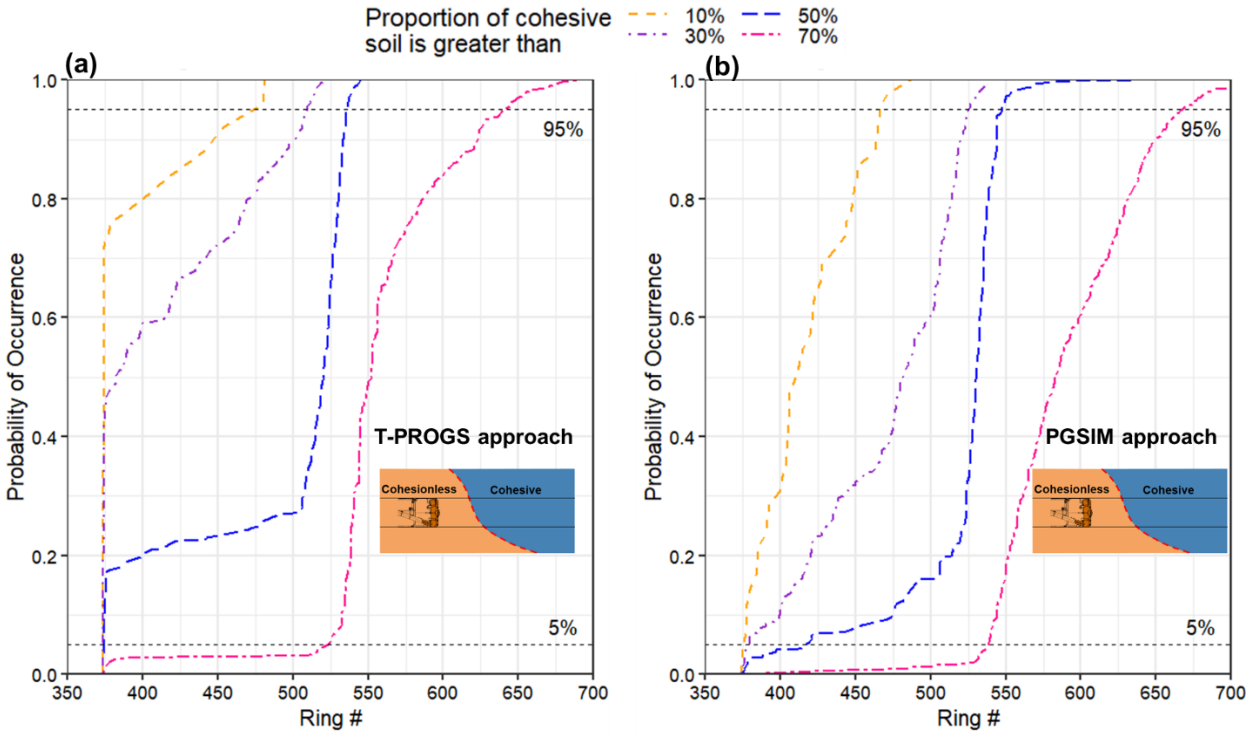

Figure 0.3 Family of empirical cumulative distribution function (ECDF) curves for varying proportions of cohesive soil for transition 2 within the tunnel envelope as evaluated from (a) TPROGS technique and (b) PGSIM technique.

Figure 0.4 shows the maximum dissipation of EPBM chamber pressure during standstill at the tunnel springline for sections of the ART alignment in the proximity of the soil transitions. Locations of transition suggested in the GBR and P_{95} observations from PGSIM and TPROGS modeling technique are presented. Results indicate that TPROGS effectively captures the P95 location of soil transition 1 within 5 rings of P_{95} observation from PGSIM technique. However, for soil transition 2 location the difference in the P_{95} observations from two techniques is about 10 rings. Based on the rate of chamber pressure dissipation reflecting the proportion of cohesionless/cohesive soil within tunnel envelope, the realizations generated from PGSIM technique capture the locations of soil transition 1 and 2 (P_{95} observations) with relatively higher accuracy compared to TPROGS. However, the accuracy of TPROGS in capturing soil transition locations is superior to interpretation from GBR.

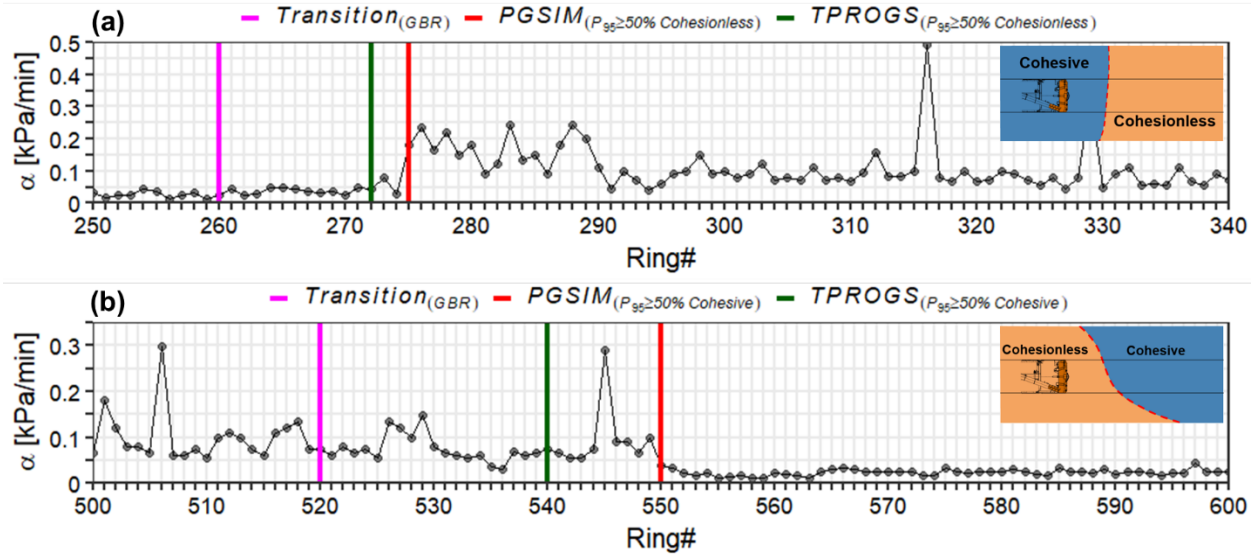

Figure 0.4 Rate of dissipation of EPBM chamber pressure as determined from the analytical fit to chamber pressure drop during EPBM standstill, in proximity of (a) soil transition 1 and (b) soil transition 2. Pink, green, and red lines indicate the soil transition from GBR, TPROGS technique, and PGSIM technique, respectively.

C.3 Conclusions

Results indicate that for a tunnel project situated in marine sedimentary geological setting, the performance of PGSIM technique in honoring the input ESU proportions is superior to TPROGS technique for the specific application of quantifying soil transition location uncertainty. For the specific application, realizations generated from PGSIM technique are found to capture the soil transition locations within tunnel envelope with relatively higher accuracy compared to the TPROGS technique. This is validated from the rate of chamber pressure dissipation observed during EPBM standstill. PGSIM technique is found to provide better predictions of ESU occurrence probabilities than TPROGS, by constraining the individual realizations to actual geological conditions observed in borehole data. Realizations generated from TPROGS technique show relatively high uncertainty (90 % CI) in soil transition location compared to the PGSIM technique. It is therefore concluded that, especially when working with sampling density typically observed in underground construction and tunnel projects, using PGSIM might represent a pragmatic yet decent ground condition modeling choice. However, a cross-validation of the developed ground models from any geostatistical modeling technique is suggested to identify the percentage accuracy of classification (or misclassification) of the categorical classes.

APPENDIX D – EFFECT OF BOREHOLE LOCATIONS ON SPATIAL UNCERTAINTY MEASURES

The effect of borehole locations on geotechnical uncertainty reduction was analyzed from virtual sampling boreholes with and without informed guidance of uncertainty in engineering soil units (ESUs). A 4 km section of the North-East Boundary Tunnel (NEBT) is considered herein. The study simulates a scenario where 15 boreholes are drilled as a part of the preliminary geotechnical site investigation (SI). Figure 0.5 presents a longitudinal profile of the drilled boreholes in terms of ESUs vis-à-vis tunnel alignment. The mean vertical sampling interval within the boreholes is approximately 0.5 m. Figure 0.6 presents the global proportions and the global vertical variability profile (also known as vertical proportion curve) of the ESUs along the NEBT alignment. The spatial continuity aspect of the simulation technique is illustrated in Figure 0.7 that presents the experimental indicator variograms of the ESUs. The indicator variograms quantify the degree of continuity for each ESU with distance. The anisotropy in the spatial continuity of the ESUs can be inferred from the indicator variograms.

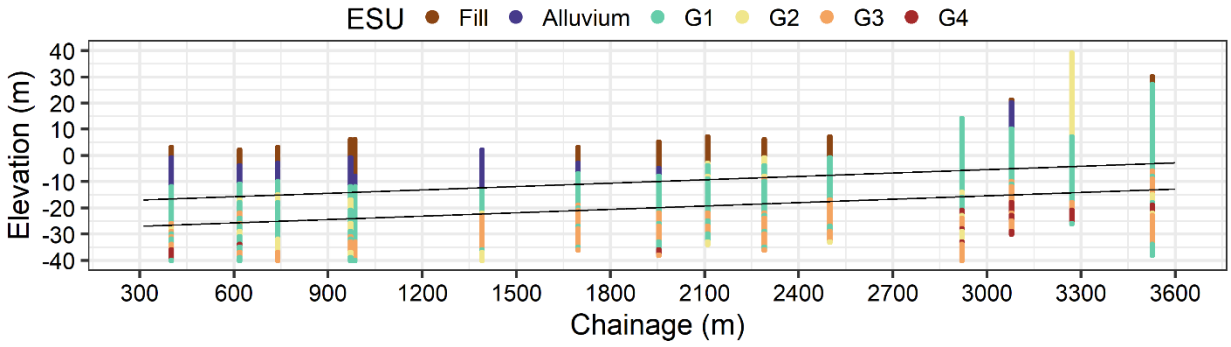

Figure 0.5 Profile view of 15 boreholes with sampled ESUs vis-à-vis tunnel alignment.

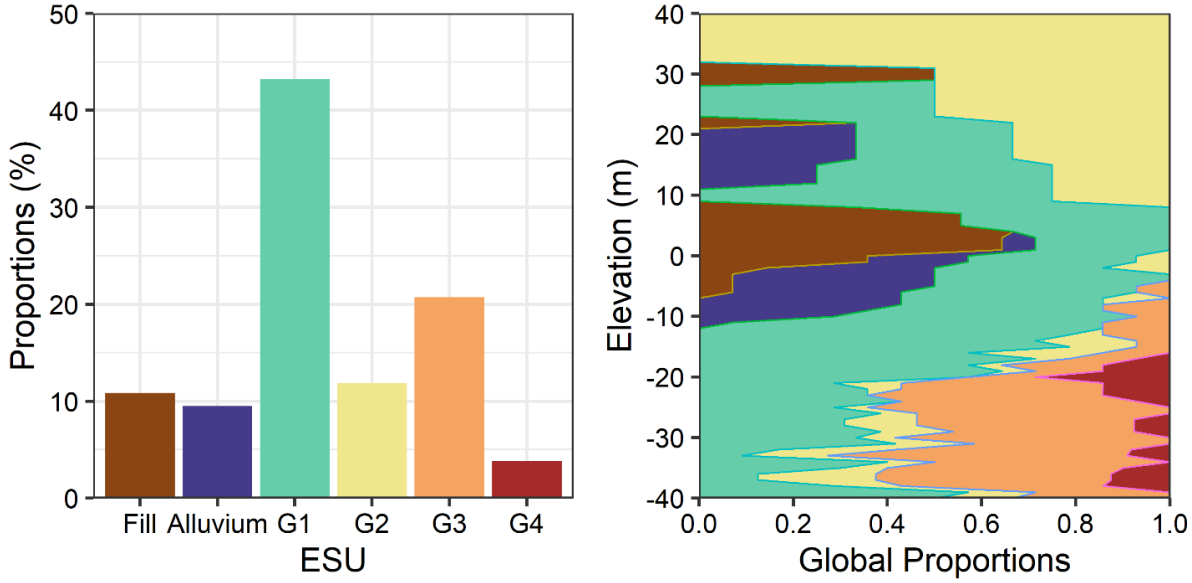

Figure 0.6 Global proportions and the global vertical variability of ESUs.

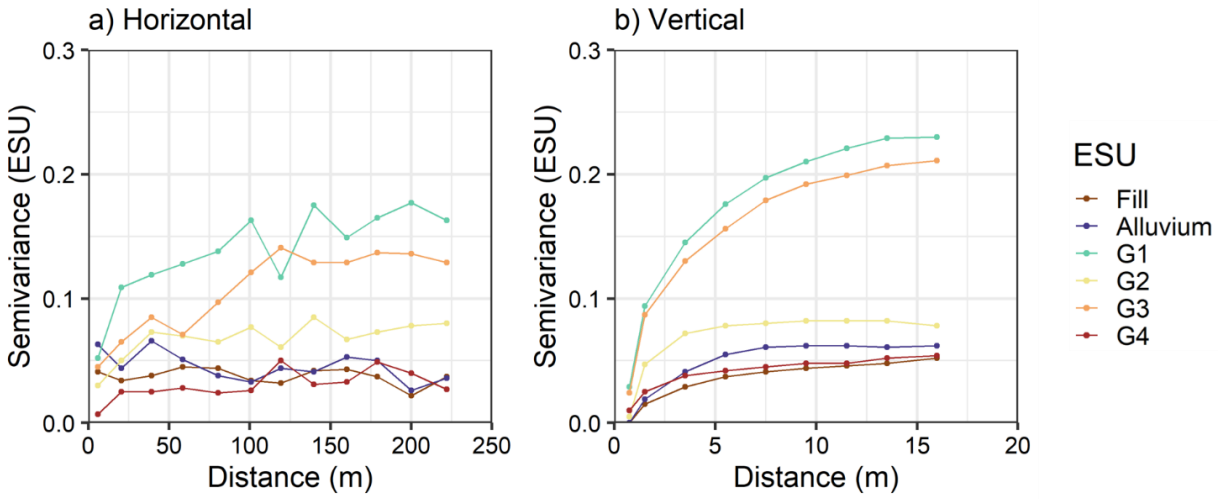

Figure 0.7 Model indicator variograms for ESUs along the horizontal and vertical directions.

In this study, a 3D random field is generated with a resolution of 5 m, 5 m, and 1 m in the longitudinal, transverse, and vertical directions, respectively. The random field extends to a transverse distance of 50 m on either side of the NEBT alignment centerline. A set of 100 realizations of ESU conditions are generated from PGSIM technique. Realizations are post-processed to quantify a most-probable ESU model (an ESU occurring the most at a voxel from all realizations) and the spatial uncertainty in ESU conditions (see Figure 0.8). The spatial uncertainty model is developed from occurrence probabilities of ESUs and is expressed in terms of information entropy. The concept of information entropy (denoted by *H*) is appealing because it based on a

metric scale of 0 to 1, with H =0 corresponding to the lowest uncertainty (only one possible outcome), and H =1 corresponding to the highest uncertainty (all outcomes are possible) (Bianchi et al. 2015).

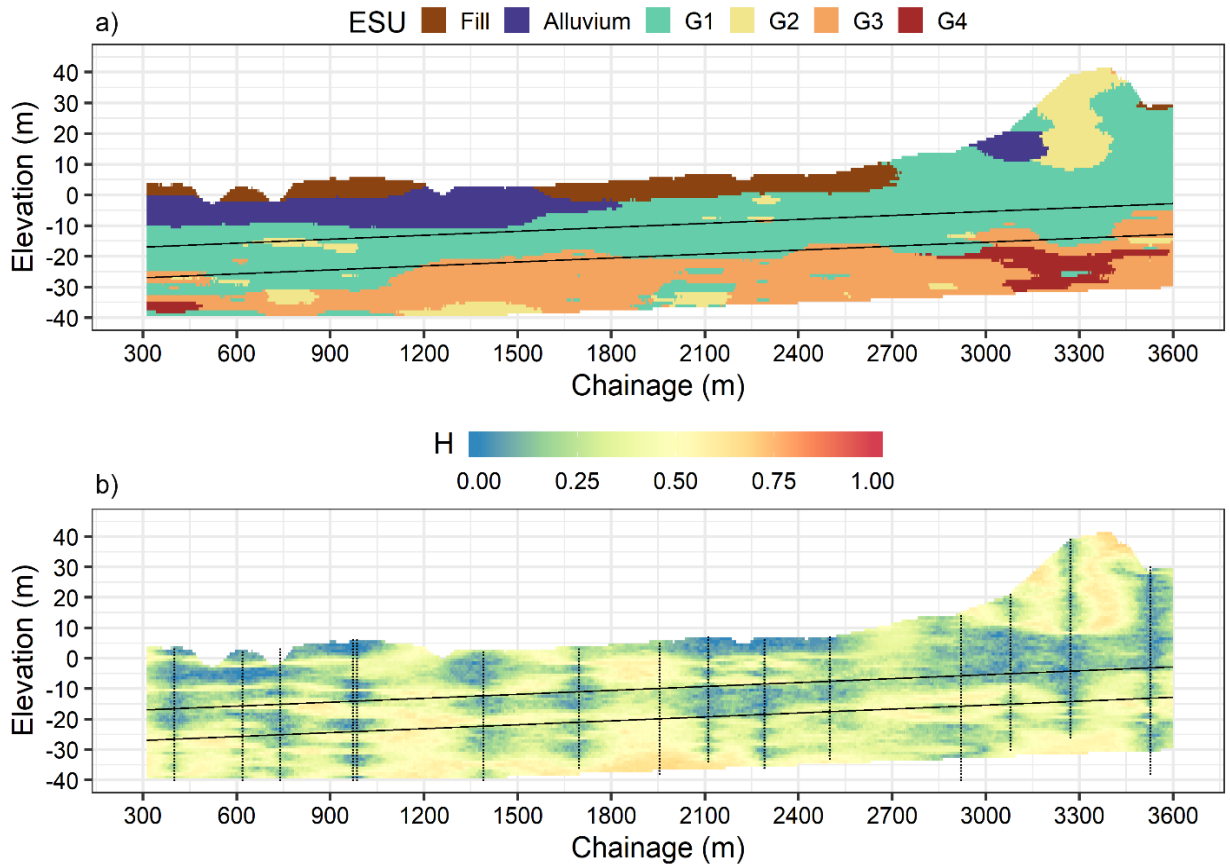

Figure 0.8 a) Most probable ESU model and (b) ESU spatial uncertainty model from preliminary geotechnical SI. Black points in (b) correspond to the borehole locations.

The study is set-up to add five boreholes after the preliminary SI (15 boreholes). Case (1) involves adding the five boreholes at the same locations as drilled in the actual project and without the knowledge of spatial uncertainty, whereas, in case (2) five boreholes are added with informed guidance of spatial uncertainty measures in ESU conditions. The ground-truth is unknown. To simulate the virtual sampling of additional boreholes, the most-probable ESU model developed from preliminary SI is considered as the ground-truth conditions. The boreholes are sampled from the 3D ground truth model.

Figure 0.9 presents a plan layout of the boreholes from preliminary site-investigation and the spatial uncertainty map (developed from preliminary SI data) superimposed on the tunnel alignment. For the risk related to tunneling-induced ground deformation, spatial uncertainty measures between the ground surface and tunnel invert are critical. Therefore, the uncertainty in ESU conditions is averaged between the ground surface and tunnel invert to develop a 2D map of spatial uncertainty. Locations of relatively higher uncertainty measures (H > 0.25) indicate that

the geostatistical model predicts multiple ESUs at these locations. A prediction of multiple ESUs at a spatial location can be attributed to (a) actual ESU transitions occurring at the location; (b) higher spatial variability of ESUs; and (c) lack of knowledge.

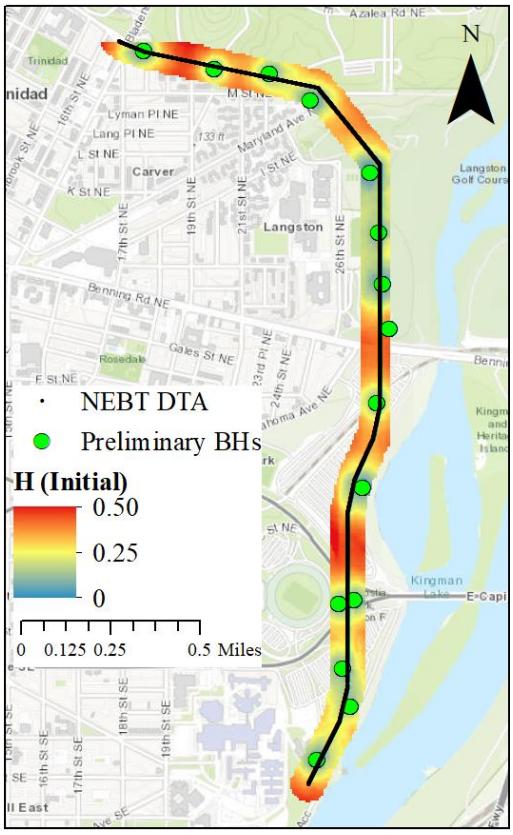

Figure 0.9 Average spatial uncertainty (*H*) between tunnel invert and ground surface superimposed on the 4 km section of NEBT alignment.

Sampling of five additional boreholes is simulated by extracting the boreholes from the 3D ground truth model. The vertical sampling interval for the 5 boreholes is kept to 1 m. All the 5 sampled boreholes, in each case, extend to at least 2 tunnel diameters below the tunnel invert. In case (1), five boreholes are drilled at the actual locations as in the NEBT project without any prior knowledge of the spatial uncertainty from the preliminary SI. In case (2), additional boreholes are drilled with the knowledge of spatial uncertainty. These five additional boreholes are added at spatial locations of relatively high uncertainty measures at least one tunnel diameter away from the NEBT alignment. Figure 0.10 presents a plan layout of the five additional boreholes from case (1) and case (2), drilled along the NEBT alignment. Next, PGSIM modeling technique is applied to develop a most-probable ESU model, ESU occurrence probability model, and a spatial uncertainty model, for both the cases.

Figure 0.11 presents a probability distribution of the spatial uncertainty measures quantified from initial SI + additional SI, for case (1) and (2). The area under each density curve for $H > 0.25$

represents the probability distribution of the number of locations with high measures of uncertainty. Distribution of spatial uncertainty from the case (2) results into relatively narrow probability distribution curve compared to the uncertainty measures from preliminary investigation and case (1), indicating a significant reduction in the uncertainty in the ESU conditions. Table 0.2 presents a summary of the area under each density curve for $H > 0.25$. The results indicate that additional SI as presented in case (1) and (2) leads to about 28 % and 50 % reduction in relatively high uncertainty measures compared to uncertainty measures from the preliminary SI.

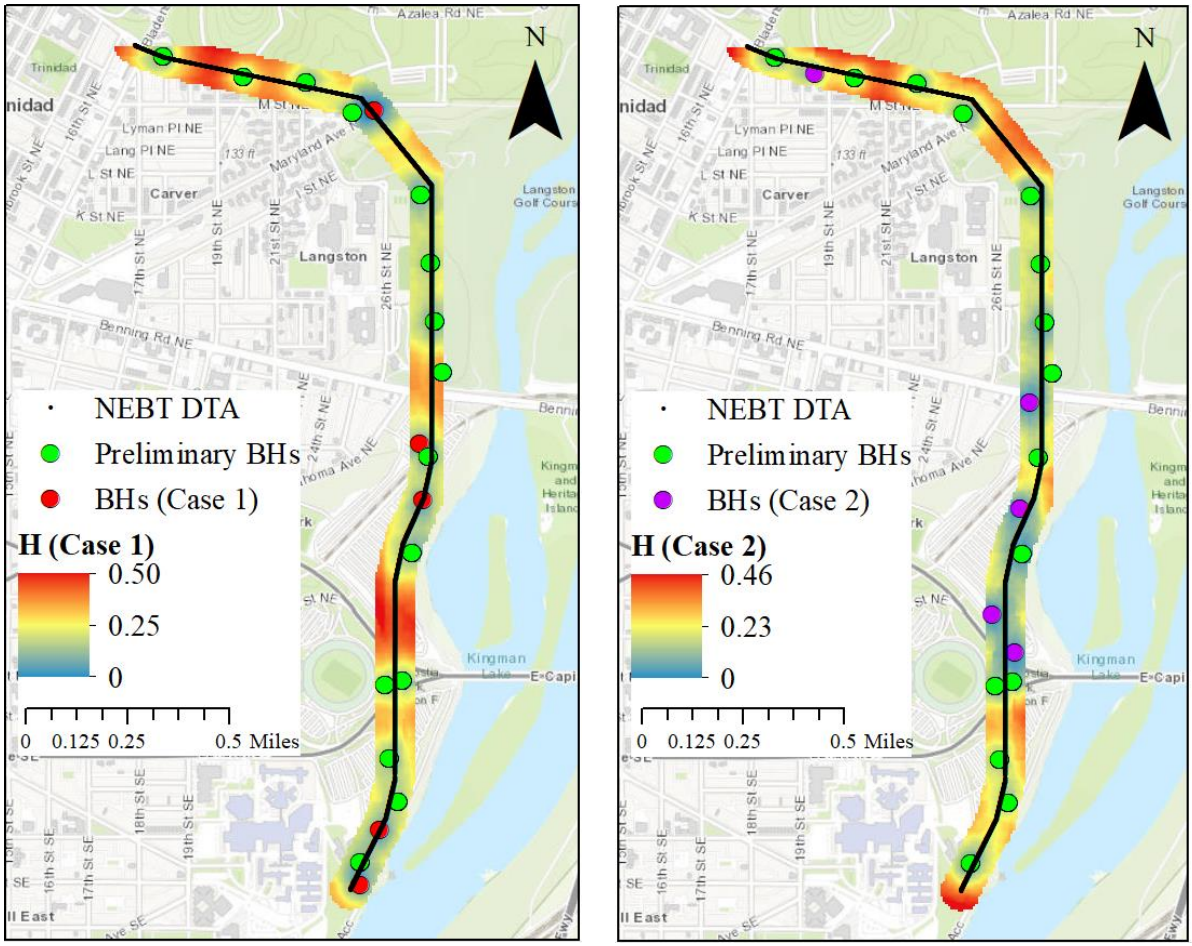

Figure 0.10 Resulting uncertainty (H) map for case (1) and case (2) with spatial locations of five additional boreholes superimposed on the 4 km section of NEBT alignment.

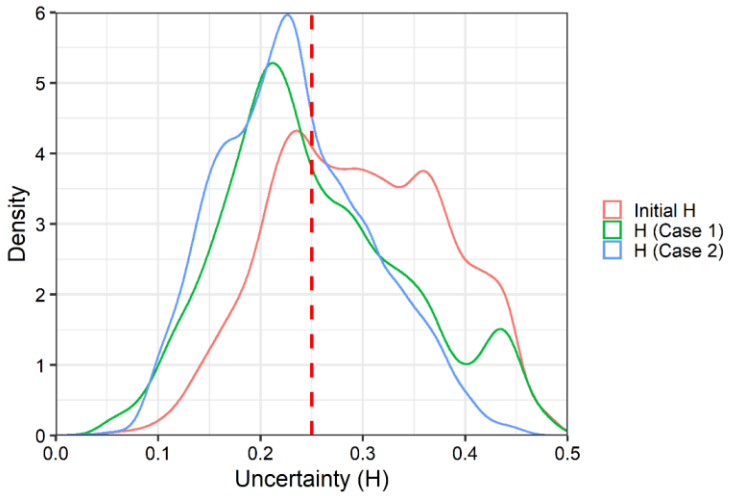

Figure 0.11 Distribution of spatial uncertainty (H) quantified from preliminary SI and additional boreholes from case (1) and case (2).

Table 0.2 The area under the probability distribution curves of spatial uncertainty.

	Preliminary SI	Case 1	Case 2
Area under the curve for $H > 0.25$	0.70	0.50	0.36

With information from additional investigations, updated spatial uncertainty maps (say H_{new}) can be developed. The knowledge gain from additional investigations (ΔH) can be quantified as the difference between the updated uncertainty (H_{new}) and uncertainty from prior measurements (H). The adaptive sampling strategy that involves locating boreholes, gaining additional information, and updating uncertainty maps to identify the next set of locations shall improve characterization of the sub surface domain. Decisions on drilling boreholes at locations of relatively lower uncertainty can be made as per the available budget and time for geotechnical SI. Further, the decisions on SI campaigns can be extended towards selecting an optimal borehole configuration that provides the highest reduction in spatial uncertainty, thus making optimal use of the allocated budget and time.

The study presents a comparative assessment of locating boreholes with the knowledge of spatial uncertainty in sub-surface domain versus the conventional approach of drilling boreholes in tunneling projects (using only a deterministic profile developed from prior investigations) and evaluates the reduction in spatial uncertainty from the two approaches. The effect of different spatial locations of the additional boreholes is captured through the reduction in uncertainty from the two approaches. A reduction in spatial uncertainty only indicates improved confidence in the knowledge of the subsurface domain.

APPENDIX E – IMPACT OF GEOSTATISTICAL MODELING GRID RESOLUTION ON TUNNEL RISK ASSESSMENT

The probabilistic subsurface models stemming from geostatistical modeling provides opportunities to enhance risk assessment and mitigation planning. Grasmick and Mooney (2020) and Gangrade et al. (2021) utilized geostatistical modeling results for tunnel risk assessment. Since geostatistical models are utilized for tunneling risk mitigation planning, it is important to examine the sensitivity of structural grid resolution on model results and interpretation towards risk assessment. The selection of appropriate structural grid resolution raises a key question, *"how do we adjudicate if the estimated geotechnical conditions, for the selected structural grid resolution, are representative of the actual ground conditions? More importantly, can we identify the structural grid resolution beyond with any reduction in the grid resolution will not have an additional benefit on model results?"*

Geotechnical site investigation (SI) data from an actual tunnel project is utilized to evaluate the influence of structural grid resolution on the risk created by tool wear. The project involves excavation of an 8-mile-long tunnel with 8 m internal diameter. As a part of the geotechnical investigation, 106 boreholes were drilled, and soil samples were visually observed and extracted for laboratory testing. To examine the grid sensitivity, four structural grids with resolution – 20m x 20m x 1m, 50m x 50m x 1m, 10m x 10m x 1m, and 5m x 5m x 1m are generated in the longitudinal (*x*), transverse (*y*), and vertical (*z*) directions along the tunnel alignment. Soil abrasivity index (SAI) conditions within the tunnel envelope are modeled to estimate the total number of ripper tool changes using the empirical prognosis model presented by Köppl and Thuro (2013) and Köppl (2014). The number of tool changes from each grid resolution are validated with the actual number of tool changes on the tunnel project site.

Köppl and Thuro (2013) listed abrasivity of the soil components, stress at the contact force between soil and cutting tool, and shape parameter of soil components as the critical factors influencing the rate of cutter tool wear. Figure 0.1 presents a longitudinal profile of the boreholes, SPT blow counts corrected for hammer efficiency and overburden stress (N1-(60)), and grain size distribution test results at sampled locations used to determine D60 along the NEBT alignment. A description of the ESUs encountered within the tunnel envelope is presented in Chapter 5. Geotechnical parameters ESU, N1-(60), and D60 are modeled stochastically, where initial investigation data is utilized to develop multiple equally probable realizations from PGSIM and SGSIM techniques on the abovementioned four different grid resolutions. Similar modeling approach to that discussed in Chapter 5 of the report is adopted to generate realizations of geotechnical conditions. A discussion on PGSIM and SGSIM techniques is presented in the earlier sections of the report.

Within each grid resolution, the developed geostatistical models of ESU, $N_{1-(60)}$, and D_{60} are transformed to estimate SAI conditions within the tunnel envelope (see Chapter 5 for details on relationship between SAI and geotechnical parameters). The variability in the equivalent quartz content (EQC) of each ESU is incorporated into SAI estimates using the Monte Carlo simulation technique (MCS), where a normal distribution with mean and 20 % standard deviation of mean EQC is generated. The distribution covers the range of EQC provided for each ESU in the geotechnical baseline report (GBR) (see Table 0.1). The expected tool wear rate (e_{wear}) is estimated from the SAI conditions within the tunnel envelope. The study considers that the rippers

tools are replaced at locations where cumulative e_{wear} is equal to 70 %. For details on e_{wear} the reader is referred to Chapter 5 of the report.

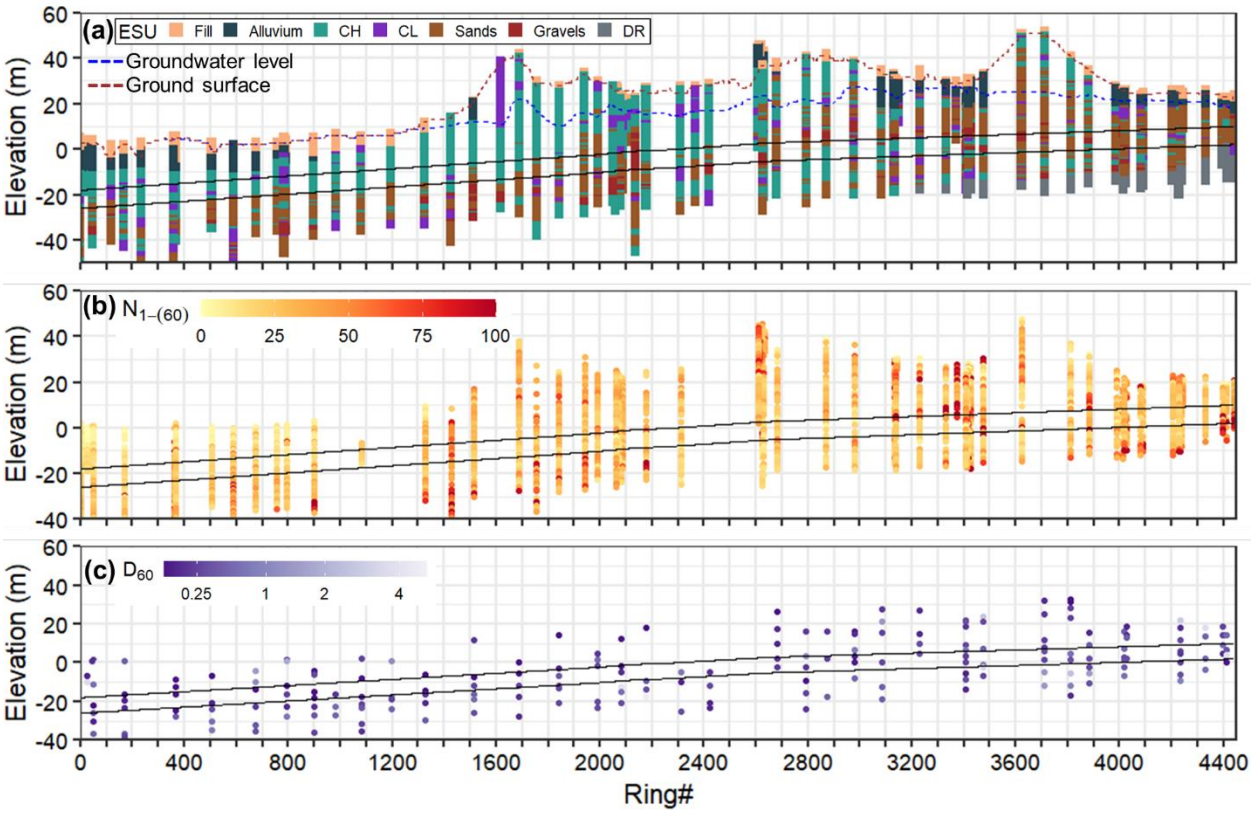

Figure 0.1 Longitudinal profile of (a) boreholes in terms of ESUs, (b) Normalized standard penetration test blow counts $N_{1-(60)}$ [2413 samples], and (c) soil particle size that 60 % of soil is smaller than D_{60} [220 samples].

Table 0.1 Geotechnical parameter values for ESUs in tunnel envelope, as reported in the GBR.

ESU	EQC [Min-Max] (%)	Mean EQC (%)
CH	[34–58]	46
CL	[36–57]	48
Sands	[65-75]	70
Gravels	[88-91]	89

Figure 0.2 presents a longitudinal profile of mean SAI conditions within the tunnel envelope for different grid resolution. Modeling results indicate that the mean SAI conditions estimated in structural grids with longitudinal and transverse resolution of 50 m and 20 m are relatively lower than that in grids with resolution of 10 m and 5 m. It is interesting to note that the difference in the mean SAI conditions is magnified after about ring #1600 where Sands (material with relatively high abrasivity) are first encountered within the tunnel envelope. The significant difference in the mean SAI conditions is reflective of the difference in the structural grids' capability in capturing the Sands. Table 0.2**Error! Reference source not found.** summarizes the number of simulation

voxels within the tunnel envelope, the runtimes of ESU modeling, and geotechnical parameter ($N_{1-(60)}$, and D_{60}) modeling for each grid resolution. In this study, runtime is the total time required to generate the geostatistical realizations and post-process the data to interpret the relevant geotechnical conditions within the tunnel envelope.

Figure 0.3 presents a comparative assessment of the occurrence probability of Sands (P (Sands)) for different grid resolutions. Results indicate that grid resolution of 5 m and 10 m show relatively higher P (Sands) than grids with resolution of 50 m and 20 m. Therefore, Sands in relatively higher proportions are predicted in grids with resolution of 5 m and 10 m than in 20 m and 50 m resolution grids. It is evident that the difference in the P (Sands) will have an impact on SAI uncertainty evaluation and consequently on the number of tool replacements.

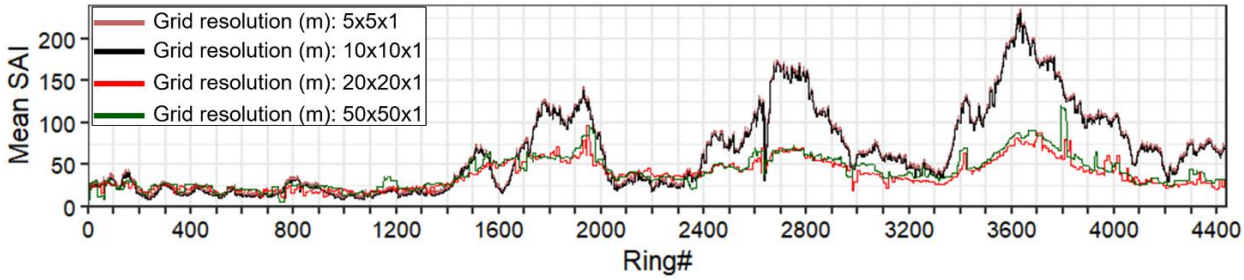

Figure 0.2 Longitudinal profile of mean SAI conditions within the tunnel envelope for different resolution of structural grid used in geostatistical modeling.

Table 0.2 Summary of geostatistical modeling runtime for different grid resolution.

Grid resolution (m)	**Number of simulation voxels**	**Runtime for ESU geostatistical modeling (hours)[1]**	**Runtime for geotechnical parameter geostatistical modeling (hours)[1]**
50 x 50 x 1	~ 1 million	0.5	1.0
20 x 20 x 1	~ 7 million	1.0	1.5
10 x 10 x 1	~ 24 million	5.0	8.5
5 x 5 x 1	~ 96 million	8.0	14.0

[1] Machine specifications: Intel (R) CPU E5-1630v4 @ 3.7 GHz; 128GB Installed memory; software- ISATIS

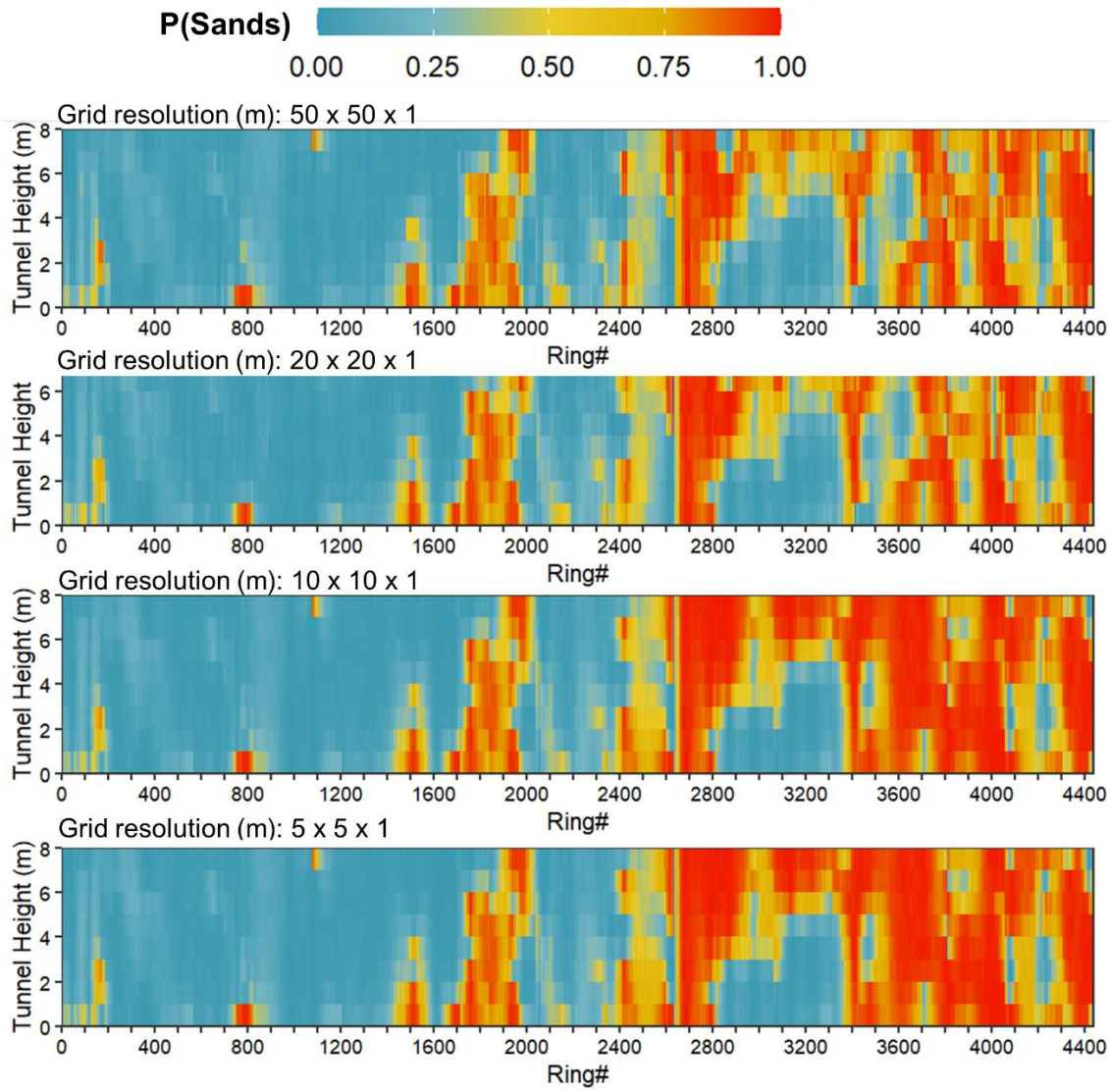

Figure 0.3 Longitudinal profile of occurrence probability of Sands within the tunnel envelope for different resolution of structural grid used in geostatistical modeling.

SAI uncertainty from different structural grid resolutions is utilized to estimate the number of ripper tool replacements for the complete tunnel excavation. The number of tool replacements required penetration rate of the shield machine as an input. Actual penetration rates from the tunnel project are considered herein. Penetration rate varied between 5 mm/rev and 70 mm/rev, with a mean and standard deviation of 22 m/rev and 6 mm/rev, respectively. Figure 0.4 presents the mean and 90 % probability interval (PI) of number of ripper tool replacements for each grid resolution. The results from the probabilistic assessment are compared with the actual number of ripper tools replaced on the tunnel project. It is to be noted that results presented only account for the number of ripper tools wearing out equal to or greater than 70 %. Any precautionary additional ripper tool replacements are not accounted herein.

As illustrated, SAI modeling results from structural grids with resolution of 50 m and 20 m underestimate the number of tool replacements due to an underestimation of SAI conditions within the tunnel envelope. As discussed in Chapter 6, EQC for each ESU is the dominant factor affecting SAI estimates. Since P (Sands) is relatively lower in 50 m and 20 m simulation grids, SAI conditions are underestimated. As observed, in certain cases, the actual number of ripper tool replacements exceed the SAI uncertainty band (90 % PI) by about three to four, which is quite significant (four rippers shall cost about ~ 12,000 USD and account for almost 20-30 % of cutterhead tools being replaced). Grids with resolution of 10 m and 5 m effectively capture the number of tool replacements predicted by the empirical model, indicating that the SAI conditions modeled the same voxel resolution are representative of the ground conditions encountered on the project site. It is observed that the difference in the SAI model results from 5 m and 10 m resolution grid are negligible. However, as illustrated in Table 0.2, the time required for modeling with a 5 m resolution grid is almost twice that 10 m grid resolution. This indicates that modeling with a finer resolution than 10 m does not effectively provide any additional benefit in terms of interpreting ground conditions. Although, model results from grid resolution > 10 m do not quite represent the ground conditions as encountered on the project site.

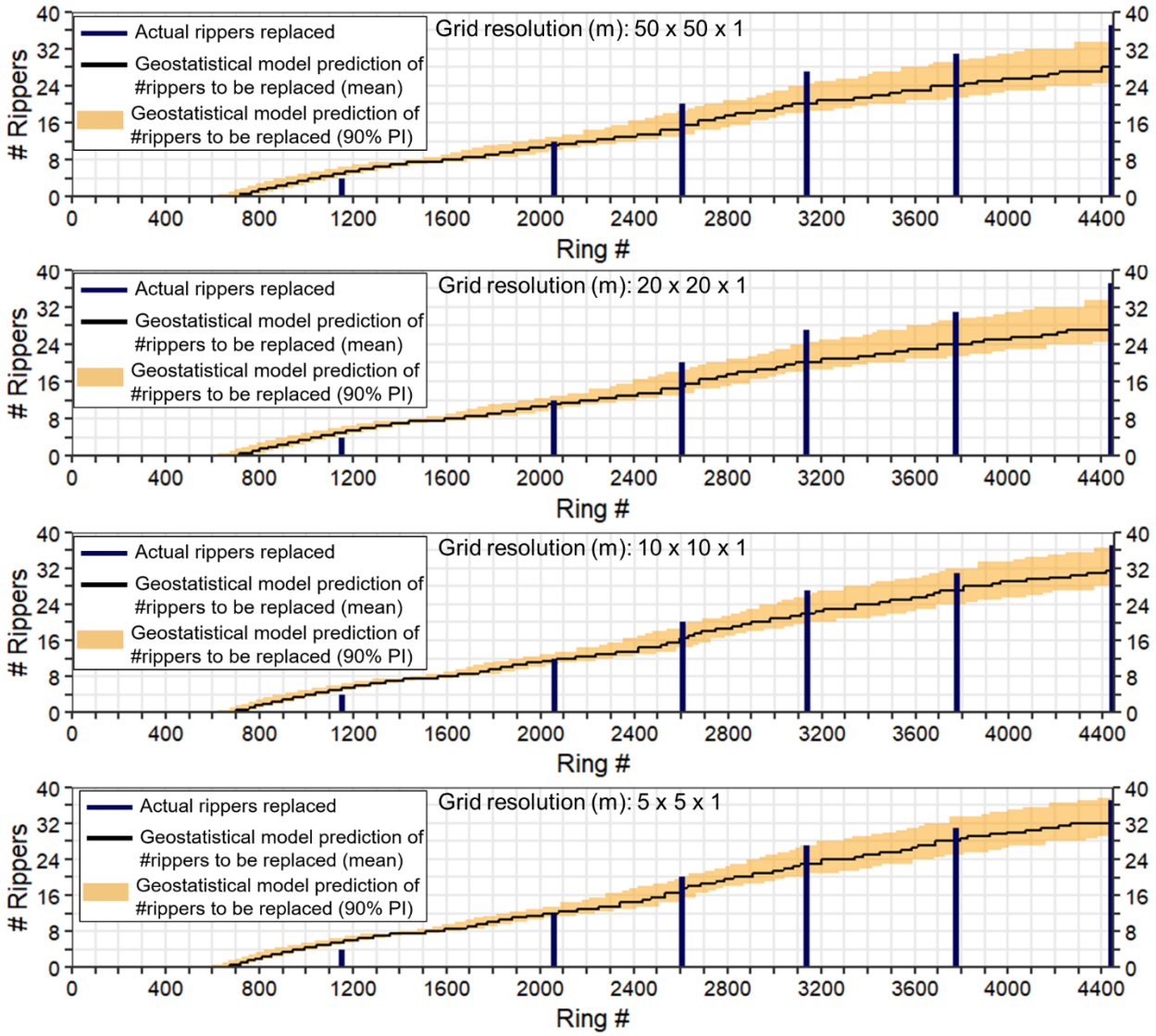

Figure 0.4 Estimated cumulative tool replacement for rippers from geostatistical modeling results of different grid resolutions compared with recorded tool changes during the project.

This study explored the extent to which tunnel risk of ripper tool replacements differs across resolutions of structural grids generated for geostatistical modeling. The prediction of geotechnical/geological conditions and their utilization in tunnel risk assessment may therefore depend on the grid resolution being used for geostatistical modeling. In the cases examined, 10 m grid resolution (in the longitudinal and transverse direction) is found to predict the number of tool replacements on an 8-mile-long tunnel project with 106 geotechnical SI boreholes. Similar results are obtained for a 5 m resolution grid, however, the geostatistical modeling runtime for 5 m grid is twice that of a 10 m grid. Coarser resolution grids of 50 m and 20 m do not effectively capture P (Sands) leading to an underestimation of SAI conditions within the tunnel envelope. It is evident that coarser resolution grids may not capture the critical soil/rock units, thus influencing tunnel risk mitigation and planning. For tunneling applications, the choice of the grid resolution depends on the modeling requirements. For a preliminary assessment of the geotechnical/geological

conditions, a coarser resolution of the grid can be selected to set up the model structure and parameters (e.g., variograms, transition probability matrices, proportions of geologic units). The preliminary assessment can be further refined using a finer grid resolution for geostatistical modeling. It is imperative and is a good practice to assess the performance of geostatistical models and their application towards tunneling risk assessment for different grid resolutions.